THE UNIVERSITY *of* EDINBURGH

Phosphoglycerate Kinase 1 as a Therapeutic Target in Motor Neuron Disease

Harriet Elizabeth McHale-Owen

THE UNIVERSITY *of* EDINBURGH

A thesis submitted in fulfilment of the requirements for the degree of Doctor of Philosophy

The University of Edinburgh, August 2025

Declaration

I confirm that the work presented in this thesis has been composed by me, except where explicitly stated otherwise in the text. This work has not been submitted for any other degree of professional qualification.

Harriet McHale-Owen

August 2025

Acknowledgements

I would like to firstly thank my supervisors Professor Tom Gillingwater and Professor Kiterie Faller for their consistent support and guidance throughout this project and their unending tolerance for my questions. Without Tom's positivity and Kiterie's healthy pragmatism this project would not have been possible. The rest of the Gillingwater lab team must also be recognised for being excellent colleagues who have turned into excellent friends. Without Helena Chaytow, Hannah Smith, Nikky Huang, Kim Morris, Federica Genovese, Hannah Crick, Rizwan Farrukh, Shahd Qutifan and others, my PhD experience would have been far less enjoyable and my lunches far more lonely.

I would also like to thank Professor Richard Mellanby and the rest of the ECAT team for supporting and funding this project via the Wellcome Trust. My previous mentors Clive Bate, Julie Simpson and Paul Heath should also be thanked for encouraging a love of research in me which has led me to be where I am now.

This manuscript would still be in its draft phase without the continued encouragement of my husband, Connor, who has kept me supplied with much needed caffeine (Pepsi Max) and who has supported me through the many, early starts, long nights and weekends where I've needed to write up or finish experiments. I would also like to thank my family who have supported me both emotionally and financially since before vet school – I promise this is the last time I plan on graduating! `

Finally, I would like to thank my good friends Sophie, Scott and my cat Tim, who helped keep me grounded and reminded of the world outside the project.

Lay Abstract

Motor Neuron Disease (MND) is a fatal condition where the nerve cells that control different muscles in the body progressively die. There is a lack of effective treatments for this condition and efforts to find treatments have been hampered by the complexity of the many different causes of the disease. One common feature of the diseased nerves is that they struggle to keep up with their energy demands. This can be due to an increase in energy needs due to the cell being under stress or some of their cell machinery that generates energy may be damaged. There is some evidence that increasing the activity of an important enzyme involved in cell energy production may protect nerve cells and slow down cell death. This enzyme is called phosphoglycerate kinase 1 (PGK1). Clinical trials are in their early stages to investigate whether a drug called terazosin, a PGK1 activator, may be beneficial in patients. However, terazosin was not designed to be a PGK1 activator and interacts with other important pathways in the body. Side effects of terazosin treatment have been reported in patients related to the other effects of terazosin. This has left the field with two key questions:

1. Is increasing PGK1 activity safe?
2. Can a PGK1 activator that is more effective or more specific than terazosin be found?

To help address these questions, I increased the levels of PGK1 in cells in a dish and found that no potentially harmful cell pathways were affected. I then screened a group of compounds in cells to see whether they affected PGK1 activity. The compounds that increased PGK1 activity the most were then tested in a zebrafish model of MND to see how they affect diseased nerves as part of a whole body system. Based on the findings of those screens, I realised we needed a better model system to screen potential PGK1 activating compounds. So, I developed an alternative cell model using stressed cells with genetic mutations associated with MND that could be applied to future compound screens. My work shows that cells can tolerate large amounts of

additional PGK1 but that finding new PGK1 activators that could be developed into therapies remains challenging. Future screening studies should consider using stressed cells or disease models (such as the zebrafish model) as these appear to be more sensitive to changes in PGK1 activity.

Scientific Abstract

Metabolic dysfunction and cellular stress are common features in neurodegenerative conditions like motor neuron disease (MND) and supporting cell energy production is an attractive strategy to improve the resilience of neurons to disease pathology. Phosphoglycerate kinase 1 (PGK1) is a key enzyme in the first ATP-producing step in the glycolysis pathway. PGK1 may have multiple other roles in cells apart from its role in glycolysis but these are less well understood, and the consequences of increased PGK1 activity in cells and therefore its suitability as a therapeutic target is not known. Overexpression of PGK1 has been shown to be beneficial in multiple models of MND but the most commonly used PGK1 agonist, terazosin, is non-specific and so there is a need to develop more effective and more specific alternatives.

In this thesis, I demonstrate that increased PGK1 activity in HEK-293 cells is well tolerated and does not result in the upregulation or downregulation of any cellular pathways supporting the further exploration of PGK1 agonists as potential future therapeutics. A metabolic assay in HEK-293 cells was used to identify the most promising PGK1 activators from a compound library. These lead compounds were then screened in a C9orf72 knockdown zebrafish model of MND. This work highlighted the importance of using a disease model for screening, as adding extra PGK1 to cells with adequate levels shows little observable effect.

An alternative model is needed to test compounds for PGK1 activation more effectively. NSC-34 cell lines stably overexpressing human TDP-43 that are subjected to an osmotic stressor are a promising cell model to use for future assessments of potential PGK1 agonists. My work suggests that whilst PGK1 is a promising target, it is challenging to find suitable alternatives to terazosin. Future PGK1 studies should consider using stressed cellular models of disease as a screening method rather than traditional cell lines.

Table of Contents

Declaration *2*

Lay Abstract *4*

Scientific Abstract *6*

Abbreviations *12*

Chapter 1: Introduction *13*

1.1 Thesis Structure **13**

1.2 Motor Neuron Disease (MND) **14**

1.2.1 Genetics of ALS 15

1.2.2 Current Therapies for ALS 16

1.2.3 TDP-43 17

1.3 Phosphoglycerate Kinase 1 ..... **19**

1.3.1 PGK1 structure, role in glycolysis and regulation 22

1.4 Other PGK1 functions **25**

1.4.1 Protein kinase 25

1.4.2 Modulation of autophagy 25

1.4.3 Modulation of inflammation 26

1.4.4 Disulphide reductase activity 26

1.4.5 DNA replication 26

1.4.6 Further suggested roles of PGK1 27

1.5 PGK1 in Cancer **29**

1.6 PGK1 in Neurological Conditions **29**

1.6.1 Motor Neuron Diseases 30

1.6.2 Parkinson's Disease 31

1.6.3 Other neurological conditions 34

1.7 PGK1 Activators **36**

1.7.1 Terazosin 36

1.7.2 The search for alternative PGK1 activators 37

1.8 Thesis Aims **40**

Chapter 2: Methods 41

2.1 Cell Protocols 41

2.1.1 Cell Maintenance 41

2.1.2 Transfection of HEK-293 cells 41

2.1.3 Bacterial transformation and purification of the PGK1 plasmid 42

2.1.4 Immunocytochemistry 44

2.1.5 Protein extraction 45

2.1.6 Protein quantification 45

2.1.7 Protein detection with western blot 46

2.1.8 PGK1 metabolic assay 48

2.1.9 Preparation for the Seahorse assays 51

2.1.10 Cell Mito Stress Test Seahorse assay 52

2.1.11 Glycolytic Stress Test Seahorse assay 53

2.1.12 Seahorse assay normalisation methods 54

2.1.13 RNA extraction and quality assessment 55

2.1.14 RNA Sequencing 56

2.1.15 NSC-34 cell differentiation and application of cell stressor 57

2.2 Zebrafish Protocols 59

2.2.1 Ethics 59

2.2.2 Microinjection of C9orf72 morpholino 59

2.2.3 Treatment and collection of zebrafish embryos 60

2.2.4 Motor axon analysis of zebrafish embryos 61

2.3 Statistics 61

2.3.1 Mixed Effects Models 61

Chapter 3: Effects of increased PGK1 activity in HEK-293 cells 62

3.1 Introduction 62

3.1.1 Transfecting HEK-293 cells 62

3.1.2 Assessing PGK1 overexpression 63

3.1.3 RNA-sequencing 64

3.2 Aims 65

3.3 Results 66

3.3.1 Overexpression of functional PGK1 66

3.3.2 Optimisation of Seahorse assays for HEK-293 cells 72

3.3.3 Cellular respiration is unaffected by PGK1 overexpression 77
3.3.4 RNA sequencing reveals minimal changes following PGK1 overexpression 84

3.4 Discussion 90

3.4.1 PGK1 transfection and Seahorse Assays 90
3.4.2 Upregulated genes identified by RNA-sequencing 91
3.4.3 Future work 95
3.4.4 Conclusion 96

Chapter 4: Screening potential PGK1 activating compounds in HEK-293 cells 97

4.1 Introduction 97

4.1.1 The lack of alternative PGK1 activators 97
4.1.2 Atomwise PGK1 compound library 98
4.1.3 PGK1 Metabolic Assay 98

4.2 Aims 99

4.3 Results 100

4.3.1 Optimisation of the PGK1 metabolic assay 100
4.3.2 Screening the Atomwise compound library for PGK1 activity 104
4.3.3 Selection of lead compounds 107

4.4 Discussion 111

4.4.1 Selection of lead compounds 111
4.4.2 Future work 111
4.4.3 Conclusion 112

Chapter 5: Screening potential PGK1 activating compounds in zebrafish. 113

5.1 Introduction 113

5.1.1 Zebrafish in bioscience research 113
5.1.2 The C9orf72 knockdown zebrafish model 116
5.1.3 Lead compounds 117

5.2 Aims 118

5.3 Results 119

5.3.1 The C9orf72 knockdown model 119
5.3.2 Screening lead compounds in the C9orf72 knockdown model 122
5.3.3 Screening additional compounds in the C9orf72 knockdown zebrafish model 126

5.3.4 Further exploring compound D11 in the C9orf72 knockdown zebrafish model..... 129

5.4 Discussion 133

5.4.1 Screening lead compounds in zebrafish 133

5.4.2 Clutch and Model Variability 133

5.4.3 Compound 12b 134

5.4.4 B11 134

5.4.5 Future Work 135

5.4.6 Conclusion 136

Chapter 6: Investigating other cell models for improved PGK1 screening. 137

6.1 Introduction 137

6.1.1 NSC-34 Cells 137

6.1.2 NSC-34 cells stably transfected with TDP-43 138

6.2 Aims 139

6.3 Results 140

6.3.1 Expression of TDP-43 and GFP in NSC34 lines 140

6.3.2 PGK1 in undifferentiated NSC-34 cells 143

6.3.3 Optimising the Seahorse assay for NSC-34 cells 145

6.3.4 Seahorse assay pilots with undifferentiated NSC-34 cells 147

6.3.5 Differentiating NSC-34 cells 152

6.3.6 PGK1 function in differentiated NSC-34 cells 152

6.3.7 Optimising cell stressor administration 154

6.3.8 Cellular metabolism and PGK1 function in stressed, differentiated NSC34 cells .. 156

6.3.9 The effect of potential PGK1 activating compounds on recovery from osmotic stress in differentiated NSC-34 cells 160

6.4 Discussion 169

6.4.1 The NSC-34 cell lines 169

6.4.2 Differentiation of NSC-34 cells 169

6.4.3 Assessing cellular metabolism following cell stressor 170

6.4.4 Compound screen in NSC-34 cell lines 171

6.4.5 Future Work 172

6.4.6 Conclusion 173

Chapter 7: General Discussion 174

7.1 Summary of Thesis Findings 174

7.1.1 Overexpression of PGK1 in HEK-293 cells is well tolerated 174
7.1.2 Screening potential PGK1 activators 174
7.1.3 NSC-34 cells show promise as a potential model system for future compound screens 175
7.1.4 Compound D11 has shown promise as a PGK1 activator in multiple models..... 175
7.2 PGK1 as a therapeutic target: the challenges 176
7.2.1 Model systems for drug screening..... 176
7.2.2 PGK1: a challenging target..... 179
7.3 Future work 180
7.4 Final thoughts..... 181
References*..... *182

Abbreviations

ALS	Amyotrophic Lateral Sclerosis
ASO	Antisense Oligonucleotide
BCA	Bicinchoninic Acid
DMSO	Dimethyl Sulphoxide
ECAR	Extracellular Acidification Rate
FTD	Frontotemporal Dementia
HEK	Human Embryonic Kidney
hpf	Hours post fertilisation
ICC	Immunocytochemistry
MND	Motor Neuron Disease
MO	Morpholino
NSC-34	Mouse Motor Neuron-Like Hybrid Cell Line
OCR	Oxygen Consumption Rate
PD	Parkinson's Disease
PGK1	Phosphoglycerate Kinase 1
PLL	Poly-L-lysine
ROS	Reactive Oxygen Species
SMA	Spinal Muscular Atrophy
TDP-43	TAR DNA-binding protein – 43 kDa
Tz	Terazosin
ZF	Zebrafish

Chapter 1: Introduction

1.1 Thesis Structure

This thesis investigates targeting of the enzyme phosphoglycerate kinase 1 (PGK1) for the development of future therapeutics for motor neuron disease (MND). The thesis comprises four results chapters and is structured as follows:

- **Introduction**: to put the results of this thesis into the context of current knowledge, the introduction will cover the need for novel therapeutics in neurodegenerative diseases like MND, the role of dysregulated metabolism in its pathogenesis and recent studies demonstrating the therapeutic potential of increased PGK1 activity. It will also discuss the current challenges faced in the field and introduce the aims of this thesis.
- **General materials and methods:** protocols that are used throughout the thesis are described here. Alterations to these protocols for specific experiments are described in the relevant results chapter.
- **Results chapters:**
    1. The effect of increased PGK1 activity *in vitro*
    2. Screening of potential PGK1 activators *in vitro*
    3. Screening of lead potential PGK1 activators *in vivo*
    4. Exploring an alternative *in vitro* model to improve compound screening
- **Discussion and final conclusions**: this chapter aims to bring together the conclusions of the individual results chapters and suggest next steps for researchers.

1.2 Motor Neuron Disease (MND)

Motor neuron diseases are a group of neurodegenerative disorders characterised by the progressive loss of motor neurons. Clinical presentations are varied as symptoms are dependent on the location of neuronal loss. Amyotrophic lateral sclerosis (ALS) is the most common motor neuron disease with global incidence estimated around 1-2 per 100,000 person-years (Marin et al. 2017; Xu et al. 2020). In terms of epidemiology, the average age of onset is approximately 65 years old and males are more commonly affected (Talbot 2009).

ALS is a progressive and ultimately fatal condition affecting both the upper and lower motor neurons. The prognosis of ALS is typically very poor with a median survival time of approximately 2-4 years following disease onset (Chio et al. 2009). However, ALS is a heterogenous disorder and there is large variation in survival times with up to 10% of patients surviving for more than 10 years (Chio et al. 2009). A key factor in this variation is in the ALS phenotype as patients that present with the bulbar, classic or respiratory forms have been found to have lower survival times (Wolf et al. 2014). There is also a recognised overlap between ALS and frontotemporal dementia (FTD) and the presence of FTD further reduces survival (Chio et al. 2009; Ferrari et al. 2011).

Reflecting the heterogenous nature of the clinical presentation of the disease, the causes of ALS are complex with multiple genetic and environmental factors identified (Feldman et al. 2022). ALS can be categorised as being either familial or sporadic. Familial cases are cases where there is a family history and make up approximately 10% of ALS cases with the rest being categorised as sporadic (Feldman et al. 2022; Barberio et al. 2023). Ubiquitinated transactive response DNA binding protein (TDP-43) cytosolic aggregates are an almost universal feature of ALS pathology and are indicative of some

common mechanisms in this highly diverse disease (Suk and Rousseaux 2020).

1.2.1 Genetics of ALS

Genome-wide association studies and other investigations into familial ALS cases have allowed for the detection of ~40 ALS-associated genes so now a genetic mutation can be pinpointed in approximately 75% of familial cases and 20% of sporadic cases (Chia, Chio, and Traynor 2018). Of the genes identified so far, four have received particular attention from researchers as between them they account for ~50% of familial cases and ~5% of sporadic cases (Goutman et al. 2022). These four genes are superoxide dismutase 1 (*SOD1*), chromosome 9 open reading frame 72 (*C9orf72*), fused in sarcoma (*FUS*) and TAR DNA binding protein (*TARDBP*).

SOD1 is an antioxidant protein and mutations in *SOD1* were the first to be associated with ALS in the 1990s (Rosen et al. 1993). *SOD1* cases of ALS are atypical in that they do not show pathological TDP-43 depositions common to the other forms of ALS suggesting that the mechanisms underlying the pathology of these cases may be different (Mackenzie et al. 2007).

The discovery of the hexanucleotide repeat expansion (GGGGCC) in the C9orf72 gene was a breakthrough in 2011 as this gene is responsible for ~40% of familial cases and ~7% of sporadic cases (Majounie et al. 2012). The mechanism behind why these expanded repeats are neurotoxic are unclear but both loss and gain of function mechanisms have been proposed including the dysregulation of RNA metabolism (Akcimen et al. 2023).

FUS and *TARDBP* mutations provide further evidence that dysregulated RNA metabolism is a common feature of ALS as these both encode RNA-binding proteins. Between them they account for <10% of familial cases and ~1-2% of

sporadic cases (Akcimen et al. 2023). Mutations in *FUS* seem to result in a more aggressive, early onset disease phenotype (Hubers et al. 2015). Interestingly both FUS and TDP-43 (the protein encoded by TARDBP) have been associated with altered stress granule dynamics suggesting important roles for these proteins in response to cellular stresses (Bosco et al. 2010; Khalfallah et al. 2018).

Despite the advances in genetics there remains a substantial number of ALS cases, particularly sporadic cases, where a specific gene mutation cannot be identified. Progress has been made towards designing therapies for some of the known gene mutations but given the heterogenous nature of ALS therapies that target specific genes will only benefit certain subsets of patients (Faller, Chaytow, and Gillingwater 2025).

1.2.2 Current Therapies for ALS

Despite the severity and impact of the disease, there is no cure and limited therapies are available to patients diagnosed with ALS. Riluzole was the first licensed therapeutic for ALS and confers some neuroprotection by inhibiting glutamate release in the CNS (Doble 1996). It can be given for all forms of ALS but only increases median survival by 6-19 months (Andrews et al. 2020). Retrospective analysis of patients has shown that riluzole increases survival by prolonging the last clinical stage rather than by uniformly slowing down disease progression (Fang et al. 2018). The antioxidant drug edaravone is reported to be well tolerated by patients but its effect on clinical outcomes to date appears to be relatively modest (Witzel et al. 2022; Gao et al. 2023). Developing therapies that are effective in all patient subgroups of this heterogenous condition is clearly going to be very challenging and it has been recognised since at least the 1990s that combinations of synergistic therapies are needed to achieve the most beneficial effects for patients (Mitsumoto and Olney 1996). In terms of targeting specific groups of patients, there have been

some promising recent breakthroughs in the field of antisense oligonucleotides (ASOs) which bind to mRNA of mutated genes to reduce the expression of their target genes. These are highly specific treatments and are most effective for groups of patients with specific mutations in proteins that cause a toxic 'gain of function'. Tofersen is an ASO that targets SOD1 and so may benefit patients that carry a *SOD1* mutation (Miller et al. 2022). Other ASOs are under development for patients that carry *C9orf72* or *FUS* mutations but although there is evidence they are able to reduce the expression of their target proteins, so far their clinical benefit remains unproven (Faller, Chaytow, and Gillingwater 2025).

Whilst the development of ASOs is exciting, even if they are successful therapeutics they will only be able to benefit patients with those specific mutations. There remains a need to develop therapeutics targeting common mechanisms that may benefit a broader range of patients and slow down disease progression at earlier clinical stages to help preserve patient's quality of life for as long as possible. Common mechanisms that could be targeted include metabolic dysregulation, RNA processing, protein aggregation and inflammation and ultimately a combination of approaches may be needed (Faller, Chaytow, and Gillingwater 2025).

1.2.3 TDP-43

The discovery of ubiquitinated TDP-43 deposits in the cytoplasm of postmortem tissue from the central nervous system (CNS) of ALS and FTD patients by two groups in 2006 marked a significant shift in ALS research (Neumann et al. 2006; Arai et al. 2006). These TDP-43 aggregates are found in an estimated 97% of ALS cases including both familial and sporadic forms (Arai et al. 2006; Neumann et al. 2006). TDP-43 is a ubiquitously expressed protein encoded by the *TARDBP* gene (Winton et al. 2008). Following the identification of TDP-43 aggregates, more than 80 *TARDBP* mutations

associated with ALS have been described with these mutations accounting for 3-5% of familial ALS cases (Balendra et al. 2025). Under normal physiological conditions TDP-43 is predominantly located in the nucleus of cells with a small proportion continuously shuttling between the nucleus and cytoplasm (Ayala et al. 2008). TDP-43 is a heterogeneous nuclear ribonucleoprotein that plays a key role in RNA regulation in the nucleus by repressing non conserved cryptic exons thereby conserving intron integrity (Ling et al. 2015). TDP-43 mislocalisation from the nucleus to the cytoplasm results in the inclusion of these cryptic exons resulting in dysfunctional proteins. Along with the reduction of normal TDP-43 function in the nucleus, mislocalisation of TDP-43 results in gain of toxic functions in the cytoplasm (Floare and Allen 2020). Both depletion and overexpression of TDP-43 results in cell death and motor function deficits in animal models and so its normal expression is tightly regulated (Kabashi et al. 2010; Xu et al. 2010; Wu, Cheng, and Shen 2012; Schmid et al. 2013). Pathological TDP-43 found in cytoplasmic aggregates has typically undergone phosphorylation and ubiquitination but the exact mechanism underlying TDP-43 aggregation is unknown (Neumann et al. 2009; Arai et al. 2006; Suk and Rousseaux 2020). Aggregates of TDP-43 have been found to co-localise with stress granules in the cytoplasm suggesting a link between TDP-43 pathology and altered cellular response to stress (Dewey et al. 2012). TDP-43 is expressed in many different cell types with aggregates found in both neurons and oligodendrocytes of ALS and FTD patients (Kawakami, Arai, and Hasegawa 2019). Interestingly, TDP-43 cytoplasmic aggregates are not always found to accompany cell toxicity in the overexpression of either wild type or mutant forms of TDP-43 when investigated in multiple *in vitro* and *in vivo* models (Hergesheimer et al. 2019). One reason for this may be related to the distribution of TDP-43 in the brains of ALS patients as the brainstem, hippocampus, spinal cord and motor cortex appear to be particularly susceptible to TDP-3 pathology whereas the occipital cortex and cerebellum are relatively protected in early disease stages (Geser et al. 2009). TDP-43 pathology is also relevant to other neurodegenerative conditions, particularly

in Alzheimer's disease where a staging scheme has been developed based on the location of TDP-43 deposits in the brain which correlates with clinical decline and imaging findings (Josephs et al. 2016).

1.3 Phosphoglycerate Kinase 1

Neurons, particularly motor neurons, need large amounts of energy to maintain their normal functions of propagating action potentials, maintaining synapses and the axonal transport of proteins along their long neurites (Vandoorne, De Bock, and Van Den Bosch 2018). The availability of intracellular ATP appears to be critical to maintaining normal motor neuron function (Le Masson, Przedborski, and Abbott 2014). ATP can be produced by neurons by multiple routes including mitochondrial oxidative phosphorylation and aerobic glycolysis (Wei et al. 2023). Mitochondrial oxidative phosphorylation is the most efficient in terms of ATP production, but it also results in an increase in toxic reactive oxygen species (ROS) within the cell (Turrens 2003). In aerobic glycolysis, the pyruvate produced by glycolysis is directed away from the oxidative phosphorylation pathway and is instead converted into lactate (Figure 1.1).

Whilst aerobic glycolysis is much less efficient in terms of ATP production and thought to predominantly occur in pathological conditions, recent work has found that even in the absence of increased energy needs, this was the preferred pathway for ATP generation in neuronal cell bodies (Wei et al. 2023). When the neurons were forced to switch to favour oxidative phosphorylation via the deletion of the glycolytic enzyme pyruvate kinase 1 there was increased oxidative damage and cell death (Wei et al. 2023). The upregulation of glycolysis has been reported in fibroblasts isolated from SOD1 ALS patients and upregulation of the glycolytic enzyme phosphofructokinase has also been reported in motor neurons with TDP-43 pathology (Allen et al. 2014; Manzo et

al. 2019). This upregulation of glycolysis has been suggested to be a compensatory mechanism and may be neuroprotective in conditions like ALS (Tang 2020). The enzyme phosphoglycerate kinase 1 (PGK1) has recently been established as a rate-limiting component of glycolysis in neurons which has important implications for multiple neurological conditions where increased neuronal energy production may be beneficial (Kokotos et al. 2024).

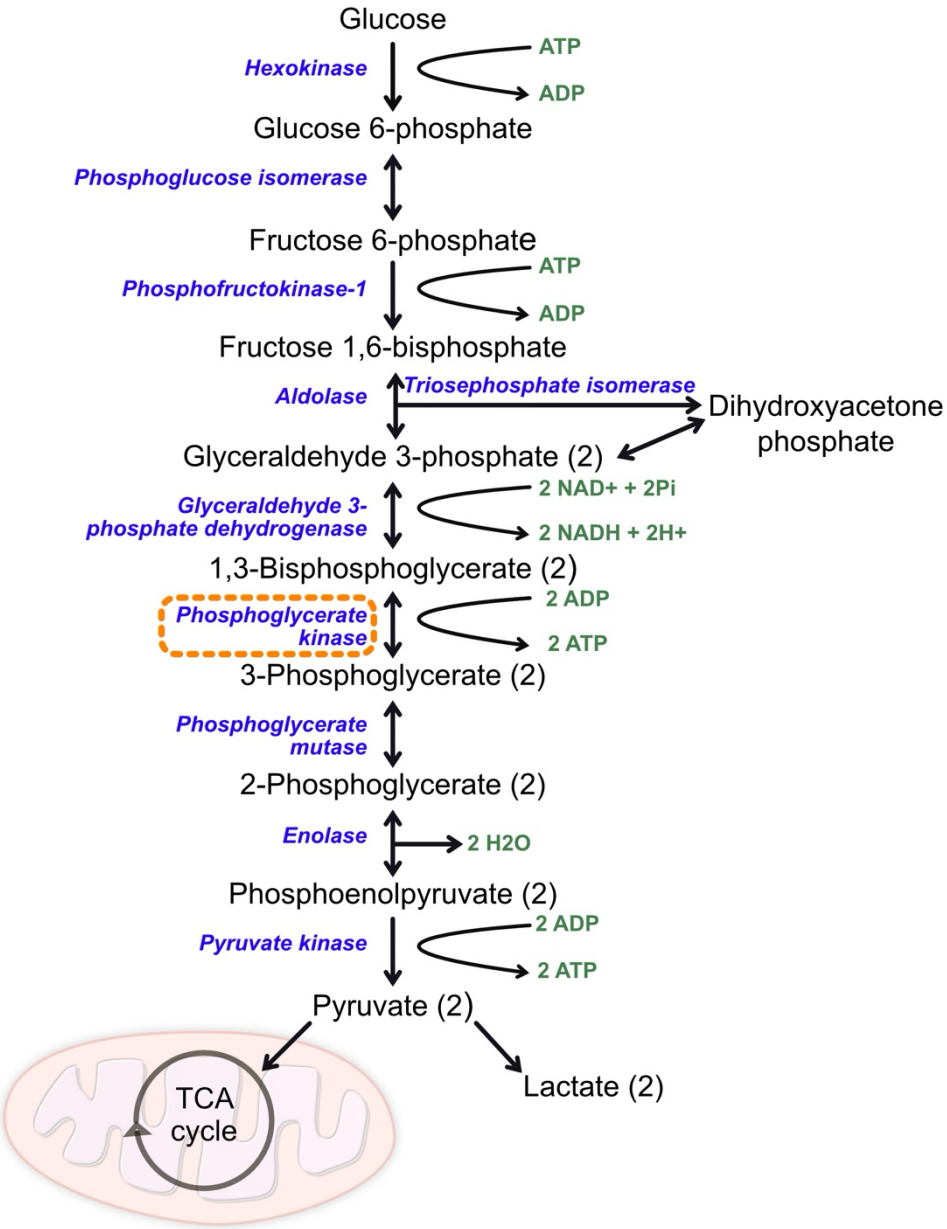

Figure 1.1. Glycolysis pathway reproduced from McHale-Owen et al (McHale-Owen et al. 2025). The position of the reaction catalysed by PGK1 is highlighted (orange box). The other enzymes in the pathway are in blue with NAD+/NADH and ADP/ATP shown in green. Once glucose has been transformed to pyruvate then it can either enter the tricarboxylic acid (TCA) cycle, commonly referred to as the Krebs cycle or be converted to lactate.

1.3.1 PGK1 structure, role in glycolysis and regulation

Phosphoglycerate kinase 1 (PGK1) is an important glycolytic enzyme responsible for catalysing the first ATP-producing step in glycolysis. PGK1 is highly conserved across species and as it has such a key role in cellular energy production it is expressed in all somatic cells (Watson and Littlechild 1990). There are two isoforms of the PGK enzyme with PGK2 being an isozyme of PGK1 expressed only during spermatogenesis to replace the glycolytic function of PGK1 and contributes significantly to sperm motility and overall male fertility (Danshina et al. 2010). PGK1 is a monomeric enzyme made up of 417 amino acids that form two alpha helix domains of similar size with a cleft in the centre (Watson et al. 1982)(Figure 1.2). Both of these domains, referred to as the N- and C- terminal domains, bind substrates and are necessary for PGK1's function in glycolysis. The step of glycolysis catalysed by PGK1 is the production of 3-phosphoglycerate (3-PG) and adenosine triphosphate (ATP) by the reversible transfer of a phosphate group from 1,3-biphosphoglycerate (1,3-BPG) to adenosine diphosphate (ADP). The N-terminal domain of PGK1 binds to 1,3-BPG/3-PG and the C-terminal domain binds to ADP/ATP. The cleft between the two domains acts like a hinge. When there are no bound substrates then PGK1 has an open conformation that closes when the substrates bind to the N- and C- terminal domains. This aids the transfer of the phosphate group by bringing the substrates closer together (Rojas-Pirela et al. 2020; Palmai et al. 2009).

The activity of PGK1 is highly regulated at the transcriptional, post-transcriptional and post-translational level (Zhang, Sun, and Kang 2023). Multiple transcription factors have been associated with increased PGK1 expression in various cancers. The oncogene MYC which functions as a transcription factor has been shown to interact with the promotor region of *PGK1* and upregulate PGK1 expression (Tang et al. 2009). Hypoxia-inducible factor 1 (HIF-1) is another important transcription factor which has been associated with increased PGK1 expression under hypoxic conditions (Kaluz,

Kaluzova, and Stanbridge 2008; Firth et al. 1994). Additionally, knockdown of Nuclear Factor of Activated T-Cells 5 (NFAT5) was found to reduce cell proliferation by reducing PGK1 expression (Jiang et al. 2019). Various noncoding RNAs (ncRNAs) have been implicated in the regulation of PGK1 in multiple cancers (Zhang, Sun, and Kang 2023). For example, the long noncoding RNA (lncRNA) nuclear paraspeckle assembly transcript 1 (*NEAT1*) is overexpressed in glioma and has been suggested to stabilise PGK1 levels by inhibiting its ubiquitination-induced degradation (Liang et al. 2022). *NEAT1* is commonly upregulated in patients with cancer and has been associated with an increase in glycolytic rate (Park et al. 2021). A mechanism for this has been proposed whereby *NEAT1* is able to bind and form a scaffold to facilitate assembly of a multienzyme complex of PGK1, phosphoglycerate mutase and enolase improving substrate channelling for glycolysis and contributing to the observed Warburg effect in cancer models (Park et al. 2021). In addition to ubiquitination, PGK1 has been shown to undergo other posttranslational modifications (PTMs) including acetylation (Wang et al. 2015), phosphorylation (Zhang et al. 2018), O-GlcNAcylation (Nie et al. 2020), succinylation (Luo et al. 2023) and crotonylation (Guo et al. 2024).

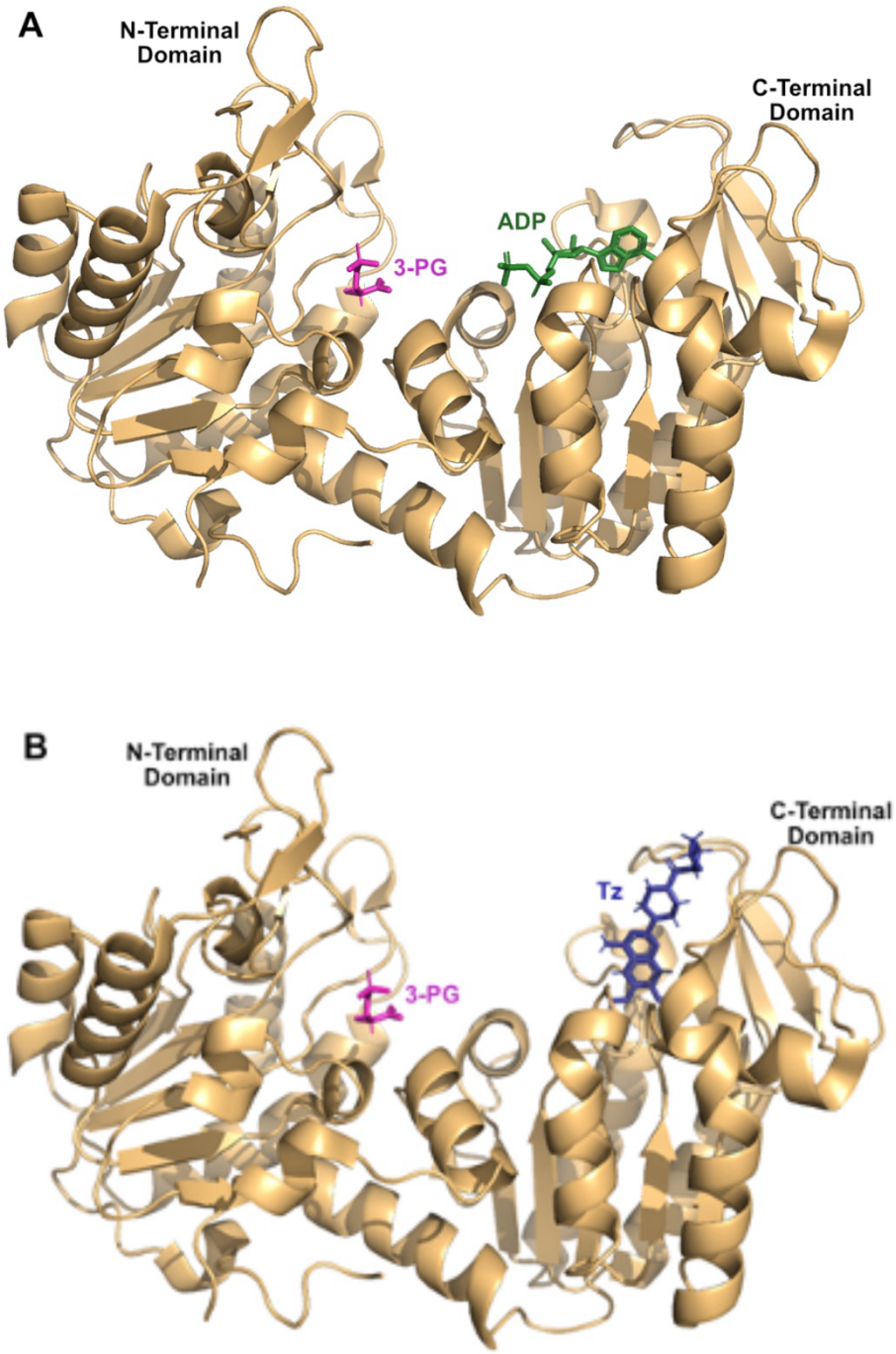

Figure 1.2: PGK1 structure and location of key binding sites. **(A)** PGK1 molecule (yellow) showing its interactions of 3-PG (pink) and ADP (green). **(B)** PGK1molecule (yellow) showing its interactions of 3-PG (pink) and terazosin (Tz, blue). Figures adapted from McHale-Owen et al (McHale-Owen et al. 2025). Molecular structure images created using PyMOL (Version 2.1) with structures sourced from the RCSB Protein Data Bank (Kumar et al. 1999; Bowler 2013; He et al. 2021; Shimizu et al. 2020).

1.4 Other PGK1 functions

PGK1 is primarily found in the cytoplasm of cells for its role in glycolysis but additional functions have been attributed to PGK1 associated with its presence in other locations such as the mitochondria (Chen, Wang, et al. 2024), cell nuclei (Li et al. 2018) and even extracellularly (Fu, Chen, et al. 2023)(Figure 1.3). These additional functions have led to PGK1 being referred to as a 'moonlighting' protein which are a heterogenous group of approximately 300 proteins that perform multiple physiologically relevant functions (Jeffery 2017). The additional roles of PGK1 are generally not well characterised and there is a need for further research in these areas. However, these non-canonical roles could have significant implications for therapies that aim to affect PGK1 activity and so it is worth considering them here.

1.4.1 Protein kinase

Under hypoxic conditions, such as the tumour microenvironment, PGK1 has been found to translocate to the mitochondria where it acts as a protein kinase phosphorylating pyruvate dehydrogenase kinase 1 (PDHK1) which then inhibits the pyruvate dehydrogenase complex (Li et al. 2016; Nie et al. 2020). This results in decreased mitochondrial pyruvate utilisation and increased glycolysis and lactate production.

1.4.2 Modulation of autophagy

PGK1, acting as a protein kinase, under normal conditions phosphorylates PRAS40 which is a protein important in the Akt and mTOR signalling pathways (Zhang et al. 2022). The phosphorylation of PRAS40 was found to reduce autophagy mediated cell death promoting cell growth. The relationship between PGK1 and PRAS40 changes in hypoxic conditions and instead PGK1 phosphorylates Beclin 1 which induces autophagy (Qian et al. 2017).

1.4.3 Modulation of inflammation

PGK1 has been reported to be a regulator for multiple aspects of inflammation. A direct link between PGK1 and the Keap1-Nrf2 signalling pathway has been demonstrated with reduced PGK1 activity resulting in the activation of the Nrf2 signalling pathway (Bollong et al. 2018). This occurs as inhibition of PGK1 leads to the accumulation of methylglyoxal (MGO) which results in the post translational modification of KEAP1 through a crosslink between the proximal cysteine and arginine. This results in the dimerization of KEAP1 and increased Nrf2 (Bollong et al. 2018). Inhibition of PGK1 reduced the expression of IL-6 indicating a role of PGK1 in the JAK/STAT pathway (Liao et al. 2022). PGK1 has also been shown to be able to bind to and regulate the stability of the acute phase protein inter-α-trypsin inhibitor heavy chain 4 (ITI-H4) (Park, Choi, and Baek 2023).

1.4.4 Disulphide reductase activity

Extracellular PGK1 may have a role in angiogenesis, at least in the context of cancer, where the administration of PGK1 to mice with HT1080 tumours increased angiostatin levels and inhibited tumour growth (Lay et al. 2000). It was suggested that PGK1 is secreted by tumours and acts as a disulphide reductase to reduce the disulphide bonds in plasmin which releases angiostatin.

1.4.5 DNA replication

PGK1 also has a reported role in DNA replication. CDC7 (cell division cycle 7) is a protein kinase which is activated during the S phase of the cell cycle and inhibited by ADP. CDC7 is a potential target in cancer therapies as it is often upregulated in tumour cells (Bonte et al. 2008). Nuclear PGK1 can be phosphorylated by casein kinase 2α activated by epidermal growth factor receptor (EGFR) activation (Li et al. 2018). Phosphorylated PGK1 was found

to phosphorylate the ADP product of the CDC7-ASK complex to ATP thereby relieving the inhibitory effect of ADP and promoting DNA replication and cell proliferation (Li et al. 2018).

1.4.6 Further suggested roles of PGK1

In another link between PGK1 and EGFR, phosphorylated PGK1 can be recruited to the endosomal membrane where it acts as a cargo adaptor by binding to EGFR aiding the lysosomal transport of EGFR (Chu et al. 2024). PGK1 may also have a role in regulating ferroptosis which is a process of cell death characterised by iron-dependent lipid peroxidation with PGK1 potentially playing a protective role (Wang et al. 2024).

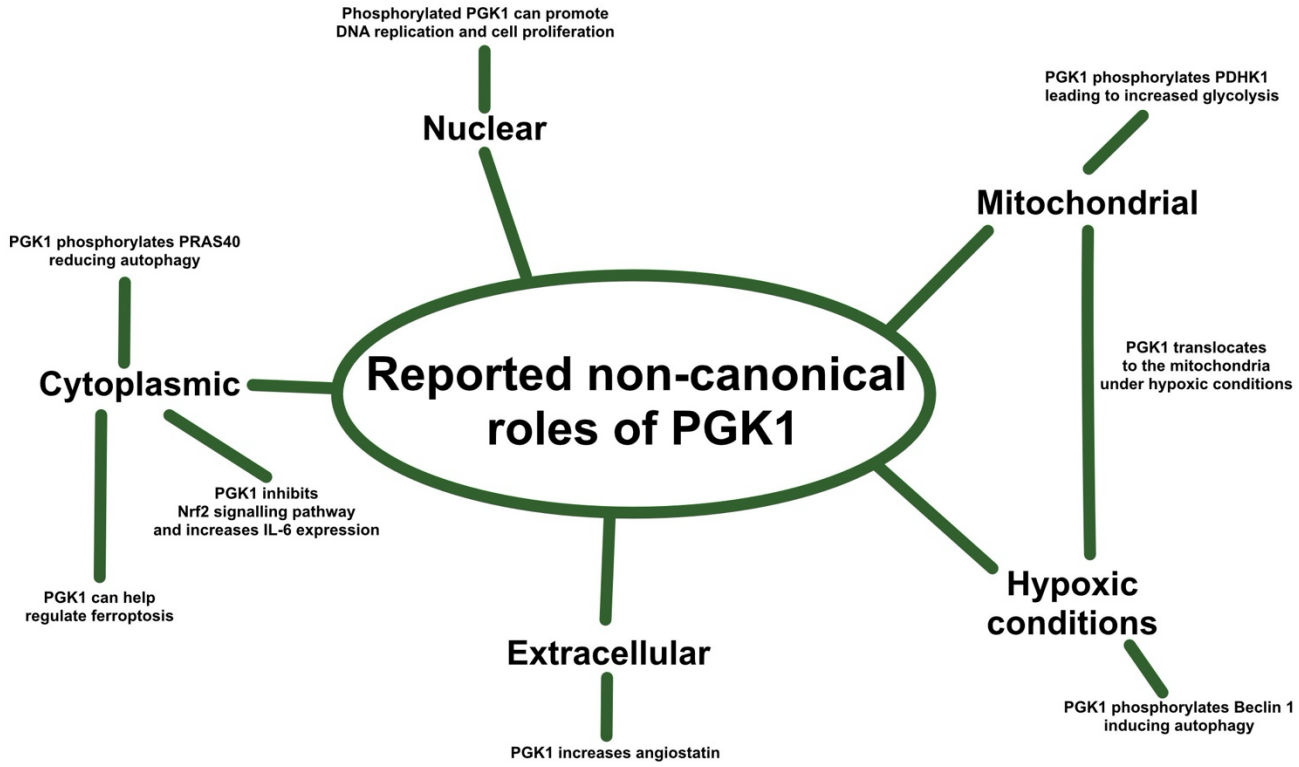

Figure 1.3: Summary of reported non-canonical roles of PGK1. PGK1 has multiple other reported functions, aside from its role in glycolysis, in different parts of the cell (nuclear, cytoplasmic, mitochondrial, extracellular) as well as under different cellular conditions (hypoxia).

1.5 PGK1 in Cancer

Historically, PGK1 targeted therapies have been a topic of research primarily in the field of cancer rather than in neurological disease. The metabolism of cancer cells has been extensively studied and a switch to aerobic glycolysis also known as the Warburg effect is a common finding (Vander Heiden, Cantley, and Thompson 2009). Aerobic glycolysis is where glucose is metabolised to pyruvate that is converted to lactate rather than proceeding into the oxidative phosphorylation pathway. This may be a more inefficient way of producing energy in terms of yield but may allow cells to produce energy at a faster rate giving them a selective advantage in a tumour microenvironment (Pfeiffer, Schuster, and Bonhoeffer 2001; Vander Heiden, Cantley, and Thompson 2009; Liberti and Locasale 2016). High PGK1 expression has been found in many types of cancer and has been associated with both a poorer prognosis and increased resistance to treatments (Qiu et al. 2024; Ding et al. 2014). Therefore, inhibiting PGK1 activity is being explored as a potential adjunctive therapy in multiple forms of cancer (Chen et al. 2025; Li et al. 2023).

1.6 PGK1 in Neurological Conditions

The positive association of high PGK1 levels on cell survival in many cancers suggests that increased PGK1 may be of interest in conditions where cell death is a prominent feature such as in neurodegenerative diseases. Neurons seem to be particularly vulnerable to dysregulated energy production as they have high metabolic demands to support their neuronal projections and synapses (Pacelli et al. 2015; Muddapu et al. 2020). Whilst this thesis is mainly focussed on exploring PGK1 activation for the purpose of therapy development in motor neuron disease, there are other neurological conditions which may also benefit from the development of improved PGK1 activators. Additionally, it must be recognised that a significant amount of research in this area has

come from the Parkinson's disease field and this must be understood to appreciate the progress and challenges of where we are now.

1.6.1 Motor Neuron Diseases

Metabolic dysfunction is commonly reported in ALS and other motor neuron diseases like spinal muscular atrophy (SMA). There is evidence that the metabolic switch to aerobic glycolysis that is common to many forms of cancer also occurs in ALS (Valbuena et al. 2016; Allen et al. 2014). This has been proposed to be a compensatory mechanism in response to increased energy demands to support cell survival (Tang 2020). The G93A SOD1 mouse model of familial ALS shows impaired glucose utilisation and reduced cortical ATP levels (Browne et al. 2006). This is supported by evidence from the TDP-43 mouse model with the A315T mutation that also show reduced ATP production and impaired mitochondrial function in the motor cortex (Gautam et al. 2022). What is intriguing is that not all neurons are equally vulnerable to disease with some subgroups being particularly vulnerable or resistant to disease. In SMA, examples of these subgroups can all be found in the hindlimb with the *extensor digitorum longus* (resistant), *tibialis anterior* (vulnerable) and the *gastrocnemius* (intermediate) providing a range of known vulnerability to disease which is not associated with their morphological characteristics (Thomson et al. 2012). A comparison of the transcriptomic profiles of pools of these vulnerable and resistant motor neurons from wild-type mice revealed PGK1 as one of a cluster of genes that have a lower expression in the vulnerable neurons (Boyd et al. 2017). Knockdown of PGK1 in zebrafish embryos reduced axon length and increased motor axon branching in a similar manner to the phenotype observed in SMA and ALS models (Boyd et al. 2017; Ciura et al. 2013; Chaytow et al. 2022). Additionally, the overexpression of PGK1 or treatment with the PGK1 agonist terazosin rescued the motor axon phenotype seen in a zebrafish model of SMA (Boyd et al. 2017). This was further supported by work in the severe Thy1-hTDP-43 mouse model of ALS

where terazosin treatment improved survival and motor function. Terazosin treatment was also neuroprotective in ESC-derived motor neurons expressing TDP-43 with the M337V mutation (Chaytow et al. 2022). This evidence that terazosin may be neuroprotective in ALS by targeting PGK1 has led to a clinical trial of terazosin in ALS (ISRCTN45028842). Fibroblasts cultured from patients with sporadic ALS have a 1.7 fold decrease in PGK1 expression compared with controls (Raman et al. 2015). Given how tightly PGK1 expression is controlled this suggests a degree of dysregulation however whether PGK1 expression is altered in the CNS of ALS patients is currently unknown.

1.6.2 Parkinson's Disease

Parkinson's disease (PD) is another neurodegenerative condition but unlike MND it is characterised by the loss of dopaminergic neurons in the substantia nigra and the accumulation of intracellular α-synuclein (Poewe et al. 2017). Like ALS, the pathogenesis of PD is complex with multiple patient and environmental factors contributing to disease onset and progression (Morris et al. 2024). Aberrant cellular metabolism and mitochondrial dysfunction have been identified as occurring early on in the disease, particularly related to deficiency in complex I that is associated with increased levels of oxidative stress (Swerdlow et al. 1996; Morris et al. 2024). As with the MNDs ALS and SMA, not all neurons are equally vulnerable to disease. The more vulnerable dopamine containing neurons of the substantia nigra compacta have been found to have a higher density of axonal mitochondria with a higher basal rate of both mitochondrial oxidative phosphorylation and oxidative stress compared with the less vulnerable dopamine neurons of the ventral tegmental area (Pacelli et al. 2015). In terms of genetics, multiple genes associated with familial PD such as Parkin, PINK1 and PARK7/DJ-1 are also associated with energy metabolism (Poewe et al. 2017). Interestingly, PARK7/DJ-1 has recently been suggested to have a role in PGK1 regulation with PARK/DJ-1

expression being required for the improved synaptic resilience in neuronal cultures seen with increased PGK1 activity (Kokotos et al. 2024).

PGK1 deficiency is a rare X-linked recessive genetic condition with patients presenting with a range of symptoms including epilepsy and early onset or juvenile Parkinsonism (Morales-Briceno et al. 2019). It has also been suggested that carriers of a *PGK1* mutation may be at increased risk of also developing early onset Parkinsonism which could be related to the location of the *PGK1* gene on PARK12 which is a known susceptibility locus for PD (Sakaue et al. 2017). The association between PGK1 deficiency and PD-like symptoms is supported by *in vivo* work with a PGK1 knockdown in the dopaminergic neurons of *Drosophila* resulting in reduced CNS dopamine levels and locomotive deficits akin to those seen with PD (Shimizu et al. 2020).

PGK1 overexpression or treatment with the PGK1 agonist terazosin has been beneficial in multiple *in vitro* and *in vivo* models of PD (Cai et al. 2019; Kokotos et al. 2024). Increased neuronal PGK1 expression using an adeno-associated virus in the substantia nigra of mice which then received a 6-hydroxydopamine (6-OHDA) injection to model PD was found to protect axonal integrity and improve cell survival (Kokotos et al. 2024). Overexpression of PGK1 was also neuroprotective in a *Drosophila* model of PD induced by exposure to the mitochondrial complex I inhibitor rotenone (Cai et al. 2019). This is supported by *in vitro* work where increased PGK1 expression in neuronal cell cultures improved ATP production and synaptic function in low glucose conditions (Kokotos et al. 2024). A similar improvement in synaptic function in the primary neuronal cultures in low glucose conditions with 10 μM terazosin treatment (Kokotos et al. 2024). Terazosin treatment also increased ATP levels and improved the phenotype of the rotenone exposed *Drosophila* model as well as improving the motor function and dopamine levels in both MPTP- treated mice and 6-OHDA-treated rats (Cai et al. 2019).

These preclinical findings have led to multiple interrogations of patient databases to assess the impact of terazosin on PD incidence and progression as terazosin is already prescribed clinically for benign prostatic hyperplasia (Cai et al. 2019; Gros et al. 2021; Simmering et al. 2021; Sasane et al. 2021; Simmering et al. 2022; Weber et al. 2023; Opheim et al. 2024). Terazosin, doxazosin and alfuzosin are all α1-adrenergic receptor antagonists that contain similar PGK1 binding sites, tamsulosin is commonly prescribed for the same conditions but lacks the PGK1 binding site (Simmering et al. 2021). Initial retrospective database analyses of male patients in North America and Denmark showed that patients receiving terazosin, doxazocin or alfuzosin had a reduced risk of being diagnosed with PD and patients with PD showed a slower decline in their motor function than the control group receiving tamsulosin (Cai et al. 2019; Gros et al. 2021; Simmering et al. 2021). An observational study was then published which suggested that it was not that terazosin, doxazosin and alfuzosin were protective, but rather that tamsulosin treatment increased the incidence of PD raising questions over the use of tamsulosin treated patients as a control group (Sasane et al. 2021). A follow up study by a group that performed one of the initial database analyses used patients treated with 5α-reductase inhibitors (5ARI) as an additional alternative control group (Simmering et al. 2022). They found that treatment with terazosin, doxazosin or alfuzosin reduced the risk of PD compared with treatment with either tamsulosin or 5ARI. A meta-analysis of these studies supported the initial findings that the incidence of PD was lower in people taking terazosin, doxazosin or alfuzosin compared with people taking tamsulosin (Ribeiro et al. 2024). Subsequent studies also found that PD patients taking terazosin, doxazosin or alfuzosin had fewer recorded PD events and a lower risk of being diagnosed with dementia compared with PD patients receiving tamsulosin suggestive of slower disease progression (Weber et al. 2023; Opheim et al. 2024). The first randomised controlled pilot of terazosin in people with PD found that terazosin may increase ATP levels but did not affect clinical outcomes in the 12-week course of the study (Schultz

et al. 2022). Side effects in the group taking terazosin related to its α1-adrenergic receptor inhibitor activity resulted in three out of eight participants withdrawing which needs to be taken into consideration in future trials. A follow-up phase 2 study is currently underway investigating the effect of terazosin treatment in PD (NCT05109364).

1.6.3 Other neurological conditions

Since PGK1 activation targets a common disease mechanism rather than a specific genetic cause of disease, it has broad therapeutic potential across a range of diseases. In terms of other neurodegenerative diseases, the effect of terazosin treatment or PGK1 overexpression has been explored in Alzheimer's disease (AD) (Chen et al. 2023), multiple system atrophy (MSA) (Chen et al. 2023), dementia with Lewy bodies (DLB) (Hart et al. 2024) and spinocerebellar ataxia type 3 (SCA3) (Chen, Hong, et al. 2024). Terazosin treatment was found to reduce tau protein aggregates in both *Drosophila* and mouse models of AD as well as improving the performance of an amyloid precursor protein/presenilin 1 mouse model in memory tests (Chen et al. 2023). This study looked at the effect of terazosin treatment on protein aggregation in a range of models of different neurodegenerative diseases and also found that terazosin improved the motor function of a rat model of MSA that was associated with an increase in brain ATP and reduced α-synuclein protein levels (Chen et al. 2023). The same group that performed some of the retrospective database analyses of terazosin, doxazosin and alfuzosin in PD also found that men on one of these medications had a reduced risk of developing DLB compared with those taking either tamsulosin or 5ARI (Hart et al. 2024). PGK1 decreased polyQ expression in a HEK-293 cell model of SCA3 (Chen, Hong, et al. 2024). A liposomal system was then employed to deliver PGK1 intranasally to a mouse model of SCA3 and was found to improve motor performance and reduce polyQ expression (Chen, Hong, et al. 2024).

The role of PGK1 in other pathological neurological states such as neuroinflammation and hypoxia is less clear. PGK1 has potential roles in the modulation of inflammation via interactions with Nrf2 and inter-α-trypsin inhibitor heavy chain 4 (Bollong et al. 2018; Park, Choi, and Baek 2023). Inhibition of PGK1 using CBR-470-1 was found to be protective in SH-SY5Y neuroblastoma cells when exposed to the neurotoxin MPP+ via activation of the Nrf2 pathway (Zheng et al. 2020). This was supported by a later study which found that overexpression of PGK1 inhibits the Nrf2 pathway and worsened the pathology seen in a rat model of cerebral ischaemia reperfusion injury achieved with middle cerebral artery occlusion reperfusion (Liu et al. 2023).

Hypoxia can occur as part of multiple neurological conditions in an acute, chronic, systemic or focal manner. A lot of the research regarding PGK1 in hypoxia relates to the tumour microenvironment in various cancers, but some more recent work is more relevant to neurological disease. Upregulation of PGK1 by HIF-1α as an adaptive response in systemic hypoxic conditions has been observed in multiple cell models as well as animal and human population studies (Li, Ko, and Whitlock 1996; Wang et al. 2007; Lam et al. 2007). A mouse model of post-operative cognitive dysfunction induced with etomidate found that the increased expression of HIF-1α and associated increase in PGK1 resulted in increased levels of oxidative stress with downregulation of HIF-1α being protective (Lu et al. 2024). However, the increased expression of PGK1 seen in hypoxic conditions has been associated with better outcomes in hypoxic-ischaemic encephalopathy in infants in keeping with the suggestion that the upregulation of PGK1 is a compensatory mechanism (Yip et al. 2023). Under chronic hypoxic conditions PGK1 can translocate to the mitochondria and phosphorylate PDHK1, increasing its activity and also promoting cell proliferation (Li et al. 2016). This translocation of PGK1 to mitochondria was associated with a decrease in cytosolic PGK1 and found to increase neuronal cell death in a cell model of ischaemic neuronal injury (Chen, Wang, et al.

2024). However, another study found that the translocation of PGK1 to the mitochondria could be beneficial in primary hippocampal neurons and a mouse model of acute hypobaric brain injury via interactions with TRAP1 (Liu et al. 2024). Hypoxia also affects post translational modifications of PGK1 with a decrease in lysine crotonylation and increase in cell proliferation and glycolysis observed in hypoxic conditions (Guo et al. 2024). The effect of the various PTMs of PGK1 is not fully understood but a report of reduced expression of succinylated PGK1 in the hippocampus of a rat model of epilepsy suggests that these PTMs may play a significant role [22].

One of the reasons why we may be seeing a discrepancy between whether PGK1 is beneficial or harmful in such conditions is in the amount of PGK1 overexpression. A study using modified PGK1 in a gerbil model of hippocampal ischemia found that whilst a low dose (0.1 mg/kg) reduced neuronal death, the higher dose (1.0 mg/kg) was not protective (Hahn et al. 2022). A similar finding was seen separately in a middle cerebral artery occlusion rat model treated with the PGK1 agonist terazosin where the higher dose of terazosin (0.08 mg/kg) was not neuroprotective but the lower dose (0.03 mg/kg) was (Chen et al. 2015). However, the effect seen with terazosin treatment is perhaps more likely due to the biphasic relationship between PGK1 and terazosin rather than differences in PGK1 activity itself (see below).

1.7 PGK1 Activators

1.7.1 Terazosin

Terazosin is used in many studies as a PGK1 agonist and clinical trials investigating whether it is beneficial in PD or ALS are ongoing. Terazosin was not designed as a PGK1 activator; it has been used clinically since the 1980s as an α-1 adrenergic receptor antagonist (Kyncl 1986). The interaction between terazosin and PGK1 is separate to its function as an α-1 adrenergic

receptor antagonist as when the quinazoline ring of terazosin is modified to reduce its ability to bind to α-1 adrenergic receptors 1000-fold, the effect of terazosin on PGK1 is preserved (Chen et al. 2015). Terazosin binds to PGK1 via its 2,4-diamino-6,7-dimethoxyisoquinazoline structural motif which fits into the PGK1 C-terminal domain which typically binds ADP/ATP (Figure 1.2.B) (Chen et al. 2015; Riley et al. 2024). The position of the terazosin binding site may explain a reported peculiarity where as well as being a PGK1 agonist, at concentrations of 2.5 μM and above, terazosin can also inhibit PGK1 (Chen et al. 2015). At low concentrations, the binding of terazosin is thought to accelerate the release of ATP whereas at higher concentrations terazosin may compete with ADP for the binding site and therefore inhibit PGK1 activity (Riley et al. 2024). This biphasic response is suggestive of a complex relationship between the two which could have significant implications for dose optimisation as there may be quite a narrow therapeutic window. However, this is not the only challenge regarding the use of terazosin as a PGK1 agonist as its non-specificity and α-1 adrenergic receptor antagonist properties are also a concern. In a recent pilot study, three out of eight participants with PD withdrew because they developed dizziness and/or orthostatic hypotension whilst being treated with terazosin (Schultz et al. 2022).

1.7.2 The search for alternative PGK1 activators

Since the identification of terazosin as a PGK1 agonist there has been a search for alternatives, with recent studies published investigating similar compounds that could be repurposed (Cai et al. 2019; Liu et al. 2024), structural analogs of terazosin (Wang, Qian, et al. 2022) and virtual screening to try to identify novel PGK1 activators (Qiang et al. 2022).

Alfuzosin and doxazosin are both very similar molecules to terazosin and contain the quinazoline motif thought to increase PGK1 activity (Cai et al. 2019). However, these are also both used clinically as α-1 adrenergic receptor antagonists and so the side effects reported with terazosin treatment are likely

to also be an issue for patients given these drugs. Meldonium (mildronate) is another drug that has been proposed to activate PGK1. Treatment with meldonium was found to improve the pathology of a rat model of PD and has been suggested to have both anti-apoptotic and anti-inflammatory properties in a neurotoxicity rat model (Klusa et al. 2010; Pupure et al. 2010). However, the mechanism of these observed protective effects are unclear with virtual docking studies suggesting meldonium could bind to both PGK1 (Liu et al. 2024) and phosphofructokinase (Wang, Liu, et al. 2022) with other work suggesting more mitochondrial focussed mechanisms of neuroprotection via the Akt/GSK-3β signalling pathway (Yang et al. 2024). Another complication of meldonium is that it does not have marketing authorisation in the European Union and it was added to the list of illicit substances of the World Anti-Doping Agency in 2016 for its performance enhancing effects seen due to the inhibition of L-carnitine synthesis (Berlato and Bairros 2020).

Terazosin analogs have been synthesised and compared in *in vitro* experiments; they have shown that the ability of terazosin to activate PGK1, to increase relative ATP levels and to reduce reactive oxygen species (ROS) levels can be improved upon with modifications to its structure (Wang, Qian, et al. 2022). The most promising of the analogs tested was formed by combining terazosin with a bioisostere of the piperonyl group found in piribedil. Piribedil is a dopamine agonist which has also shown some neuroprotective and antiperoxidative effects *in vivo* (Calzi et al. 1997). Whilst these analogs are perhaps likely to show a similar biphasic effect on PGK1 activity as terazosin given their binding sites are similar, this work is exciting as it provides some evidence that the increase in PGK1 activity seen with terazosin could be enhanced (Wang, Qian, et al. 2022).

A virtual screen using molecular docking has been performed in the search for novel PGK1 activators (Qiang et al. 2022). From an initial screen of 73355 compounds, the researchers went on to screen 11 of their top 19 hit

compounds in a *Drosophila* model of neurotoxicity of which five compounds showed a neuroprotective effect. Three of those, 7979989, Z112553128 and AK-693/21087020, increased PGK1 activity at multiple concentrations. 7979989 and Z112553128 have similar structures and were both also shown to inhibit cellular inflammation. The study did not directly compare these hit compounds with terazosin but the biphasic response seen with terazosin is not so apparent in their dose response experiments (Qiang et al. 2022; Chen et al. 2015). This provides some optimism that their mechanism of action may be slightly different to that of terazosin and that further novel PGK1 activators may be discovered.

These recent studies into terazosin analogues and novel PGK1 activators give us some evidence that it may be possible to find compounds that activate PGK1 either more specifically or more effectively than is currently possible clinically with terazosin. Finding good alternatives to terazosin is key to maximising the potential benefits of increased PGK1 activity that have been reported both in *in vitro* and *in vivo* models of ALS and is likely to be of wider importance in the field of neurodegenerative diseases.

1.8 Thesis Aims

It is hypothesised that increasing PGK1 activity is safe and has considerable therapeutic potential but that superior agonists to terazosin are needed.

This thesis aims to address some of the important outstanding questions regarding developing PGK1 activators as potential therapeutics for ALS.

- To investigate the consequences of increased PGK1 activity in cells that are not PGK1 deficient.
- To screen potential PGK1 activating compounds identified by artificial intelligence *in vitro*.
- To see if the lead compounds from the *in vitro* screen improve the phenotype in a zebrafish model of ALS.
- To explore the suitability of a novel *in vitro* model system for screening potential PGK1 activating compounds.

Chapter 2: Methods

This chapter contains details of the methods used in the subsequent results chapters. Experiment-specific details and optimisations of these methods can be found in the relevant chapters where applicable.

2.1 Cell Protocols

2.1.1 Cell Maintenance

All cell lines were maintained in a standard cell growth media which was Dulbecco's modified eagle medium (Gibco DMEM, Thermo Fisher Scientific) with 10% foetal bovine serum and 1% penicillin/streptomycin (Weiskirchen et al. 2023). The cell culture incubator that the cells were grown in was kept at 37 °C and 5% CO_2. HEK-293 cells were maintained in T75 flasks and split every 2-3 days when confluency in the flask was approaching 80%. NSC-34 cells were also maintained in T75 flasks and split every 3-5 days when flask confluency was approaching 80%. NSC-34 cells were not kept beyond passage 30 (Weiskirchen et al. 2023).

2.1.2 Transfection of HEK-293 cells

HEK-293 cells were plated at a seeding density of $1x10^6$ cells per well in six well plates 24 hours before transfection. Two 1.5 ml Eppendorf tubes were prepared for each well, one for the lipofectamine mix and one for the DNA mix and 150 μl of antibiotic free cell media was added to each Eppendorf tube. 9 μl of the transfection agent lipofectamine (Lipofectamine 2000, Thermo Fisher Scientific) was added to half of the tubes and 4.2 μg of PGK1 DNA plasmid (pscAAV-CMV-PGK, Vigene Biotech) were added to the remaining tubes (Invitrogen 2013). The lipofectamine and DNA mixes were incubated at room temperature for 5 minutes before mixing one lipofectamine tube with one DNA tube per well to be transfected. These were incubated again for 5 minutes at

room temperature. The media was then removed from the six well plate containing the cells to be transfected and they were gently washed with PBS. 2 ml of antibiotic-free media was added to each well before adding the 300 μl of lipofectamine-DNA complex mix prepared per well. The six well cell plates were incubated for 4 hours at 37 °C before the media containing the transfection agent was removed and replaced with standard cell growth media which was Dulbecco's modified eagle medium (DMEM) with 10% foetal bovine serum and 1% penicillin/streptomycin.

2.1.3 Bacterial transformation and purification of the PGK1 plasmid

Bacterial transformation was used to make up more of the PGK1 plasmid (pscAAV-CMV-PGK, Vigene Biotech) by taking advantage of the ampicillin resistance included within the plasmid. Agar plates were made up by adding 3.5g LB Agar powder to 100 ml sterile water and then autoclaving the mixture. Ampicillin was added to the mix after autoclaving at a concentration of 100 μg/ml and the solution poured into petri dishes and kept at 4 °C until use. Competent bacterial cells (New England Biolabs) were brought up from laboratory stocks stored at -80 °C incubated with the PGK1 plasmid at a 1:50 dilution on ice for 30 minutes and then heat shocked by heating the tube to 42 °C for 1 minute and then returning to the ice. 20 μl of the transformed bacteria were spread onto the Agar plates containing ampicillin and incubated in a 37 °C oven overnight. Two individual colonies were selected and transferred to different conical flasks each containing 50 ml LB broth containing ampicillin. The conical flasks were then incubated in a shaking incubator overnight at 37 °C. The following day glycerol stocks were made from the LB broth by adding 700 μl of the bacterial broth to 300 μl glycerol and stored at -80 °C.

To purify the DNA plasmid from the remaining bacterial broth the PureYield™ Plasmid Midiprep System was used. The cells were pelleted by centrifugation at 5000 g for 10 minutes and the supernatant discarded. The cells were then

resuspended in 3 ml of the kit's Cell Resuspension Solution and 3 ml of the Cell Lysis Solution was added and the solution gently mixed. 5 ml of the Neutralization Solution was then added to the lysed cells, gently mixed in and then allowed to rest at room temperature for 3 minutes. The lysate was added to a PureYield clearing column and allowed to rest again for 2 minutes to allow the cell debris to separate out. The clearing column was centrifuged at 1500 g for 5 minutes and then the flowthrough added to the PureYield Binding Column which was centrifuged at 1500 g for 3 minutes. To wash the DNA in the binding column, 5 ml of Endotoxin Removal Wash solution was added to the column and it was centrifuged at 1500 g for 3 minutes. The flowthrough was discarded and 20 ml of Column Wash Solution added to the column before centrifuging again at 1500 g for 5 minutes. The flowthrough was discarded and the column centrifuged again at 1500 g for a further 10 minutes. The DNA was then eluted by adding 600 μl nuclease free water to the binding column membrane. To achieve a plasmid concentration of 2.4 μg/μl ethanol precipitation was performed. 2.5x the volume of DNA mix of 95% ethanol was added to the DNA along with 1/10 the volume of the DNA mix of 3 M sodium acetate (pH 5.2). The tube was placed in the -80 °C freezer for 1 hour. The DNA was then pelleted out by centrifuging at 13000 rpm for 10 minutes at 4 °C and then as much ethanol removed as possible without disturbing the DNA pellet. The DNA pellet was then resuspended in nuclease-free water and concentration checked using a NanoDrop spectrophotometer (NanoDrop™ 2000, Thermo Fisher).

For the digestion of the plasmid with HindIII, 1 μl of the DNA plasmid was incubated with 1 μl of 10U/μl HindIII diluted in 20 μl nuclease free water for 3 hours at 37 °C. To allow visibility on the gel 1 μl dye was added to the mix before the sample was run on an agarose gel alongside a sample of the plasmid that had not been digested and instead incubated with the same volume of nuclease free water.

2.1.4 Immunocytochemistry

For immunocytochemistry (ICC) of the HEK-293 cells, the HEK-cells were first transfected with PGK1 or Lipofectamine only. The cells were seeded at $0.06x10^6$ cells per well in a 24 well plate containing round coverslips that had been coated with 0.01 mg/ml poly-L-lysine (PLL). The following day the HEK-cells were then transfected with the PGK1 plasmid as described earlier with the volumes adjusted to keep the concentration per well the same as in the 6 well plates. Therefore, 1.8 μl lipofectamine and 0.84 μg of the PGK1 DNA plasmid were used per well in the transfection protocol.

The ICC was started 48 hours after transfection. The coverslips were first washed for 5 minutes in PBS then fixed using 4% paraformaldehyde (PFA) for 10 minutes at room temperature before washing again twice with PBS. The cells were permeabilised with 0.1% Triton X-100 for 15 minutes at room temperature before being blocked with 2% bovine serum albumin (BSA) for 1 hour at room temperature. The polyclonal rabbit anti-PGK1 primary antibody (ab90787, Abcam) was used at a dilution of 1:50 with 50 μl of the primary antibody mix used to cover the cells of each coverslip. The cells were incubated with the primary antibody overnight at 4 °C. The following day the coverslips were washed with three 10 minute washes in PBS before the secondary antibody (donkey anti-rabbit IgG, Alexa Fluor 594, ab150076, Abcam) was added. The secondary antibody was made up at a 1:500 concentration in BSA block. Again 50 μl of the secondary antibody mix was used for each coverslip. The secondary antibody was left to incubate on the cells for 1 hour at room temperature before the coverslips were washed three times with PBS for 10 minutes. Then the cells were stained with DAPI (4',6-diamidino-2-phenylindole) by adding 300 μl of 300 nM DAPI (D1306, Life Technologies) to each coverslip and incubating for 5 minutes at room temperature. The coverslips were again washed three times with PBS for 10 minutes and then the slips were mounted onto microscope slides using 6 μl of

mowiol mounting media per slide. The slides were left to dry before imaging was performed using a Nikon Ti2 epifluorescent microscope.

2.1.5 Protein extraction

To extract the protein from cells, they were trypsinised using 0.5 ml 0.25% trypsin-EDTA (Gibco™) per well of a six well plate. The cells were suspended in 0.5 ml standard cell growth media and transferred into Eppendorf tubes. These were centrifuged for 5 minutes at 4 °C at 13,000 rpm. The media was then suctioned away leaving behind a cell pellet in each tube. The cell pellets were dissolved into radioimmunoprecipitation assay (RIPA) buffer (Thermo Scientific) containing 1X Halt™ protease inhibitor cocktail (Thermo Scientific). The samples were put on a rotating wheel at 4 °C for 30 minutes and then centrifuged for 10 minutes at 4 °C at 13,000 rpm. The supernatant containing the extracted protein from each sample tube was then transferred to fresh Eppendorf tubes to be stored at -80 °C.

2.1.6 Protein quantification

Multiple cell assays were normalised to total protein levels which were measured using a bicinchoninic acid (BCA) assay (Pierce™ Micro BCA Protein Assay Kit, Thermo Fisher Scientific). Protein samples were loaded into a 96 well plate in duplicate. Due to differences in protein concentration between experiments and cell types, 3 μl of sample was added per well for the HEK-293 experiments and 5 μl of sample was added per well for the NSC-34 experiments to ensure all samples fell within the range of the standard curve. Working reagent for the BCA assay was made up according to the manufacturer's instructions by adding 25 parts of Reagent A to 24 parts of Reagent B with 1 part of Reagent C. Bovine serum albumin (2 μg/μl BSA) standards were loaded in duplicate in wells for a standard curve for eight different final concentrations of protein (μg/ml): 0, 10, 20 ,30, 40, 50, 100 and

200. 200 μl of the working reagent mix was added to each well. The plate was then incubated at 60 °C for 10 minutes. Absorption in each well was measured at 560 nm using a plate reader. The absorption of protein sample duplicates were averaged and protein concentration calculated by comparing them to the standard curve plotted from the BSA standard results.

2.1.7 Protein detection with western blot

Western blots were performed for PGK1 in transfected HEK-293 cells and for PGK1, TDP-43 and GFP in NSC-34 cell lines. The same method was followed for all the western blot experiments and was based on the standard protocols used by the Gillingwater group (Huang et al. 2019). Cell pellets were collected and protein extracted and quantified with a BCA assay as per the protein extraction and quantification methods. 50 μl of 2 μg/μl of each protein sample acquired from the HEK-293 cells was then made up with 1X NuPAGE LDS sample buffer (Thermo Fisher) and deionised water. The protein concentrations in some of the NSC-34 cell samples was lower and so to ensure all the samples had the same protein concentration, the NSC-34 protein samples were made to a concentration of 1.4 μg/μl instead in the same way. These samples that were prepared for use in the western blot were incubated in a heat block at 70 °C for 10 minutes and then kept on ice.

After the protein samples had been prepared, 10 μl of each sample was loaded into the wells of a NuPage 4-12% Bis-Tris 1.0mm Gel (Invitrogen) along with 3 μl of a protein ladder (Chameleon Duo Pre-Stained Protein Ladder, Licor / Novex Sharp Pre-Stained Protein Standard, Life Technologies). The proteins were separated out in the gel by electrophoresis performed in NuPAGE MES SDS running buffer (Invitrogen). The voltage was initially set to 80 V for 15 minutes to allow the proteins to settle in the stacking gel and then the voltage was increased to 150 V and run for a further 50 minutes. Gel transfer was performed using iBlot 2 PVDF Mini Stacks (Thermo Fisher) in an iBlot 2 Gel

Transfer System (Thermo Fisher). The membrane containing the protein was rehydrated with methanol and then washed with PBS for 5 minutes and then washed with deionised water. 10 ml of Revert 520 Total Protein Stain (Li-COR) was added to the membrane and it was incubated at room temperature on a shaker for 5 minutes before being washed with Revert 520 Wash Solution (Li-COR). Following a quick wash with deionised water, the total protein was imaged at 520 nm using a Li-COR Odyssey imager. The membrane was then destained using Revert 520 Destaining Solution (Li-COR) for 2 minutes and then the membrane was washed with deionised water. The membrane was blocked for 30 minutes using 3 ml of Intercept (PBS) Blocking Buffer (Li-COR).

The primary antibody (see Table 2.1) was made up in 3 ml of fresh blocking buffer and the membrane was placed in a 50 ml Falcon tube on a roller at 4 °C overnight. The following day, the membrane was washed six times in PBS for 5 minutes. The secondary antibody (see Table 2.1) would be made up by adding 1 μl to 3 ml of fresh blocking buffer (dilution 1:3000). The membrane would be incubated with the secondary antibody on a roller at room temperature for 1 hour. The membrane was then washed with PBS three times for 30 minutes. The membrane was then dried before being imaged again on the Li-COR Odyssey machine. The western blot images were analysed using Image Studio software (Version 5.2.2, Li-COR). To obtain the relative protein levels, the signal intensities of the visible bands of the protein of interest of each lane were divided by the signal intensity of the total protein stain for that lane.

Target	Primary Antibody	Primary Antibody Dilution	Secondary Antibody
PGK1	Rabbit polyclonal (ab90787, abcam)	1:1000	Goat anti-rabbit 680 (926-68076, Li-COR) / Donkey anti-rabbit 800 (926-32213, Li-COR)
TDP-43	Rabbit polyclonal (10782-2-AP, Proteintech)	1:1000	Donkey anti-rabbit 800 (926-32213, Li-COR)
GFP	Chicken polyclonal (ab13970, abcam)	1:1000	Donkey anti-chicken 800 (925-32218, Li-COR)

Table 2.1 Table showing the antibodies used in western blot experiments. Primary antibodies and secondary antibodies used for the different targets of the western blot experiments with their catalogue numbers and manufacturer listed.

2.1.8 PGK1 metabolic assay

The PGK1 metabolic assay was performed in both HEK-293 and NSC-34 cells. The protocol was based on similar published metabolic assays (Chung et al. 2010). The part of the glycolysis pathway that PGK1 helps facilitate is a reversible step occurring in both gluconeogenesis and glycolysis. The gluconeogenesis direction is measured by this assay as the conversion of NADH to NAD+ is relatively straightforward to measure due to differences in their absorbance at the 340nm wavelength. HEK-293 cells were seeded in 24 well plates at $6x10^4$ cells per well 48 hours before the assay. NSC-34 cells were seeded at $7.5x10^4$ cells per well 48 hours before the assay for the undifferentiated experiments and $1.5x10^4$ cells per well five days before the assay for the differentiated experiments. Compounds to be tested were added to the cells 24 hours before the assay.

For the assay itself, the cells of each well would be trypsinised by removing the cell media and adding 0.5 ml of 0.25% trypsin-EDTA (GibcoTM) per well and incubating at 37 °C for 1 minute. Then 0.75 ml of standard cell growth media would be added to each well to resuspend them. The cells would be transferred to 1.5 ml Eppendorf tubes (one tube per well) and the tubes were centrifuged for 5 minutes at 1000 rpm at room temperature. The cell media

was then removed from each tube leaving behind the cell pellet which was then dissolved in 50 μl extraction buffer (Table 2.2) with 0.5 μl Halt^{TM} protease inhibitor cocktail (Thermo Scientific), vortexed and then kept on ice for 10 minutes. Then the tubes were centrifuged for 5 minutes at 10,000 rpm at 4 °C. For each assay a standard curve of NADH was performed in duplicate in a 96 well plate using 0, 10, 20, 30, 40, 50 μl of 1 mM NADH. The reaction buffer would be prepared in advance in bulk and separated into 20 ml volumes to be stored at -20 °C. The pH of the reaction buffer was checked and adjusted to ~7.6 as necessary. Two versions of the reaction buffer (Table 2.3) would be made each time – one for the main assay and one without the NADH to use for the standard curve. After centrifuging the samples would be kept on ice whilst the assay plates were loaded. 10 μl of cell extract from each Eppendorf (which corresponds to each well of the cell plates) would be added to two wells of the 96 well assay plate so each sample was run through the assay in technical duplicates which were averaged during analysis (Figure 2.1). Once the samples were loaded, 200 μl of the reaction buffer was added to the sample wells and 150 μl of the reaction buffer without NADH was added to the standard curve wells.

When all the samples and reaction buffers had been added to the assay plate it was loaded into a plate reader. 50 μl of 10 U/ml GAPDH was added to each well just before the assay was started as this starts the reaction. The protocol measured absorbance at 340 nm every 1-2.5 minutes for 1 hour. Throughout the assay the plate reader was programmed to shake between readings and maintain a temperature of 37 °C. The HEK-293 experiments were completed with a Biotek Powerwave XS plate reader (Agilent) and the NSC-34 experiments were completed with a Multiskan FC plate reader (Thermo Fisher). The change in absorbance at 340 nm was calculated for each well and the mean calculated for technical replicates. The decrease in measured absorbance at this wavelength reflects the conversion of NADH to NAD+ (McComb et al. 1976).

Extraction Buffer Components	Desired Final Concentration	Quantity needed for 50 ml
Sodium Chloride	150 mM	438 mg
EDTA	5 mM	73 mg
Trizma base	60 mM	363 mg
Triton X	0.2 %	0.1 ml

Table 2.2: Extraction buffer components for the PGK1 Assay. Table showing the volumes of the reagents used to make up the extraction buffer and the desired final concentration of each used.
EDTA = ethylenediaminetetraacetic acid

Reaction Buffer Component	Stock Concentration	Volume to make 20 ml Reaction Buffer (ml)
EDTA	1 mM	2.5
Magnesium Chloride	20 mM	2.5
Imidazole	1M	1.25
3-PG	25 mM	5
ATP	10 mM	2.5
H_2O		1.25
NADH	1 mM	5

Table 2.3: Reaction buffer components for the PGK1 Assay. Table showing the volumes and concentrations of the reagents used to make up the PGK1 metabolic assay reaction buffer.
EDTA = ethylenediaminetetraacetic acid, 3-PG = 3-Phosphoglyceric acid, ATP = adenosine triphosphate, NADH = nicotinamide adenine dinucleotide

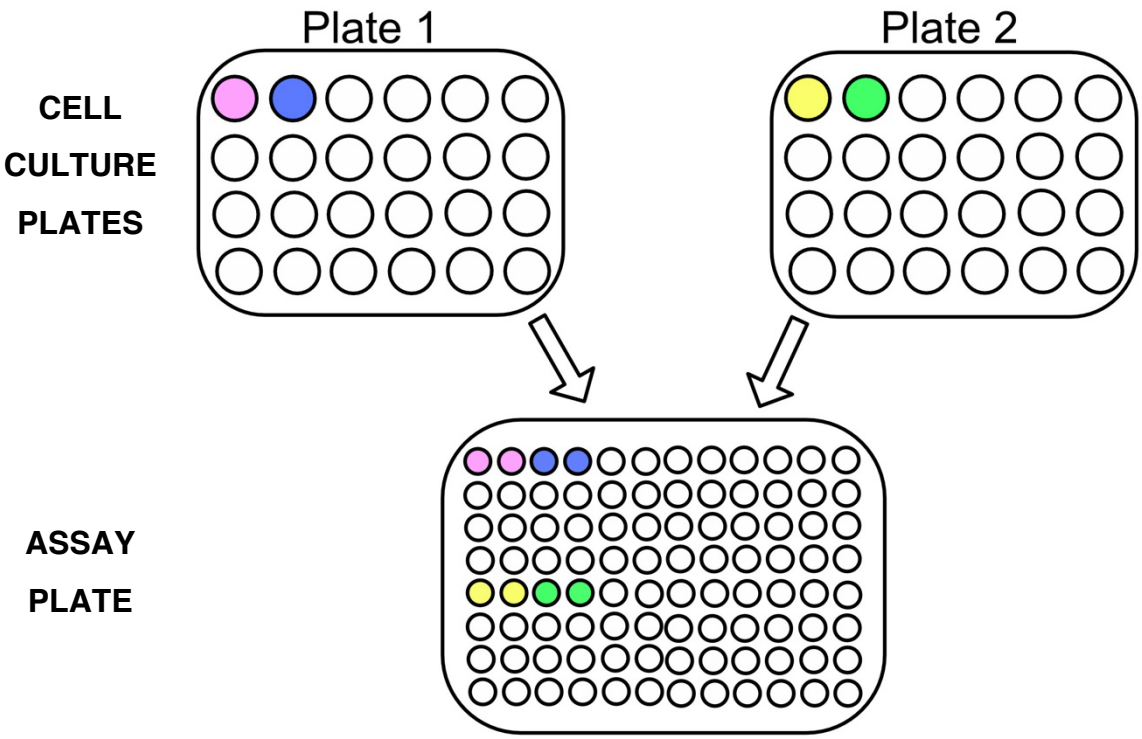

Figure 2.1: Plate layout diagram example for PGK1 assays. Wells A1 and B1 of two 24 well plates have been given colours so that the corresponding technical replicates for each can be seen in the assay plate below. Cells were grown in the 24 well cell culture plates and one compound (or DMSO control) added to each well. For the PGK1 assay, the treated wells from up to two 24 well cell culture plates would be tested in duplicate on the same 96 well assay plate.

2.1.9 Preparation for the Seahorse assays

The Cell Mito Stress Test and Glycolytic Stress Test are assays performed using the Agilent Seahorse XF analyser. Preparation for both assays is the same. The assays were performed with both HEK-293 cells and NSC-34 cells and seeding density and FCCP concentration was optimised for each. HEK-293 cells required the seahorse cell plates to be coated with PLL. This was done by adding 50 μl of 0.01 mg/ml PLL to each well of the seahorse cell plate and leaving the plate to incubate at room temperature for 1 hour. The wells were then washed three times with 100 μl PBS, wrapped with parafilm and stored at 4 °C. HEK-293 cells were plated at $4x10^4$ cells/100 μl/well the day before the assay in standard growth media leaving 4 blank cells. NSC-34 cells were plated at $7x10^4$ cells per well for undifferentiated experiments and $1x10^4$ cells per well for differentiated experiments. Differentiated cell experiments were plated five days in advance of the assay rather than 24 hours before. The cells were left at room temperature for 30 minutes and then incubated at 37 °C for 1 hour a further 150 μl of media per well was added. The plate was incubated at 37 °C before the assay was performed the following day. The Seahorse cartridge plate was also prepared the afternoon before the planned assay. 1 ml of seahorse calibrant solution (Agilent) was added to each well of the cartridge plate and the cartridge plate was incubated in a non-CO_2 incubator at 37 °C overnight.

2.1.10 Cell Mito Stress Test Seahorse assay

The Cell Mito Stress Test assays were performed according to the Agilent user guide (Technologies 2024). The cells were plated and the assay cartridge plate were prepared in advance of the assay as described above. Seahorse XF DMEM media (Agilent) was used as the base media for the assay. To make up the media to be ready for the assay, 0.5 ml 200 mM L-glutamine (final concentration: 2mM), 0.5 ml 1 M glucose (final concentration: 10mM) and 0.5 ml 200 mM sodium pyruvate (final concentration: 2mM) were added to the

Seahorse XF DMEM media to make a total volume of 50 ml. The media was pH checked and adjusted to a pH of 7.35-7.40. The media in the cell plate was then removed from all wells and replaced with 1 ml per well of the prepared Seahorse media. The cell plate was then incubated in the non-CO_2 incubator at 37 °C for 1 hour. The injections of compounds needed for the Cell Mito Stress assay were then prepared so that the final concentrations of compounds in the wells would be: 2 μM oligomycin, 1.5 μM (0.5 μM in NSC-34 cell experiments) carbonyl cyanide 4-(trifluoromethoxy)phenylhydrazone (FCCP) and 0.5 μM rotenone/antimycin A. The cartridge plate was loaded with these compounds for the injections and put in the Seahorse analyser for calibration. Once the 1 hour incubation of the cell plate was complete, the media from all the wells was removed and replaced with 450 μl of the prepared Seahorse media in each well. Following calibration, the cell plate was inserted into the analyser and the assay protocol run as per the manufacturer's instructions. The oxygen consumption rate (OCR) trace was checked for each well upon completion the assay and wells that did not respond to the compound injections or were outliers in their condition group were excluded. The OCR traces were normalised where applicable and the metabolic parameters calculated according to the analysis instructions provided by Agilent.

2.1.11 Glycolytic Stress Test Seahorse assay

The Glycolytic Stress Test Seahorse assay protocol published by Agilent was followed for these experiments (Technologies 2019). The protocol is similar to the Cell Mito Stress Test but with a few key differences. The cells and cartridge plate are prepared ahead of the assay as described previously. To make the basal media for the assay, 0.5 ml 200 mM L-glutamine was added to 49.5 ml Seahorse XF DMEM media warmed to 37 °C. The media was pH checked and adjusted to a pH of 7.35-7.40. The media was removed from the wells of the cell plate and replaced with 1 ml of the prepared basal media in each well. This

cell plate was then incubated for 1 hour in the non-CO_2 incubator at 37 °C. The compounds to be injected were prepared and added to the appropriate injection ports of the cartridge plate so that the final concentration in each well would be: 10 mM glucose, 1 μM oligomycin and 50 mM 2-deoxy-D-glucose (2-DG). The cartridge plate was then loaded into the Seahorse analyser for calibration. Following the 1 hour incubation of the cell plate, the media in the wells was removed and replaced with 450 μl of the prepared basal media before loading the cell plate into the analyser for the assay to proceed according to the settings for the protocol advised by Agilent. The extracellular acidification rate (ECAR) trace was checked for each well upon completion the assay and wells that did not respond to the compound injections or were outliers in their condition group were excluded. The ECAR traces were normalised where applicable and the metabolic parameters calculated according to the analysis instructions provided by Agilent.

2.1.12 Seahorse assay normalisation methods

To assess different normalisation strategies for the Seahorse assay, I trialled multiple methods. For normalisation to approximates of cell number both normalisation to proportion of area stained by DAPI and normalisation by particle count of DAPI stained nuclei using ImageJ (Version 2.14.0/1.54f) were trialled (Little et al. 2020). Following the Seahorse assay, the cells were stained with 300 nM DAPI (D1306, Life Technologies) by removing the media and adding 50 μl DAPI to each well and incubating for 5 minutes before removing and washing with PBS. The wells were imaged using a Nikon Ti2 epifluorescent microscope to capture a complete image of the bottom of each well with the 405 nm laser at 10X magnification. These images were analysed in ImageJ. In each image, the well was isolated and image thresholding was used to create a binary image. The proportion of thresholded pixels was calculated relative to the total number of pixels to calculate the % area of positive DAPI staining per well. For the particle count, the watershed tool in

ImageJ was used on the binarised images which separates objects in an image, in this case DAPI-stained nuclei. Then the analyse particles tool was run to count the separated particles.

2.1.13 RNA extraction and quality assessment

RNA extraction was performed using the protocol provided by the manufacturer for the purification of total RNA from animal cells using spin technology (Qiagen RNeasy Mini Kit). Cells were trypsinised from the wells of a six well plate using 0.5 ml trypsin per well. Standard growth media was added (0.5 ml per well) and the cells transferred to Eppendorf tubes. These were centrifuged at 300 g for 5 minutes and the supernatant removed leaving behind a cell pellet. The cell pellets were vortexed with 350 μl of the provided lysis buffer (Buffer RLT Plus). The lysate of each tube was transferred to a gDNA eliminator spin column, centrifuged for 30 seconds at 8000 g and the flowthrough collected. 350 μl of 70% ethanol was added to each of the flowthroughs and mixed by pipetting. The samples were then transferred to an RNeasy spin column and centrifuged for 15 seconds at 8000 g. This time the flowthrough was discarded. Then 700 μl of buffer RW1 to wash membrane-bound RNA was added to each of the RNeasy spin columns and they were centrifuged again for 15 seconds at 8000 g and the flowthrough discarded. Then 500 μl of another wash buffer – buffer RPE- was added to the spin columns and they were centrifuged again for 15 seconds at 8000 g and the flowthrough discarded. The wash with buffer RPE was repeated but instead centrifuged for 2 minutes at 8000 g. The RNeasy spin column was transferred to a fresh collection tube and centrifuged at 13000 g for 1 minute. The collection tube was replaced with a new 1.5 ml collection tube and 30 μl of RNase-free water was added directly to each spin column membrane. These were then centrifuged again for 1 minute at 8000 g to elute the RNA.

RNA concentration and quality was assessed initially using a NanoDrop spectrophotometer (NanoDrop™ 2000, Thermo Fisher). The measurement pedestal of NanoDrop was cleaned and then blanked using 1 μl RNase free water and then 1 μl of each sample was measured, ensuring to clean the pedestal between each sample. 1 μl of each RNA sample was transferred to a separate tube to the main sample to use in the Bioanalyser to avoid repeat freeze-thaw cycles.

The Agilent 2100 Bioanalyzer was used to further analyse the quality of the extracted RNA. The RNA dye concentrate was vortexed and then 1 μl was added to 65 μl of the filtered gel which was then centrifuged at 13000 g for 10 minutes at room temperature. The samples to be analysed were diluted 1:500 in nuclease free water and heated on a heat block at 70 °C for 2 minutes. The electrodes of the bioanalyzer were cleaned using one wash with 200 μl RNaseZap™ (Thermo Fisher) followed by two washes with 200 μl nuclease free water. A chip was put into the chip priming station and 9 μl of the gel-dye mix loaded into the chip in the wells marked 'G'. 9 μl of the RNA conditioning solution, 5 μl of the RNA marker and 1 μl of the ladder were added to the appropriate wells. 1 μl of each sample were added to the sample wells before the chip was vortexed for 1 minute at 2400 rpm and run through the Bioanalyser machine.

2.1.14 RNA Sequencing

RNA-sequencing was performed by Edinburgh Genomics and the analysis performed by Dr. Frances Turner. Six paired samples of RNA from transfected and non-transfected HEK-293 were submitted for analysis. Illumina sequencing was performed using a NovaSeq SP(100 cycles). Reads were trimmed using Cutadapt (version cutadapt-1.18-venv) and mapped to the reference genome Homo Sapiens version GRCh38. Each paired sample had

been collected from cells grown on the same plate and so plate was included as confounding variable in the analysis.

2.1.15 NSC-34 cell differentiation and application of cell stressor

For experiments requiring NSC-34 cell differentiation, the cells were seeded into cell plates in standard cell growth media (DMEM supplemented with 10% foetal bovine serum and 1% penicillin/streptomycin). After 24 hours, the media would be fully replaced with the differentiation media.

Differentiation media was DMEM/F12 with 0.5% foetal bovine serum, 1% MEM non-essential amino acids solution (11140-050, Gibco) and 1 μM all-*trans* retinoic acid (11017, Cambridge Bioscience Ltd). The makeup of this differentiation media was based on previous studies where NSC-34 cells were differentiated (Ding et al. 2021; Maier et al. 2013). The cells were differentiated for five complete days before experimentation with the differentiation media being replaced with fresh differentiation media every 48 hours.

For the cell stress experiments, 0.5 M of D-sorbitol (S3889, Sigma-Aldrich) were made up with differentiation media and the media on the cells was replaced with the media containing the stressor and incubated in the 37 °C, 5% CO_2 cell incubator for 30 minutes. The D-sorbitol containing media was then removed and replaced with fresh differentiation media for the recovery period of either 1 hour or 24 hours.

2.1.16 MTT assay

The MTT assay was performed using a MTT Cell Proliferation Assay Kit (Cayman chemical) according to the manufacturer's instructions. In preparation for the assays, the assay buffer tablet was dissolved in 100 ml distilled sterile water. The MTT (3-(4,5-dimethylthiazol-2-yl)-2,5-diphenyltetrazolium bromide) reagent vial (25 mg) was dissolved in 5 ml of the assay buffer. NSC-34 cells were seeded at $10x10^3$ cells per well in 96 well

plates five days prior to the assays to allow for differentiation. Two identical 96 well plates were prepared per run of the experiment to allow for two timepoints to be assessed. The cell stressor D-sorbitol was made up to concentrations of 0 M, 0.1 M, 0.2 M, 0.5 M, 0.75 M and 1 M in differentiation media. The media on the differentiated NSC-34 cells was removed and replaced with media containing the D-sorbitol so that there were three technical replicate wells per condition on each plate. The 96 well plates were then incubated with the D-sorbitol stressor for 30 minutes before the media was replaced with differentiation media.

The MTT assay was then performed on one cell plate 1 hour following the removal of the stressor and on the other plate 24 hours following the removal of the stressor. For the assay itself, 10 μl of the MTT reagent was added to each well and the plate mixed on an orbital shaker for 1 minute. The cell plate was then incubated for 3 hours at 37 °C in the 5% CO_2 cell incubator. The dark formazan crystals that had then formed in the bottom of the wells were dissolved by adding 100 μl of crystal dissolving solution from the kit (sodium dodecyl sulphate in hydrochloride) to each well. The plate was incubated for 4 hours at 37 °C in the 5% CO_2 cell incubator to dissolve the formazan crystals. The absorbance at 560 nm was then measured in each well using a plate reader (Multiskan FC plate reader, Thermo Fisher). The results for the technical replicates of each run were averaged and compared with the results from the wells of each line that were not exposed to the stressor.

2.2 Zebrafish Protocols

2.2.1 Ethics

All zebrafish used in these experiments were bred and handled in accordance with University of Edinburgh guidelines and UK Animals (Scientific Procedures) Act (ASPA), 1986. Breeding and maintenance of adult zebrafish was performed under project licence PP1017117. Experimental zebrafish embryos were not allowed to develop to 5 days post fertilisation where they would have become “protected animals” under ASPA. Adult fish were kept in a 14:10 hour light dark cycle at 26.5 °C.

2.2.2 Microinjection of C9orf72 morpholino

Zebrafish breeding pairs were set up the night before planned microinjection sessions. The fish were set up in pair tanks with a separation in place between the male and female that is removed in the morning once the microinjector station is set up. The fish begin producing eggs approximately 30 minutes after removal of the barriers. The C9orf72 morpholino was kept at a stock solution of 1 mM, this was diluted to the working concentration of 0.2 mM the morning the microinjections are taking place (Chaytow et al. 2022). To make up the working solution, an aliquot of the stock solution was incubated at 65 °C for 10 minutes. To make up 5 μl of working solution, 1 μl of stock solution would be added to 3 μl nuclease free water and 1 μl fast green dye. A pneumatic microinjection station (Narishige IM300) connected to nitrogen gas would be set to a pressure ~30 psi and an injection time of 30 milliseconds. A closed tip hollow needle pulled from thin-walled glass capillary tubes was loaded with the working solution of C9orf72 morpholino and then secured into the microinjector. A brightfield microscope was used to focus on the needle to carefully break the tip of the needle so that the loaded working solution can be ejected from it. The size of the bolus delivered by the injector was checked using a stage micrometer with a drop of mineral oil put on the top of the scale.

A bolus diameter of 0.1 mm was needed to induce the correct phenotype in the zebrafish embryos, so the needle tip or injection pressure were adjusted to get this bolus size. Due to the delicate nature of the fine needles and so that fresh working stock of the morpholino could be used each time, a new needle was set up for each injection session.

Throughout the injection of a clutch the bolus would be checked after each ~100 eggs to confirm the bolus size was still correct. The dye in the morpholino mix allowed for visual confirmation that each injection was in the correct part of the yolk sac. Eggs were collected from the breeding pairs and ~200 eggs per clutch were injected into their yolks at the 1-2 cell stage of development with one bolus of the C9orf72 morpholino solution. The rest of the eggs from each clutch were kept to check that the clutch developed normally in terms of overall mortality and to use as uninjected controls in the experiments. Following injection, the eggs were transferred into fresh E3 medium and incubated at 28.5 °C.

2.2.3 Treatment and collection of zebrafish embryos

At 6 hours post fertilisation (hpf), the zebrafish embryos were checked for normal development under a microscope. Compounds were added to fresh E3 media at a concentration of 10 μM with 6 embryos added to each well of a 24 well plate to a total volume of 1 ml per well. The 24 well plates containing the treated embryos were returned to incubate at 28.5 °C overnight. The embryos were collected at 30 hpf and dechorionated. The embryos were then fixed in 4% paraformaldehyde (PFA) for 3 hours at room temperature. Then the embryos were washed three times with PBS and stored in 70 % glycerol at 4 °C overnight. Then the embryos were deyolked and whole-mounted on slides for imaging. Z-stack images were collected at 20X magnification of each embryo using the Zeiss AxioImager M2 microscope with Apotome aiming to capture the 6 pairs of motor neurons from the first pair after the yolk sac.

2.2.4 Motor axon analysis of zebrafish embryos

Motor axon analysis was performed on the Z stack projections of the zebrafish embryos in ImageJ (Version 2.14.0/1.54f). The Blind Analysis Tool was used to blind the user to the treatment conditions of the embryos. Z-stacks were converted to maximum intensity projection images. Motor axon length was measured using the Simple Neurite Tracer plug-in for Image J. Twelve motor axons were measured per fish (6 pairs) and the mean motor axon length per embryo calculated. Each axon was given an axon phenotype score using a scale from 0 (severely affected) to 3 (healthy) and the mean axon phenotype score calculated for each embryo.

2.3 Statistics

Statistical analyses were primarily performed in GraphPad Prism (Version 10.4.2) and Microsoft Excel (Version 16.99.2). Data is displayed as mean +/- standard deviation unless otherwise stated. The statistical tests used for each analysis are listed in the figure legends. Normality was tested using the Shapiro-Wilk test due to low sample sizes. A p-value of < 0.05 was considered significant.

2.3.1 Mixed Effects Models

Mixed effects models were used for some of the zebrafish experiment to be able to analyse data from different clutches and take clutch into account as a random effect. These analyses were performed in RStudio (version 2025.05.1+513). Data was plotted in a histogram to confirm it met the assumptions for normality, then the mixed effect analysis was performed using the lmer package. A follow up ANOVA and pairwise comparison with Tukey was performed to calculate the p-values between the groups.

Chapter 3: Effects of increased PGK1 activity in HEK-293 cells

3.1 Introduction

PGK1 is a highly conserved enzyme known primarily for its key role in the first ATP producing step in the glycolysis pathway (Watson and Littlechild 1990). There has been recent interest in developing therapeutics to increase PGK1 activity to try to improve cellular energy production in multiple neurological conditions where metabolic dysfunction is a feature including Parkinson's disease and motor neuron disease. PGK1 overexpression has been shown to be beneficial in multiple models of PD and MND including in cells, *Drosophila* and zebrafish models (Cai et al. 2019; Chaytow et al. 2022). Increased PGK1 has also been shown to improve synaptic resilience and ATP production in primary neurons in low glucose conditions suggesting that, at least under certain conditions, it is rate limiting (Kokotos et al. 2024). However, there remains questions over the suitability of PGK1 as a therapeutic target, especially as there are other reported roles of PGK1 that are less well understood but which may have important consequences for therapeutic development. This chapter explores the effects of PGK1 overexpression in HEK-293 cells.

3.1.1 Transfecting HEK-293 cells

HEK-293 cells were first described in 1977, where the line was established by transforming human embryonic kidney cells with sheared fragments of adenovirus type 5 DNA (Graham et al. 1977). They are a human cell line and are fast growing, easy to maintain and have excellent transfectability which makes them an ideal cell line for these PGK1 overexpression experiments (Thomas and Smart 2005). HEK-293 cells can be transfected with the PGK1 DNA plasmid using the transfection agent lipofectamine 2000 which is known

to have a high transfection efficiency, potentially due to its ability to avoid intracellular transport mechanisms and subsequent metabolic degradation (Cardarelli et al. 2016). Lipofectamine 2000 is a cationic lipid formulation that complexes with the negatively charged nucleic acid molecules allowing them to cross the cell membrane which also has a net negative charge (Dalby et al. 2004).

3.1.2 Assessing PGK1 overexpression

Western blotting for PGK1 protein is necessary to determine whether the overexpression of PGK1 has been successful following transfection. However, increased detection of the PGK1 protein using the western blot method would not necessarily mean the enzyme produced would be functional. To show that the overexpressed PGK1 is functional two different methods have been implemented. A PGK1 metabolic assay had been developed by my supervisor Prof Kiterie Faller just prior to my starting of the project based on similar assays in the literature (Chung et al. 2010). I tested this assay for its ability to detect increased PGK1 activity in cell extracts from cells overexpressing PGK1 where we would expect there to be increased activity. Even though PGK1 is known to be a key glycolytic enzyme, it was not clear if cellular respiratory function would be affected by increased PGK1 activity as PGK1 is not traditionally considered a rate-limiting step in glycolysis (Boscá L.; Carlos Corredor 1984). To assess whether cellular respiration is affected by increased PGK1 expression in HEK-293 cells I used two different Seahorse protocols, the Cell Mito Stress Test and the Glycolytic Stress Test.

Agilent Seahorse XF analysers are used for assays that assess metabolic function in live cells and how cellular respiration is affected by different mitochondrial and glycolytic modulators. The Cell Mito Stress Test focuses on mitochondrial function and consists of injections of three different modulators. The first injection is of oligomycin which inhibits complex V of the electron

transport chain, reducing electron flow. This reduction in electron flow reduces mitochondrial respiration which is visualised in the assay by the reduction in oxygen consumption rate (OCR). The reduced OCR is associated with the amount of cellular ATP production. The second injection is of carbonyl cyanide-4 (trifluoromethoxy) phenylhydrazone (FCCP) which is a potent uncoupling agent that uninhibits electron flow and results in the maximal rate of respiration. The final injection is a combination of rotenone and antimycin A which are complex I and III inhibitors respectively. This combination stops mitochondrial respiration so that non-mitochondrial respiration can be calculated (Technologies 2024). The Glycolytic Stress Test also consists of three injections and uses changes in the extracellular acidification rate (ECAR) to assess different glycolytic parameters. At the start of this assay the cells are in media without glucose, so glycolysis only starts following the first injection of glucose. Oligomycin is the second injection which inhibits mitochondrial respiration, forcing the cells to rely more on glycolysis for energy production and so allowing us to measure glycolytic capacity. The glycolytic reserve is the difference between the cell's normal glycolytic rate and its maximum which indicates how well they can respond to an increased energy demand (Technologies 2019).

3.1.3 RNA-sequencing

Whilst the role of PGK1 in glycolysis is relatively well understood, there are reports of it having other biological roles including acting as a protein kinase and a modulator of inflammation (Li et al. 2023; Park, Choi, and Baek 2023). These roles are not fully understood and so increasing PGK1 activity may have consequences that cannot be predicted from its role in glycolysis alone. To understand which other cellular pathways may be dysregulated by PGK1 activation, I worked with Edinburgh Genomics to perform RNA-sequencing to investigate the effects of PGK1 overexpression on gene expression in HEK-293 cells. This gives us the opportunity to potentially explore these other

reported roles and interactions of PGK1 as well as identify potential problems that may result from PGK1 focussed therapies.

3.2 Aims

This chapter investigates the effects of overexpressing PGK1 in an immortalised human cell line. The primary aim was to determine whether PGK1 is an appropriate target for therapeutic development or whether increased PGK1 activity is likely to have undesirable consequences.
Secondary aims were:

1. To assess the suitability of using HEK-293 cells to screen potential PGK1 activating compounds.
2. To confirm that the metabolic assay for PGK1 activity can detect a change in PGK1 activity.

3.3 Results

3.3.1 Overexpression of functional PGK1

Before investigating the effects of overexpressing PGK1, it was important to first demonstrate that transfecting HEK-293 cells with PGK1 resulted in increased protein expression. PGK1 expression in transfected cells was explored with western blot and immunocytochemistry to visualise the protein itself and then a metabolic assay confirmed that the increased PGK1 was functional.

Preparations for PGK1 transfection experiments

A trial transfection with green fluorescent protein (GFP) confirmed that the transfection protocol worked and that the transfection agent lipofectamine produced a good level of transfection in HEK-293 cells as shown by the green fluorescence (Figure 3.1.A). Lipofectamine can be cytotoxic and so using the lowest effective concentration is desirable. I found that adding 9 μl of 1 mg/ml lipofectamine to the 2 ml of cell media used per well was the lowest dose that provided good transfection efficiency and increasing the amount to 12 μl or 15 μl lipofectamine per well did not noticeably improve transfection efficiency. Therefore, subsequent transfection experiments used 9 μl lipofectamine per well of a 6-well plate.

To complete the planned experiments more of the PGK DNA plasmid originally obtained from Vigene Biotech (pscAAV-CMV-PGK) would be needed. This was achieved by bacterial transformation and subsequent DNA purification and concentration with ethanol precipitation. This produced DNA with a concentration of ~2.4 μg/μl. The plasmid map from the original manufacturer showed expected restriction enzyme digestion sites (Figure 3.1.B) so as a confirmatory test to check the DNA that had been purified was what was expected, I digested a sample of the produced plasmid with the restriction

enzyme HindIII. Following HindIII digestion 2 bands were observed around 6000bp and 600bp which is consistent with the expected product sizes of 5699bp and 594bp predicted from the location of the two HindIII restriction sites on the plasmid map (Figure 3.1.C).

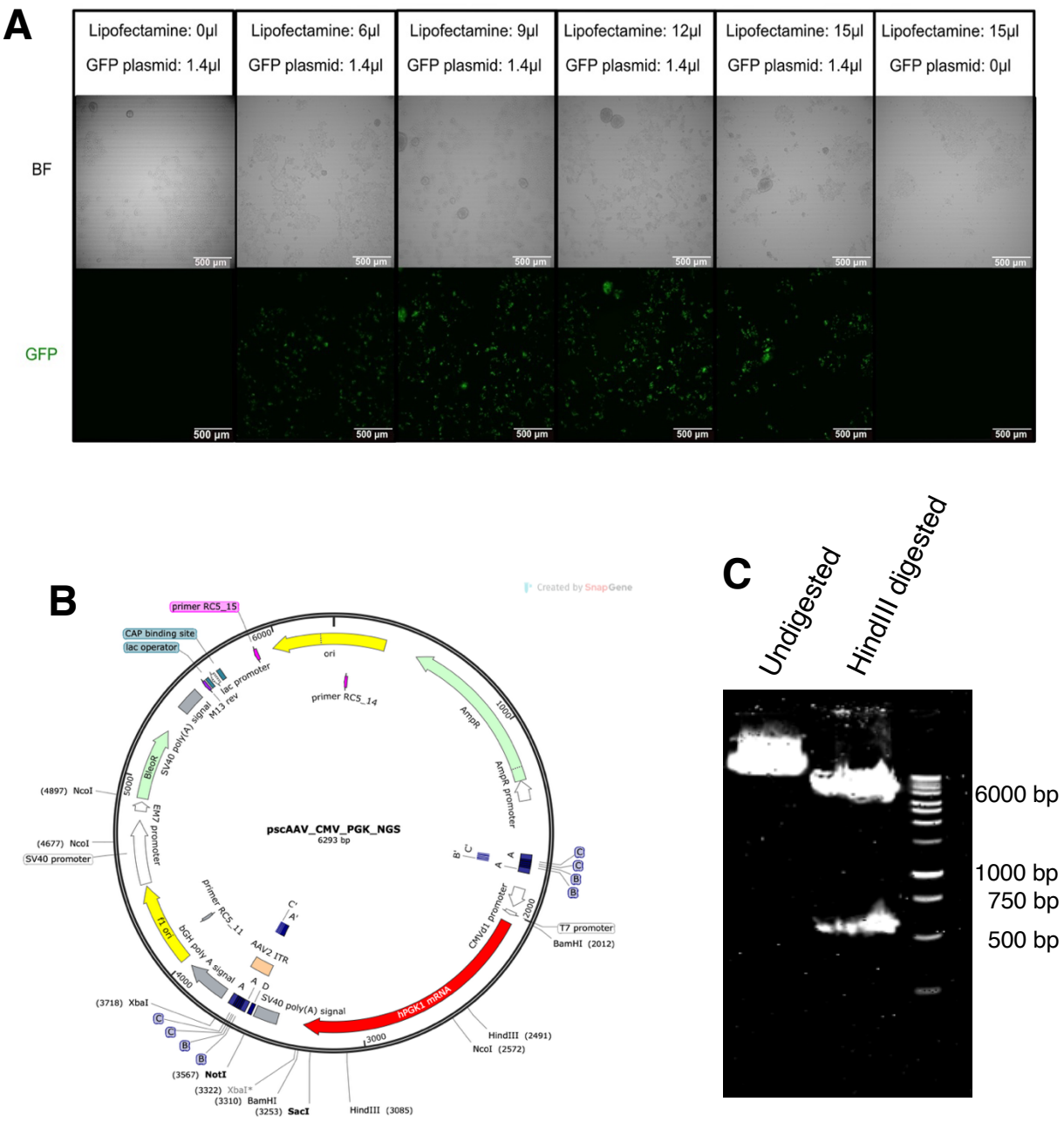

Figure 3.1: **Transfection protocol trial and HindIII digestion of PGK plasmid following bacterial transformation. (A)** Representative images from a trial transfection of HEK-293 cells with GFP (1.4μl = 3.36 μg of DNA plasmid) at different concentrations of lipofectamine transfection agent (Scale bars = 500 μm). A plasmid map of the PGK plasmid visualised using Snapgene **(B)** shows key expected enzyme sites. Two bands were visualised at around 6000 bp and 600 bp following HindIII digestion of additional plasmid produced by bacterial transformation **(C).**

Western blot

Transfections were performed in triplicate with 3 wells used per 6-well plate per condition: 3 wells were treated with lipofectamine only and 3 wells were transfected with the PGK1 plasmid. Cells were collected 48 hours following transfection. Cells were pooled from the wells of the same condition from the same plate and subsequently treated as one sample to ensure there was enough protein for repeat experiments if required. Therefore, each plate produced a pair of samples, control and PGK1 transfected. The experiment was repeated on 3 different days and the paired samples from these three separate plates were collected, protein extracted, and western blot performed for PGK1 (n=3). It showed that the transfection protocol resulted in a significant overexpression of PGK1 protein in the PGK transfected HEK-293 cells compared with control cells which were only treated with lipofectamine (Figure 3.2.A). Following normalisation of the signal to the total protein stain, analysis with a paired t-test showed a significant increase in PGK1 expression in the transfected cells of ~3-fold compared with controls ($p = 0.03$, Figure 3.2.B).

Immunocytochemistry

HEK-293 cells were grown and transfected on coverslips to allow immunocytochemistry (ICC) to be performed 48 hours post transfection. The cells were either transfected with PGK1 or treated with lipofectamine only as in the other transfection experiments. The ICC for control and transfected cells was performed and imaged at the same time using the same microscope settings. Figure 3.2.C shows representative images from the ICC showing DAPI and PGK1 channels separately and then merged. A substantial number of the PGK1 transfected cells expressed large amounts of PGK1 in the cytoplasm compared to the controls.

PGK1 metabolic assay

The PGK1 metabolic assay as described in the Methods section was performed on cell lysates from PGK1 transfected HEK-293 cells and lipofectamine only treated HEK-293 cell controls. The transfection was performed in 6-well plates with 3 wells of each condition included on each plate. Following the 4-hour incubation period with the transfection agent, the cells were trypsinised, counted and replated into a 24 well plate for the 48 hours prior to the PGK1 assay. This strategy was chosen to keep the methods for both PGK1 transfection and PGK1 metabolic assay as close as possible to the protocols used for other experiments. Each of the wells from the 6 well transfection plates were kept separate and plated into the 24 well assay plate as technical replicates. The experiment was repeated on three separate days (n=3) with 3 technical replicates per condition per repeat that reflect the original transfection wells from the 6 well plates. The raw slopes of the absorbance at 340 nm reflects the change of NADH to NAD+ as a result of PGK1 enzymatic activity.

Even before analysis there was a clear difference in the steepness of the slopes between the two groups with cells from wells that had been transfected with PGK1 having a noticeably steeper slope indicating higher PGK1 activity (Figure 3.2.D). To confirm this difference was not because of a difference in total protein of the cell which would indicate a difference in cell number between the groups, PGK1 activity was normalised to total protein by BCA. PGK1 activity was calculated using an NADH standard curve that was performed alongside each assay plate. The activity for each of the technical replicates following normalisation is shown along with the mean for each plate on the super plot to allow the better visualisation of the spread of data (Figure 3.2.E). Overall, there was significantly increased PGK1 activity in the lysates from cells that had been transfected with PGK1 compared with the controls (Figure 3.2.D, paired t-test, $p=0.03$).

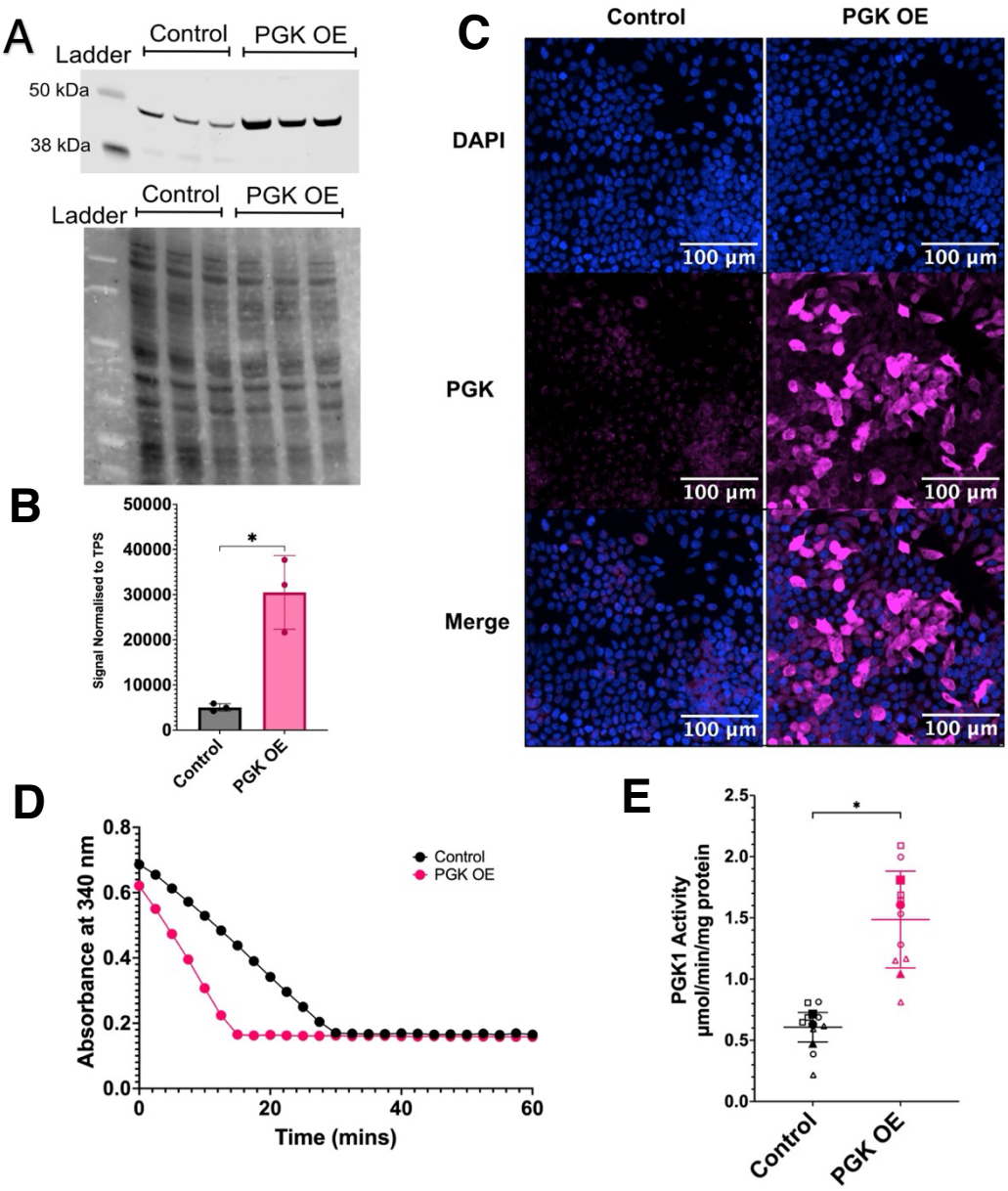

Figure 3.2: **Functional PGK1 can be overexpressed in HEK-293 cells. (A)** A western blot for PGK1 with total protein stain shown underneath shows increased PGK1 expression in PGK-transfected HEK-293 cells compared with lipofectamine treated only controls (n=3). **(B)** Quantification of western blot seen in (A) showing significant increase in PGK expression in PGK transfected cells (paired t-test, p=0.03). **(C)** Immunocytochemistry images show increased PGK1 expression in the cytoplasm of HEK-293 cells. **(D)** Example slopes from the metabolic PGK1 activity assay showing results from representative wells showing the difference in the rate of change in absorbance at 340 nm between cell lysate from a non-transfected control well (black) and a well of cells transfected with PGK1 (pink) **(E)** PGK1 activity in lysates from PGK transfected HEK-293 cells (pink) was increased compared with controls (black) (paired t-test, p=0.03). The experiment was repeated three times (n=3) with each including three technical replicates which are shown by the outlined shapes. The mean of each experiment is indicated by the solid shape of each respective shape.

3.3.2 Optimisation of Seahorse assays for HEK-293 cells

As PGK1 is a key enzyme in the glycolysis pathway, it is important to explore whether overexpressing this enzyme in the HEK-293 cells affects parameters of cellular respiration. The Seahorse XF analyzer by Agilent measures real-time changes in dissolved oxygen and free protons in the cell media and then calculate the oxygen consumption rate (OCR) and extracellular acidification rate (ECAR). This system can be used for the Mito Stress test and the Glycolytic Stress test protocols by Agilent. These test protocols deliver compounds into the cell media at set times in the protocol to probe their effect on parameters of mitochondrial respiration and glycolysis.

FCCP optimisation

One of the compounds used in the Mito Stress test is carbonyl cyanide-4-(trifluoromethoxy)phenylhydrazone (FCCP). FCCP is an uncoupler of mitochondrial oxidative phosphorylation by transporting protons through the mitochondrial membrane. This should result in a peak in the oxygen consumption rate. However, at higher concentrations FCCP can inhibit OCR. Therefore, it is recommended that the concentration of FCCP is optimised for each cell type (Technologies 2022). This was done by performing a Mito Stress assay using 4 concentrations of FCCP (0.5-2 μM) in a Seahorse plate seeded with non-transfected HEK-293 cells at $2x10^4$ cells per well. 5 wells were used per FCCP concentration although two wells were excluded based on abnormal trace shape. This is not uncommon with Seahorse experiments and so having at least 5 wells per condition per plate is preferred to allow for these types of exclusions. There was not a significant difference detected (ANOVA, p=0.078) between the FCCP concentrations (Figure 3.3.A). However, for optimisation purposes 1.5µM appeared to be the most appropriate concentration to use with the HEK-293 cells as it produced the highest mean value.

Cell seeding density

The recommended cell seeding density for the Seahorse assays is relatively broad (50-90% confluency; $1x10^4$ - $8x10^4$ cells per well), however it was observed during the FCCP concentration trial that the basal OCR of $2x10^4$ cells per well was around the lower end of the recommended basal OCR range (50-400 pmol/min) (Technologies 2017a, 2017b).

Therefore, I performed a trial Mito Stress assay with a plate containing 4 different HEK-293 cell seeding densities (1-$4x10^4$ cells/well) using 5 wells per condition. This showed a positive correlation between cell seeding density and both basal OCR (Figure 3.3.B) and maximum OCR (Figure 3.3.C) which was expected. A cell seeding density of $4x10^4$ gave a basal OCR between 100-150 pmol/min which was the most desirable of the densities tested.

Normalisation strategies

When plating different populations of cells for a Seahorse assay (for example transfected vs non transfected cells) it is possible to unintentionally introduce a systematic error in the precise number of cells plated per well between the groups. Normalising the Seahorse data to a measure of cell number is therefore important to have more confidence in any differences observed between the groups (Little et al. 2020).

During the first trial runs of the Mito Stress protocol, I found that many of the HEK-293 cells became dislodged from the bottom of the plate during the media changes resulting in the loss of cells. This was resolved by first coating the wells of the seahorse plate with 0.1 mg/ml poly-l-lysine to help the cells adhere to the bottom of the wells. However, the positive charge of the poly-L-lysine can interfere with the signal from a BCA assay meaning I could not rely on the results of a BCA assay to normalise the data to account for potential variability in cell counts between groups.

I explored other normalisation options using the maximal OCR data from the trial looking at different cell seeding densities (Figure 3.3.C). The first strategy was to image the wells after staining with DAPI and normalise to the % area stained. This proved to be a particularly unreliable method at the lowest seeding density (Figure 3.3.D), however given a higher cell seeding density is optimal anyway this wouldn't necessarily be a reason not to use this strategy. The second strategy was to use the particle analysis tool in Image J on the binarised images of the DAPI stained wells to get an automated particle count (Figure 3.3.E). The whole well was included in these analyses as the cells tended to clump, particularly around the edges of the wells so manually counting cells in random areas was not thought to be a suitable strategy. As it was thought that this clumping could also affect the accuracy of the % area and automated particle analysis strategies, a third strategy of trypsinising and resuspending the cells from the wells to perform a manual cell count was also explored (Figure 3.3.F).

The wells seeded for each different seeding density were plated from the same batch of cells, so it would be expected that successful normalisation would reduce the variation within the groups. To assess this, I compared the coefficient of variation of the groups with the different normalisation strategies (Figure 3.3.G). For this I excluded the value for the lowest seeding density normalised to % area as an outlier. There was no significant difference in the coefficient of variation between the normalisation strategies (ANOVA, $p=>0.05$). Indeed, the mean coefficient of variation of all the strategies was higher than the mean coefficient of variation of the raw data suggesting that normalising by any of strategies tested was not beneficial. However, given that the risk of introducing a systematic error when plating the cells for different groups is not insignificant, I considered at this stage that not using any normalisation process would not be appropriate. Of the strategies explored, the manual count method had the lowest mean coefficient of variation and

shouldn’t be affected by the issue of clumped overlapping cells and so this is the preferred method of those tested.

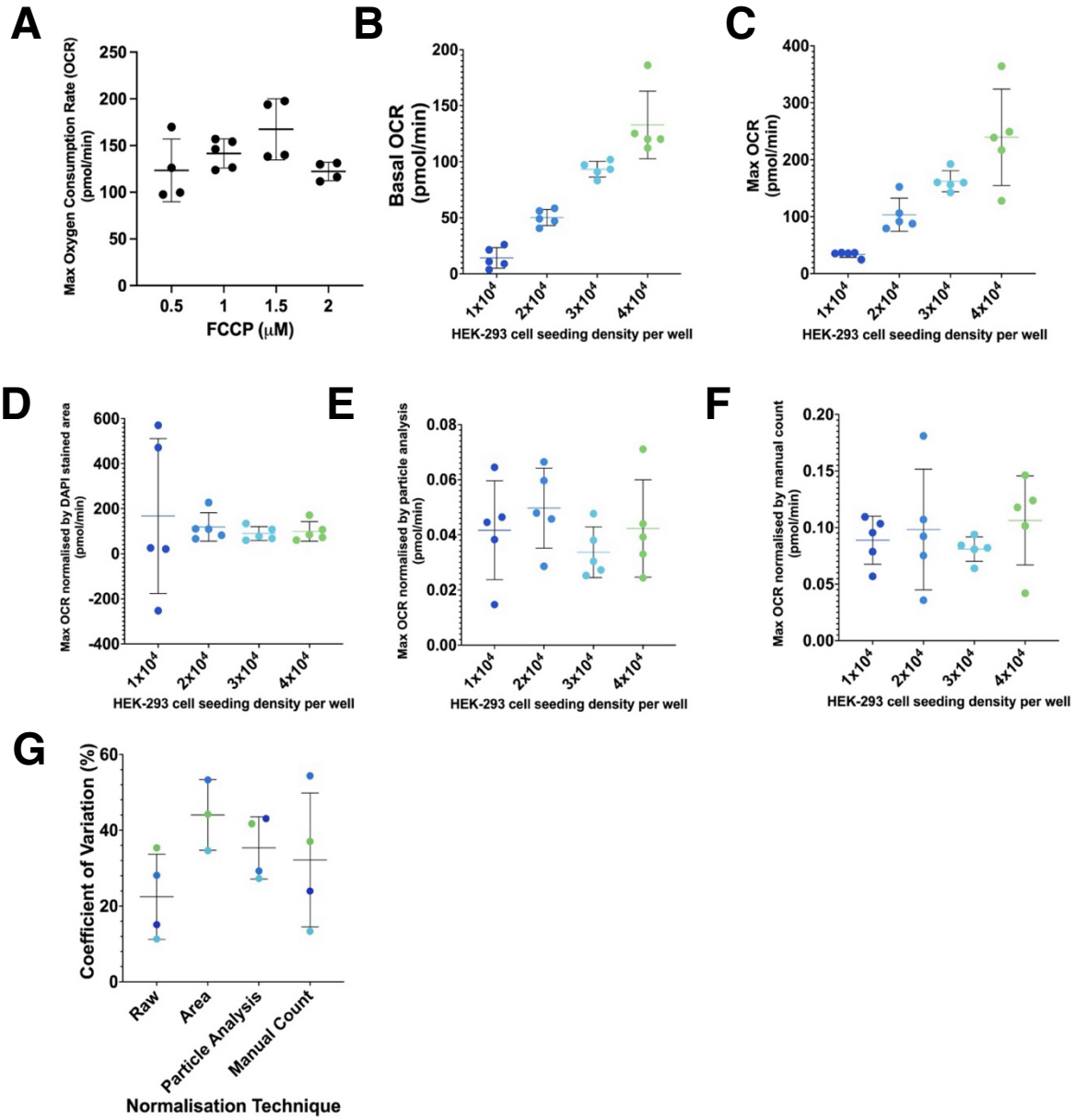

Figure 3.3: **Optimisation of FCCP, cell seeding density and normalization strategies for HEK-293 Seahorse assays (A)** Trial of the effect of different FCCP concentrations on maximum oxygen consumption rate (OCR). No significant difference between concentrations. **(B)** Effect of different cell seeding densities per well on basal OCR **(C)** Effect of different cell seeding densities per well on basal OCR. Results of (C) normalised to area stained by DAPI **(D)**, automated particle count using ImageJ **(E)** and manual cell count **(F). (G)** Comparison of the coefficient of variation from normalisation methods (D-F) excluding the value for the lowest seeding density for area. There is no significant difference between any of the methods and the non-normalised data.

3.3.3 Cellular respiration is unaffected by PGK1 overexpression

To investigate how PGK1 overexpression affected respiration in live cells both the Cell Mito Stress Test and the Glycolytic Stress Test seahorse assays were performed comparing the respiration parameters of HEK-293 cells that had been transfected with PGK1 with HEK-293 cells that had just been treated with lipofectamine.

Cell Mito Stress Test

The Cell Mito Stress Test is a protocol by Agilent that primarily uses changes in the oxygen consumption rate (OCR) following the injection of compounds that affect mitochondrial function to calculate multiple parameters of cellular respiration (Figure 3.4) (Technologies 2024).

I used the optimised cell seeding density ($4x10^4$ cells/well) and FCCP concentration (1.5 µM) and had 10 technical replicates (wells) per plate per condition. The experiment was performed in triplicate on three different days. The raw data of the means of each of the runs showed that both groups of cells showed the expected response to each of the injected compounds (Figure 3.5.A). The shape of the traces was preserved after the data was normalised to the manual cell count for each well but the variability of the data increased (Figure 3.5.B). Given that normalisation has led to increased variability but there is a risk of introducing a systematic error during the cell plating process, I assessed both the raw and the normalised data from the Cell Mito Stress Test. The parameters of mitochondrial function were calculated from both the raw and the normalised data sets. These showed no significant difference between the PGK1 transfected HEK-293 cells and the lipofectamine treated controls in terms of basal respiration, maximal respiration, ATP production, proton leak, spare capacity or non-mitochondrial oxygen consumption in either the raw data or the data normalised to manual cell count ($p=>0.05$, paired t-tests, Figure 3.5 C-H).

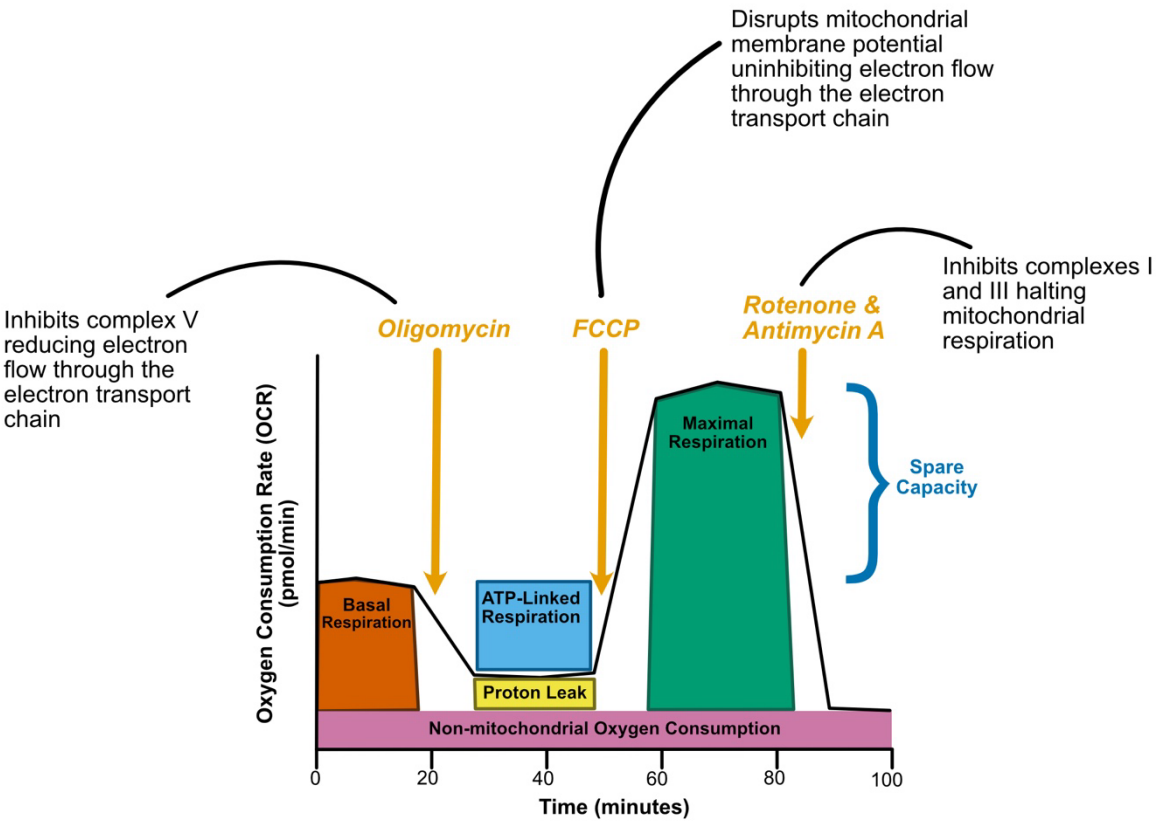

Figure 3.4: **Diagram showing a model oxygen consumption rate trace for the Mito Stress assay using Agilent Seahorse XF protocol.** The orange arrows show the approximate timings of the compound injections with their expected effects. Key parameters that can be calculated from the trace are labelled.

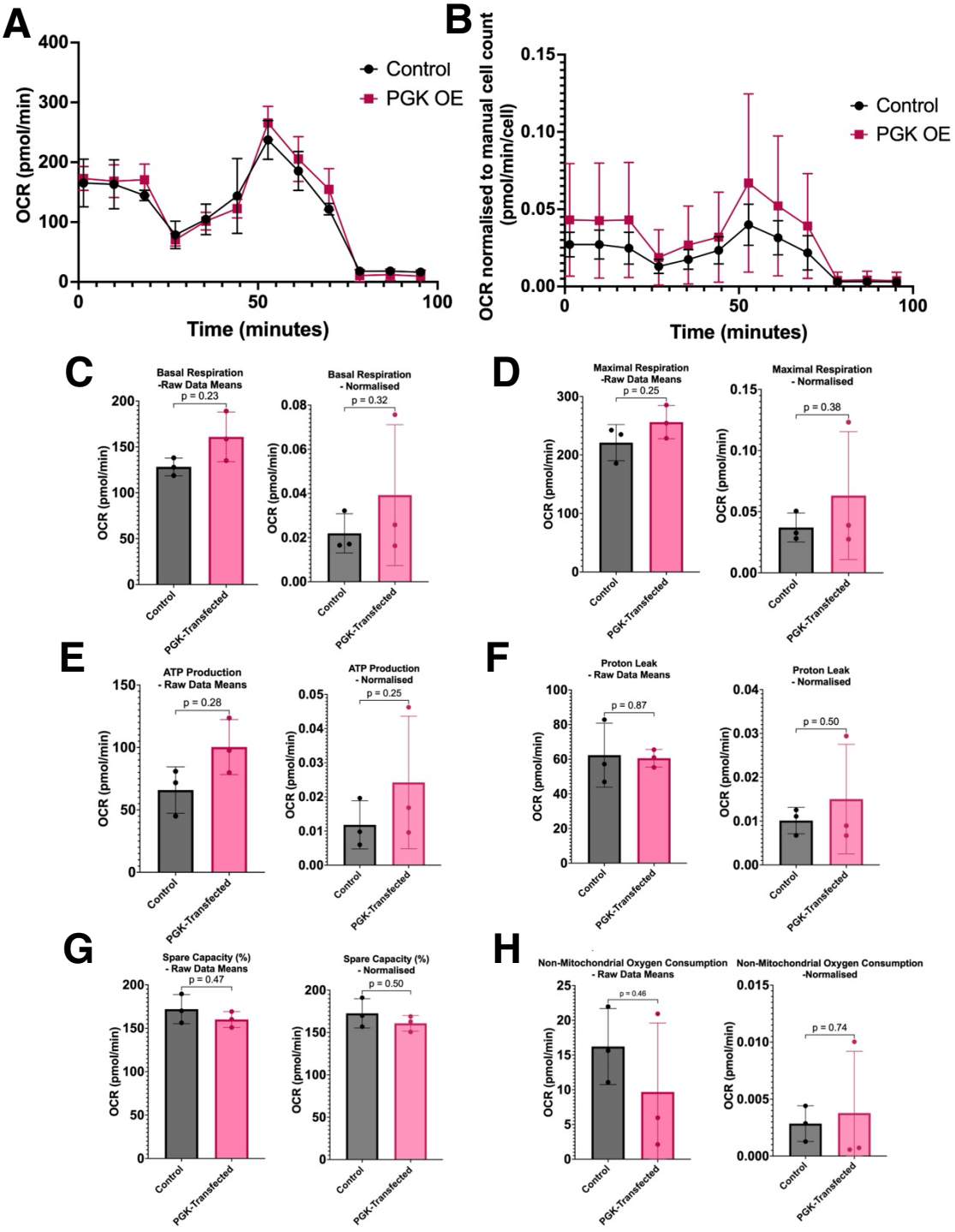

Figure 3.5: **Mito Stress Seahorse assays show no significant difference in respiration parameters between HEK-293 cells transfected with PGK1 or those treated with lipofectamine only. (A)** Raw profile data showing the mean traces from three separate plates (n=3) with the mean value for each plate being made up of the mean of 10 wells (technical replicates). **(B)** Raw profile data from (A) normalised to manual cell count. Calculated parameters of respiration from both the raw Seahorse traces and the normalised Seahorse traces showed no significant difference between the PGK-transfected cells and non-transfected control cells in any of the parameters (paired t-tests, p=>0.05) in basal respiration **(C)**, maximal respiration **(D),** ATP production **(E)**, proton leak **(F),** spare capacity **(G)** or non-mitochondrial oxygen consumption **(H).** Both the raw and normalised results are shown for each parameter with the p-values shown on the graphs.

Glycolytic Stress Test

PGK1 is known to be a key enzyme in glycolysis and whilst the Cell Mito Stress assay looks at some broad respiratory parameters, some glycolysis specific changes may not be detected. The Glycolytic Stress Test is a different Seahorse XF protocol by Agilent which is more focussed on the rate of glycolysis which it calculates by measuring the extracellular acidification rate (ECAR) following the injection of particular compounds (Figure 3.6) (Technologies 2019).

The assay was performed in triplicate on three separate days with each repeat consisting of a plate containing 10 technical replicates for each of the condition groups. The raw data taking the mean value for each timepoint for each of the three runs showed a good response to each of the injections of the protocol with no apparent difference between the PGK-transfected cells and controls (Figure 3.7.A). As with the Cell Mito Stress Test, I considered that there was a risk of introducing a systemic error during the plating of the cells for the experiment that could introduce a slightly different number of cells to wells of each treatment group and so normalising the data to a measure of cell count was important. As the manual cell count used to normalise the Cell Mito Stress Test data turned out to be quite labour intensive and not reduce the variability of the data, I decided to normalise the Glycolytic Stress Test data to the automated particle count performed in ImageJ as this method had the next lowest mean coefficient of variation when the normalisation methods were trialled and was not significantly different to the manual count method (Figure 3.3.G). The shape of the traces was retained after normalisation, but as with the Cell Mito Stress Test, the variation of the data points was increased compared with the raw data (Figure 3.7.B). This increase in variability would suggest that normalising the data has not been particularly helpful but I was still concerned about accounting for potential variation in cell number and so I decided to evaluate both raw and normalised data. Parameters of glycolysis

that can be calculated from this assay (Figure 3.6) were calculated from both the raw and normalised data. In both the raw data and data normalised to particle count, none of the parameters were significantly affected by PGK1 transfection ($p=>0.05$, paired t-tests, Figure 3.7 C-F).

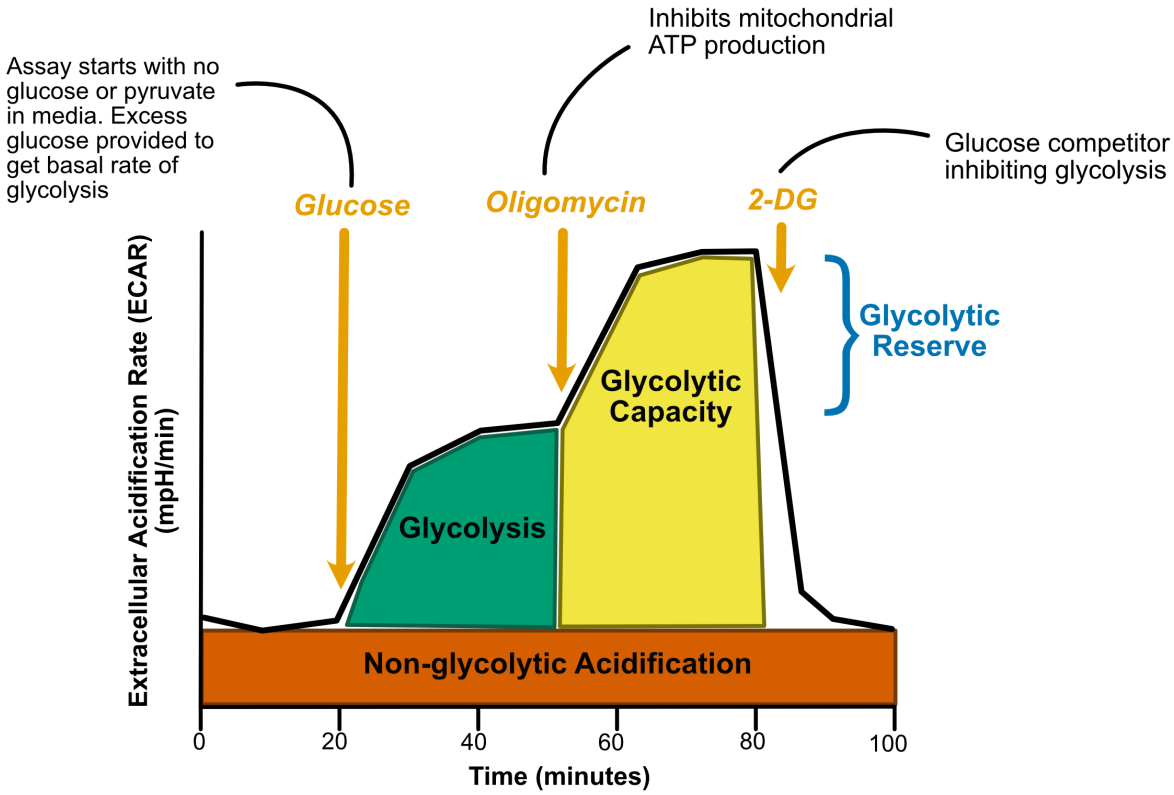

Figure 3.6: **Diagram showing a model ECAR trace for the Glycolytic Stress assay using Agilent Seahorse XF protocol.** The orange arrows show the approximate timings of the compound injections with their expected effects. Key parameters that can be calculated from the trace are labelled.

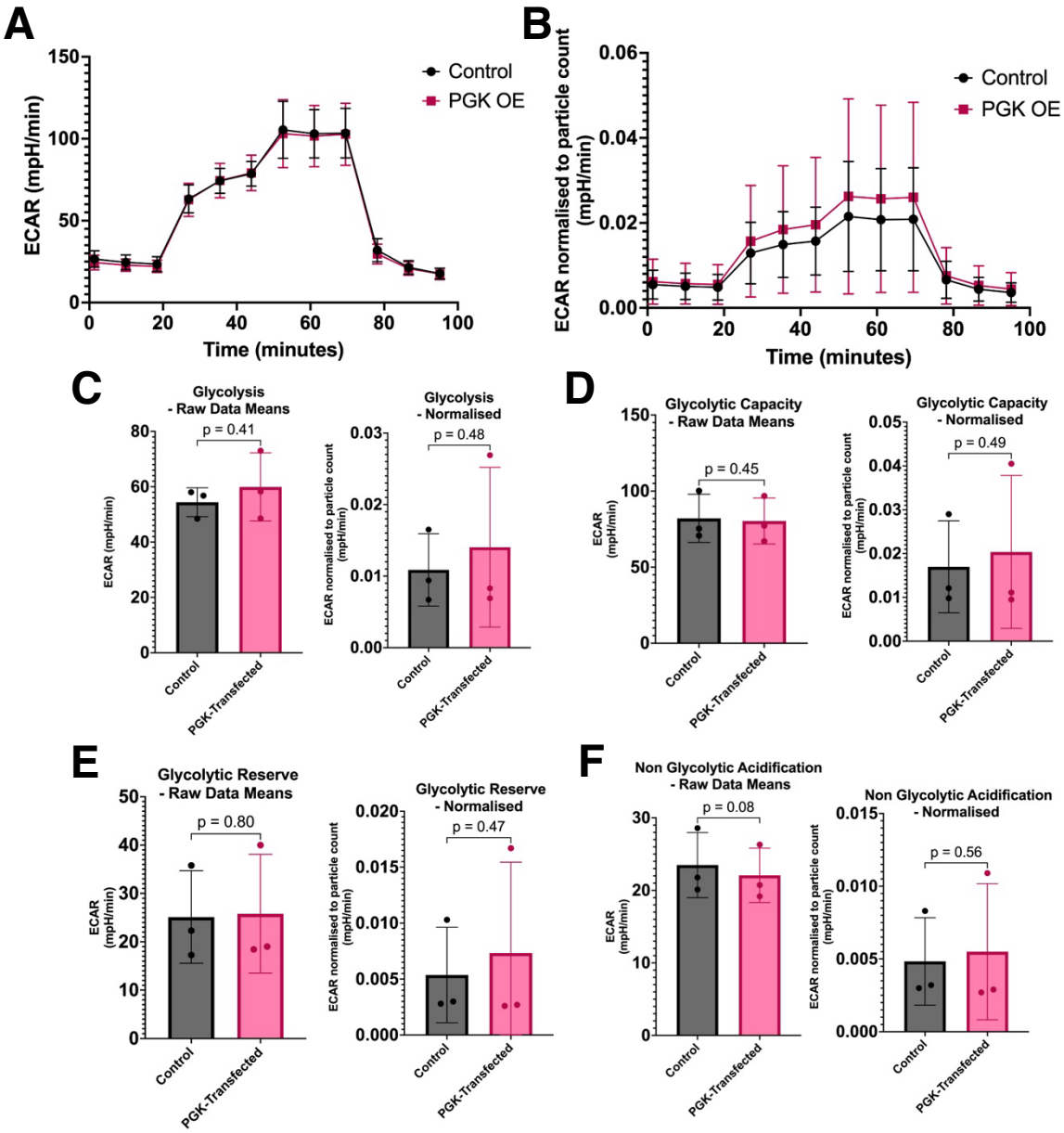

Figure 3.7: **Glycolytic Stress Seahorse assays show no significant difference in respiration parameters between HEK-293 cells transfected with PGK1 or those treated with lipofectamine only. (A)** Raw profile data showing the mean traces from three separate plates (n=3) with the mean value for each plate being made up of the mean of 10 wells (technical replicates). **(B)** Raw profile data from (A) normalised to automated particle count. Calculated parameters of respiration from both the raw Seahorse traces and the normalised Seahorse traces showed no significant difference between the PGK-transfected cells and non-transfected control cells in any of the parameters (paired t-tests, p=>0.05) in glycolysis **(C)**, glycolytic capacity **(D),** glycolytic reserve **(E)** or non-glycolytic acidification **(F).** Both the raw and normalised results are shown for each parameter with the p-values shown on the graphs.

3.3.4 RNA sequencing reveals minimal changes following PGK1 overexpression

RNA-sequencing was performed in collaboration with Edinburgh Genomics to explore if any significant cellular pathways are affected by the overexpression of PGK1 in HEK-293 cells.

RNA sample preparation

HEK-293 cells in 6-well plates were either transfected with PGK1 or treated only with the lipofectamine transfection agent as a control in technical duplicates. RNA was extracted from each well 48 hours after transfection. This was repeated for 7 plates, each plated on separate days. I selected the 6 best paired samples (one control and one PGK transfected) from different plates to send for RNA-sequencing.

To select the best samples to send for sequencing, RNA quality was assessed. To assess RNA concentration and quality both a NanoDrop and Agilent 2100 Bioanalyzer were used. The NanoDrop provided a concentration and measures of RNA purity. A 260/280 ratio of ~2 and a 260/230 ratio of between 2.0 and 2.2 were desired as an indication of low contamination in the RNA samples. Absorbance at 260 nm reflects the quantity of nucleic acids. Contamination with protein can be estimated with the 260/280 ratio and other common contaminants, particularly those that can be introduced during the RNA purification process, are reflected in the 260/230 ratio. Apart from sample 6.1, the NanoDrop results were all relatively close to the desired values indicating that the RNA extraction and purification methods were effective.

The number of samples that could be run through the Agilent 2100 Bioanalyzer was more limited than with the Nanodrop and so I excluded samples 2.1, 4.1, 5.1, 5.5, 6.1 and 6.2 following the NanoDrop results as these had either low concentrations or 260/230 ratios particularly when compared with the replicate

of the treatment condition from the same plate (Table 3.1). The bioanalyzer results also provided an estimated RNA concentration used to corroborate the NanoDrop findings. Edinburgh Genomics advised that the minimum concentration they needed for the RNA-sequencing was >85 ng/µl so all the samples were sufficiently concentrated to be sent. The decision as to which samples to send for analysis was therefore made primarily on RNA integrity number (RIN) whilst ensuring I was selected a control and PGK-transfected sample per plate. The Agilent 2100 Bioanalyzer calculates the RIN as a measure of RNA degradation from electrophoretic traces which show the ribosomal bands of the RNA samples (Schroeder et al. 2006). A RIN of 1 indicates highly degraded RNA whereas a RIN of 10 is intact RNA. RIN values for submitted samples ranged from 9.2-10 and the concentration of RNA was 637-2986 ng/µl.

RNA-sequencing data analysis

Edinburgh Genomics performed the RNA-sequencing with the Illumina NovaSeq 50PE platform and conducted the differential analyses. It was found that 'plate' impacted gene expression considerably and so analyses were performed adjusted for 'plate' to account for the variability in gene expression seen between plates. Based on the thresholds of a fold change (FC) greater than 2 and a false discovery rate (FDR) <0.05, 11 genes were found to be up-regulated in HEK-293 cells transfected with PGK1, including PGK1 itself, and no genes were found to be down-regulated (Figure 3.8.A, Table 3.2). Most of these differentially expressed genes are protein coding but there are also two that are processed pseudogenes and one that is long noncoding RNA (Figure 3.8.B). As less than 0.06 % of 19490 genes compared were found to be significantly differentially expressed between the transfected and non-transfected cells suggesting that PGK1 transfection has had a minimal effect on the HEK-293 cells.

Pathway analysis

I did attempt pathway analysis of the list of differentially expressed genes using the online tool DAVID, however even after reducing the FDR threshold to <0.2, there were only 21 genes to include. The low numbers of differentially expressed genes meant that the enrichment scores of the clusters detected were very low and so no significant pathways affected by the overexpression of PGK1 could be identified.

Sample Details				Nanodrop Results			Bioanalyser Results	
ID	Plate	Well	Condition	Conc. (ng/ul)	260/280	260/230	Conc. (ng/ul)	RIN
1.1	1	1	Control	687	2.10	1.91	637	9.5
1.2	1	2	PGK	639	2.07	1.92	1710	6.2
1.4	1	4	Control	854	2.10	1.99	ERROR	
1.5	1	5	PGK	1093	2.10	2.01	1262	9.4
2.1	2	1	Control	424	2.09	1.77	*Not Tested*	
2.2	2	2	PGK	813	2.10	2.12	1106	9.4
2.4	2	4	Control	988	2.10	2.01	1366	9.3
2.5	2	5	PGK	740	2.09	2.09	825	9.5
3.1	3	1	Control	754	2.11	1.96	1389	9.3
3.2	3	2	PGK	1194	2.10	2.15	1306	9.6
3.4	3	4	Control	974	2.11	2.05	ERROR	
3.5	3	5	PGK	767	2.10	2.10	948	9.4
4.1	4	1	Control	404	2.08	2.05	*Not Tested*	
4.2	4	2	PGK	1280	2.11	2.20	2987	9.5
4.4	4	4	Control	445	2.08	2.03	872	10.0
4.5	4	5	PGK	528	2.09	2.12	742	9.8
5.1	5	1	Control	787	2.09	1.99	*Not Tested*	
5.2	5	2	PGK	852	2.09	2.00	1649	9.5
5.4	5	4	Control	795	2.09	2.05	1731	9.8
5.5	5	5	PGK	638	2.11	2.08	*Not Tested*	
6.1	6	1	Control	ERROR/Contamination			*Not Tested*	
6.2	6	2	PGK	608	2.02	1.86	*Not Tested*	
6.4	6	4	Control	583	2.04	1.74	897	9.2
6.5	6	5	PGK	588	2.02	2.03	965	9.1
7.1	7	1	Control	554	2.08	2.09	986	8.7
7.2	7	2	PGK	786	2.07	2.12	1171	10.0
7.4	7	4	Control	769	2.06	2.15	938	9.2
7.5	7	5	PGK	604	2.08	1.98	1270	9.6

Table 3.1: **Analysis of samples sent for RNA-sequencing.** Table showing the results of NanoDrop spectrophotometer and Agilent 2100 Bioanalyzer analyses to assess RNA concentration and quality of the extracted RNA samples from HEK-cells transfected with PGK or the lipofectamine only treated controls. The seven cell plates were plated on separate days with two wells plated per treatment condition. The NanoDrop provided both a concentration and indicators of RNA purity in 280/260 and 260/230 ratios. The bioanalyser also provided a concentration but also an RNA integrity number (RIN). These results were used to select the best six pairs of samples with the highest concentration and most optimal RNA quality to send for RNA-sequencing. Samples highlighted in yellow are the 6 paired samples from different plates that were selected for RNA-sequencing.

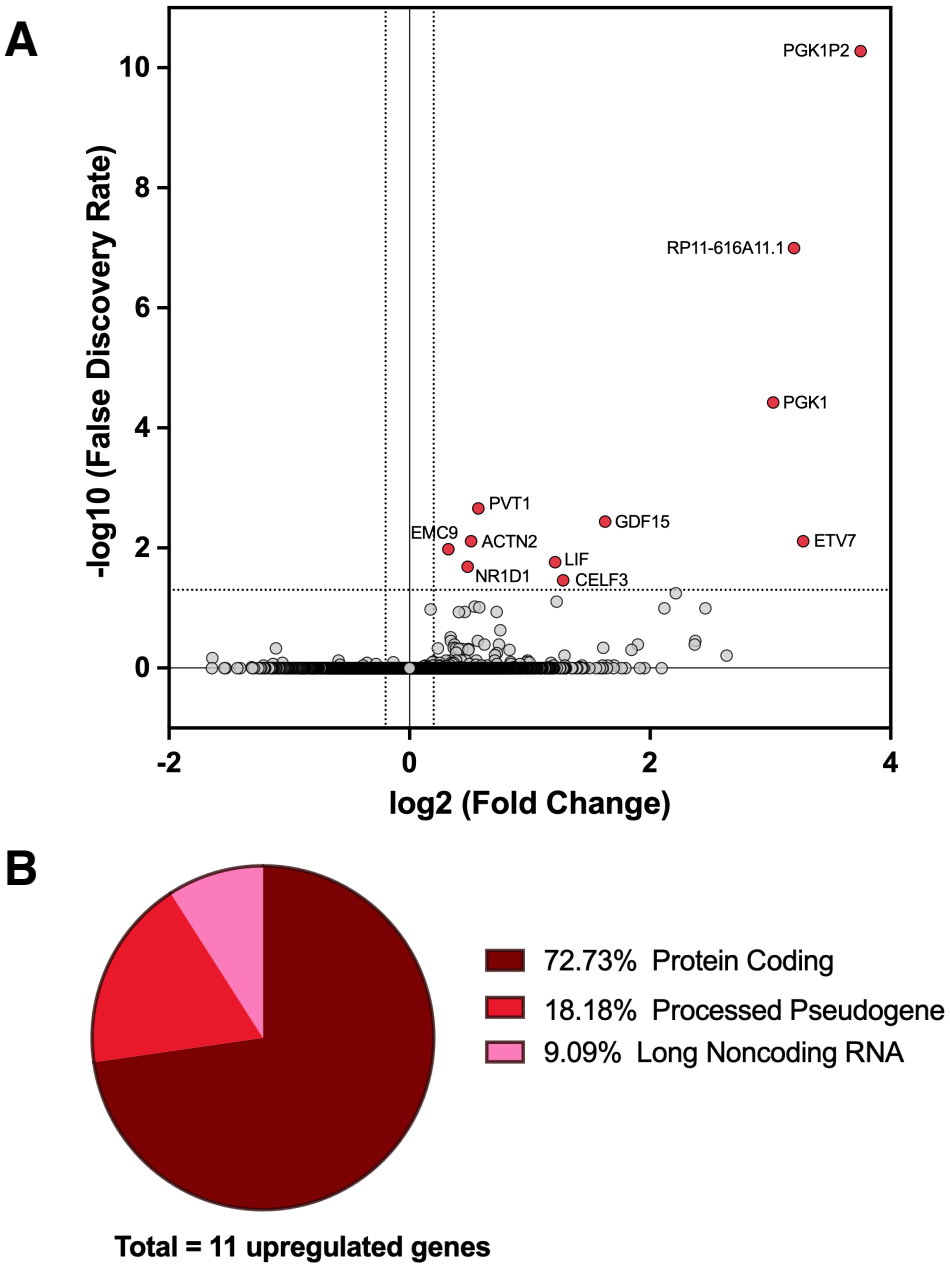

Figure 3.8: **RNA sequencing reveals 11 upregulated genes in PGK transfected cells compared with lipofectamine treated controls. (A)** Volcano plot showing differential expression between 6 paired RNA samples from control and PGK transfected cells with the FDR adjusted for plate effect. The dashed lines represent the thresholds set for significance of a fold change >2 and an FDR <0.05. **(B)** Pie chart illustrating the distribution of gene biotypes in the 11 upregulated genes in PGK transfected cells vs controls.

Gene	Gene ID	Gene Biotype	LogFC (Transfected vs Control)	P Value (Transfected vs Control)	FDR (Transfected vs Control)
PGK1P2	ENSG00000213290	Processed pseudogene	3.75	2.72E-15	5.29E-11
RP11-516A11.1	ENSG00000228328	Processed pseudogene	3.20	1.03E-11	1.00E-07
PGK1	ENSG00000102144	Protein coding	3.02	5.78E-09	3.76E-05
PVT1	ENSG00000249859	lincRNA	0.57	4.49E-07	2.19E-03
GDF15	ENSG00000130513	Protein coding	1.62	9.29E-07	3.62E-03
ACTN2	ENSG00000077522	Protein coding	0.51	2.44E-06	7.71E-03
ETV7	ENSG00000010030	Protein coding	3.27	2.77E-06	7.71E-03
EMC9	ENSG00000100908	Protein coding	0.32	4.31E-06	1.05E-02
LIF	ENSG00000128342	Protein coding	1.21	7.93E-06	1.72E-02
NR1D1	ENSG00000126368	Protein coding	0.48	1.05E-05	2.05E-02
CELF3	ENSG00000159409	Protein coding	1.28	1.94E-05	3.44E-02

Table 3.2 Table of the 11 differentially expressed genes in PGK transfected cells compared with lipofectamine treated controls that met the thresholds of having a fold change (FC) >2 and a false discovery rate (FDR) <0.05. The gene ID and gene biotype for each gene is also shown.

3.4 Discussion

3.4.1 PGK1 transfection and Seahorse Assays

PGK1 was successfully transfected into HEK-293 cells with significant increase in PGK1 expression which was visualised in the cytoplasm of the cells with ICC. The PGK1 metabolic assay showed that the overexpressed PGK1 was functional with significantly increased activity in the cell extracts from transfected cells. However, this increased PGK1 activity did not significantly affect cell respiratory parameters that were measured using the Seahorse assays. This confirms that in the HEK-293 cells, PGK1 is not a rate-limiting factor in glycolysis which is consistent with the literature (Boscá L.; Carlos Corredor 1984; Jin et al. 2020). This does not mean that a PGK1 targeted therapy would not be working via its role in glycolysis as PGK1 has been found to be rate-limiting in primary neuronal cultures subjected to stress (Kokotos et al. 2024). This would suggest that cell type and cell conditions have significant influence on cellular metabolism. So, in HEK-293 cells, where PGK1 is not the primary rate-limiting factor in glycolysis, a difference in PGK1 activity can be assessed using the PGK1 metabolic assay, but the Seahorse assays would not be able to detect increased PGK1 activity. This makes the Seahorse assays inappropriate to use for screening compounds in HEK-293 cells for increased PGK1 activity which I needed to consider in future chapters.

Optimisation of the methods generally went smoothly; however, the normalisation of the Seahorse traces should be discussed. The transfections were performed in 6-well plates and then the cells were replated into the Seahorse assay plates with the two groups counted and plated separately (but at the same time and from the same 6-well plate). This meant that there was a real risk of introducing a systematic error in terms of the number of cells plated per well that would introduce a fundamental difference between the two groups. Ideally, I would have used the BCA assay to normalise to total protein, however I was concerned that the positively charged PLL coating needed to

help the cells adhere to the surface of the wells would interfere with the BCA assay. Instead, I tried multiple methods which were all essentially variations of cell count. None of these methods improved the variation of the data compared with the raw traces and actually increased observed variability in the experiments. Despite this, given the risk of introducing an error related to cell number during plating, I looked at both the normalised and non-normalised data and neither showed any significant changes following PGK1 transfection. It should also be noted that the pyruvate added to the Seahorse media in the Mito Stress Seahorse assays may have masked subtle changes in the mitochondrial outputs as pyruvate is a substrate at the end of glycolysis pathway that feeds into the TCA cycle. Future experiments should consider optimising a protocol where exogenous pyruvate is not added to look for more subtle changes.

3.4.2 Upregulated genes identified by RNA-sequencing

As there were only 11 differentially expressed genes identified using the thresholds of a fold change >2 and an FDR <0.05 and no significantly altered pathways could be identified using DAVID analysis, I instead researched each gene in the literature to try to identify potential associations or consequences of upregulation to cell health.

PGK1P2, RP11-516A11.1, PGK1

PGK1 and associated pseudogenes PGK1P2 (phosphoglycerate kinase 1, pseudogene 2) and RP11-516A11.1 (phosphoglycerate kinase 1, pseudogene 1) were unsurprisingly the most differentially expressed genes detected by the RNA-sequencing. Their presence reassures us that the transfection method was successful. Pseudogenes are genomic sequences which have a very high similarity to a protein-coding gene but contain mutations, which mean they are unable to produce functional proteins (Cheetham, Faulkner, and Dinger 2020). Historically, pseudogenes have been presumed to be nonfunctional, however

there is increasing evidence that they may play specific roles in certain processes. Some pseudogenes can influence the expression of their parent gene by acting as long or short non-coding RNA or they can influence expression of neighbouring genes by affecting chromatin structure (Pink et al. 2011). Deficiency in the pseudogene PGK1P2 has been implicated in preeclampsia in humans (Tong et al. 2018). The same report also found that levels of PGK1P2 correlated with those of PGK1 and suggested PGK1P2 helps to regulate PGK1 expression (Tong et al. 2018). This provides some preliminary evidence that these pseudogenes may play a role in diseases. The current literature does not include PGK1P2 or RP11-516A11.1 as any of the few pseudogenes found to encode functional peptides, however this is a developing field and further information on the roles of these pseudogenes may be discovered in the future (Lin et al. 2025).

PVT1

Plasmacytoma variant translocation 1 (PVT1) is a long non-coding RNA locus. It has been reported as a potential oncogene and may play a role in regulating apoptosis (Zhang et al. 2023; Fu, Tian, et al. 2023).

GDF15

Growth differentiation factor 15 (GDF15) is a widely expressed protein that is part of the transforming growth factor – β (TGF-β) superfamily. Increased expression has been associated with both intracellular metabolic stress and extracellular stresses to the extent that it has been suggested that GDF15 may be a useful biomarker of mitochondrial disorders and some cardiovascular conditions (Yatsuga et al. 2015; Luo et al. 2021; Yu et al. 2025). Circulating GDF15 increases in the absence of disease with age and elevated levels that correlate with inflammation markers are seen after strenuous physical exercise (Conte et al. 2020). These increased levels of GDF15 have been proposed to be protective with reduced GDF15 levels being associated with obesity and increased mortality in acute inflammation in mice (Luan et al. 2019; Tran et al.

2018). Whilst GDF15 being associated with mitochondrial dysfunction is interesting given PGK1's role in glycolysis, increased GDF15 appears to be a non-specific compensatory response to stress.

ACTN2

Actinin alpha 2 (ACTN2) is part of a family of cytoskeletal proteins that anchors actin to intracellular structures. ACTN2 is typically associated with cardiac and skeletal muscle where it stabilises the contractile muscle apparatus (Sjoblom, Salmazo, and Djinovic-Carugo 2008). Variants in ACTN2 have long been associated with cardiomyopathies (Noureddine et al. 2025). ACTN2 is also expressed in brain tissue and more recently expression has been associated with a subtype of oligodendrocytes in Alzheimer's disease, however its specific role in these cells is unclear (Mills et al. 2001; Sadick et al. 2022).

ETV7

ETS variant transcription factor 7 (ETV7) is a transcription factor which has been associated with multiple cancers. Its association with multiple cancers appears to be closely linked with immune system regulation with interactions with NOTCH1, TNFR1 and IFIT3 all reported in the literature (Salameti et al. 2019; Meskyte et al. 2023; Chai et al. 2024). ETV7 is a potential target for anti-cancer therapies as ETV7 interacts with the mechanistic target of rapamycin (mTOR) and is a key component in the assembly of mTORC3 (Harwood et al. 2018). ETV7 is not known to be directly associated with PGK1 or cellular respiration but there is a potential link with PGK1 via the mTOR pathway.

EMC9

Endoplasmic reticulum protein complex subunit 9 (EMC9) is part of the endoplasmic reticulum protein complex (EMC). The EMC is highly conserved and needed for transmembrane protein insertion in the endoplasmic reticulum (Chitwood et al. 2018). Apart from a role in embryonic neural crest

development, the functions of EMC9 specifically are unclear (Marquez, Aslam, and Khokha 2023).

LIF

LIF interleukin 6 family cytokine (LIF – previously leukemia inhibitory factor) plays a regulatory role in inflammation and is involved in the acute phase response (Weber et al. 2005). LIF signalling also has broader roles in cell proliferation and tumorigenesis and it has been found to activate the AKT-mTOR pathway providing a weak link between LIF and ETV7 (Li et al. 2014). Further to this, there is a link between PGK1 and the mTOR pathway via its proposed function as a protein kinase, as PGK1 phosphorylates PRAS40 (proline-rich Akt substrate of 40kDa) which is a key part of mTOR pathway activation suppressing autophagy (Zhang et al. 2022; Qian et al. 2017).

NR1D1

Nuclear receptor subfamily 1 group D member 1 (NR1D1, also known as REV-ERB alpha) is a transcription factor with a key role in regulating the circadian clock and participates in the feedback loop by inhibiting Bmal1 expression (Yin, Wu, and Lazar 2010). NR1D1 has also been associated with inflammation, in particular neuroinflammation, which particularly interesting given that circadian rhythm dysfunction is often seen in neurodegenerative disorders such as Alzheimer's disease and Parkinson's disease (Griffin et al. 2019).

CELF3

CUGBP Elav-like family member 3 (CELF3) is an RNA-binding protein involved with pre-mRNA alternative splicing and has been identified as being able to activate the splicing of tau exon 10 (Wang et al. 2004). CELF3 expression has been shown to be restricted to the brain and testes and it is enriched in a subpopulation of primary sensory neurons (Grlickova-Duzevik et al. 2023; Ladd, Charlet, and Cooper 2001).

There are features of this group of differentially expressed genes that are interesting, a few have broad links to metabolism and their levels may be increased as a protective response to cellular stress whereas others have associations with various neurological conditions. However, there is not much information available in the literature to suggest that there is much to link the genes and certainly no clear pathways can be said to be affected by overexpression of PGK1.

Ultimately, the reason for and potential consequences of the upregulation of most of these genes is unclear at this stage. As the transfection increased PGK1 expression by approximately 3-fold, it is perhaps surprising that there weren't more changes to the gene expression of the transfected cells. This suggests that the HEK-293 cells are relatively tolerant of both the additional PGK1 protein and the additional PGK1 enzyme activity.

3.4.3 Future work

In this chapter I have used HEK-293 cells as an initial model system to explore how a relatively generic human cell line would respond to the overexpression of a key metabolic enzyme. However, the results have left some unanswered questions. Whilst the differentially expressed genes from the RNA-sequencing could be explored further, given there are so few of them and there are no significantly affected pathways it was not considered worth exploring further at this time. Future work investigating the additional roles reported for PGK1 may find it more fruitful to investigate its function in association with its cellular location rather than its absolute level of activity.

The PGK1 metabolic assay is useful as a compound screening tool as it is able to detect increased PGK1 activity even when it may not be resulting in changes to cellular respiration. However, finding a cellular model of disease where PGK1 is a rate-limiting factor of glycolysis would be desirable so that

compounds could be tested for their effect on energy production using the Seahorse assays.

3.4.4 Conclusion

In summary, overexpression of the glycolytic enzyme PGK1 in HEK-293 cells did not affect cellular respiration or result in the up- or downregulation of any identifiable cellular pathways.

The primary aim of this chapter was to determine if increased PGK1 activity was likely to have undesirable consequences. The overexpression of PGK1 in HEK-293 cells only had a modest impact on the transcriptome with only 11differentially expressed genes identified. This would suggest that increased PGK1 activity in cells unaffected by disease is not likely to be a huge concern which is important when considering developing systemic therapies. However, the results of the RNA-sequencing have not provided much further insight into the potential non-canonical roles of PGK1 that have been reported.

The secondary aims relate to the suitability of the methods for later chapters. HEK-293 cells are easy to work with, however because PGK1 is not a rate-limiting factor in the glycolysis pathway of these cells, the Seahorse assays were not able to detect any significant change in cells overexpressing PGK1. This means that for compound screening the Seahorse assays are not likely to be useful, however as the PGK1 metabolic assay was able to detect increased PGK1 activity then this would be a suitable method to use to try to screen potential activators.

Chapter 4: Screening potential PGK1 activating compounds in HEK-293 cells

4.1 Introduction

Terazosin is a known PGK1 activator which is being explored for its therapeutic potential as a repurposed drug in both Parkinson's disease and amyotrophic lateral sclerosis (ALS) (Schultz et al. 2022). Terazosin has been in clinical use since the 1980s as an alpha-1 adrenergic antagonist which is separate from its capability to activate PGK1 (Riley et al. 2024; Kyncl 1986). The alpha-1 adrenergic antagonist activity of terazosin has led to reports of side effects in patients which have been significant enough to result in some patients withdrawing from trials (Schultz et al. 2022). This means that whilst there is interest in increasing PGK1 activity as a therapy in multiple diseases, there is a need for novel PGK1 activators that are more specific than terazosin. In this chapter, I take a set of compounds that have been predicted by artificial intelligence (AI) to interact with PGK1 and screen them in HEK-293 cells for their ability to increase PGK1 activity.

4.1.1 The lack of alternative PGK1 activators

Despite the interest in PGK1 as a therapeutic target and the issues with terazosin, there is a lack of alternative PGK1 activators. Ideally, a more specific compound would be found to develop further into a potential therapeutic which may be either more effective or have fewer side effects than terazosin.

The current search for alternatives is discussed in more detail in the thesis introduction but it is important to highlight here that there have been other recent attempts to improve on terazosin. *In vitro* testing of synthesised structural analogs of terazosin has shown improved PGK1 activation (Wang, Qian, et al. 2022). A database screen for novel PGK1 activators using a virtual screen followed by testing in a *Drosophila* model of oxidative stress and *in vitro*

models also found three compounds that showed some promise (Qiang et al. 2022). Whilst these were not directly compared with terazosin or tested in mammalian models, they do provide some reassurance that the effect of terazosin on PGK1 is not unique and so there is some cause for optimism that alternatives can be found.

4.1.2 Atomwise PGK1 compound library

Developments in machine learning and artificial intelligence capabilities have led to interest in how these tools can be used to assist in drug discovery. The biotechnology company Atomwise have developed the AtomNet computational model to screen synthetic chemical libraries as an alternative to the more traditional high throughput screen physical libraries (Wallach, Dzamba, and Heifets 2016). To help validate this platform, Atomwise collaborated with 296 external academic projects (Atomwise 2024). An average of 85 compounds were identified per project and Atomwise has reported a 73% success rate for detecting at least one bioactive compound for the project's target amongst those identified compounds. These screenings have led to recent publications from collaborators of Atomwise identifying successful hits including a new 6-phosphofructo-2-kinase/fructose-2,6-biphosphatase inhibitor (Eyster et al. 2025). We received a library of compounds predicted to target PGK1 from the Atomwise AtomNet project containing 89 compound samples and 2 DMSO negative controls to which I was blinded. The compounds are made up to 10 mM with 100% DMSO which is why DMSO is used as the negative control.

4.1.3 PGK1 Metabolic Assay

The PGK1 metabolic assay used to screen the compounds is the same as the one used in Chapter 3. As discussed previously, the metabolic assay was able to detect increased PGK1 activity in HEK-293 cells which were overexpressing

PGK1. NADH has a strong absorbance at 340 nm whereas the NAD+ that forms following the reaction facilitated by PGK1 has almost no absorbance at 340 nm (McComb et al. 1976). The PGK1 metabolic assay uses a spectrometer to measure absorbance at 340 nm over time so the rate of change of absorbance can be used to measure the reaction rate with an increased rate signalling increased PGK1 activity.

4.2 Aims

In this chapter I used the PGK1 metabolic activity assay to screen the Atomwise compound library for their ability to activate PGK1 in HEK-293 cells. The aims of this chapter are:

- To show the optimisation of the PGK1 metabolic assay
- To identify the most promising compounds in terms of PGK1 activation capability to take forward as lead compounds into a disease model system.

4.3 Results

4.3.1 Optimisation of the PGK1 metabolic assay

Different factors of the PGK1 metabolic assay were optimised with the HEK-293 cells before proceeding to screening compounds:

- Seeding density of the HEK-293 cells in the 24 well plates
- Acquiring the linear part of the reaction curves
- Normalisation of the reaction slopes
- Confirming the reliable detection of NADH

Seeding density of the HEK-293 cells in the 24 well plates

Cells were seeded at three different seeding densities in a 24 well plate: $0.05x10^6$, $0.06x10^6$ and $0.07x10^6$ cells per well with three wells per condition 48 hours before the assay. The PGK1 assay was completed in a single 96 well plate (see Methods) using 10 μl of cell extract from each of the experimental wells. Absorbance at 340 nm declines over the 60-minute time course of the assay, which is expected with the conversion of NADH to NAD+ as a result of PGK1 activity (Figure 4.1.A). A steeper slope indicates a faster rate of conversion of NADH to NAD+ and therefore higher PGK1 activity. As expected, PGK1 activity was highest from the cell extracts from wells seeded with the highest number of cells. As I was screening compounds with the aim to increase PGK1 activity there needed to be scope within the assay to detect an increased rate and at the highest seeding density of $0.07x10^6$ this may be more limited. It was noted that looking at the raw slopes of PGK1 activity there was not an observable difference between the extracts from wells seeded with $0.05x10^6$ and $0.06x10^6$ cells per well.

Acquiring the linear part of the reaction curves

The linear part of the progress curve is where the reaction is occurring at its highest rate and this needs to be isolated for the subsequent analysis. Towards

the end of the assay the rate of the reaction slows down and the curve flattens. This is particularly prominent in the $0.07x10^6$ cells per well group where the reaction occurs at the fastest rate and is likely due to the substrate in the well being used up. The first couple of readings in all the groups also do not fit the linear relationship seen in the rest of the assay and should also be excluded to ensure the analysis is consistently performed on the linear part of the kinetic curves (Figure 4.1.B). The raw progress curves did not show a difference in reaction rate between the lower seeding densities. This may be due to differences in cell growth between the wells or in the effectiveness of the trypsinisation of the wells. If either of these are the case then it would be expected that the total protein levels would reflect this, and normalisation to total protein would help account for some of the potential sources of variability.

Normalisation of the reaction slopes

It was initially concerning that there was not an observable difference in the absorbance slopes between the $0.05x10^6$ and $0.06x10^6$ cells per well groups as it would be expected that wells containing more cells would have more PGK1 and therefore would have a faster reaction rate (Figure 4.1.C). To try to standardise the assay, normalisation was attempted by performing a BCA assay on each cell extract to allow for normalisation of the slope to total protein which reduced the difference between the means of the two highest cell seeding densities (Figure 4.1.D).

Confirming the reliable detection of NADH

A standard curve was performed using different volumes of 1 mM NADH in each well which contain reaction buffer but no cell extracts. The absorbance in each of these wells was stable over the time of the assay and increased consistently with the concentration of NADH (Figure 4.1.E). Repeats were performed for the 20 μl and 50 μl volumes of 1 mM NADH which are shown in magenta in Figure 4.1.E and demonstrate a good level of consistency with the

assay. A trendline that includes these repeats had a coefficient of determination (R^2) of 0.9979 indicating a very high goodness of fit of the linear regression model.

Optimisation Conclusions

The PGK1 metabolic assay is able to detect different concentrations of NADH based on absorbance at 340 nm. Using 10 μl of cell extract per well from HEK-293 cells plated at $0.06x10^6$ cells per well provided a good reaction rate with capability within the assay to measure increased rates if a strong PGK1 agonist is found. The linear part of the kinetic curve is used for analysis by excluding the first and last few readings but is checked on a well-by-well basis to ensure just the linear part of the reaction is included. Increasing the frequency of the absorbance measurements from every 5 minutes to every 2.5 minutes increases the number of data points available to help assess this more precisely. Normalisation of the slope values to the BCA result for each well reduces variation in the assay and is a relatively straightforward step to include to help standardise the assay and account for known potential sources of variability such as cell number or cell growth rate.

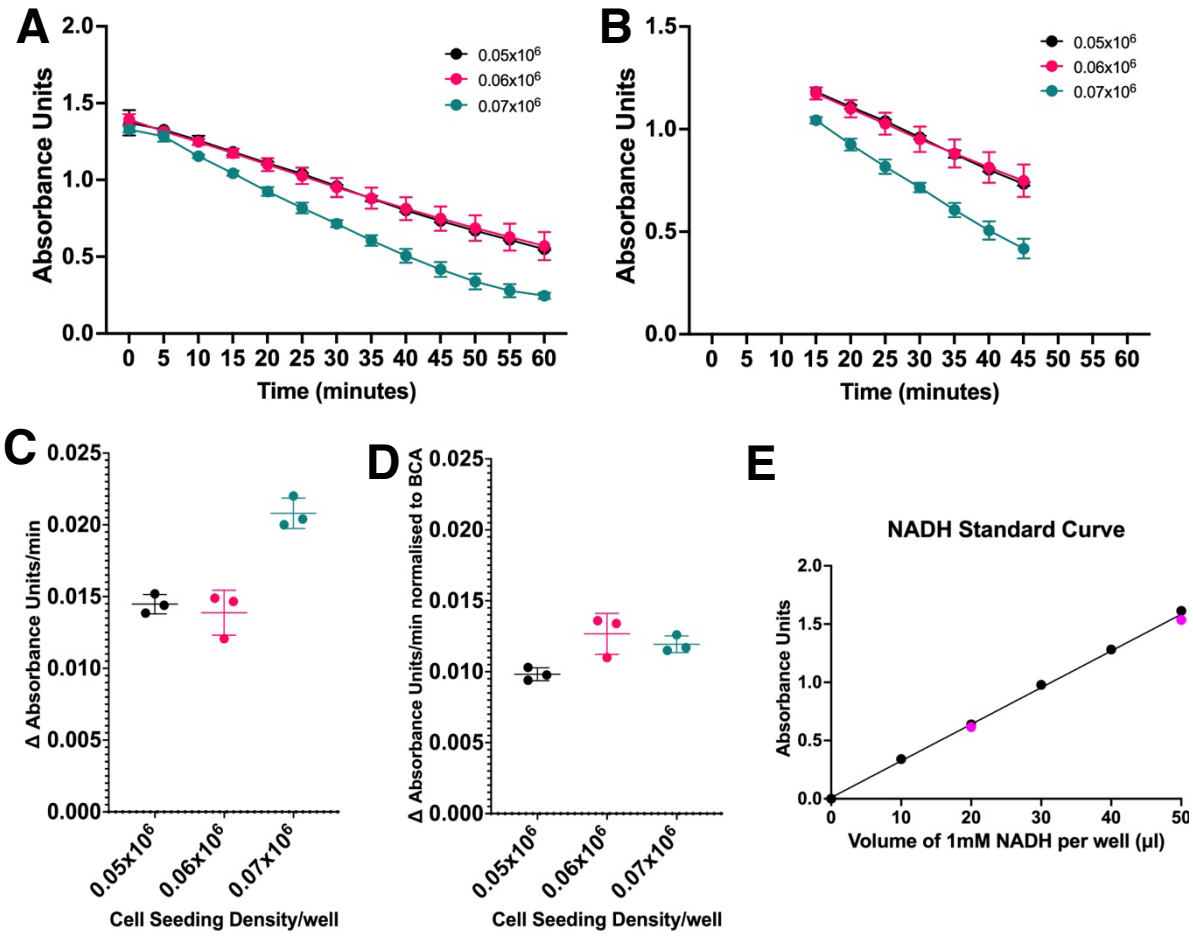

Figure 4.1: **Optimisation of the PGK1 metabolic assay. (A)** Raw absorbance curves at 340 nm from wells seeded at different seeding densities that were tested in triplicate (A). **(B)** Isolated linear parts of the progress curves from the raw absorbance curves in (A) showing the period where the reaction rate is constant. **(C)** Change in absorbance at 340 nm per minute calculated from the slopes from the linear part of the raw reaction curves indicating the reaction rate. **(D)** Rate of reaction normalised to the BCA result for each well to adjust reaction rate to total protein. **(E)** The NADH standard curve showing strong correlation between absorbance at 340nm and NADH. Repeats of 20 μl and 50 μl volumes of NADH are shown in magenta. Coefficient of determination (R^2) = 0.9979.

4.3.2 Screening the Atomwise compound library for PGK1 activity

The optimised PGK1 metabolic activity assay was performed on all 89 compounds identified by AI drug discovery company Atomwise as being predicted to interact with PGK1 and two hidden DMSO negative controls. HEK-293 cells were plated in 24 well plates at $0.06x10^6$ cells per well. The compounds were added 24 hours after plating and the metabolic assay was performed 24 hours after the compounds were added. An initial testing concentration of 10 μM is typical for a high throughput discovery screen with the concentration of promising compounds then being optimised by performing dose response experiments (Bell et al. 2024). Cells were plated in 24 well plates and to achieve the desired initial compound concentration of 10 μM, 0.5 μl of 10 mM stock compound was added to each well to make a total volume of 0.5 ml per well with three wells per 24 well plate used for DMSO controls. I was blinded to the additional two negative DMSO controls that were amongst the 91 samples from Atomwise.

Unfortunately, it was not practical to perform the metabolic assay on all compounds at the same time due to the time sensitivity of the metabolic assay. Instead, the compounds were spread across five 24 well cell plates with three DMSO control wells included on every plate (Figure 4.2 A-E). For the metabolic assay, cell lysates were acquired from each well of the 24 well cell plates and tested in technical duplicate in 96 well assay plates. This meant that two of the 24 well cell plates could be tested on the same assay plate but a total of three metabolic assay plates were still needed per screen to include all the compounds and controls. The full screen was run in total three times (n=3) so that each compound was tested on three separate occasions in technical duplicate each time and the mean PGK1 activity was calculated for each compound in each screen. PGK1 activity is shown normalised to the BCA result for each well to account for variation in cell number, particularly between plates and runs. After normalisation to BCA, I also normalised to the mean result for the DMSO controls. This allows us to visualise the increase or

decrease in PGK1 activity more easily as a result higher than 1 indicates that the compound produced a relative increase in PGK1 activity whereas a result lower than 1 indicates that the compound reduced PGK1 activity relative to the DMSO control. For each of the 24 well cell plates I have chosen to include the mean values for each DMSO control well along with the compound treated wells so that the variability of assay can be appreciated. It should be noted that variability does seem to vary per plate, and this was taken into consideration when selecting lead compounds (Figure 4.2.C, Figure 4.2.D).

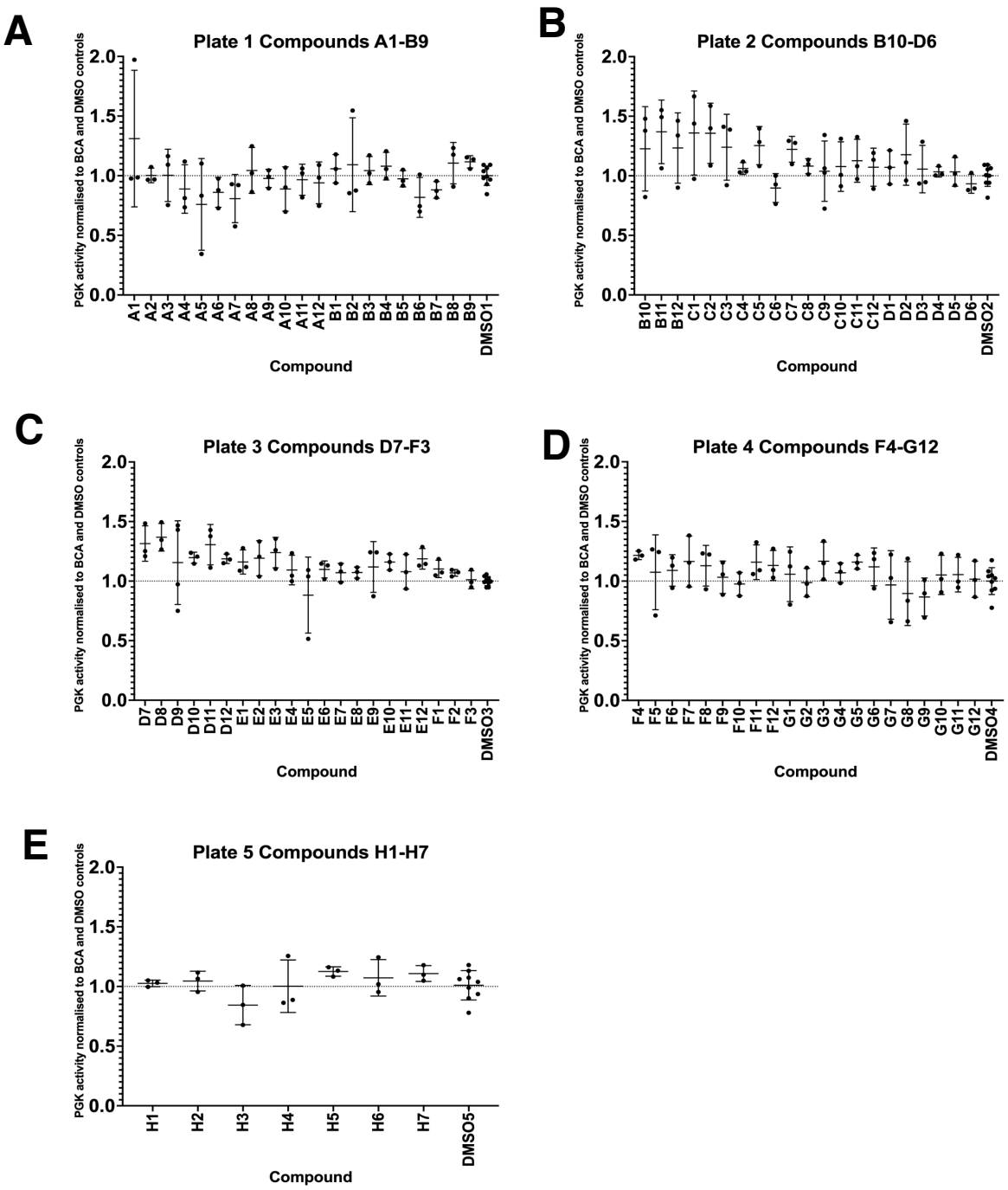

Figure 4.2: **Screening results showing PGK1 activity normalised to BCA and mean DMSO control following administration of compounds to HEK-293 cells separated by 24 well cell plate. (A)** Shows results of compounds A1-B9 and the DMSO controls **(B)** Shows results of compounds B10-D6 and the DMSO controls **(C)** Shows results of compounds D7-F3 and the DMSO controls **(D)** Shows results of compounds F4-G12 and the DMSO controls **(E)** Shows results of compounds H1-H7 and the DMSO controls. The dotted line at 1.0 represents the mean activity of the DMSO controls for that plate so that mean values above 1.0 represent increased PGK1 activity and means below 1.0 represent decreased PGK1 activity. The mean for each well is shown of each of the three repeat screens. Three wells per plate per screen were for DMSO controls so the mean of all 9 DMSO wells in total is shown for each plate.

4.3.3 Selection of lead compounds

Due to the number of compounds to be screened and the setup of the metabolic activity assay not all the compounds could be screened within the same plate or on the same day. However, I needed to be able to compare the compounds to select a group of lead compounds to take forward into models of disease along with terazosin. Figure 4.3 shows the graphs from Figure 4.1 combined so that the relative scale of PGK1 activation can be more clearly visualised between the compounds from different plates. The PGK1 activity screen was completed for each compound on three separate occasions (n=3). For each experiment, PGK1 activity was normalised to both the BCA assay result for the well to normalise to total protein levels and then normalised to the result from the DMSO treated wells from the same plate. This attempts to account for some of the expected variability between plates and gives the increase or decrease in PGK1 activity relative to the controls. Looking across the plates it was clear that the variability of the assay was not consistent, therefore just taking the compounds with the greatest level of PGK1 activation may not be the best approach to select lead compounds. There are multiple statistical methods described for determining 'hit' compounds from libraries including comparing compounds with the mean result of a negative control +/- 2-3 standard deviations and comparing compounds with the mean across the whole plate (Malo et al. 2006; Gero et al. 2013). Given this is a relatively small, targeted compound library and there may be proportionally more active compounds than a more typical high throughput screen, I decided to compare compounds to the mean and standard deviation of the control wells of DMSO included on each plate. I found that using the mean +/- 2 standard deviations appeared to provide a good balance in trying to identify some potential PGK1 activators to take forward whilst separating out enough probable background noise. I calculated the mean DMSO result for each run of each plate +/- 2 standard deviations (SD) and recorded whether the result for each compound was greater or lower than this range. Seven compounds, shown in blue in Figure 4.3, showed increased PGK1 activity greater than the mean DMSO

+2SD in all three runs of the screen. A further 15 compounds, shown in yellow in Figure 4.3, showed increased PGK1 activity greater than the mean DMSO +2SD in two runs of the screen. There were 3 compounds which had reduced PGK1 activity lower than the mean DMSO -2SD in two of the three runs of the screen, these compounds have potential PGK1 inhibitor activity.

Compounds selected to take forward as lead compounds:

D7, D8 and D11 had the highest mean PGK1 activity of those compounds that increased PGK1 activity greater than the mean DMSO + 2SD on all three runs of the screen.

D12 also showed increased PGK1 activity that was greater than the mean DMSO + 2 SD on all three screens. This has been selected despite others having higher overall means due to how consistent the results from this compound were with very little variability seen between screens.
All the compounds that showed an increased PGK1 activity greater than the mean DMSO + 2SD on all three screens were all found on the same plate (Plate 3). The variability in the DMSO control wells will be contributing to this to a degree and this varies slightly by plate. Multiple compounds from Plate 2 showed increased activity greater than the DMSO mean + 2SD on two of the three screens and as **B11** had the highest mean of these, it was included in our lead compound group.

Like B11, **F4** was selected because it increased PGK1 activity greater than the DMSO mean +2SD on two of the screens and was on another plate. F4 was also very consistent with little variability between the three runs of the screen.
B6 is a potential inhibitory compound. It showed decreased PGK1 activity of less than the mean DMSO – 2SD on two of the three screens and had the lowest mean PGK1 activity of the potential inhibitory compounds. A novel PGK1 inhibitor would also be interesting to help understand more about the

enzyme and potentially include as a comparator in future screening experiments.

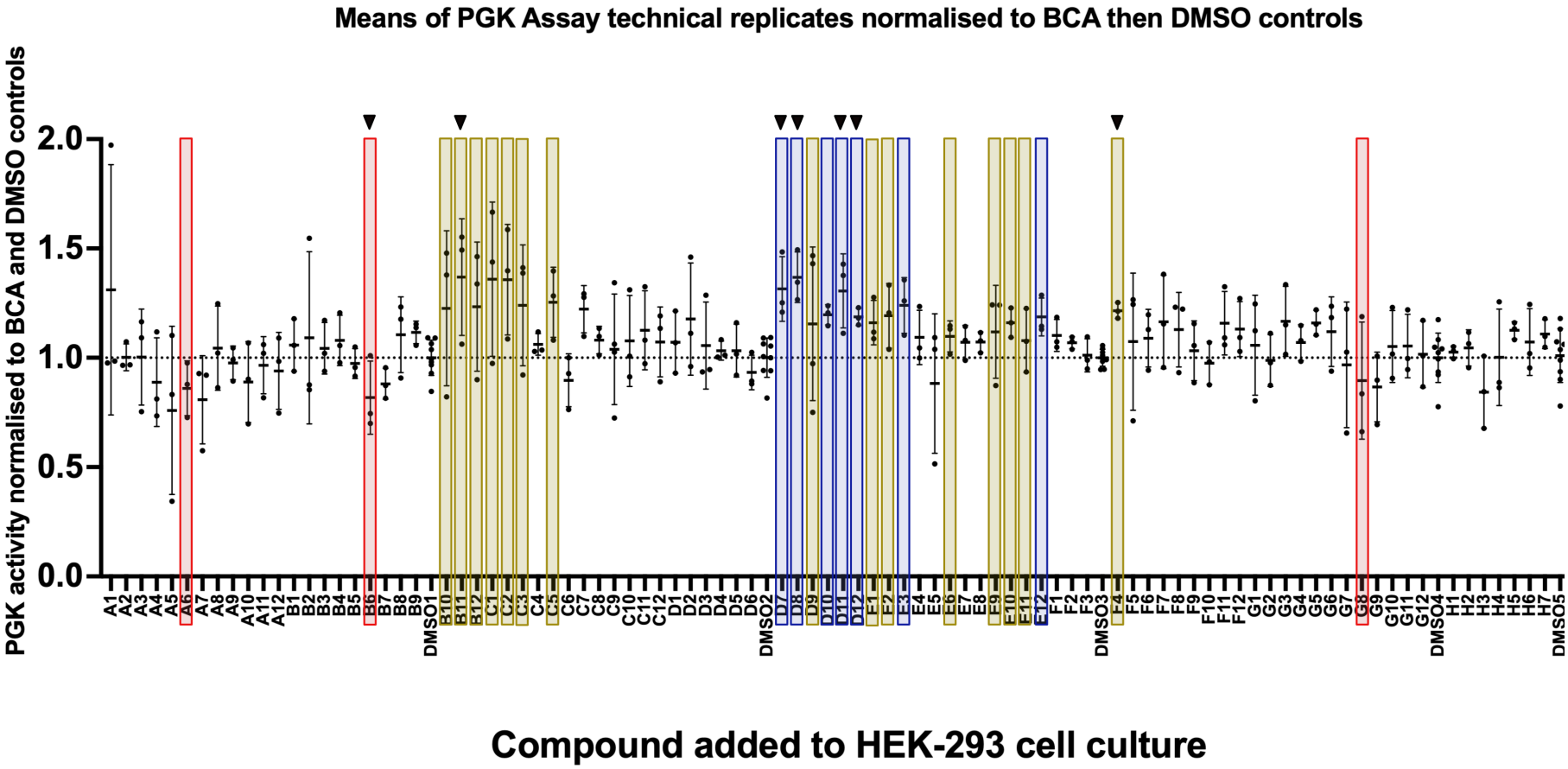

Figure 4.3: **Combined graph showing PGK1 activity normalised to BCA and mean DMSO control following compound administration.** PGK1 activity normalised to BCA and DMSO controls from the 5 separate cell plates visualised on a combined graph with DMSO controls from each plate also shown showing the effect of each compound on PGK1 activity in HEK-293 cells. The 7 compounds highlighted in blue produced increased PGK1 activity in the HEK-293 cells that was greater than the mean +2SD of the DMSO controls on all 3 runs of the screen. The 15 compounds highlighted in yellow showed increased PGK1 activity greater than the mean +2SD on 2 runs of the screen. The 3 compounds highlighted in red showed reduced PGK1 activity less than the mean -2SD of the DMSO controls on at least 2 of the screens This figure allows for the visualisation of the compounds selected to take forward as lead compounds which are indicated by the black triangles.

4.4 Discussion

In this chapter, I took advantage of the fast growing and easy to maintain nature of the HEK-293 cells to screen a compound library of small molecules for their ability to increase PGK1 activity. I was blinded to the molecule structures so that the screen could be completed impartially.

4.4.1 Selection of lead compounds

Lead compounds were selected from the screen based on both the magnitude of PGK1 activation as well as the consistency of that activation across the three runs of the screen. The strongest candidate for PGK1 inhibition was also included in this group to test in other models as this may prove to be a useful negative control compound. The criteria for selection into the lead compound group is relatively arbitrary and given that many of the compounds show similar degrees of PGK1 activation several of the other compounds would also have been suitable for inclusion in the lead compound group. This does mean that should none of the lead compounds show any promise in future experiments, it would be possible to return to the PGK1 activity screen and reselect a set of new promising compounds. It should be noted that I remain blinded to the structural properties of these compounds and so selection into the lead compound group is not based on any pharmacological properties and is solely based on the effect on PGK1 activity seen following administration to HEK-293 cells.

4.4.2 Future work

The work in this chapter has delivered a group of compounds that show promise in terms of their ability to increase PGK1 activity in HEK-293 cells based on the PGK1 metabolic assay. The next step to check their therapeutic potential is to test these compounds in an *in vivo* model system.

Should any of the compounds show promise in disease models, investigating their interaction with PGK1 and in particular how they activate PGK1 would be important. Terazosin is thought to increase PGK1 activity by binding at the same site as ADP (Chen et al. 2023). This binding site is likely to be why a biphasic response to terazosin has been observed, where terazosin can be inhibitory at higher doses (Riley et al. 2024). Whilst beyond the scope of this specific project, finding a way of increasing PGK1 activity that uses an alternate binding site would be valuable to further PGK1 targeted therapy development.

4.4.3 Conclusion

In this chapter, I showed the optimisation of the PGK1 metabolic assay using HEK-293 cells. Using this PGK1 metabolic assay I was able to screen the AI generated compound library for PGK1 activity and select a group of lead compounds that showed the most promising increase in PGK1 activity based on both the extent and consistency of activation.

Chapter 5: Screening potential PGK1 activating compounds in zebrafish

5.1 Introduction

Lead compounds that increased PGK1 activity in HEK-293 cells were identified using a PGK1 metabolic assay (Chapter 4). To understand whether any of them have the potential to be developed further into a therapeutic, it is important to know whether they also have an effect *in vivo*. By using a zebrafish model, I can screen all the lead compounds relatively quickly to select the most promising compound to take forward. In this chapter, I used the C9orf72 knockdown ALS model on a hb9:GFP transgenic zebrafish background line to screen potential PGK1 activating compounds as identified from the previous HEK-293 cell screen (Ciura et al. 2013; Flanagan-Steet et al. 2005).

5.1.1 Zebrafish in bioscience research

Zebrafish (*Danio rerio*) are small freshwater fish native to South Asia. They have been used to model human disease since 1980s due to their ability to regularly produce large clutches of quickly developing eggs and their high genetic homology to humans (Streisinger et al. 1981; Howe et al. 2013). Zebrafish eggs are fertilised and develop outside the body of the mother and do not fall under the Animals (Scientific Procedures) Act (ASPA) 1986 regulations until they are 5 days old when they exhaust their yolk and begin independently feeding. The breeding of zebrafish also makes them attractive to researchers, as in the wild spawning is triggered by dawn and so the timing of clutch production can be planned using light cycles. This means that it is straightforward to deliver interventions to the embryos at planned developmental timepoints. A detailed annotated zebrafish reference genome is available allowing the easier identification of zebrafish orthologues to genes

of interest making zebrafish an even more popular model for transgenic research (Howe et al. 2013). This reference genome should be consulted before embarking on a set of zebrafish experiments as the last common ancestor between zebrafish and humans was around 340 million years ago and so there are many significant genetic differences between the species that need to be considered (Amores et al. 2011). Fortunately, around 70% of human genes do have a zebrafish orthologue (Howe et al. 2013). PGK1 is a highly conserved enzyme and the zebrafish pgk1 gene is one of those that is orthologous to human PGK1 (Figure 5.1).

Compounds can be administered to the zebrafish embryos for drug screening purposes by adding them to their water. This adds an additional variable that would not be present in mammals in that there is an assumption that the compounds are able to cross into the egg in such a way that all embryos are exposed to the same concentration of compound which may not always be the case. However, being able to administer drugs in this manner is practical for larger scale approaches as it avoids the need to administer the compounds to each individual embryo separately. Drug screening in this manner has been performed for multiple neurological conditions including spinal muscular atrophy (Oprisoreanu et al. 2021), seizures (Sourbron et al. 2019) and Parkinson's disease (Vaz et al. 2020) .

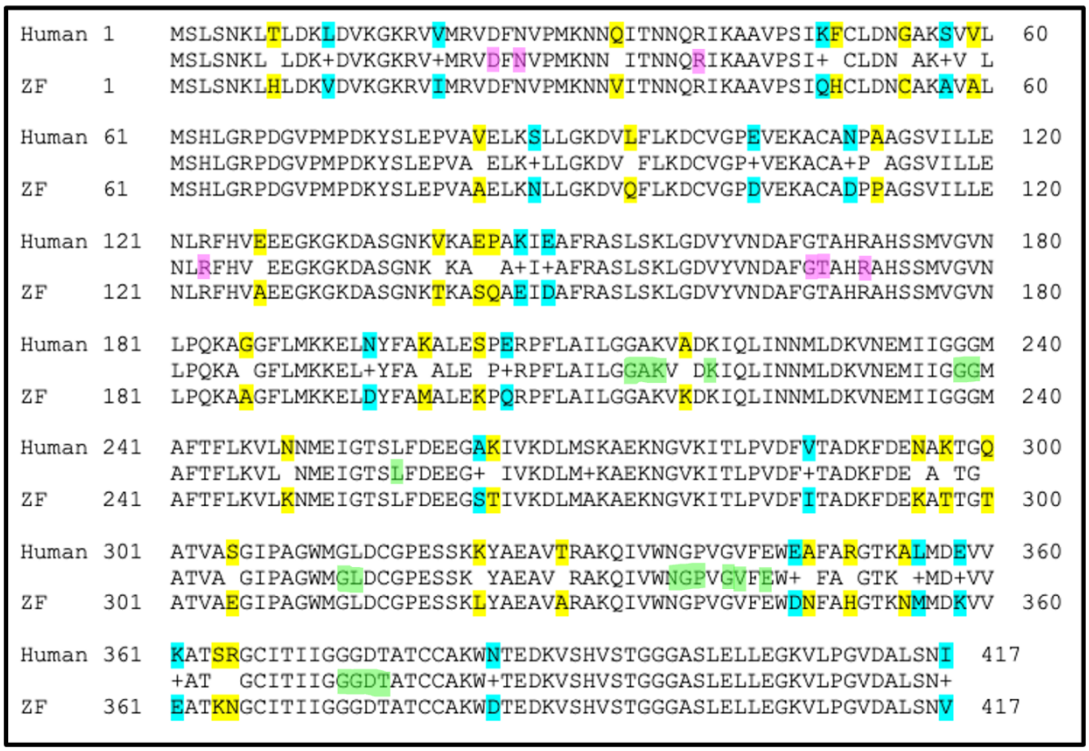

Figure 5.1: Comparison of the human and zebrafish (ZF) PGK1 proteins conducted using the Protein Basic Local Alignment Search Tool (BLASTp) (Altschul et al. 1997). The aligned amino acid sequence is shown where the positions highlighted in yellow represent where there is a mismatch in amino acid sequence and the positions highlighted in blue show where there is a different but similar amino acid between the two sequences. 88% of the total amino acids are identical between the two proteins. The key residues involved in the binding of 3-PG (pink) and ADP (green) which allow the kinase function of PGK1 are also shown and these are 100% conserved between the two sequences (Fiorillo et al. 2018).

5.1.2 The C9orf72 knockdown zebrafish model

As neuroanatomical features and neurotransmitter systems have been shown to be well conserved in zebrafish they have become an important tool to investigate disease mechanisms and conduct drug screenings in multiple neurological conditions (Rosa, Lima, and Lopes-Ferreira 2022; Saleem and Kannan 2018). Despite the similarities in the nervous system of zebrafish and humans, there are key differences including the ability of adult zebrafish to regenerate spinal cord neurons which need to be considered (Becker et al. 1997).

The hb9:GFP zebrafish line is a transgenic line which expresses GFP protein in cells that are positive for the transcription factor hb9 (*Mnx1*) which is considered specific for spinal cord motor neurons (Flanagan-Steet et al. 2005).The advantage of this line is that as they are also transparent the developing motor axons of the embryonic fish can be easily visualised and imaged. The model is induced in each embryo individually by injecting the egg with a morpholino. A morpholino is a synthetic single-stranded oligonucleotide which binds to the mRNA of the protein of interest to block protein translation (Bill et al. 2009). To knockdown endogenous C9orf72, the hb9:GFP zebrafish eggs are injected when they are at the 1-2 cell stage with the ATG-targeting phosphorodiamidate morpholino oligomer (MO) (ATTGTGGAGGACAGGCTGAAGACAT) (Ciura et al. 2013). This means the breeding of the zebrafish needs to be controlled the morning of the microinjections as the embryos typically develop beyond the 2-cell stage only around 1 hour post fertilisation (hpf) (Kimmel et al. 1995). This approach has been shown to produce an axonopathy that can be partially rescued by treatment with 10 μM terazosin or PGK1 overexpression (Ciura et al. 2013; Chaytow et al. 2022). In this model, the embryos are collected for analysis at 30 hpf. This is comfortably within the 5 days post fertilisation (5 dpf) permitted by ASPA but enough time for the motor axons of the embryos to have

developed enough for analysis. In zebrafish, the spinal motor neurons develop in two stages with axons following predictable paths. Initially all primary motor neurons extend along a common pathway. The horizontal myoseptal region is at the distal end of the common pathway and it is at this point where the primary motor neurons split into their cell-specific pathways (Beattie 2000). It is a common point where development stops in the case of an axonopathy and whether an axon develops past the horizontal myoseptal region is considered when scoring the axon phenotype (Oprisoreanu et al. 2021). In normally developing embryos, the caudal primary motor axon has a straight unbranched axon extending from the spinal cord to the ventral edge of the somite at 30 hpf. This makes measuring the length and phenotype of the caudal primary motor axons at the 30 hpf timepoint ideal as outputs to assess changes in axon development in response to treatments.

5.1.3 Lead compounds

In this chapter I screened the lead compounds identified from the metabolic assay performed in HEK-293 cells in Chapter 4: B11, F4, D7, D8, D11 and D12. B6 will also be screened as a potential PGK1 inhibitor. Terazosin was included as a positive control as there is previous published data from our lab that shows treatment with 10 μM terazosin improved the motor axon length and phenotype in this model (Chaytow et al. 2022). Another compound that I am interested in is compound 12b. Compound 12b is not from the AI generated compound library but instead has been published by another group researching terazosin analogs (Wang, Qian, et al. 2022). Compound 12b showed the strongest PGK1 agonist activity of the compounds tested and had neuroprotective properties in the MPP^+ induced SH-SY5Y cell injury model of Parkinson's disease that were superior to terazosin at their testing concentration of 2.5 μM. However, there is not yet any published data on the effectiveness of compound 12b *in vivo* or in models of ALS. Including compound 12b in the zebrafish screen is a good opportunity to see how a

compound that has performed well in multiple *in vitro* experiments performs in an *in vivo* model and it may prove to be a useful comparison compound for the ones from the AI compound library.

5.2 Aims

The aim of this chapter was to screen the lead compounds identified by the PGK1 metabolic activity screen in HEK-293 cells in an *in vivo* model system of ALS. To achieve this, I:

1. Demonstrate the C9orf72 knockdown model induces a phenotype in the motor axons of hb9:GFP zebrafish embryos.
2. Evaluate the lead compounds for their ability to improve motor axon length and branching phenotype in the zebrafish model.
3. Assess whether there is sufficient evidence to take the most promising compound into another *in vivo* model.

5.3 Results

5.3.1 The C9orf72 knockdown model

To induce the C9orf72 knockdown, a microinjection of 1 nl of 0.02 mM C9orf72 morpholino (MO) was injected into the yolk of a fertilised zebrafish egg at the 1-2 cell stage (Flanagan-Steet et al. 2005). The method (see Methods) relies on a breeding pair of fish producing a healthy clutch of eggs to be used for the microinjections. Although I was using an established transgenic line, in the beginning I had multiple instances where the breeding pairs did not produce eggs, produced too few eggs or produced eggs that did not develop normally. Clutches with a survival of less than 90% in the uninjected control group were discarded. The unreliable production of good clutches meant that the compound screening progressed more slowly than expected. The poor breeding was likely due to a combination of issues including the adult zebrafish getting older and having been inbred for multiple generations to maintain the hb9:GFP transgene. To address these problems, I bred the fish to raise new breeding adults in two ways – both an in-cross and an out-cross with a wild type line on an alternative background strain kept by the facility for this purpose. Embryos were sorted at around the 30 hpf stage to only keep the embryos for future breeding that demonstrate the GFP expression in their spinal cord and motor axons (Figure 5.2.A). As data collection had already begun by the time the new breeding fish had reached sexual maturity, the following zebrafish experiments were all performed on clutches from the original fish or the in-cross so as to not introduce variability in the experiments by including clutches from a different background strain of zebrafish.

The C9orf72 morpholino was injected into the eggs at the 1-2 cell stage and the eggs incubated at 28.5 °C until they reach 30 hpf where they are collected. The embryos were dechorionated and fixed in PFA before the yolks are removed so that they could be positioned relatively flat on microscope slides to image the GFP.

The motor axons of the zebrafish embryos are adversely affected by the knockdown of endogenous C9orf72 with the C9orf72 MO. This results in reduced motor axon length, more branching and absent axons in severe cases (Figure 5.2.B). To assess the effect of the compounds in this model I measured motor axon length and assess the branching phenotype of the motor axons. Measuring of the length of the motor axons was done using the Simple Neurite Tracer plugin in ImageJ. A scoring system is in place to score the phenotype of each axon on a scale from 0 (severely affected) to 3 (healthy) to take into account the branching abnormalities that can result from the C9orf72 MO (Figure 5.2.C). Healthy axons have developed normally with no branching and extended far beyond the horizontal myoseptum (grade 3). Mildly affected axons have developed past the horizontal myoseptum but may be either truncated or distally branched (grade 2). Moderately affected axons may have stalled their development in the horizontal myoseptum region or show proximal branching (grade 1). Axons that are absent or have not extended as far as the horizontal myosteptum were considered to be severely affected (grade 0).

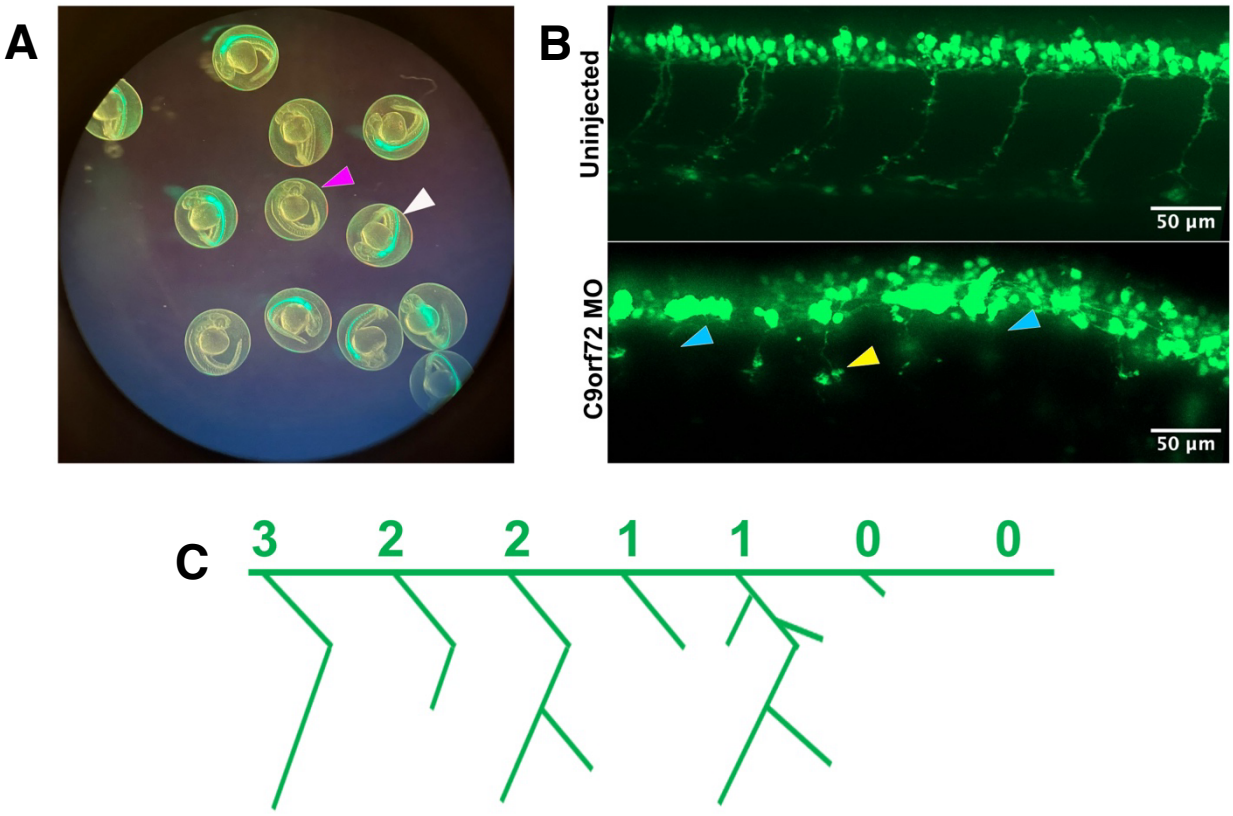

Figure 5.2: The C9orf72 knockdown model in an hb9:GFP zebrafish line. (A) Example zebrafish embryos at approximately 30 hpf being sorted for GFP expression where the embryos expressing GFP in their motor neurons (white arrow) were separated from those not expressing GFP (magenta arrow). **(B)** Example images of the maximum intensity image projections of the first 6 motor neurons following the yolk sac from both an uninjected control hb9:GFP fish and an hb9:GFP fish from the same clutch injected with C9orf72 morpholino. Examples of absent motor axons (blue arrows) and shortened motor axon length (yellow arrow) Scale bar = 50 μm. **(C)** Scoring system used to score the phenotype of each axon from 3 (healthy) to 0 (severely affected).

5.3.2 Screening lead compounds in the C9orf72 knockdown model

The lead compounds identified from the screen for increased PGK1 activity in HEK-293 cells were B11, F4, D7, D8, D11 and D12. B6 had the greatest potential as a PGK1 inhibitor and so was also included. Similar published experiments showed that terazosin did improve the motor axon length and phenotype in this model, so terazosin was included as a positive control (Chaytow et al. 2022). The eggs from each clutch were randomly assigned to one of four groups, an uninjected control group, an injected group treated with DMSO and then two injected groups that would each be treated with one of the lead compounds. The embryos were separated into groups of 6 in a 24 well plate for the treatments which were added to the water and so a total of 36 embryos per condition. The numbers of embryos analysed for each group as shown at the bottom of each graph (Figure 5.3.A-D) is typically substantially less than this. This loss of embryos is typical and multifactorial with both clutch and experimental issues involved. In some clutches not all the eggs may have been fertilised, and the health of the clutch would vary which is why an uninjected control group is always included for every clutch. Some embryos would be lost due to the physical damage from the injection. The precise severity of the phenotype induced by the C9orf72 MO injections could be affected by multiple factors as well between clutch and between batch effect so the injected C9orf72 treated with DMSO was also an essential control. Occasionally whole clutches would need to be excluded because the phenotype was so severe that axons could not be clearly identified or whole groups had not survived. However, the most common cause of embryo loss from analysis was during the mounting of the embryos onto the microscope slides as even with the yolk removed they had a tendency to roll or twist which made acquiring the images needed for reliable analysis impossible.

Motor Axon Length

Treatment with 10 μM terazosin did significantly improve the motor axon length in the C9orf72 MO injected zebrafish (p=<0.001) whereas the potential inhibitor B6 did not significantly affect motor axon length (p=0.81). None of the lead compounds were found to affect mean axon length compared with the DMSO treated injected control: B11 (p= >0.99), F4 (p=0.11), (D7 p= 0.12), (D8 p=0.93), D11 (p= 0.18) and D12 (p=0.77)(Figure 5.3 A-D). The clutch in Figure 5.3.D shows a greater standard deviation and a less normal distribution than the other three clutches in Figure 5.3.A-C. It appears that there was a population of embryos in this clutch where the injection of C9orf72 MO was not effective and so did not produce a phenotype. Additionally, in this clutch the mean axon length of the other injected embryos in this clutch are relatively short suggesting a relatively severe phenotype in the embryos where the injection has appeared to have an effect. Therefore, I had less confidence in the results from this clutch screening D11 and D12.

Motor Axon Phenotype Score

The motor axon phenotype scoring system is more subjective than the mean motor axon length measurement, and I used the blinding tool in ImageJ to be blinded to the treatment conditions for both analyses. Twelve motor axons were scored from 0-3 for each embryo as discussed previously and the mean axon score calculated. Treatment with terazosin was found to improve motor axon phenotype (p=0.006) which is consistent with previously published work (Chaytow et al. 2022). Again, the potential inhibitor B6 (p=0.63) and lead compounds B11 (p=0.64), F4 (p=0.52), D11 (p=0.40) and D12 (p=0.43) did not affect the mean axon phenotype score compared with the DMSO treated controls (Figure 5.2.E,F,H). However, lead compounds D7 (p=0.04) and D8 (p=0.017) both showed a small improvement in mean axon phenotype score compared with the DMSO treated injected controls (Figure 5.2.G). Like the analysis for mean axon length, the clutch analysing the effect of D11 and D12

showed large standard deviations in the injected embryos supporting my suspicion from the results of mean axon length that the phenotypes induced by the C9orf72 MO injections in this clutch were too inconsistent to be considered reliable.

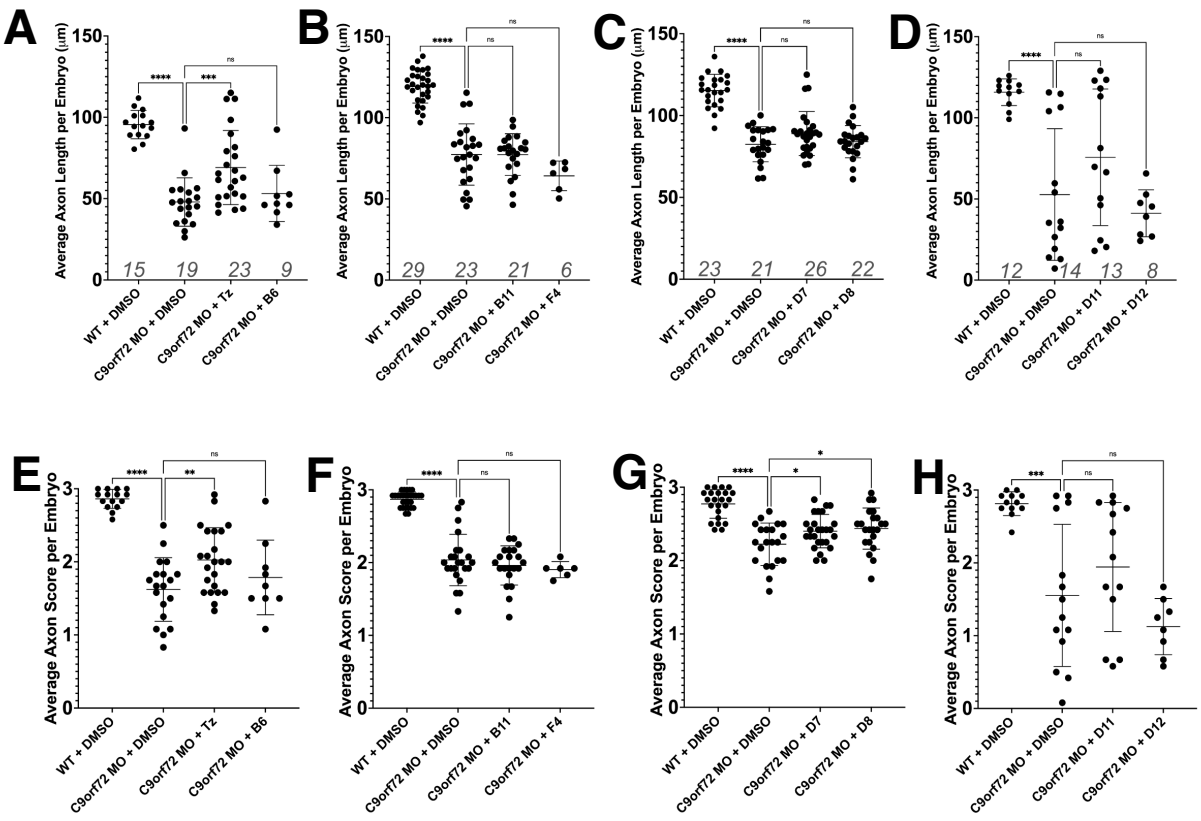

Figure 5.3: Screening lead compounds in a C9orf72 knockdown model in a HB9:GFP zebrafish line. Mean motor axon length per zebrafish embryo is shown following treatment with DMSO control and compared with treatment with one of the selected lead compounds: Terazosin (Tz) and B6 **(A)** B11 and F4 **(B),** D7 and D8 **(C),** D11 and D12 **(D).** The number of embryos analysed per group is shown in italics above the x axis. Each graph shows a single clutch with uninjected controls (WT) showing expected normal motor axon length development. Each axon was also scored based on its development and branching. The mean axon score for each embryo following treatment with DMSO control compared with treatment with one of the lead compounds: Tz and B6 **(E)** B11 and F4 **(F),** D7 and D8 **(G),** D11 and D12 **(H).** 6 pairs of motor axons were measured and scored per embryo. Statistical analysis was performed using an ANOVA with Dunnett's post hoc test to compare each mean with C9orf72 + DMSO.

5.3.3 Screening additional compounds in the C9orf72 knockdown zebrafish model

The results of the initial lead compound screen in the zebrafish C9orf72 knockdown model successfully repeated the findings of published work showing that terazosin treatment results in an improved phenotype but the lead compounds from the HEK-293 screen did not appear to have much effect. The clutch that screened compounds D11 and D12 produced an unreliable phenotype and so I rescreened these compounds in new clutches. In addition, a novel terazosin analog that showed improved PGK1 agonist activity in cells had been identified and published by another group (Wang, Qian, et al. 2022). I obtained a sample of this analog, known as compound 12b, and wanted to see whether the increased PGK1 activity observed in cells would translate to improved rescue of the C9orf72 MO model. To improve the chance of finding a promising compound to take forward, I also went back to the combined data from the HEK-293 screen and selected 3 more compounds that increased PGK1 activity in the HEK-293 cells: C1, C3 and D9.

Motor Axon Length

The compound C1 did not affect motor axon length in the C9orf72 MO injected embryos compared with the DMSO treated controls (Figure 5.4.A, p=0.26). Interestingly, the published terazosin analog compound 12b also did not improve motor axon length (Figure 5.4.B, p= 0.093). More promisingly, compound C3 (Figure 5.4.A, p=0.0060) and the repeat screens for compounds D11 (Figure 5.4.B, p=<0.0001) and D12 (Figure 5.4.C, p=0.0074) all showed an improvement in motor axon length compared with the DMSO treated controls.

Motor Axon Phenotype Score

Compound C1 also did not have an effect on motor axon phenotype compared with DMSO controls (Figure 5.4.D, p=0.56). Despite the effect seen on motor

axon length, neither C3 (Figure 5.4.D, p=0.81) or D12 (Figure 5.4.F, p=0.38) had an effect on motor axon phenotype score. Conversely, the terazosin analog compound 12b which did not affect motor axon length, did improve the mean motor axon phenotype score (Figure 5.4.E, p= 0.0005). D11 was the only compound screened which like terazosin which improved both motor axon length and motor axon phenotype score (Figure 5.4.E, p=<0.0001).

Compound D9

Compound D9 was screened in the same clutch as D12 (Figure 5.4.C and F), however none of the motor axons from the D9 treated embryos (n=14) could be analysed or even detected due to the embryos failing to develop properly (Figure 5.4.G). Compared with an embryo that developed normally the yolk sac was larger (not shown), there was no visible sign of ocular development and the D9 treated embryo was comparatively smaller (Figure 5.4.H). There was no detectable GFP expression in the D9 treated embryos to take fluorescent images for analysis.

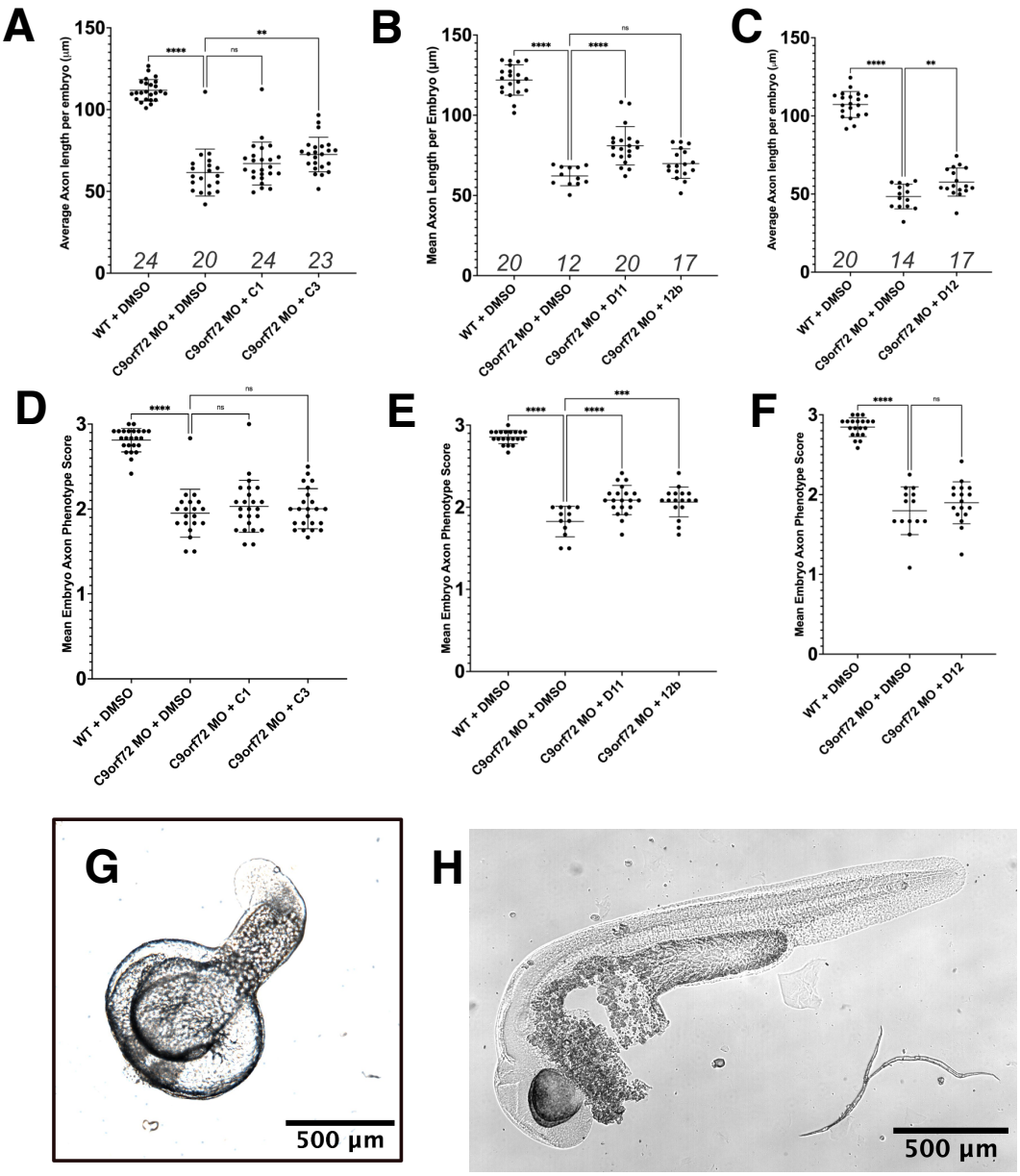

Figure 5.4: Screening additional compounds in a C9orf72 knockdown model in a HB9:GFP zebrafish line. Mean motor axon length per zebrafish embryo is shown following treatment with DMSO control and compared with treatment with one of the compounds: C1 and C3 **(A),** D11 and 12b **(B),** D12 **(C).** The number of embryos analysed per group is shown in italics above the x axis. Each graph shows a single clutch with uninjected controls (WT) showing expected normal motor axon length development. Each axon was also scored based on its development and branching. The mean axon score for each embryo following treatment with DMSO control compared with treatment with one of the lead compounds: C1 and C3 **(D),** D11 and 12b **(E),** D12 **(F).** 6 pairs of motor axons were measured and scored per embryo. Statistical analysis was performed using an ANOVA with Dunnett's post hoc test to compare each mean with C9orf72 + DMSO. A representative image of an embryo at 30 hpf following D9 administration is shown **(G).** A brightfield image taken of an embryo with its yolk sac removed at 30 hpf that has developed normally taken from another clutch by my colleague Dr. Hannah Smith is shown in **(H).**

5.3.4 Further exploring compound D11 in the C9orf72 knockdown zebrafish model

Given D11 was the only novel compound which improved both the motor axon length and phenotype score it was considered worthy of further investigation. There is some debate in zebrafish research about whether embryos from a single clutch can be considered individuals or if these are just technical replicates (Bedell et al. 2025). To address this, I repeated the D11 screen using two new clutches to achieve 3 independent experiments and analyse the results both at the level of the individual embryo and per clutch. Figure 5.5.A shows representative images of the axons of uninjected and C9orf72 MO injected controls to compare with the axons from D11 treated C9orf72 MO injected embryos.

Mean Axon Length

Mean axon length per clutch was not significantly changed by treatment with compound D11 (Figure 5.5.B, ANOVA, Tukey, p=0.88). If the embryos from the three clutches are considered as individual data points and clutch taken into account by using a mixed effects model then the mean motor axon length was improved by D11 treatment (Figure 5.5.C, mixed effects model followed by ANOVA and Tukey, p=0.0034).

Mean Axon Phenotype Score

A similar finding was found when the mean axon phenotype scores for the three clutches were analysed where the grouped mean axon scores per embryo did not show an improvement with D11 treatment at clutch level (Figure 5.6.A, ANOVA, Tukey, p=0.86). When a mixed effect model was used to analyse the mean scores from each embryo and take clutch into account as a random effect then D11 was found to improve axon phenotype (Figure 5.6.B, mixed effect model followed by ANOVA and Tukey, p=0.024). The spread of the grouped phenotype scores is shown for uninjected control embryos (Figure

5.6.C), injected DMSO treated control embryos (Figure 5.6.D) and injected D11 treated embryos Figure 5.6.E). The condition groups were compared to see whether the proportion of axons scored as healthy (Figure 5.6.F), mild (Figure 5.6.G), moderate (Figure 5.6.H) or severe (Figure 5.6.I) were different between the groups. D11 did increase the percentage of axons scored as healthy (ANOVA, Tukey, $p=0.0083$) but not the % of axons scored as mild (ANOVA, Tukey, $p=0.63$), moderate (Kruskal-Wallis, Dunn's, $p=0.052$) or severe (Kruskal-Wallis, Dunn's, $p=0.34$) when compared with the DMSO treated injected controls.

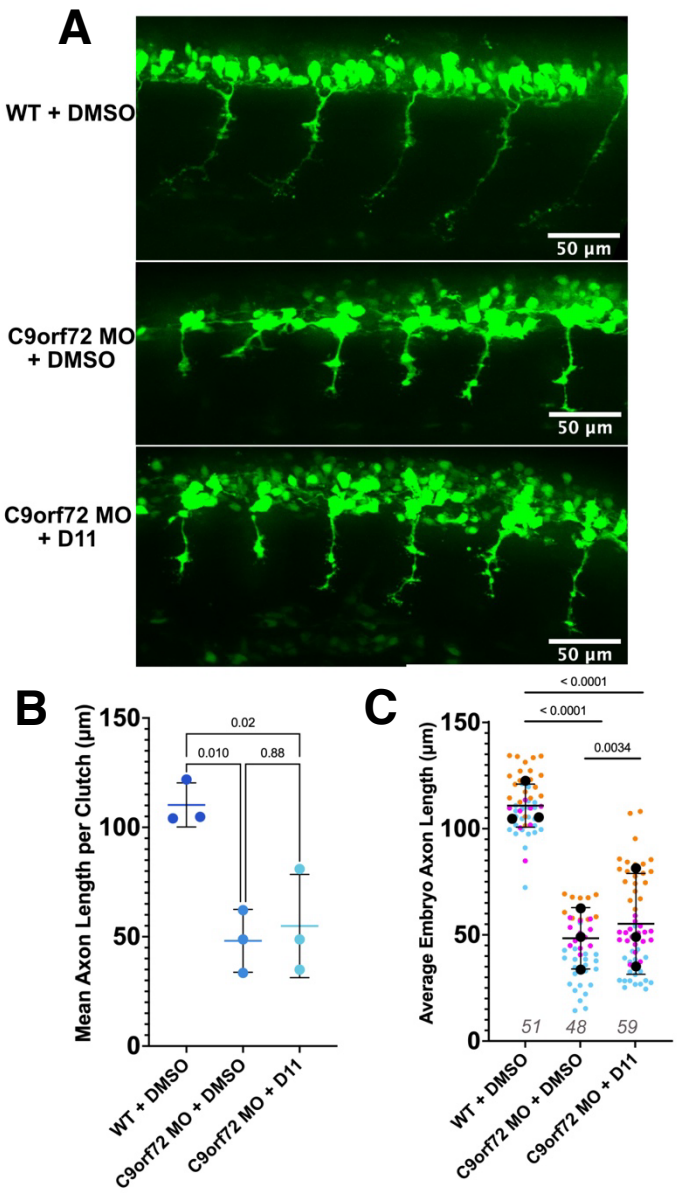

Figure 5.5: The effect of compound D11 treatment on mean axon length in a C9orf72 knockdown model in a HB9:GFP zebrafish line. (A) Example fluorescent images showing the maximum projection images of primary motor neuron outgrowth from an uninjected WT control, a C9orf72 knockdown and a C9orf2 knockdown treated with compound D11. **(B)** The mean axon length shown per clutch for each of the three different clutches analysed (n=3) showing D11 treatment did not significantly affect mean axon length following C9orf72 knockdown at clutch level. Statistical analysis was performed using an ANOVA with Tukey's multiple comparison post hoc test. **(C)** shows the mean axon length per embryo rather than per clutch with the mean of each clutch superimposed on top in black. Each of the three clutches is shown in a different colour (yellow, pink, blue). This was analysed using a mixed effects model to take clutch into account as a random effect. This showed that D11 did significantly improve mean axon length in C9orf72 MO injected fish compared with DMSO treated controls ($p = 0.0034$). The number of embryos analysed per group is shown in grey italics above the x axis. 6 pairs of motor axons were measured per embryo. P-values are displayed on the graphs.

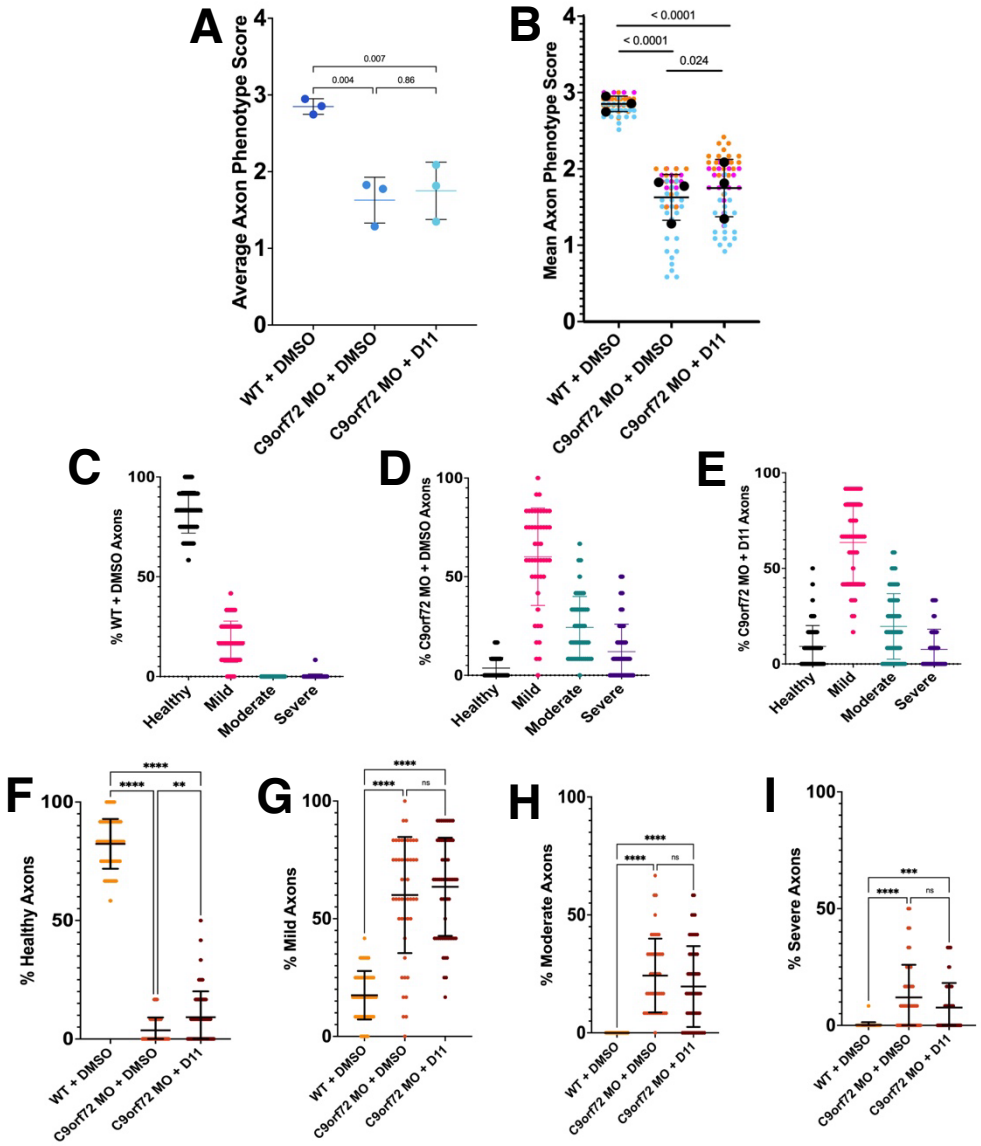

Figure 5.6: The effect of compound D11 treatment on axon phenotype in a C9orf72 knockdown model in a HB9:GFP zebrafish line. (A) Mean axon phenotype score per clutch (n=3) in uninjected WT fish and C9orf72 morpholino injected fish treated with either DMSO or compound D11 showing that D11 treatment did not significantly affect mean axon score following C9orf72 knockdown at clutch level (p= 0.86). Statistical analysis was performed using an ANOVA with Tukey's multiple comparison post hoc test. **(B)** The mean axon score shown per embryo with embryos from each of the three clutches displayed in a different colour (yellow, pink, blue). This was analysed using a mixed effect model to take clutch into account as a random effect. This found that D11 did improve axon phenotype score compared with DMSO treatment (p= 0.024). The spread of mean axon phenotype scores per embryo is shown in **(C)** uninjected WT, **(D)** C9orf2 morpholino injected embryos treated with DMSO and **(E)** C9orf72 morpholino injected embryos treated with D11. Comparison of percentage of **(F)** healthy axons, **(G)** mild axons, **(H)** moderately affected axons and **(I)** severely affected axons per embryo in uninjected WT fish and C9orf2 morpholino injected fish treated with either DMSO or D11. After checking the data for normality, statistical analysis was either performed using an ANOVA with Tukey's multiple comparison or a Kruskal-Wallis Test followed by Dunn's multiple comparison test if the data did not have a normal distribution. The percentage data in graphs C-I was transformed using arcsine transformation before analysis. 6 pairs of motor axons were scored per embryo.

5.4 Discussion

5.4.1 Screening lead compounds in zebrafish

The initial lead compounds and additional compounds selected from the HEK-293 screen detailed in Chapter 4 were screened in the C9orf72 knockdown zebrafish embryo model. Terazosin was included in the screen as a positive control as there is published data showing a positive effect in this model with terazosin treatment (Chaytow et al. 2022). The results of my screen replicate the published terazosin findings with an improvement in both motor axon length and motor axon phenotype score observed with terazosin treatment. Of the other compounds screened, including the terazosin analog compound 12b, only compound D11 showed improvement in both motor axon length and phenotype score in the first clutch. However, this finding was not replicated when the experiment was repeated in a further two clutches.

5.4.2 Clutch and Model Variability

Small changes can affect the development of the normal zebrafish embryos including husbandry and parental factors. The variation in means of motor axon length and phenotype score seen across the uninjected control fish groups are due to these interclutch effects and demonstrate the importance of including this control group to help assess the overall health of the clutch and confirm that the disease phenotype has been induced by the injection of the C9orf72 MO rather than another cause of impaired development. Another important source of variability with the model was the variation in the precise severity of the disease model induced by the C9orf72 MO injection. This can be seen in the differences in the mean axon lengths of the C9orf72 MO injected embryos treated with DMSO between the clutches. To make the experiments as consistent as possible, the injection bolus volume used for each clutch was measured using a stage graticule. Despite this some clutches developed a more severe phenotype than others. There is therefore a concern that the

phenotype of some clutches may have been too severe for a rescue effect to be observed. This may have been the case for the additional D11 clutches as the rescue effect was only observed in the least severe clutch.

5.4.3 Compound 12b

It was interesting that whilst treatment with compound 12b mildly improved the axon phenotype in the embryos of the clutch it was tested in, it did not improve axon length and so a rescue effect was far from conclusive. Whilst an effect may be observable if further clutches were analysed, any effect of compound 12b on the C9orf72 MO injected embryos would seem to be very mild which was not predicted from its performance in multiple *in vitro* experiments (Wang, Qian, et al. 2022). It may be that compound 12b behaves very differently in cells compared with a whole organism, as appears to be the case with compound D9 which appears to be toxic to the zebrafish. Another reason that compound 12b may not have behaved as expected may be due to the concentration used. Compound 12b is an analog of terazosin and as discussed previously, the relationship between terazosin and PGK1 is complex which has resulted in a published biphasic dose-response effect (Chen et al. 2015). The published *in vitro* experiments showing the beneficial effects of compound 12b were performed at 2.5 μM whereas I tested it at 10 μM in the zebrafish model to maintain consistency between all the compounds tested. Unfortunately, it was not practical to do a full dose response curve for all of the identified lead compounds for this thesis.

5.4.4 B11

Following the zebrafish screen, I unblinded myself to the identity of the compounds included in the library that was screened in the HEK-293 cells in Chapter 4. Disappointingly, B11 was one of the hidden DMSO controls which was identified as a potential PGK1 activator in the HEK-293 cell screen.

Reassuringly for the zebrafish screen, B11 did not affect either motor axon length or motor axon phenotype score but this does suggest that the HEK-293 screen may not have been sensitive or reliable enough to select the most promising compounds. Looking back to Chapter 3 where I investigated the effect of PGK1 overexpression in HEK-293 cells, it can be seen that HEK-293 cells are relatively unaffected by increased PGK1 activity. An alternative cell model more similar to the zebrafish where a rescue effect can be observed may need to be explored to potentially rescreen the initial compound library.

5.4.5 Future Work

As I briefly touched upon earlier, further work could include dose-response experiments of the lead compounds to identify the optimal dose of each compound. This would have been performed if I felt like I had a strong enough candidate from the initial zebrafish screen to take into another disease model but it was not feasible to perform in all of the identified lead compounds. Measurements of motor axon length and motor axon phenotype score do not necessarily reflect the function of the fish. The C9orf72 MO model could be explored further with motor function tests such as the touch-evoked escape response test which measures the distance travelled after the tail of the embryo is touched. The C9orf72 MO model is also only one zebrafish model of MND and the effect of the most promising compounds could be investigated in others such as a TDP overexpression model or even a model of spinal muscular atrophy using an *smn* morpholino since the aim of targeting PGK1 is to target a common pathway in neurodegeneration.

For future zebrafish embryo experiments where the embryos are collected at 30 hpf, I would exclude clutches where the mean axon length of the injected control group is below 50 μm. A mean axon length below 50 μm would mean that the majority of the axons of the C9orf72 MO injected embryos did not

reach the horizontal myoseptal region and a phenotype that severe may be too extreme to reasonably expect to see a rescue.

5.4.6 Conclusion

In this chapter, I screened the lead compounds identified in Chapter 4 in a zebrafish model of ALS. Whilst using a zebrafish model has a lot of benefits, it does require considerable time and skill to get the most consistent disease phenotypes with this model as it requires microinjecting each egg. D11 was the most promising compound but ultimately the rescue effect was not significant at clutch level. The reveal of B11 as one of the DMSO controls hidden among the potential PGK1 agonists means that potentially better PGK1 agonists may have been missed by the initial HEK-293 screen. Finding a suitable alternative screening model to assess compounds for their ability to increase PGK1 activity is now a priority.

Chapter 6: Investigating other cell models for improved PGK1 screening

6.1 Introduction

Results of screens in HEK-293 cells and in a zebrafish model of ALS have shown the need to develop an alternative *in vitro* model to screen potential PGK1 activating compounds. When PGK1 was overexpressed in HEK-293 cells, I showed that PGK1 overexpression was well tolerated and had little effect on the cells (see Chapter 3). This may explain why the screen of potential PGK1 activators in HEK-293 cells may not have resulted in the best PGK1 activators being selected as lead compounds (see Chapter 4). A model where there is a deficit in PGK1 activity that could be rescued by a PGK1 activator would be preferred for the purposes of compound screening.

6.1.1 NSC-34 Cells

NSC-34 cells are a hybrid murine cell line of neuroblastoma cells with motor neuron enriched spinal cord preparations that were described in 1992 (Cashman et al. 1992). They are used regularly to investigate mechanisms of MND as they share multiple properties with motor neurons when differentiated including having long neurite outgrowths, the ability to establish contacts with myotubes in culture and expressing neurofilament proteins (Cashman et al. 1992). Differentiation protocols for NSC-34 cells vary, with both retinoic acid and prostaglandin E_2 used for differentiation. Prostaglandin E_2 has been reported to result in faster differentiation compared with retinoic acid, but as retinoic acid seems to be the most common method, I used differentiation media containing retinoic acid for this set of experiments (Nango et al. 2020). Even within the papers that use retinoic acid there are differences in protocols, particularly in regards to how long cells are differentiated for, with published papers reporting times from 4 days through to 4 weeks (Johann et al. 2011;

Madji Hounoum et al. 2016). Differentiation of the NSC-34 cells using 1 μM all-*trans* retinoic acid was found to increase both the number and length of neurite outgrowths from 4 days of differentiation so this should be sufficient at least for initial differentiation experiments (Maier et al. 2013).

6.1.2 NSC-34 cells stably transfected with TDP-43

The NSC-34 cells seemed promising as a starting point, but what we wanted was a cell model that may be a model of disease rather than just a model of a cell-type as this would be more likely to show a metabolic deficit. Mutations in TDP-43, such as the missense mutations A315T and M337V, have been associated with many familial cases of ALS (Gitcho et al. 2008; Tamaoka et al. 2010). Both these mutations fall within the glycine rich region of the TDP-43 protein which has been shown to be necessary for the association of TDP-43 with stress granules (Dewey et al. 2011). Stress granules are dynamic assemblies of non-translating mRNA protein complexes that form in the cytoplasm in response to various forms of stress (Protter and Parker 2016). When a cell is exposed to a stressor, TDP-43 is exported from the nucleus to the cytoplasm and is associated with other stress granule proteins, the stress granules then disassemble when the stressor is removed and under normal conditions TDP-43 returns to the nucleus (Yang et al. 2020; Uechi et al. 2025). The M337V mutation has been shown to reduce stress granule formation in response to oxidative stress in mouse ESC-derived motor neurons as well as disturbing other protein interactions (Feneberg et al. 2020).

The Noakes group based in the University of Queensland, Australia published a group of NSC-34 cell lines in 2021 that they reported to be stably transfected with different forms of human TDP-43 (Ding et al. 2021). Following five days differentiation with all-*trans* retinoic acid they subjected the different NSC-34 cell lines to a stressor and found that 1 hour and 24 hours following exposure to the osmotic stressor D-sorbitol, the cell lines expressing TDP-43 with either

the A315T or M337V mutations had both a greater number and larger stress granules than the cell line expressing wild type (WT) TDP-43. Mutated TDP-43 seems to interfere with stress granule dynamics, and therefore these NSC-34 lines may respond to cellular stressors differently. These differences may result in observable differences in cellular metabolism which could prove to be useful as a screening tool for potential PGK1 activators, and this chapter will focus on exploring this.

6.2 Aims

In this chapter, I investigated NSC-34 cells as a model to use for screening potential PGK1 activators. This chapter aims:

- To confirm and compare TDP-43 expression in the different NSC-34 lines
- To assess cellular metabolism and PGK1 activity in undifferentiated NSC-34 lines using the Seahorse assays and PGK1 metabolic assay
- To differentiate the NSC-34 cell lines and assess if this changes the measured parameters of metabolism
- To use a cell stressor on differentiated NSC-34 cells to see if an affected metabolic parameter is rescuable by PGK1 activators and therefore be a potential screening platform for further compounds.

6.3 Results

6.3.1 Expression of TDP-43 and GFP in NSC34 lines

We received multiple vials of frozen cells from the Noakes group from the four NSC-34 cell lines they have previously shown to stably be transfected with different forms of human TDP-43 (hTDP-43) (Ding et al. 2021). Before proceeding further experimentally with them, I wanted to confirm that the TDP-43 expression of the lines was what would be expected from the published data. Two forms of TDP should be present across the lines, endogenous mouse TDP-43 and hTDP-43 fused with enhanced green fluorescent protein (GFP). I will refer to the four lines as:

- **GFP**: NSC-34 cells only transfected with GFP and so expected to only express endogenous TDP-43
- **WT**: NSC-34 cells transfected with wild-type hTDP-43 fused with GFP
- **A315T**: NSC-34 cells transfected with hTDP-43 with the A315T mutation fused with GFP
- **M337V**: NSC-34 cells transfected with hTDP-43 with the M337V mutation fused with GFP

I cultured all four cell lines and extracted protein from three different passages of each line on separate days to give three independent biological replicates for the western blot for TDP-43 (n=3). The TDP-43 polyclonal antibody used (Proteintech, 10782-2-AP) binds to both human and mouse TDP-43 so two bands are expected in all the lines except the GFP line as the exogenous hTDP-43 is fused with GFP and so should be larger (~70 kDa) than the endogenous TDP-43 (~43 kDa). The western blot for TDP-43 had strong bands visible in the two expected regions (Figure 6.1.A). To confirm that the bands visible around 70 kDa are the GFP fused hTDP-43 proteins I performed a western blot for GFP (Figure 6.1.B). As the bands seen at ~60-70 kDa in the TDP-43 blot correlated with the size and shape of the visible band at ~60-70 kDa in the GFP blot, I was confident that the positive signal in this region was due to the exogenous TDP-43 fused with GFP. The red boxes in Figure 6.1.A-

B show the regions of signal that was quantified in the first WT lane as an example. The band seen at ~30 kDa in the GFP cell line is consistent with unfused GFP. In the TDP-43 western blot there is another distinct band visible in all lines at ~43 kDa consistent with endogenous mouse TDP-43. Total TDP-43 was increased in the lines transfected with hTDP-43 (Figure 6.1.C). Endogenous TDP-43 was detected in all lines but was significantly lower in the M337V cell line compared with the GFP cell line (ANOVA followed by Bonferroni's multiple comparisons test, $p=0.03$; Figure 6.1.D). Endogenous TDP-43 levels were not significantly different across the hTDP-43 transfected lines. Similarly, there was not a significant difference in the expression levels of the hTDP-43 across the lines that were transfected with a form of hTDP-43 (Figure 6.1.E). This was reassuring going into further experiments that any observed differences between those lines are not due to significant differences in TDP-43 expression.

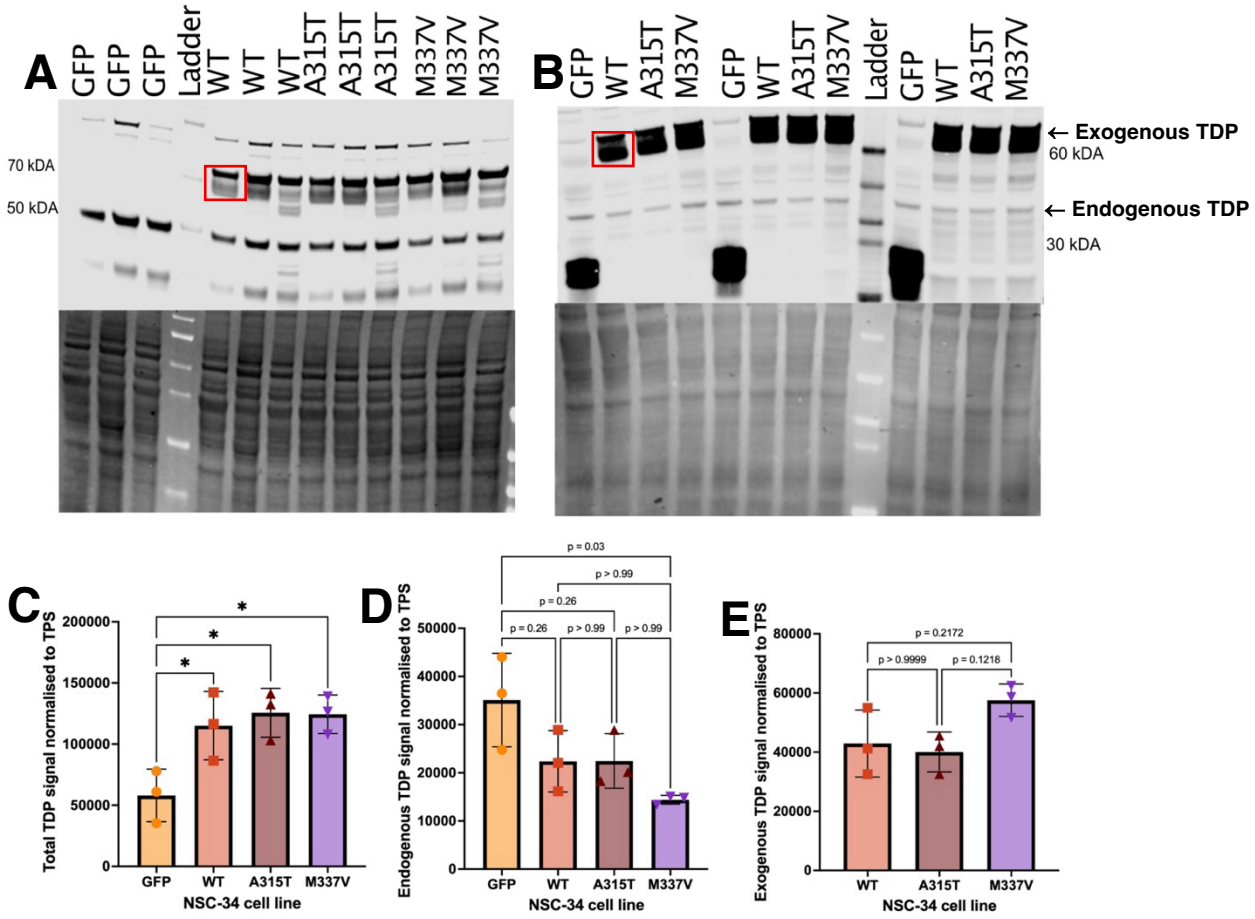

Figure 6.1: **TDP-43 expression in NSC-34 cell lines. (A)** Western blot for TDP-43 with total protein stain shown underneath shows expression of exogenous TDP tagged with GFP at ~70 kDa in the TDP transfected lines, WT, A315T and M337V. Protein was extracted from cells collected from three different passages of each line on separate days (n=3). A strong band is visible in all lines around 43 kDa which is the expected location for the endogenous TDP. The red box outlines the area of signal that was quantified for exogenous TDP in the first WT lane as an example. **(B)** Western blot for GFP with total protein strain shown underneath shows high GFP expression around ~70 kDa consistent with the GFP tagged exogenous TDP in the TDP – transfected lines. This is absent from the GFP transfected only line (GFP) which has high GFP signal at ~27 kDa instead. The red box in the first WT lane correlates with the same area of signal as the red box in (A). **(C)** Quantification of total TDP signal including both main bands from the exogenous and endogenous TDP regions for each NSC-34 cell line normalised to total protein stain (TPS). All the TDP transfected cell lines had increased total TDP compared with the GFP transfected only line: WT (p=0.03), A315T (p=0.01), M337V (p=0.01). **(D)** Quantification of the endogenous TDP signal normalised to TPS with p-values displayed on the chart. Only M337V had a significantly decreased endogenous TDP compared with the GFP only transfected cell line (p=0.03). **(E)** Quantification of exogenous TDP in the cell lines transfected with hTDP normalised to TPS showed there was no significant difference in the amount of exogenous TDP expressed by the different TDP transfected NSC-34 lines. Statistical analysis was by ANOVA followed by Tukey's multiple comparisons test (n=3).

6.3.2 PGK1 in undifferentiated NSC-34 cells

To establish whether there was a difference in PGK1 expression or activity between the NSC-34 cell lines I performed a western blot and PGK1 metabolic activity assay on non-differentiated cells.

PGK1 expression in undifferentiated NSC-34 cell lines

A western blot for PGK1 was performed on protein extracted from cells collected from three separate passages of each of the four NSC-34 lines on three separate days (n=3). A clear band was observed in all lines at ~45 kDa which was the expected size for PGK1 (Figure 6.2.A). The signal was normalised to the total protein stain (TPS) and no significant difference in PGK1 expression was seen between the four NSC-34 lines (ANOVA with Tukey's multiple comparison test, Figure 6.2.B).

PGK1 activity in undifferentiated NSC-34 lines

A PGK1 metabolic assay was performed using cell lysates from the four NSC-34 cell lines three times on three separate days (n=3). Each cell line was plated at both 0.75 $x10^5$ and $1x10^5$ cells per well 48 hours before the planned assay. As the wells plated at $0.75x10^5$ cells per well had all reached between 80-90% confluency at the 48 hour timepoint, it was these that were used for the metabolic assays. Each run was performed with technical duplicates and the mean for each line calculated. The change in absorbance at 340 nm is due to the conversion of NADH to NAD+ due to PGK1 activity and this rate is normalised to the BCA for each well to account for differences in cell number that can occur during plating. There was not a significant difference in PGK1 activity between any of the four NSC-34 cell lines (ANOVA with Tukey's multiple comparison test, Figure 6.2.C).

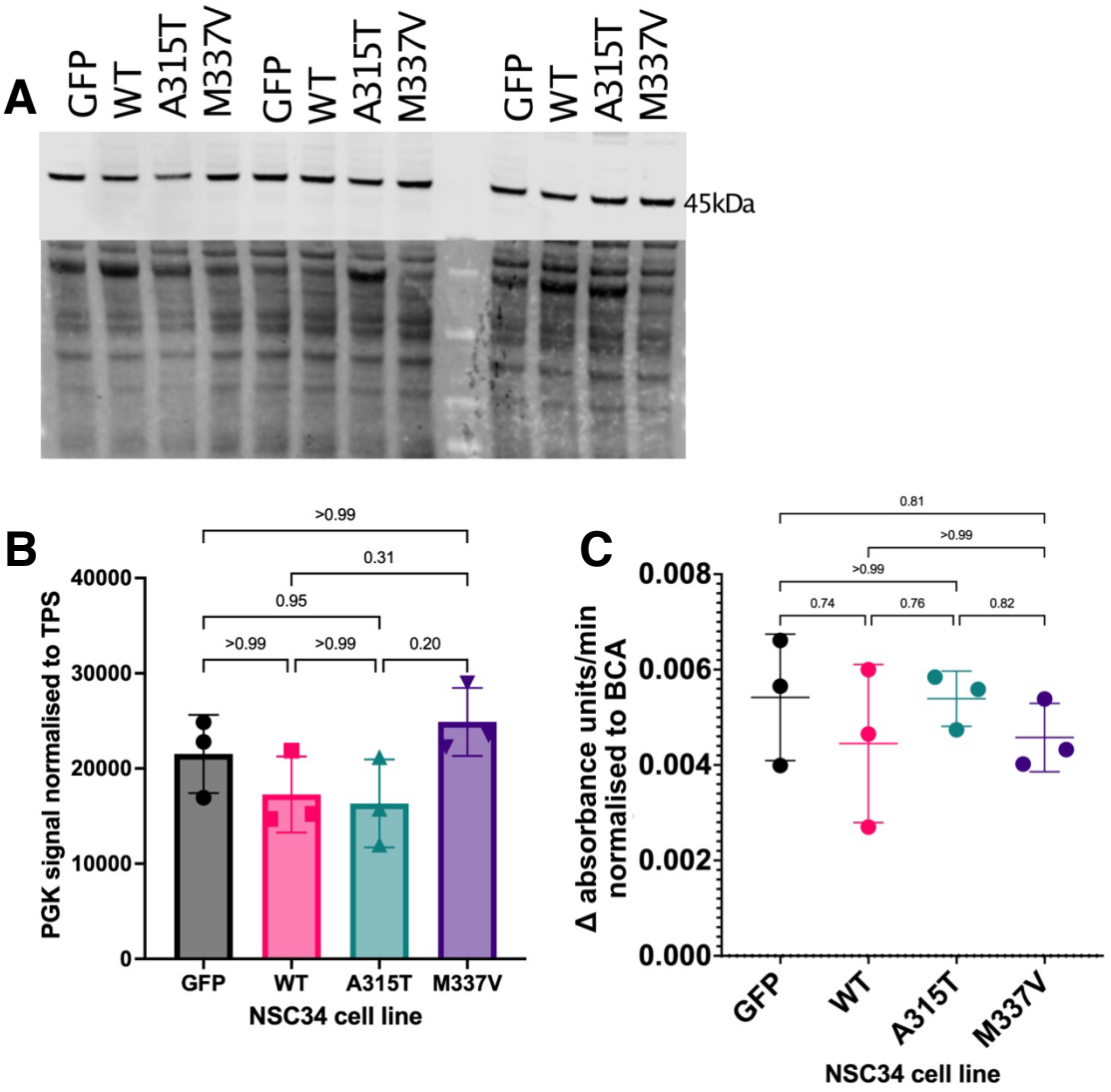

Figure 6.2: **PGK1 expression and activity in non-differentiated NSC-34 cell lines expressing different forms of TDP. (A)** Western blot for PGK in protein samples from four different NSC-34 cell lines showing a strong signal in all cell lines at the expected size ~45 kDa for PGK1. Protein was extracted from cells collected from three separate passages of each line on different days (n=3). The associated total protein stain is shown below the western blot for PGK. **(B)** Quantification of the western blot for PGK in the four different NSC-34 lines normalised to TPS. There was no significant difference in PGK1 expression between the lines. **(C)** PGK1 metabolic activity assay performed on cell lysates from the four NSC-34 cell lines showing the change in absorbance at 340 nm per minute normalised to BCA. This was repeated on three separate days, and the mean of each experiment is shown (n=3). There was no significant difference in PGK1 activity between the four NSC-34 cell lines. Statistical analysis was performed using ANOVA followed by Tukey's multiple comparison test and p-values are displayed on the charts.

6.3.3 Optimising the Seahorse assay for NSC-34 cells

Before I used the NSC-34 cell lines for the Cell Mito Stress Test Seahorse assay, I needed to optimise both the seeding density and the FCCP concentration as recommended by Agilent as these will vary by cell type (Technologies 2017a, 2022).

Cell Seeding Density

To optimise NSC-34 cell seeding density I used the GFP cell line and seeded a 24 well seahorse assay plate with four different cell seeding densities (5-11 $x10^4$ cells/well) with five wells per condition. The recommended basal oxygen consumption rate (OCR) is 50-400 pmol/min and only the wells seeded at $7x10^4$ cells per well consistently had a basal OCR within that range (Figure 6.3.A).

FCCP Concentration

To optimise FCCP concentration, I plated a 24 well seahorse assay plate with $7x10^4$ cells/well of the GFP NSC-34 cell line and prepared the seahorse cartridge plate to inject four different FCCP concentrations (0.5-2 μM) with five wells per condition. The wells with an FCCP concentration of 0.5 μM had the greatest mean maximal respiration and as FCCP can inhibit OCR at high concentrations, I chose to continue with using an FCCP concentration of 0.5 μM for further NSC-34 cell seahorse assays (Figure 6.3.B).

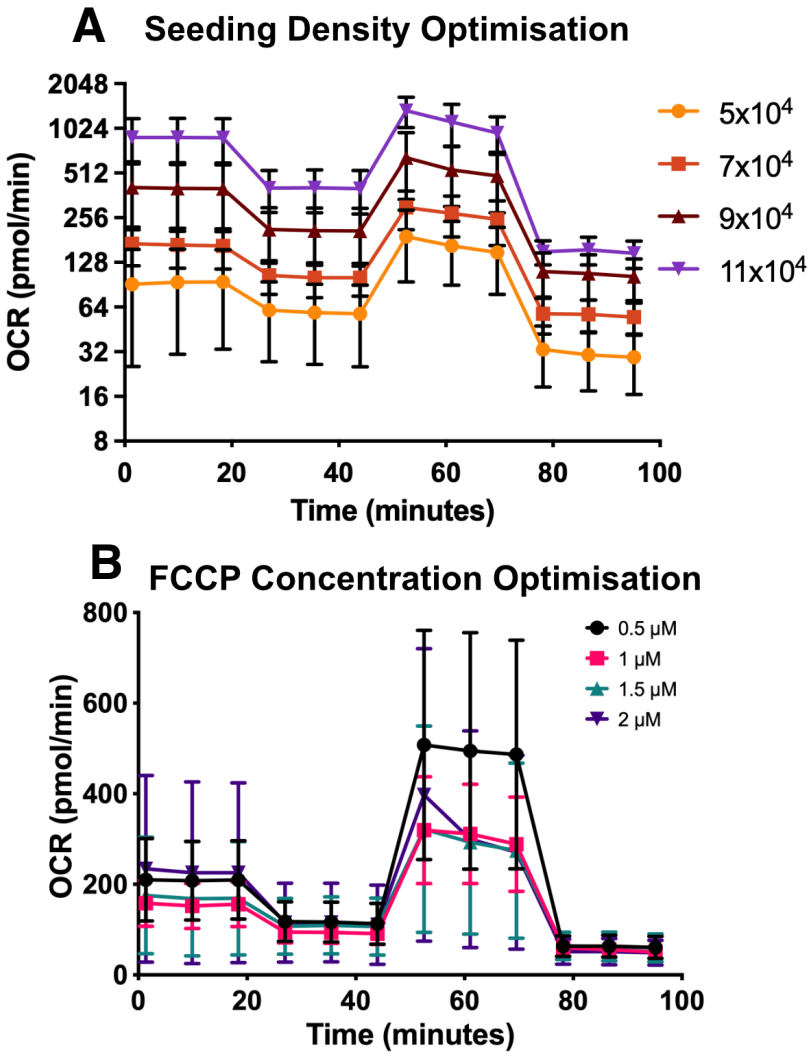

Figure 6.3: **Optimisation of the Mito Stress Seahorse assay for NSC-34 cells. (A)** Optimisation of cell seeding density for NSC-34 cells performed using the GFP transfected NSC-34 cell line. Cells were seeded onto Seahorse plates 24 hours before assay with 5 wells per condition included on the same assay plate. The wells with a seeding density of $7x10^4$ cells per well had the most consistent basal oxygen consumption rate (OCR) within the recommended range of 50-400 pmol/min. OCR is presented on a log2 scale. **(B)** Optimisation of FCCP concentration for NSC-34 cells performed using the GFP transfected NSC-34 cell line and a seeding density of $7x10^4$ cells per well. Four different FCCP concentrations were trialled with 5 wells per condition included on the same assay plate. A FCCP concentration of 0.5 μM resulted in the highest mean maximal respiration.

6.3.4 Seahorse assay pilots with undifferentiated NSC-34 cells

To gain an initial understanding of potential differences in cellular metabolism between the NSC-34 lines I performed pilot Cell Mito Stress Test and Glycolytic Stress Test Seahorse assays using the same protocols as I used with the HEK-293 cells in Chapter 3 but with the seeding density and FCCP concentration optimised for the NSC-34 cells. If a clear difference between the lines emerged, then one or both assays could be a platform for screening potential PGK1 activating compounds. The advantage of this would be that if there is a metabolic parameter in one of the lines that can be targeted with compounds without the need to differentiate the cells first then the process of screening multiple compounds would be much faster. However, given the published work with the NSC-34 cell lines showing differences in stress granule formation and disassembly was performed in differentiated cells and my previous results with the HEK-293 cells, I suspected that differentiating the cells would be necessary. This is why I decided to perform a pilot experiment of each assay first, where a separate plate is used for each test with each plate containing five wells of each cell line plated at $7x10^4$ cells/well 24 hours before the assay.

Cell Mito Stress Test

The raw oxygen consumption rate (OCR) from the Cell Mito Stress Test initially appeared to show that the WT and M337V lines had an increased basal respiration compared with the GFP and A315T lines (Figure 6.4.A). This may be due to different growth rates between the lines or due to an unintentional systemic error that can be introduced in the cell counting process during the seeding of the cell plates. Normalisation of Seahorse assay traces was discussed previously in Chapter 3 however working with the NSC-34 cells has been slightly different as they adhered better to the Seahorse assay plates than the HEK-293 cells. As the PLL coating was not considered necessary, I felt confident using BCA assays to measure total protein per well which I did

as soon as each assay was completed to allow for normalisation to the BCA result. The OCR traces after normalisation showed less distinct differences between the cell lines (Figure 6.4.B). To interrogate the results of the trial further I looked at four key parameters that can be calculated from the OCR traces of the Cell Mito Stress Test using the normalised data. Statistics were not performed as only a single plate was used. The maximal respiration of the A315T cell line wells in this plate was higher than both the GFP and WT cell lines. The A315T line also had increased spare respiratory capacity but reduced ATP production compared with the WT line. The M337V line had increased basal respiration and reduced ATP production compared with the GFP line. Overall, the picture is mixed with no clear pattern emerging across the parameters of a consistent difference between the lines.

Glycolytic Stress Test

The Glycolytic Stress Test is another Seahorse assay protocol that can be used to assess measures of cellular metabolism. As with the Cell Mito Stress Test, I performed a trial with a plate containing 5 wells of each NSC-34 cell line to see if there were clear differences between the lines that may negate the need to differentiate them for the purposes of compound screening. Similar to the Cell Mito Stress Test, looking at the raw extracellular acidification rate (ECAR) traces it appeared there may be a difference in metabolic profiles between the WT and M337V lines and the GFP and A315T lines (Figure 6.5.A). However, after the ECAR traces were normalised to the BCA results of each well the differences between the lines appeared to be less clear (Figure 6.5.B). Statistics were not performed as only a single plate was used. Looking more closely at the parameters that can be calculated from these normalised traces again reveals some potential differences between the lines but not a clear overall picture (Figure 6.5.C-F). The M337V line had reduced glycolysis but increased glycolytic reserve and non-glycolytic acidification compared with the GFP and A315T lines. The A315T line was not significantly different to the

GFP line in any of the parameters and was only significantly different to the WT line in terms of glycolytic capacity (Figure 6.5.D). There was no clear difference in glycolytic capacity between any of the lines (Figure 6.5.E).

Conclusion of Seahorse assay pilots

In both the pilot assays, it was interesting that there wasn't a clearer pattern between the three lines overexpressing TDP or the two lines expressing mutated forms of TDP. Even after normalisation the A315T line behaved most similarly to the GFP line and the M337V line behaved most similarly to the WT line. Ultimately, whilst these preliminary results suggest that there may be some metabolic differences between the lines, those differences do not seem to be substantial enough to justify not experimenting with differentiated cells.

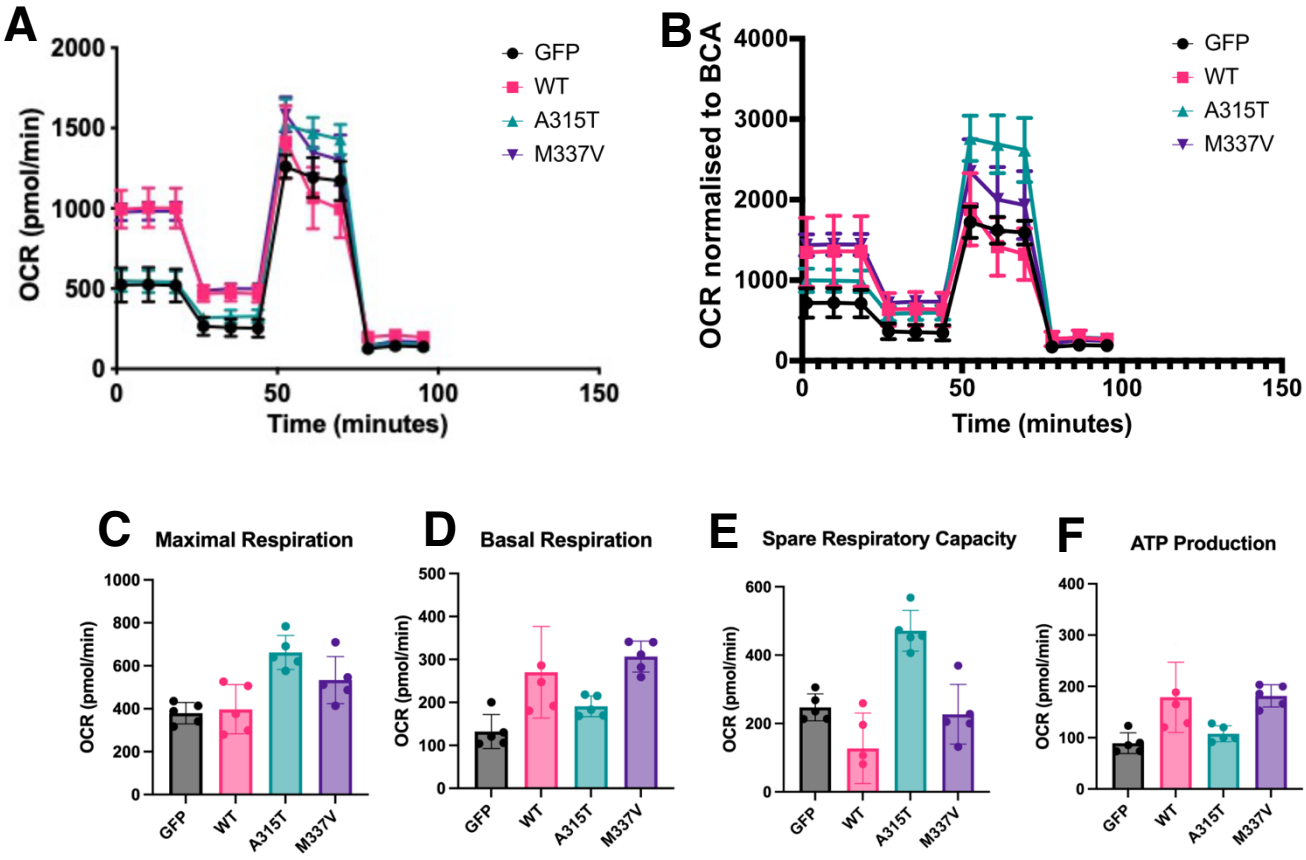

Figure 6.4: **Cell Mito Stress Test seahorse assay trial with undifferentiated NSC-34 cell lines (A)** Raw oxygen consumption rate (OCR) traces from a single Mito Stress Seahorse assay containing five wells of each NSC-34 cell line. The key to the cell lines is displayed on the graph with black line representing the mean of the GFP only transfected cells, pink representing the mean of cells transfected with WT hTDP and turquoise and purple representing the mean from cells transfected with hTDP with the A315T and M337V mutations respectively. **(B)** OCR traces from the Mito Stress Seahorse assay normalised to BCA to account for potential variation in cell number that can occur when plating different lines. **(C)** Maximal respiration from the normalised OCR data. **(D)** Basal respiration from the normalised OCR data. **(E)** Spare respiratory capacity calculated from the normalised OCR data **(F)** ATP production calculated from the normalised OCR data.

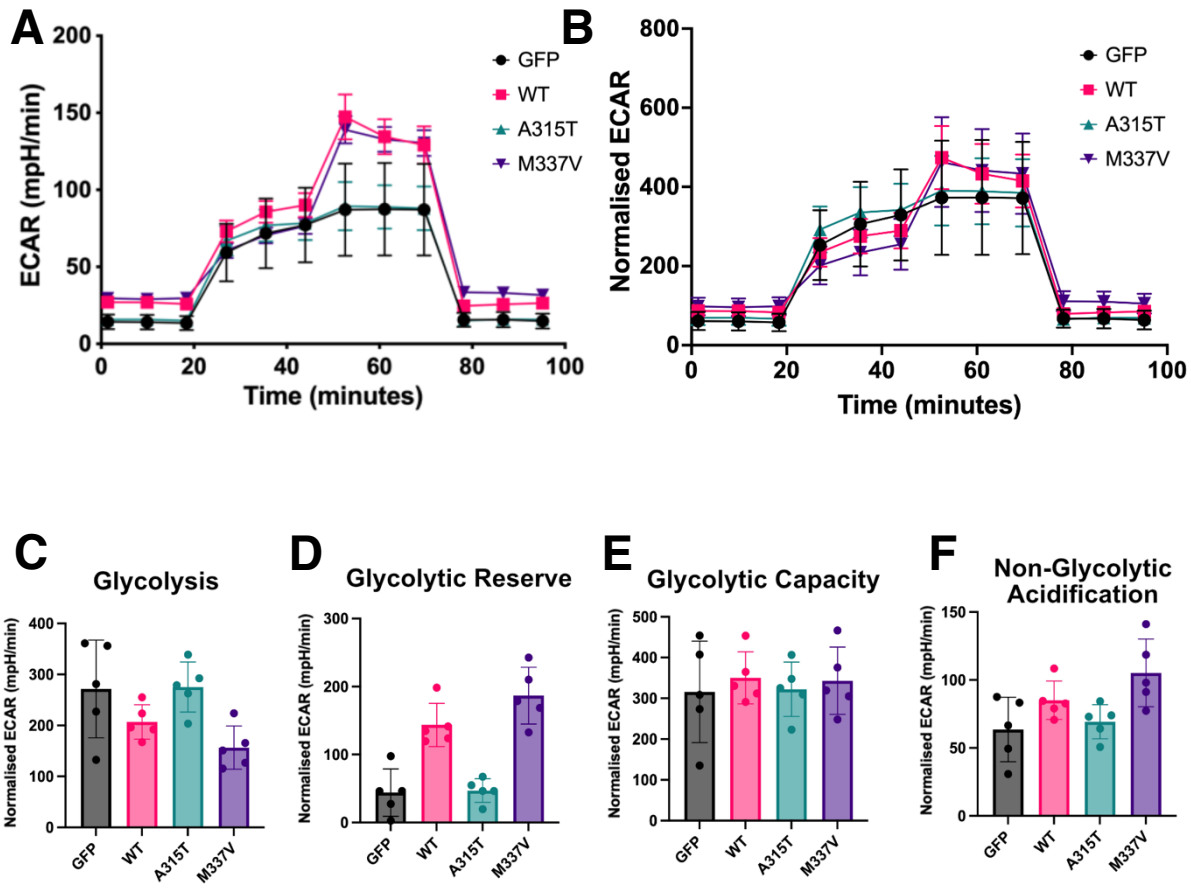

Figure 6.5: **Glycolytic Stress Seahorse assay trial with undifferentiated NSC-34 cell lines (A)** Raw extracellular acidification rate (ECAR) traces from a single Glycolytic Stress Seahorse assay containing five wells of each NSC-34 cell line. The key to the cell lines is displayed on the graph with black line representing the mean of the GFP only transfected cells, pink representing the mean of cells transfected with WT hTDP and turquoise and purple representing the mean from cells transfected with hTDP with the A315T and M337V mutations respectively. **(B)** ECAR traces from the Glycolytic Stress Seahorse assay normalised to BCA to account for potential variation in cell number that can occur when plating different lines. **(C)** Glycolysis rate calculated from the normalised ECAR data. **(D)** Glycolytic reserve for each NSC-34 cell line calculated from the normalised ECAR data. **(E)** Glycolytic capacity calculated from the normalised ECAR data **(F)** Non-glycolytic acidification calculated from the normalised ECAR data.

6.3.5 Differentiating NSC-34 cells

The NSC-34 cells were differentiated for five days. For experiments requiring the differentiated cells, the cells were seeded into plates using standard growth media which was changed to differentiation media (see methods) after 24 hours. Differentiation media was replaced every 48 hours. To check the differentiation process I seeded the four NSC-34 cell lines at $15x10^3$ cells per well in a 24 well plate with six wells seeded per line. After 24 hours in standard media, the media in 3 wells per line was switched for differentiation media and then refreshed every 48 hours for five days. Wells of both undifferentiated and differentiated cells of each line were imaged with brightfield microscopy to assess cell morphology (Figure 6.6.A). Subjectively it appeared that there were more cells present in the undifferentiated wells and neurite outgrowths were longer and more commonly seen in the differentiated cells. These are good indicators that the differentiation process had been successful.

6.3.6 PGK1 function in differentiated NSC-34 cells

To see whether differentiation affected PGK1 activity in the NSC-34 cell lines, I performed the PGK1 metabolic assay on undifferentiated and differentiated cells from each line. The experiment was repeated three times on separate days (n=3). For each run, a 24 well plate was seeded with six wells of each NSC-34 cell line at $15x10^3$ cells per well. Three of the wells of each line were differentiated for 5 days whereas the other three wells were maintained in standard growth media. Results were normalised to BCA and the means for each run used for analysis. None of the lines showed a significant difference in PGK1 activity between undifferentiated and differentiated cells (Figure 6.6.B). When the PGK1 activity of the differentiated NSC-34 lines were compared to each other, the M337V line showed an increased PGK1 activity compared with the GFP ($p=0.03$) and WT ($p=<0.01$) lines. This indicates that the M337V line, once differentiated, may be metabolically different to these other lines.

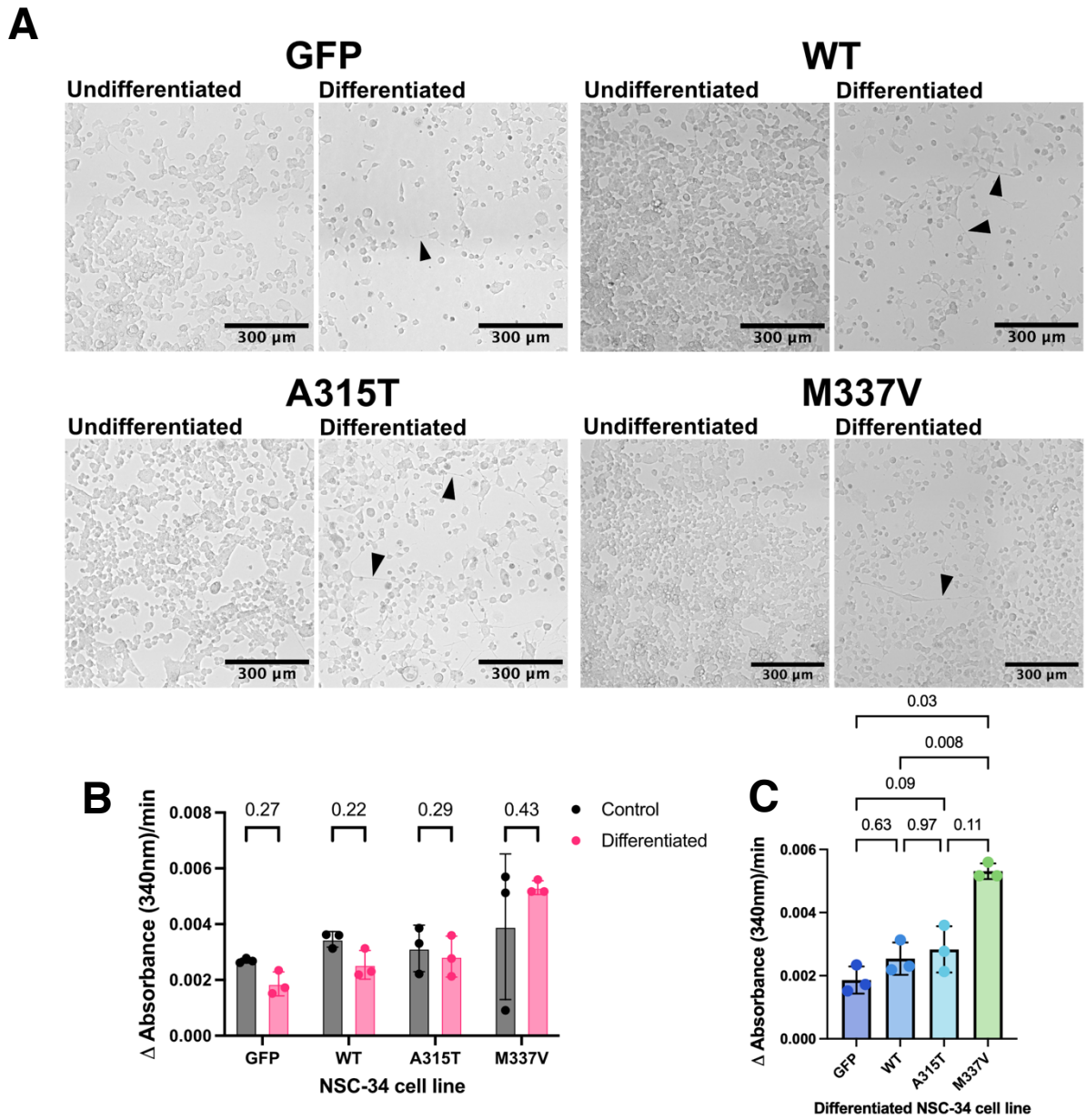

Figure 6.6: **NSC-34 cell line differentiation and PGK1 activity in differentiated NSC-34 cell lines. (A)** Representative images of NSC-34 cells after 5 days differentiation to compare with NSC-34 cells after 5 days in standard cell growth media that were cultured on the same plate. Cells grown in differentiation media appear to have fewer cells and a greater number of neurite outgrowths (black triangles) than undifferentiated cells. **(B)** PGK1 metabolic assay results comparing PGK1 activity in differentiated cells with non-differentiated cells of the same cell line. Differentiation did not significantly affect PGK1 activity in any of the four NSC-34 lines. **(C)** PGK1 assay results comparing the differentiated NSC-34 lines. The M337V line had increased PGK1 activity compared with both the GFP and WT lines.

For the PGK1 assays, cells were plated at the same time on the same plate and the rate NADH was converted to NAD+ as measured by the change in absorbance at 340 nm was normalised to BCA. The experiment was repeated three times on three separate days (n=3). Statistical analysis was by multiple t-test analysis comparing differentiated cells with controls for each line and the adjusted p-values are shown on the graphs.

6.3.7 Optimising cell stressor administration

As differentiation had resulted in a change in cell morphology but not significantly affected PGK1 function, I decided to proceed on to using D-sorbitol as a cell stressor to see if the NSC-34 lines respond differently to stress. The cells were assessed at both 1 hour and 24 hours after exposure to D-sorbitol so that the ability of the cells to recover from the stressor could be evaluated. Similar experiments in the literature, including the 2021 paper from the Noakes group, treated cells with 0.5 M of D-sorbitol for 30 minutes (Ding et al. 2021).To make sure that this concentration of D-sorbitol would not be lethal to the cells I used an MTT assay to assess the cell viability of all four NSC-34 lines 1 hour and 24 hours after exposure to five different concentrations of D-sorbitol (0.1-1 M). NSC-34 cells were seeded onto a 96 well plate so that each concentration of D-sorbitol could be tested on each line in technical triplicate replicates on the same plate with the mean result for each plate used for analysis. This was repeated three times on three separate days (n=3). The MTT assays were performed 1 hour after the stressor (Figure 6.7.A) and 24 hours after the stressor (Figure 6.7.B). Only treatment with 1 M D-sorbitol was sufficient to significantly reduce cell viability across the four lines at both 1 hour ($p=0.01$) and 24 hours ($p=<001$). However, mean cell viability does begin to fall at 0.75 M, and so for the purposes of optimisation I decided to use a concentration of 0.5 M. This is also consistent with the reported concentration used for similar experiments in the literature.

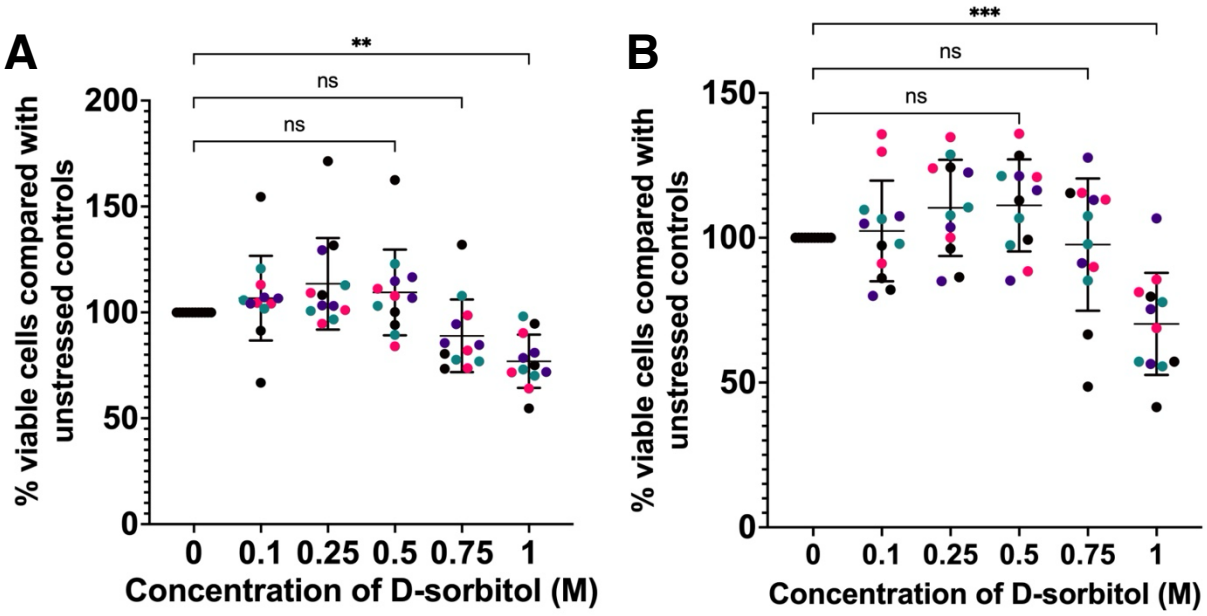

Figure 6.7: **Optimisation of the stressor D-sorbitol using the MTT assay** MTT assay results showing % of viable cells as a proportion of viable cells in the non-stressed wells of the same cell line on the same plate. All four NSC-34 lines were included on each plate and the experiment was repeated on three separate days (n=3). These graphs combine the results of all lines: GFP-only transfected cells (black), TDP^{WT} cells (pink), TDP^{A315T} cells (turquoise), TDP^{M337V} cells (purple). **(A)** Cell viability compared with non-stressed cells 1 hour after exposure to the D-sorbitol stressor. Mean cell viability is only significantly different at 1 M (p=0.01, ANOVA, Dunnett's multiple comparisons test). (**B)** Cell viability compared with non-stressed cells 24 hours after exposure to the D-sorbitol stressor. Again, the mean cell viability is only significantly different at 1 M (p= <0.001). Statistical analysis by ANOVA followed by Dunnett's multiple comparisons test.

6.3.8 Cellular metabolism and PGK1 function in stressed, differentiated NSC34 cells

To assess the NSC-34 cell lines response to the D-sorbitol stressor, I performed the Cell Mito Stress Test Seahorse assay to compare parameters of cellular metabolism and the PGK1 metabolic assay to assess PGK1 activity.

Cell Mito Stress Test

The Cell Mito Stress Test Seahorse assay was performed on all four NSC-34 cell lines 1 hour and 24 hours after a 30 minute exposure to 0.5 M D-sorbitol. Cells were plated at $10x10^3$ cells per well and stressed with D-sorbitol after five days of differentiation. For each run of the experiment two plates were seeded and stressed at the same time, one plate for the 1 hour timepoint and the other for the 24 hour timepoint. Three runs of the experiment were completed on three different days (n=3). The OCR traces were normalised to the BCA for each well. There were five wells per condition included on each Seahorse plate and wells that did not respond to any of the injected compounds or had very atypical traces compared with the other wells of that condition would be excluded. The average of the remaining wells was used for further analysis. Assessing the full traces, the WT line appeared to have a higher basal and maximal respiration 1 hour following the stressor (Figure 6.8.A). The GFP line looked like it may recover in terms of maximal respiration at the 24 hour timepoint but there was considerable variability in the data (Figure 6.8.B). Looking more closely at the parameters for cellular metabolism that can be calculated from the OCR traces shows that none of the lines showed a significant difference in basal respiration, ATP production, spare respiratory capacity, maximal respiration, proton leak or non-mitochondrial respiration between the 1 hour and 24 hour timepoints (Figure 6.8. C-H). Not seeing a significant change even in the GFP or WT lines means that this method may not be suitable for screening compounds.

PGK1 metabolic assay

The PGK1 metabolic assay specifically looks at PGK1 activity in cell lysates. Cells from all four NSC-34 lines were plated at 15 x10^3 cells per well with three wells used for each cell line in a 24 well plate. Two plates were plated per run of the experiment, one for the 1 hour timepoint and one for the 24 hour timepoint. The cells were differentiated for five days before being exposed to 0.5 M D-sorbitol for 30 minutes. The PGK1 assay was then performed (see methods) at 1 hour and 24 hours post stressor exposure. The experiment was repeated three times on three separate days (n=3). The mean of the wells of each cell line was calculated for each run and used for analysis. The WT line was the only NSC-34 line that showed a significant increase in PGK1 activity 24 hours after stressor exposure compared with 1 hour (p=0.03, Figure 6.9.A). The % improvement of PGK1 activity was calculated by calculating the change in absorbance at 340 nm at 24 hours as a percentage of the change in absorbance at 1 hour. The GFP line which is only transfected with GFP showed huge variability in terms of percentage of improvement (Figure 6.9.B). When the cells that are overexpressing hTDP were compared, I found that both the lines expressing a mutated hTDP had a significantly lower recovery in PGK1 activity 24 hours after the stressor compared to 1 hour, relative to the line expressing WT hTDP (Figure 6.9.B). This appears to be a promising output to use for a screening platform for compounds to see whether treatment with a compound improves the recovery of PGK1 activity in one of the mutated hTDP cell lines.

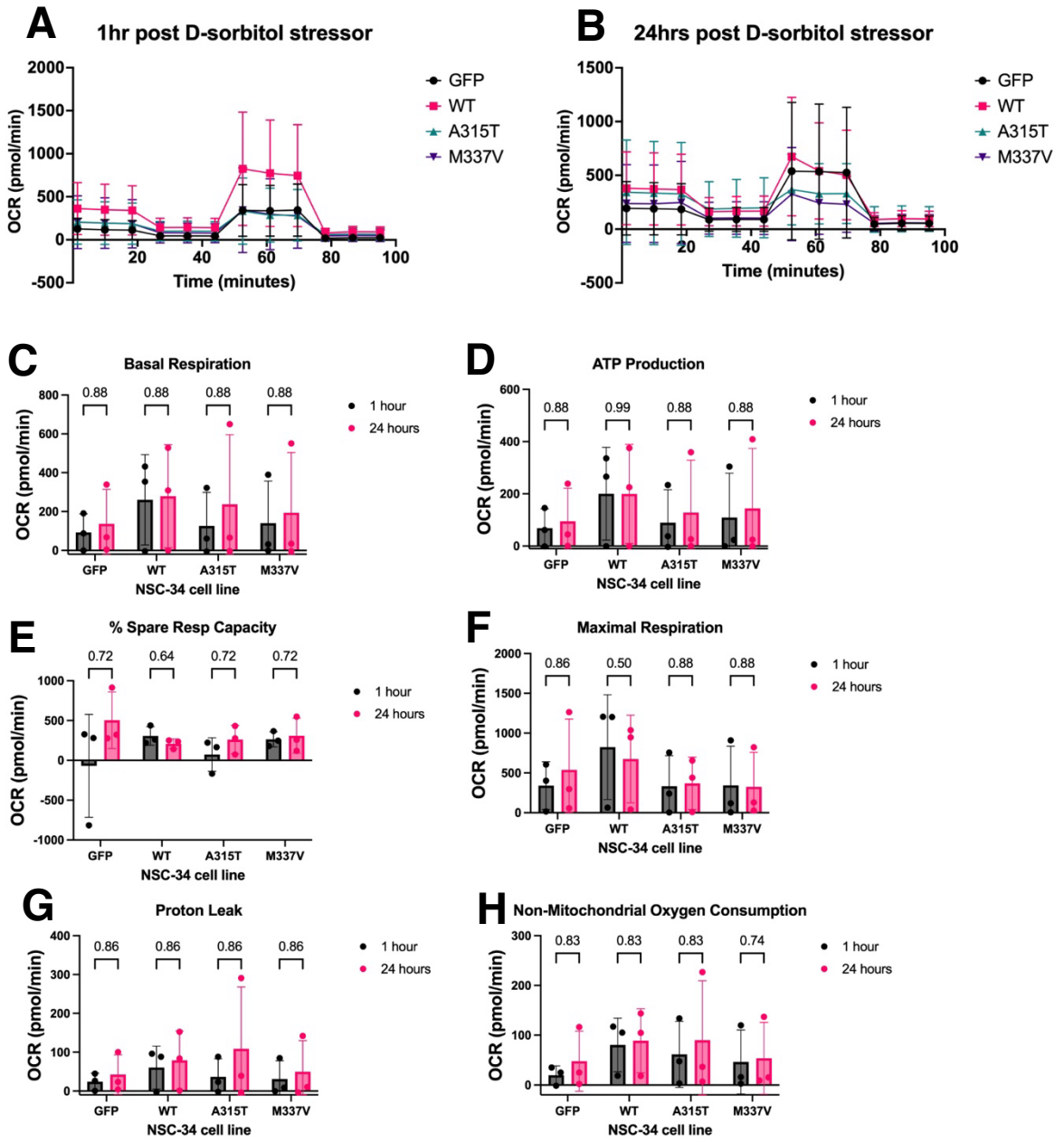

Figure 6.8: Cell Mito Stress Seahorse assay differentiated NSC-34 cell lines at 1 hour and 24 hours post exposure to D-sorbitol stressor. Oxygen consumption rate (OCR) traces from the Cell Mito Stress Seahorse assay of each NSC-34 cell line **(A)** 1 hour and **(B)** 24 hours after a thirty minute exposure to 0.5 M D-sorbitol. Cells were differentiated for 5 days before exposure to the stressor. Traces were normalised to the BCA for each well. Five wells of each line were included on each plate with the mean and SD shown on the graph and the experiment was repeated three times on separate days (n=3). The key to the cell lines is displayed on the graph with black line representing the mean of the GFP only transfected cells, pink representing the mean of cells transfected with WT hTDP and turquoise and purple representing the mean from cells transfected with hTDP with the A315T and M337V mutations respectively. There was no significant change in **(C)** basal respiration, **(D)** ATP production, **(E)** spare respiratory capacity, **(F)** maximal respiration, **(G)** proton leak or **(H)** non-mitochondrial oxygen consumption between the 1 hour and 24 hour timepoints in any of the cell lines. Statistical analysis was performed using multiple paired t-tests with the adjusted p-values shown on the graphs.

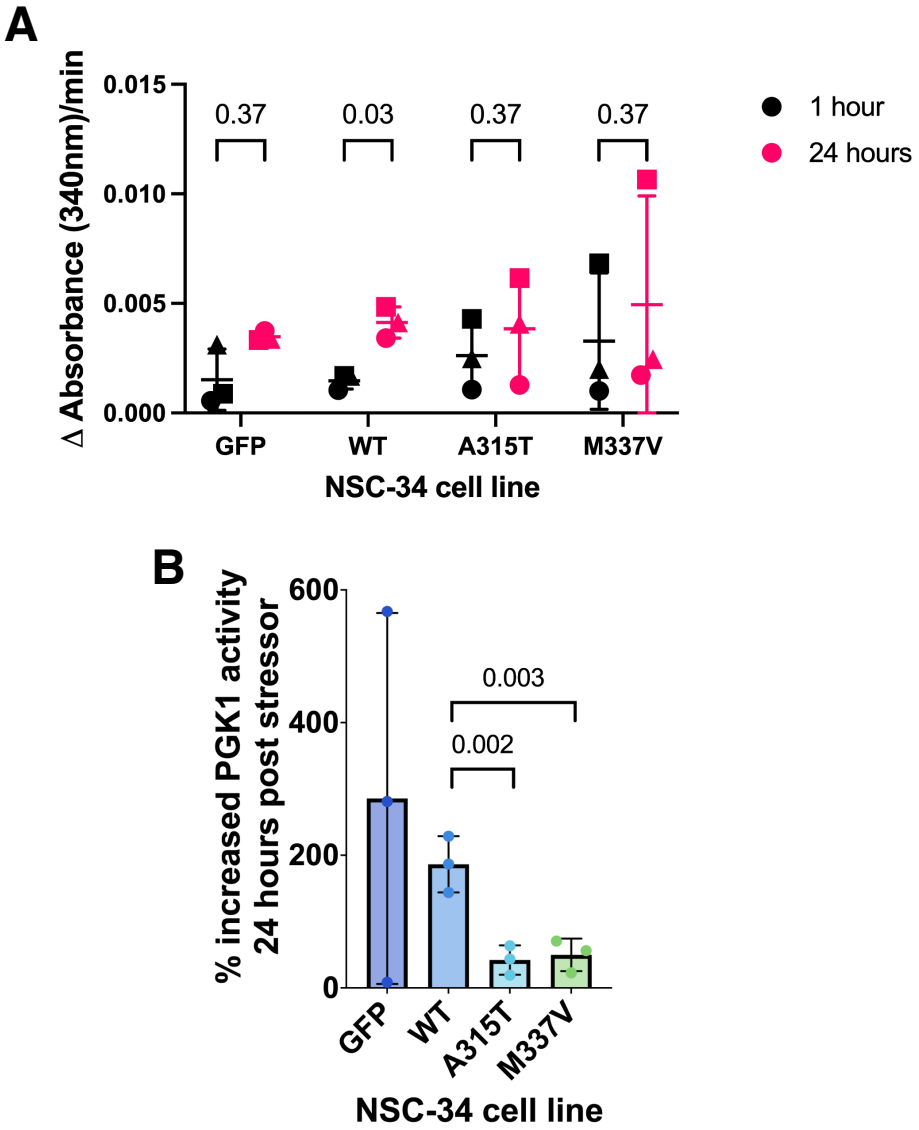

Figure 6.9: PGK1 metabolic activity assay results showing change in absorbance rate in the NSC-34 cell at 1 hour compared with 24 hours after stressor exposure. (A) Change in absorbance at 340nm normalised to BCA shown at 1 hour and 24 hours following 30 minute exposure to 0.5M D-sorbitol as an osmotic stressor. The experiment was repeated three times on separate days (n=3) with each of these runs shown as a separate symbol (circle, triangle, square). Statistical analysis between the 1 hour and 24 hour timepoints was by multiple paired t-tests with the adjusted p-values shown on the graph. In the cells expressing WT human TDP there was a significant increase in PGK1 activity 24 hours after the stressor (p=0.03). **(B)** PGK1 metabolic assay results from NSC-34 cell lines where PGK1 activity at 24 hours post stressor is shown as a percentage of PGK1 activity at 1 hour post stressor. The NSC-34 cells lines transfected with mutated human TDP (A315T and M337V) are compared with NSC-34 cells transfected with WT human TDP. The cells expressing mutated TDP had a reduced increase in their PGK1 activity at 24 hours compared with their PGK1 activity at 1 hour post stressor exposure. Statistical analysis was performed using ANOVA followed by Dunnett's multiple comparison test and p-values are displayed on the graph.

6.3.9 The effect of potential PGK1 activating compounds on recovery from osmotic stress in differentiated NSC-34 cells

Finally, I wanted to assess the most interesting compounds from earlier chapters in both the Cell Mito Stress Test Seahorse assay and the PGK1 metabolic assay in the differentiated NSC-34 cells to see if they affect how the cells recover from the stressor. Whilst the PGK1 metabolic assay has seemed the most promising screening platform to use from my earlier experiments, the Seahorse assay does allow the assessment of a wider range of measures of cellular metabolism. The compounds I decided to test initially were terazosin as a known PGK1 activator, the published compound 12b and compounds D7 and D11 from the Atomwise compound library.

Cell Mito Stress Test compound screen

Only four conditions can be included per Seahorse plate whilst maintaining five wells per condition so the compounds were split into two groups (terazosin with 12b, and D7 with D11) and run as two plates per run of the experiment. I decided to use the WT line as a control line as although it was not significant, it did appear to have a higher maximal respiration following the stressor than the other lines. Both the A315T and M337V lines performed similarly following exposure to the stressor so I could have selected either to trial the compounds on. For this set of experiments, I used the M337V line. For each Seahorse plate I plated five wells of the WT line and fifteen wells of the M337V line at $10x10^3$ cells per well. As with the previous compound screen, DMSO is used as a control treatment and all treatments were added at a concentration of 10 μM. Each plate contained five M337V wells treated with DMSO and two sets of five wells treated with one of the compounds to be tested.

Cells were differentiated for five days and compounds were added 24 hours before a 30 minute exposure to 0.5 M D-sorbitol. Following removal of the stressor, the compounds were re-added. The Cell Mito Stress Test was then

performed 24 hours after the stressor. This was repeated three times on three separate days (n=3). To try to reduce the variability in the assay in addition to excluding wells that either did not respond to the injections or had atypical trace shapes, I decided to exclude wells with a basal OCR of less than 25 or more than 800 pmol/min. This would be less than half or more than double the recommended basal OCR that is targeted when optimising for seeding density. The raw OCR traces for the three plates which tested terazosin and compound 12b (Figure 6.10.A) appears to show that the cells treated with 12b seemed to have a persistently lower OCR and this effect was visible even after normalisation to BCA (Figure 6.10.B). There was no observable effect in the OCR traces of cells treated with terazosin, D7 or D11, even following normalisation (Figure 6.10.A-D). When the parameters of cellular metabolism were calculated from the normalised data and analysed, the effect of 12b was not found to be significant in any of the measured outputs (Figure 6.11.A-F). Treatment of the M337V cells with terazosin, D7 or D11 was also found to have no significant effect on measures of cellular metabolism in the Cell Mito Stress Test.

PGK1 metabolic assay compound screen

Screening the compounds by seeing if they improve PGK1 activity recovery between 1 hour and 24 hours post stressor exposure was the most promising method from my work so far. I was able to include more conditions in the PGK1 metabolic assays as I was not as limited by the size of the plate, so I decided to include all four of the NSC-34 cell lines for this experiment. I used the same method as previously so for each run cells were seeded at 15 $x10^3$ cells per well in four 24 well plates, 24 wells per NSC-34 line in total and these were differentiated for five days. There were six treatment conditions: untreated, DMSO, terazosin, 12b, D7 and D11. The cell lines and treatment conditions were spread equally across the four plates so that each plate contained all four lines and all six treatment conditions. Compounds were added at 10 μM 24

hours before a 30 minute exposure to 0.5 M D-sorbitol and then the compounds were re-added. Two of the plates in each run were used for the 1 hour post-stressor timepoint and the other two were used for the 24 hour post-stressor timepoint ensuring that there were two wells per condition for each timepoint in case a well needed to be excluded. Six runs that included both 1 hour and 24 hour timepoints for all conditions were completed in total and percentage of increase in PGK1 activity was calculated following normalisation to BCA.

There was significant variability between runs, and it was apparent that some of the runs did not show much difference in PGK1 activity in any of the NSC-34 cell lines despite no apparent alterations in the method (Figure 6.12.A). There are two main reasons why wells may not show an improvement in activity, either the cells did not recover from the stress or they were not significantly affected by the stress in the first place. Looking at the change in absorbance data from the GFP and WT lines from the six runs, the PGK1 activity at the 1 hour timepoint of runs 2, 5 and 6 does not seem to have been affected by the stressor as much as in previous experiments. Run 4 does seem to be affected by the stressor at the 1 hour timepoint but then does not seem to show a noticeable recovery in either the GFP or WT lines at the 24 hour timepoint (Figure 6.12.B). To be able to assess the compounds they needed to be tested in conditions where there may be a phenotype to be improved so I only wanted to include runs where the GFP and WT lines had shown signs of recovery. In the first experiment where I used this assay in these cell lines to assess PGK1 activity following stress, the results for the GFP line were highly variable, but the WT line was more consistent and had a mean increase of >150% (Figure 6.9.C).

I decided to assess the untreated GFP and WT results from each run and include the runs where there had been a mean increase in PGK1 activity of at least 50% in these cell lines (Figure 6.12.C). The results from the two runs all

showed increased PGK1 activity at the 24 hour timepoint compared with at the 1 hour timepoint but no compound in any of the lines showed a clear improvement or change in PGK1 activity compared to treatment with the DMSO control (Figure 6.13). There remains quite considerable variability between the two runs at both timepoints in all lines. The compounds also had no clear effect on the increase in PGK1 activity between 1 hour and 24 hours post stressor in the GFP, WT and M337V lines (Figure 6.14). However, D11 looked like it might improve the increase in PGK1 activity in the A315T line compared with the DMSO treated control (Figure 6.14.C). This suggests that D11 may be protective in cells expressing TDP-43 with the A315T mutation, however this finding needs to interpreted cautiously at this stage as only two runs have been included (n=2) and the DMSO result in the A315T line is relatively low compared with the other lines and so it may be that there is an increased sensitivity to DMSO in this line, rather than benefits associated with D11 treatment.

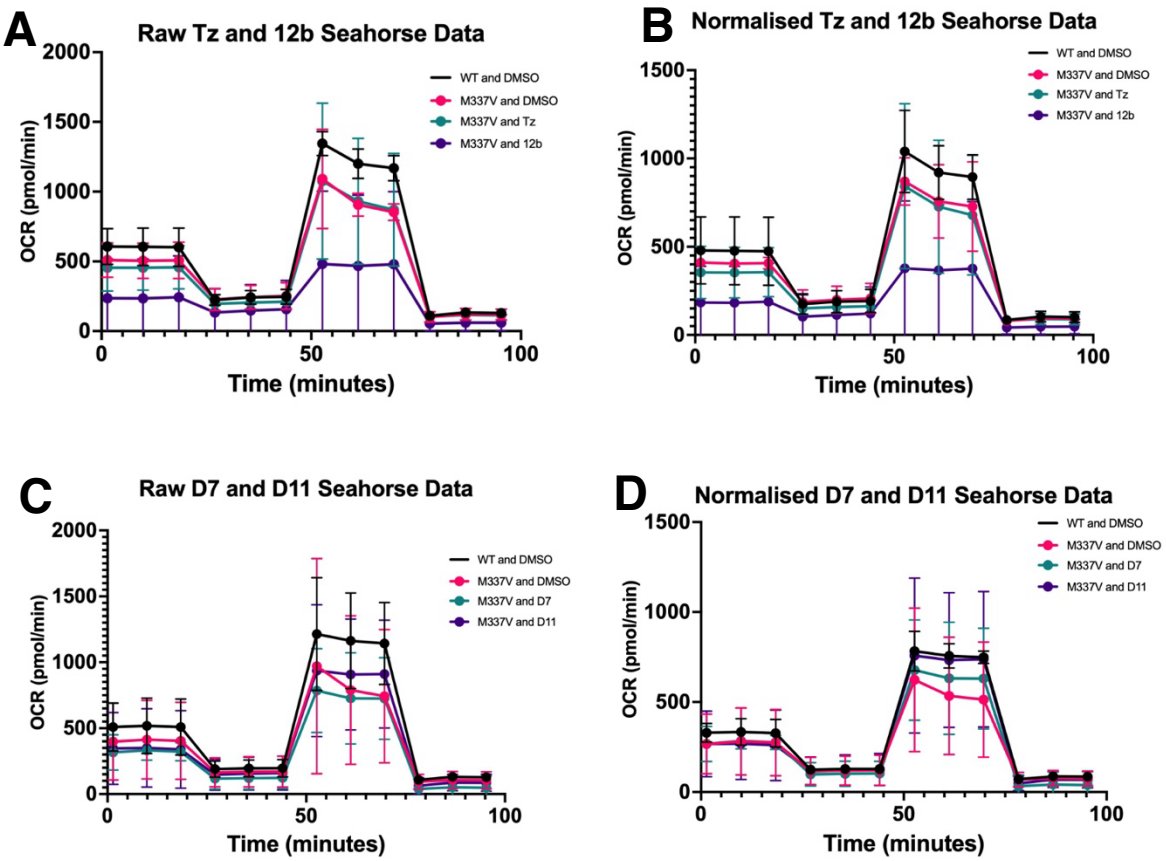

Figure 6.10: **Mito Stress Seahorse assay on treated differentiated NSC-34 cells 24 hours following stressor exposure. (A)** Raw oxygen consumption rate (OCR) traces from the Mito Stress Seahorse assay with the M337V NSC-34 cell line treated with 10 μM terazosin (Tz) or compound 12b to compare with DMSO treated control and the WT NSC-34 cell line also treated with DMSO. 5 wells per condition were included on each plate. The experiment was repeated three times on separate days (n=3). **(B)** OCR traces from the Mito Stress Seahorse assays in (A) where each well has been normalised to BCA. **(C)** Raw oxygen consumption rate (OCR) traces from the Mito Stress Seahorse assay with the M337V NSC-34 cell line treated with 10 μM D7 or D11 to compare with DMSO treated control and the WT NSC-34 cell line also treated with DMSO. 5 wells per condition were included on each plate. The experiment was also repeated three times on separate days (n=3). **(D)** OCR traces from the Mito Stress Seahorse assays in (C) where each well was normalised to BCA.

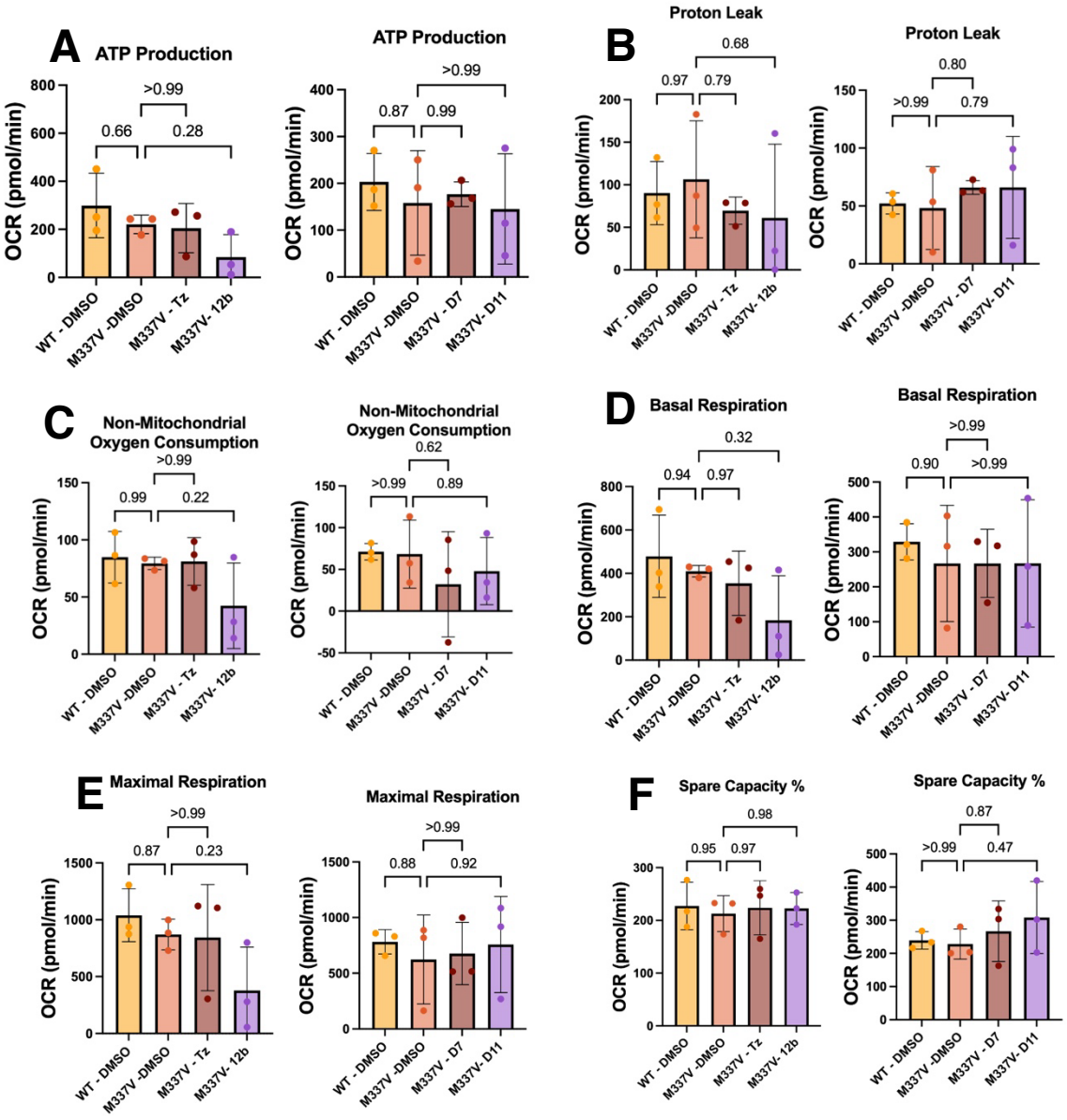

Figure 6.11: Parameters of respiration from the normalised OCR traces of the Mito Stress Seahorse assay performed on treated differentiated NSC-34 cell lines at 24 hours post exposure to D-sorbitol stressor as shown in Figure 6.10. Analysis of different parameters of cellular respiration calculated from the normalised data from the Mito Stress Seahorse assay performed on NSC-34 cells 24 hours after a thirty minute exposure to 0.5 M D-sorbitol. Five wells were included per plate per condition. The experiment was repeated three times on separate days (n=3). Cells were treated with 10 μM DMSO, Tz, 12b, D7 or D11 24 hours before the stressor. Only four conditions could be included per plate, so data is displayed to only include comparisons that were from the same plate. None of the compounds significantly affected **(A)** ATP production, **(B)** proton leak, **(C)** non-mitochondrial oxygen consumption, **(D)** basal respiration, **(E)** maximal respiration or **(F)** spare capacity in the M337V NSC-34 cell line. Statistical analysis was performed using ANOVA followed by Dunnett's multiple comparisons test with the p-values displayed on the graphs.

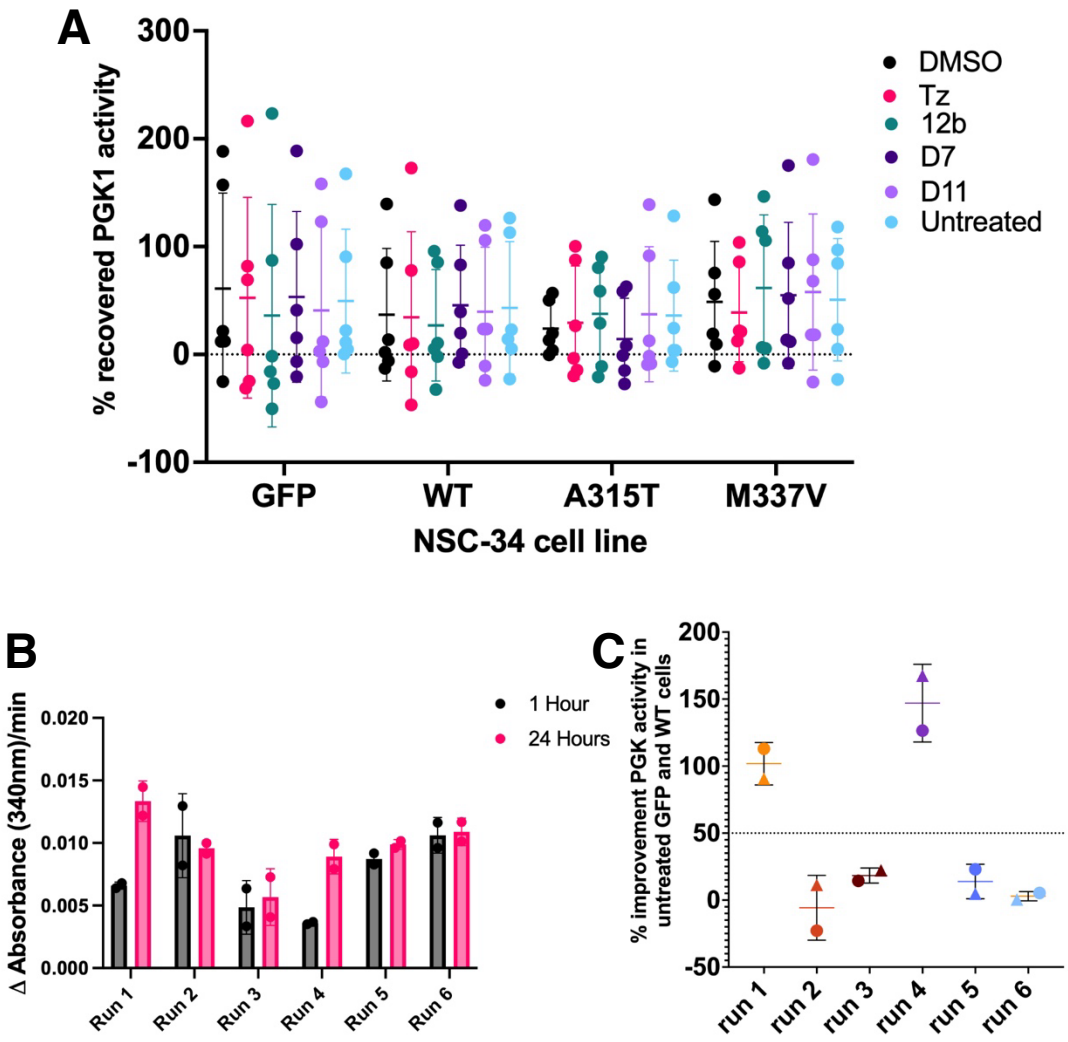

Figure 6.12: Variability in improvement in PGK activity across 6 experimental runs looking at the effect of compounds on recovery after stress. (A) PGK1 activity in treated and untreated NSC-34 cells 24 hours after exposure to a stressor expressed as a percentage of activity compared with PGK1 activity 1 hour after exposure to the stressor to assess how PGK1 activity has recovered. The experiment was repeated six times (n=6) but showed high variability across runs. **(B)** Change in absorbance measured at 340 nm in the untreated GFP and WT NSC-34 cell lines 1 hour and 24 hours after exposure to the cell stressor. **(C)** Improvement in PGK1 activity at 24 hours post stressor relative to PGK1 activity 1 hour post stressor in the untreated GFP NSC-34 cell line (triangles) and WT NSC-34 cell line (circles) in each of the six runs of the experiment. Only two runs showed a mean increase in PGK1 activity in these lines greater than 50% 24 hours following stressor exposure.

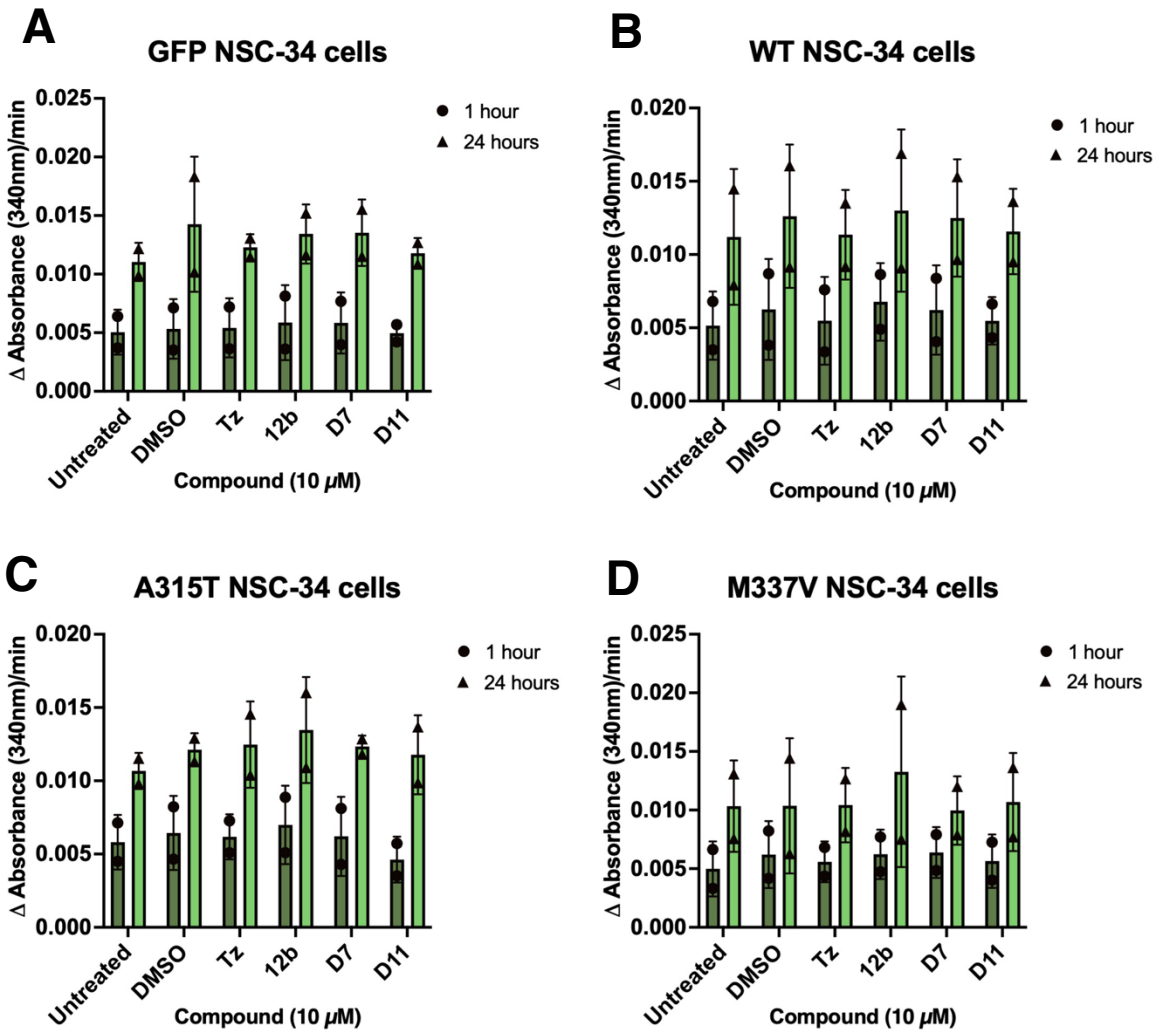

Figure 6.13: PGK1 metabolic activity assay results showing change in absorbance rate in the NSC-34 cell lines treated with compounds at 1 hour compared with 24 hours after stressor exposure. Change in absorbance at 340 nm normalised to BCA shown at 1 hour (circles) and 24 hours (triangles) following 30 minute exposure to 0.5M D-sorbitol as an osmotic stressor. Compounds were applied to treated cells 24 hours before stressor exposure and readded to cells after the stressor. Data is shown only for the two runs of the experiment where the untreated GFP and WT cells had an increased PGK1 activity of at least 50%. Each run included all four cell lines and each condition. Each run was performed on separate days and included two cell plates, one for each timepoint, which were plated at the same time from the same cell stocks. The effect of compounds on PGK1 activity following stressor is shown in **(A)** the NSC-34 cell line transfected with only GFP **(B)** the NSC-34 cell line transfected with WT human TDP **(C)** the NSC-34 cell line transfected with human TDP with the A315T mutation **(D)** the NSC-34 cell line transfected with human TDP with the M337V mutation.

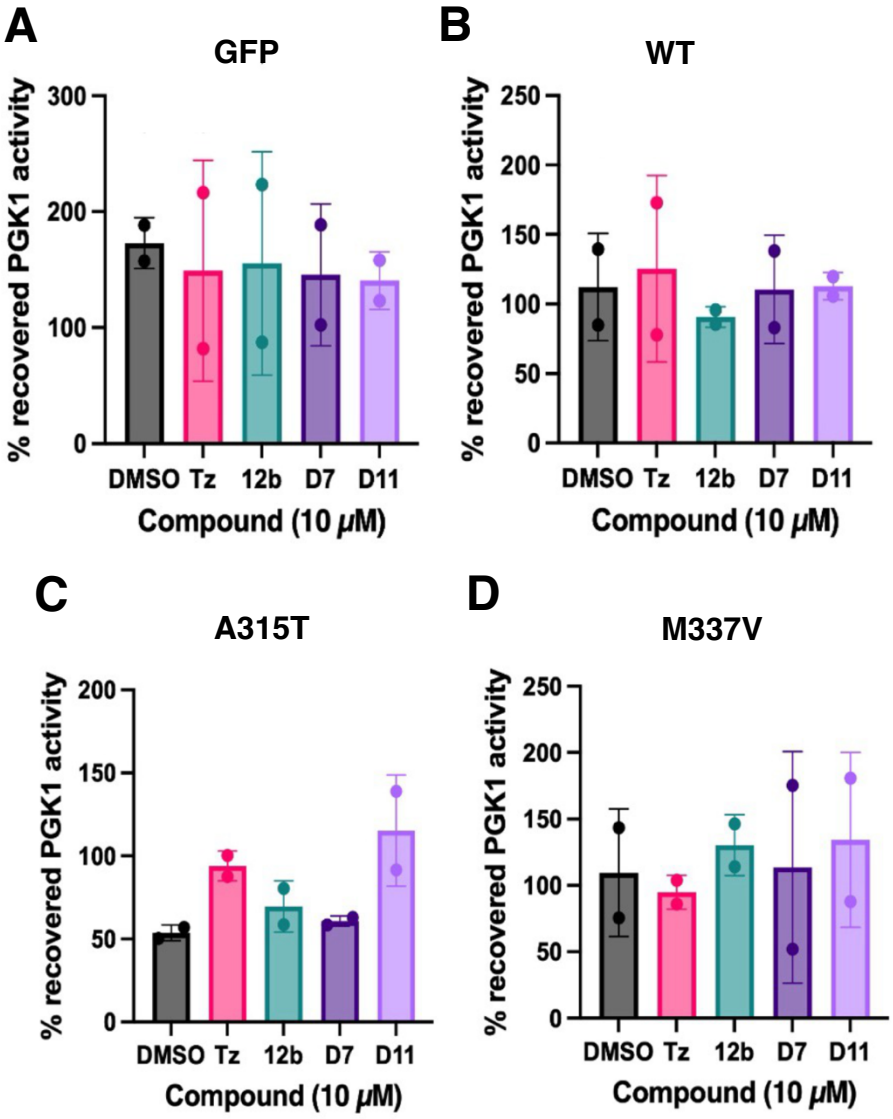

Figure 6.14: **Increased PGK1 activity rate at 24 hours post stressor as a percentage of PGK1 activity at 1 hour post stressor.** PGK1 metabolic assay results from the four different NSC-34 cell lines treated with compounds looking at how much PGK1 activity is increased 24 hours after 0.5M D-sorbitol stressor exposure compared with 1 hour post stressor exposure to assess the cells' ability to recover from the stressor. The two runs of the experiment where a recovery of at least 50% was observed in the untreated GFP and WT cells were included. **(A)** NSC-34 cell line transfected with only GFP, **(B)** NSC-34 cell line transfected with WT human TDP, **(C)** NSC-34 cell line transfected with human TDP with the A315T mutation, **(D)** NSC-34 cell line transfected with human TDP with the M337V mutation.

6.4 Discussion

6.4.1 The NSC-34 cell lines

The first step in this chapter was to confirm the TDP-43 overexpression in the WT, A315T and M337V lines. Consistent with the findings of the Noakes group, the three lines that overexpress different forms of human TDP were found to be overexpressing similar amounts of exogenous TDP (Ding et al. 2021). Endogenous TDP was significantly downregulated in the M337V NSC-34 line, this is consistent with published work showing that in transgenic mice overexpressing TDP-43 with the M337V mutation, endogenous mouse TDP-43 was downregulated (Xu et al. 2011). Although the Noakes group found that both the A315T and M337V NSC-34 lines had significantly reduced endogenous TDP-43 compared with the WT line (Ding et al. 2021). All four lines in their undifferentiated form were found to have similar levels of PGK1 expression and PGK1 activity and whilst there may have been some mild differences in the cellular metabolism profiles from the Seahorse trials, these were judged not to be substantial enough to justify proceeding without differentiating the NSC-34 cell lines.

6.4.2 Differentiation of NSC-34 cells

There are multiple published protocols for the differentiation of NSC-34 cells. I decided to use all-*trans* retinoic acid and differentiate the cells for five days as this was the method used by the Noakes group in the paper reporting differences in stress granule assembly and disassembly following stressor exposure in the differentiated NSC-34 cell lines (Ding et al. 2021). After five days of differentiation, all four of the NSC-34 cell lines developed visible neurite outgrowths. Differentiation alone did not affect PGK1 activity so I decided to proceed directly onto experiments to see whether the NSC-34 lines had differences in recovery from a cell stressor that could be measured with either a Seahorse assay or PGK1 metabolic assay.

6.4.3 Assessing cellular metabolism following cell stressor

Following five days of differentiation, the NSC-34 cell lines were exposed to 30 minutes of 0.5 M D-sorbitol. D-sorbitol is an osmotic stressor which has been shown to mediate TDP-43 localisation to stress granules in multiple cell types (Dewey et al. 2011). Other types of cell stressor were considered, particularly sodium arsenite which is an oxidative stressor. NSC-34 lines expressing mutated TDP-43 were shown by the Noakes group to have slower stress granule disassembly following exposure to sodium arsenite than the NSC-34 line expressing WT TDP-43, but this difference was only observed at the 3 hour timepoint (Ding et al. 2021). In comparison, differences in stress granule size and number were observable between the lines at 1 hour and 24 hours after exposure to D-sorbitol. This longer period where there was a significant difference between the lines made me more confident that differences between the lines would be detected using D-sorbitol as a stressor, but using a different stressor such as sodium arsenite in the future could be considered.

The Cell Mito Stress Test Seahorse assay did not show any significant recovery in any of the NSC-34 cells lines between 1 hour and 24 hours after D-sorbitol exposure. Wells that do not respond to any of the injected compounds or that had grossly abnormal OCR/ECAR traces compared with the rest of the wells of that condition on each plate were excluded from each seahorse assay experiment. Despite this, the Seahorse assay, as seen in previous chapters, suffers from high variability even within the same run and with or without normalisation. This variability may be limiting our ability to detect some changes in cellular metabolism with this method. I introduced stricter criteria for the compound screening Seahorse experiments based on the basal OCR but potentially future experiments could introduce tighter inclusion criteria. However, given the potential for bias when deciding on these criteria, they should be decided upon before conducting the assays. Another potential avenue to improve Seahorse variability would be to more precisely optimise seeding density and concentrations of Seahorse compounds,

particularly oligomycin and FCCP, as well as trialling using media that does not contain additional pyruvate in the Cell Mito Stress assay.
The line expressing WT TDP-43 showed significantly increased PGK1 activity 24 hours after the stressor compared with 1 hour after the stressor. The lines expressing mutated TDP-43 showed reduced PGK1 activity recovery following the stressor compared with the line expressing WT TDP-43. This difference between the lines was significant and was the most promising method to pursue in terms of developing a practical screening platform.

6.4.4 Compound screen in NSC-34 cell lines

I proceeded on to testing four compounds in the differentiated NSC-34 lines to see if any of them affected how the metabolism of the NSC-34 cells responded to the D-sorbitol stressor. The four compounds selected for this small screen were terazosin, compound 12b and compounds D7 and D11 from the Atomwise compound library (see Chapter 4). Terazosin is a known PGK1 activator and so was included as a positive control. Compound 12b is a published terazosin analogue that increased PGK1 activity and had similar neuroprotective properties to terazosin in SH-SY5Y cells but did not improve the axon phenotype of the C9orf72 zebrafish model of ALS (see chapter 5) (Wang, Qian, et al. 2022). Compounds D7 and D11 were selected as the most promising compounds from the Atomwise compound library based on the HEK-293 and zebrafish screens.

As suspected from the previous Seahorse assay results, none of the compounds were found to significantly affect any of the parameters of cellular metabolism that can be calculated from the Cell Mito Stress Test. This may be because the compounds had no effect at all, or that the high variability in the method is obscuring any effect. However, it may be that the stressor applied was too mild to alter cellular metabolism to the extent that there are observable differences as it is highly regulated.

Assessing the recovery of PGK1 activity between 1 hour and 24 hours post stressor exposure had seemed like the most promising method to use to screen compounds. In reality, this method proved to be less straightforward as in four of six runs of the experiment there was no improvement of PGK1 activity even in untreated WT cells. In these runs it appeared that either PGK1 was not affected by stressor exposure or that an unknown factor was limiting the ability of the cells to increase their PGK1 activity. To be able to assess the compounds' ability to improve recovery of PGK1 activity following exposure to a stressor the conditions must be suitable so that recovery of PGK1 activity is observable. For this reason, I excluded the four runs where the untreated control lines (GFP and WT) did not show an improvement in PGK1 activity of at least 50% between the 1 hour and 24 hour timepoints. The data from the two included runs suggested that compound D11 may improve the recovery of PGK1 activity in the A315T cell line.

6.4.5 Future Work

The results of this chapter suggest that there is a difference in how the metabolism of the differentiated NSC-34 cells responds to a cell stressor. Examining how the PGK1 activity of the cells recovers following stressor exposure using the PGK1 metabolic assay was the most promising method of screening potential PGK1 activators. Further optimisation of this method to improve consistency between runs would be advisable before proceeding with further compound screens. Next steps for optimisation could include differentiating the cells for longer, experimenting with a higher concentration of D-sorbitol or by using an alternative cell stressor. Using the current method, D11 was the most promising compound of those tested, but so far only a concentration of 10 μM has been used which may not be the optimal concentration for this compound so retesting D11 in the A315T line at multiple

different concentrations would be interesting, particularly before moving on to any further *in vivo* models.

6.4.6 Conclusion

In this chapter, I have attempted to use NSC-34 cell lines expressing different forms of TDP-43 as a screening platform for potential PGK1 activating compounds. To achieve this, I assessed both cellular metabolism and PGK1 activity in undifferentiated and differentiated NSC-34 cells and in differentiated NSC-34 cells after exposure to a stressor. The most promising method to use as a basis for future screening platforms was using the PGK1 metabolic assay to assess the recovery of PGK1 activity at 24 hours post exposure to D-sorbitol relative to PGK1 activity at 1 hour post exposure. However, this method has had variable results in that some runs did not seem to stress the cells much initially and so there wasn't a deficit to recover from and so would benefit from further optimisation. From the runs that did produce a potentially recoverable phenotype, compound D11 did improve recovery of PGK1 activity in the A315T cell line and so is worthy of further investigation.

Chapter 7: General Discussion

7.1 Summary of Thesis Findings

7.1.1 Overexpression of PGK1 in HEK-293 cells is well tolerated

RNA-sequencing showed that overexpression of the glycolytic enzyme PGK1 did not meaningfully change gene expression profile in HEK-293 cells. The increased expression of functional PGK1 protein also had no effect on cellular metabolism when measured in real-time using mitochondrial and glycolytic stress Seahorse assays. These results suggest that increased PGK1 activity in cells under basal conditions that are not deficient in PGK1 does not have adverse effects on the cells. This is a reassuring finding when considering developing PGK1 activators as systemic therapies for conditions where cells are affected to different extents by disease pathology and tissues and cells that are unaffected by the disease will be exposed to the therapy.

7.1.2 Screening potential PGK1 activators

Lead compounds were identified from a screen in HEK-293 cells of 89 potential PGK1 activating compounds and they were tested in a zebrafish embryo ALS model. I was able to confirm previous findings that treatment with the known PGK1 activator terazosin was able to improve the phenotype of the C9orf72 knockdown zebrafish model (Chaytow et al. 2022). Unlike terazosin, the lead compounds identified from the HEK-293 screen did not significantly improve the phenotype of the zebrafish model. One of the lead compounds selected was a control compound exposing a key weakness in the initial HEK-293 screen. Given that additional PGK1 activity had little effect on HEK-293 cells, it would seem that they are not an appropriate model system to screen for potential PGK1 activating compounds. Model systems like the zebrafish model where there is a phenotype to rescue would seem to be the most appropriate

to assess compounds but inducing a phenotype is a delicate and labour intensive process.

7.1.3 NSC-34 cells show promise as a potential model system for future compound screens

NSC-34 cells that express hTDP with either the A315T or M337V mutation have a reduced ability to recover PGK1 activity levels compared to NSC-34 cells expressing WT hTDP. Preliminary results suggest that this difference can be used to screen compounds for their ability to improve this recovery, particularly in the A315T line. For this method the cells need to be both differentiated and exposed to the osmotic stressor D-sorbitol to induce a phenotype where a rescue effect can be observed.

7.1.4 Compound D11 has shown promise as a PGK1 activator in multiple models

Despite the challenges in screening the potential PGK1 activating compounds, a candidate worthy of further investigation did emerge. Only a small group of lead compounds from the initial HEK-293 screen were taken into the zebrafish model and then the NSC-34 model but in both of these compound D11 was the most promising of the drugs tested. In the preliminary work in the NSC-34 cells it performed better than terazosin at improving the recovery of PGK1 activity in the A315T cells following a stressor. Whilst there is not enough evidence to say conclusively that compound D11 is a PGK1 activator, these early results suggest D11 should be examined further and reassure us that it may be possible to find a PGK1 activator comparable or superior to terazosin in the future.

7.2 PGK1 as a therapeutic target: the challenges

7.2.1 Model systems for drug screening

There has been a growing movement towards using drug screening platforms that are centred on modelling human diseases *in vitro* (Loewa, Feng, and Hedtrich 2023). This has been driven by a lack of clinical success from drugs that have performed well in animal models as well as the costs and ethical concerns related to maintaining these models (Franco and Cedazo-Minguez 2014). Modern methods of modelling disease have become more complex with the advancement of *in silico* models and patient derived cell models including fibroblast cultures, induced pluripotent stem cells (iPSCs) and organoids.

Fibroblasts can be collected from ALS patients and controls and cultured. These fibroblasts carry genetic mutations and can show age related changes which is an important consideration when modelling a degenerative condition which is typically late in onset (Gerou et al. 2021). These have been used to show that changes in metabolism associated with ageing are different between healthy controls and patients with different causes of ALS (Allen et al. 2015; Gerou et al. 2021). Whilst these are relatively easily accessible and can be a good model for certain aspects of the disease, particularly cellular ageing, fibroblasts are not one of the main cell types showing pathological changes in ALS and so findings need to be validated in neuronal or glial models.

The production of pluripotent stem cells from human fibroblasts using four transcription factors (OCT4, SOX2, KLF4 and c-MYC) was a landmark discovery (Takahashi et al. 2007). These iPSCs can be differentiated into any cell type including neurons and glia and as they can be derived from cells acquired from living patients, they carry mutations both known and unknown that are relevant for ALS pathology (Ferraiuolo and Maragakis 2021). The field has progressed quickly, but reprogramming efficiency is still low with reported efficiencies typically <1% with the differentiation process taking around 3-4

weeks (Du et al. 2023). Despite this they have already proven useful in ALS research with iPSC motor neurons being used to test therapeutics and investigate mechanisms (Fujimori et al. 2018). The advantage of being able to differentiate into different cell types has also allowed the investigation into the roles that different cell types play in pathology for example that both motor neurons and astrocytes with C9orf72 mutations show dysfunction (Devlin et al. 2015; Birger et al. 2019).

Organoids are in vitro models that can be derived from different types of stem cells (including iPSCs) which aim to replicate 3D tissues (Zhao et al. 2022). They offer an exciting intermediary model between traditional 2D cell cultures and animal models by trying to model more of the complexity of tissue structure. Neuromuscular organoids made using iPSCs derived from C9orf72 ALS patients have been shown to be able to model aspects of the disease including electrophysiological dysfunction, autophagy and denervation with contraction deficits (Gao et al. 2024). Cerebral organoids have also been described, also made from iPSCs derived from C9orf72 ALS patients, which showed pathologic changes in astrocytes and neurons (Szebenyi et al. 2021). There are concerns regarding how faithfully organoids model the *in vivo* environment and their reproducibility in part related to inherent heterogeneity (Zhao et al. 2022).

In silico modelling makes use of multiple computer techniques to screen drug candidates, predict binding sites and help predict toxicity (Shaker et al. 2021). They are already commonly found to be used in the early stages of drug screening and have been used to help identify potential PGK1 activators (Qiang et al. 2022). However, they are reliant on existing knowledge and require other experimental data to validate findings. The rise of artificial intelligence technology is likely to further accelerate the use of these models and has already been associated with the tripling of the number of innovative

drugs approved for the Chinese market between 2014 and 2020 (Wu et al. 2024).

Despite the rise in popularity of these methods, the more traditional models used in this project still have considerable value. The history of these models' usefulness in drug screens as well as the relative ease of getting these models up and running should not be overlooked. HEK-293 cells are known for both their transfectability and ability to perform post-translational modifications (Hu et al. 2018). Zebrafish have many analogous genes to humans, including PGK1, and so are a great first step in trialling compounds in a high-throughput vertebrate model (Patton, Zon, and Langenau 2021). Then the immortalised NSC-34 cell lines that express human TDP43 sit in a nice middle ground of being a stable cell line that also model an important feature of ALS (Ding et al. 2021).

Investigations of the benefits of PGK1 do seem to be best done in a model of the disease. The response of the NSC-34 lines to the D-sorbitol osmotic stressor did seem to expose that the more pathological lines generally had more difficulty recovering from the stress which would fit within existing literature suggesting that PGK1 has an important role in stress granule regulation (Ding et al. 2021). However, I only looked at one type of stress here – namely an acute osmotic stressor – and it is known that multiple stress granule subtypes exist (Reineke and Neilson 2019). Indeed, the same NSC-34 cell lines I am working with showed different stress granule dynamics when recovering from osmotic stress than they did when recovering from the oxidative stressor sodium arsenite (Ding et al. 2021). However, as PGK1 has been found to be rate-limiting in synaptic firing in primary cultures of rat hippocampal neurons in low glucose conditions there is evidence that PGK1 is important in cell functions under multiple types of stressor (Kokotos et al. 2024). Further exploration into the role of PGK1 in how the cells respond to

different types of stress could reveal more mechanisms that are relevant to ALS pathology.

Ultimately, no single model can encapsulate the complexity of a human disease and combining findings of multiple models whilst advancing the complexity of the models until reaching human trials remains the primary process of drug discovery. Indeed, corroborating preclinical findings like target engagement and disease pathway modulation in multiple model systems is recommended in a recent white paper prepared by an ALS expert working group (Talbot K 2023).

7.2.2 PGK1: a challenging target

The difficulties in finding novel compounds that bind and affect the activity of PGK1 is not limited to the search for PGK1 activators. There has also been research into developing PGK1 inhibitors in multiple forms of cancer where PGK1 has been found to enhance tumour proliferation, increase resistance to therapies and has been associated with a poorer prognosis (He et al. 2019). Whilst some small molecule inhibitors of PGK1 have recently been reported in the literature, there is a lack of effective lead compounds suitable to take forward into trials (He et al. 2024). Multiple approaches have been trialled to develop novel PGK1 inhibitors including modulating the PGK1 activity by targeting PTMs, using a non-ATP-competitive inhibitor or using a competitive inhibitor of 1,3 BPG or ADP/ATP (Zhang, Sun, and Kang 2023). Reducing K323 acetylation of PGK1 has been shown to inhibit PGK1 activity but there are concerns that targeting PTMs like this is likely to be a very nonspecific method of inhibiting PGK1 activity (Zhang, Sun, and Kang 2023; Hu et al. 2017). The compound GQQ-792 is suggested to inhibit PGK1 by binding to C799 and C380 of PGK1 which sit near the ADP/ATP binding site and blocks the binding of ADP/ATP without directly competing for the same site (Wang et al. 2021). Whilst theoretically bisphosphonate analogues of 1,3-BPG could be

used to inhibit PGK1 activity, this has not yet been demonstrated beyond 3D modelling techniques (Kotsikorou, Sahota, and Oldfield 2006). Terazosin binds to the same domain of PGK1 as ADP and is thought to increase the rate of ATP release at low concentrations but inhibit enzyme activity at higher concentrations through a competitive binding mechanism (Riley et al. 2024; Chen et al. 2023). Other ATP competitive molecules, CBR-470-1 and DC-PGK1, have been identified through screens and used to explore the role of PGK1 in the Nrf2 pathway but their effectiveness in vivo is yet to be fully ascertained (Bollong et al. 2018; Liao et al. 2022; Zheng et al. 2020).

Activators that use a novel mechanism to that of terazosin would be preferred to avoid the complexity of a compound that has both inhibitory and activator qualities. However, it should be considered that some PGK1 inhibitors may show activator properties similar to those of terazosin at different concentrations, particularly those also targeting the ADP/ATP binding site.

7.3 Future work

There are two clear avenues of further investigation that this project has uncovered. Firstly, an optimised method for screening for PGK1 activation is needed. The NSC-34 lines have shown promise as a screening model for PGK1 activators but further optimisation to improve the consistency of the effect of the D-sorbitol stressor is needed. From the work here it is clear that a metabolic deficit is required so that a rescue effect can be seen and measured. Secondly, once a more consistent screening model is in place, the potential PGK1 activators identified by the Atomwise project should be rescreened. From the preliminary screens here, compound D11 does look like it has potential, but superior compounds may have been passed over in the original HEK-293 screen. If multiple promising compounds can be identified, then comparing their structure to that of terazosin to try to identify compounds that interact with PGK1 in dissimilar ways would be desirable. Alternative in vitro or

in vivo models can be considered but future researchers should consider the difficulty in observing metabolic changes with increased PGK1 activity where there was not previously a deficit.

7.4 Final thoughts

PGK1 activators such as terazosin are an exciting area of research as increased PGK1 activity has been shown to be beneficial in multiple pre-clinical models of neurodegenerative diseases for which there is an urgent need for novel therapeutics. However, the side effects associated with terazosin and the complex nature of how it interacts with PGK1 mean that there is a need to develop alternatives. Cells which are not deficient in PGK1 are not affected by increased PGK1 activity meaning that screening for increased PGK1 activity is not straightforward and improved screening models are needed. Significant steps towards finding a suitable screening model have been made here but further optimisation is required as, ultimately, the clinical relevance of PGK1 activation will be limited without the discovery of novel activators.

References

Akcimen, F., E. R. Lopez, J. E. Landers, A. Nath, A. Chio, R. Chia, and B. J. Traynor. 2023. 'Amyotrophic lateral sclerosis: translating genetic discoveries into therapies', *Nat Rev Genet*, 24: 642-58.

Allen, S. P., L. M. Duffy, P. J. Shaw, and A. J. Grierson. 2015. 'Altered age-related changes in bioenergetic properties and mitochondrial morphology in fibroblasts from sporadic amyotrophic lateral sclerosis patients', *Neurobiol Aging*, 36: 2893-903.

Allen, S. P., S. Rajan, L. Duffy, H. Mortiboys, A. Higginbottom, A. J. Grierson, and P. J. Shaw. 2014. 'Superoxide dismutase 1 mutation in a cellular model of amyotrophic lateral sclerosis shifts energy generation from oxidative phosphorylation to glycolysis', *Neurobiol Aging*, 35: 1499-509.

Altschul, S. F., T. L. Madden, A. A. Schaffer, J. Zhang, Z. Zhang, W. Miller, and D. J. Lipman. 1997. 'Gapped BLAST and PSI-BLAST: a new generation of protein database search programs', *Nucleic Acids Res*, 25: 3389-402.

Amores, A., J. Catchen, A. Ferrara, Q. Fontenot, and J. H. Postlethwait. 2011. 'Genome evolution and meiotic maps by massively parallel DNA sequencing: spotted gar, an outgroup for the teleost genome duplication', *Genetics*, 188: 799-808.

Andrews, J. A., C. E. Jackson, T. D. Heiman-Patterson, P. Bettica, B. R. Brooks, and E. P. Pioro. 2020. 'Real-world evidence of riluzole effectiveness in treating amyotrophic lateral sclerosis', *Amyotroph Lateral Scler Frontotemporal Degener*, 21: 509-18.

Arai, T., M. Hasegawa, H. Akiyama, K. Ikeda, T. Nonaka, H. Mori, D. Mann, K. Tsuchiya, M. Yoshida, Y. Hashizume, and T. Oda. 2006. 'TDP-43 is a component of ubiquitin-positive tau-negative inclusions in frontotemporal lobar degeneration and amyotrophic lateral sclerosis', *Biochem Biophys Res Commun*, 351: 602-11.

Atomwise, Aims Program. 2024. 'AI is a viable alternative to high throughput screening: a 318-target study', *Sci Rep*, 14: 7526.

Ayala, Y. M., P. Zago, A. D'Ambrogio, Y. F. Xu, L. Petrucelli, E. Buratti, and F. E. Baralle. 2008. 'Structural determinants of the cellular localization and shuttling of TDP-43', *J Cell Sci*, 121: 3778-85.

Balendra, R., J. Sreedharan, M. Hallegger, R. Luisier, H. A. Lashuel, J. M. Gregory, and R. Patani. 2025. 'Amyotrophic lateral sclerosis caused

by TARDBP mutations: from genetics to TDP-43 proteinopathy', *Lancet Neurol*, 24: 456-70.

Barberio, J., C. Lally, V. Kupelian, O. Hardiman, and W. D. Flanders. 2023. 'Estimated Familial Amyotrophic Lateral Sclerosis Proportion: A Literature Review and Meta-analysis', *Neurol Genet*, 9: e200109.

Beattie, C. E. 2000. 'Control of motor axon guidance in the zebrafish embryo', *Brain Res Bull*, 53: 489-500.

Becker, T., M. F. Wullimann, C. G. Becker, R. R. Bernhardt, and M. Schachner. 1997. 'Axonal regrowth after spinal cord transection in adult zebrafish', *J Comp Neurol*, 377: 577-95.

Bedell, V. M., P. Dubey, H. B. Lee, D. S. Bailey, J. L. Anderson, A. Jamieson-Lucy, R. Xiao, E. V. Leonard, M. J. Falk, M. A. Pack, M. Mullins, S. A. Farber, R. G. Eckenhoff, and S. C. Ekker. 2025. 'Zebrafishology, study design guidelines for rigorous and reproducible data using zebrafish', *Commun Biol*, 8: 739.

Bell, L. E., C. Bardelle, M. J. Packer, J. Kastl, G. A. Holdgate, and G. Davies. 2024. 'Characterisation of high throughput screening outputs for small molecule degrader discovery', *SLAS Discov*, 29: 100162.

Berlato, Dener Gomes, and André Valle de Bairros. 2020. 'Meldonium: Pharmacological, toxicological, and analytical aspects', *Toxicology Research and Application*, 4: 2397847320915143.

Bill, B. R., A. M. Petzold, K. J. Clark, L. A. Schimmenti, and S. C. Ekker. 2009. 'A primer for morpholino use in zebrafish', *Zebrafish*, 6: 69-77.

Birger, A., I. Ben-Dor, M. Ottolenghi, T. Turetsky, Y. Gil, S. Sweetat, L. Perez, V. Belzer, N. Casden, D. Steiner, M. Izrael, E. Galun, E. Feldman, O. Behar, and B. Reubinoff. 2019. 'Human iPSC-derived astrocytes from ALS patients with mutated C9ORF72 show increased oxidative stress and neurotoxicity', *EBioMedicine*, 50: 274-89.

Bollong, M. J., G. Lee, J. S. Coukos, H. Yun, C. Zambaldo, J. W. Chang, E. N. Chin, I. Ahmad, A. K. Chatterjee, L. L. Lairson, P. G. Schultz, and R. E. Moellering. 2018. 'A metabolite-derived protein modification integrates glycolysis with KEAP1-NRF2 signalling', *Nature*, 562: 600-04.

Bonte, D., C. Lindvall, H. Liu, K. Dykema, K. Furge, and M. Weinreich. 2008. 'Cdc7-Dbf4 kinase overexpression in multiple cancers and tumor cell lines is correlated with p53 inactivation', *Neoplasia*, 10: 920-31.

Boscá L.; Carlos Corredor, C. 1984. 'Is phosphofructokinase the rate-limiting step of glycolysis?', *Trends in Biochemical Sciences*, 9: 372-73.

Bosco, D. A., N. Lemay, H. K. Ko, H. Zhou, C. Burke, T. J. Kwiatkowski, Jr., P. Sapp, D. McKenna-Yasek, R. H. Brown, Jr., and L. J. Hayward. 2010. 'Mutant FUS proteins that cause amyotrophic lateral sclerosis incorporate into stress granules', *Hum Mol Genet*, 19: 4160-75.

Bowler, M. W. 2013. 'Conformational dynamics in phosphoglycerate kinase, an open and shut case?', *FEBS Lett*, 587: 1878-83.

Boyd, P. J., W. Y. Tu, H. K. Shorrock, E. J. N. Groen, R. N. Carter, R. A. Powis, S. R. Thomson, D. Thomson, L. C. Graham, A. A. L. Motyl, T. M. Wishart, J. R. Highley, N. M. Morton, T. Becker, C. G. Becker, P. R. Heath, and T. H. Gillingwater. 2017. 'Bioenergetic status modulates motor neuron vulnerability and pathogenesis in a zebrafish model of spinal muscular atrophy', *PLoS Genet*, 13: e1006744.

Browne, S. E., L. Yang, J. P. DiMauro, S. W. Fuller, S. C. Licata, and M. F. Beal. 2006. 'Bioenergetic abnormalities in discrete cerebral motor pathways presage spinal cord pathology in the G93A SOD1 mouse model of ALS', *Neurobiol Dis*, 22: 599-610.

Cai, R., Y. Zhang, J. E. Simmering, J. L. Schultz, Y. Li, I. Fernandez-Carasa, A. Consiglio, A. Raya, P. M. Polgreen, N. S. Narayanan, Y. Yuan, Z. Chen, W. Su, Y. Han, C. Zhao, L. Gao, X. Ji, M. J. Welsh, and L. Liu. 2019. 'Enhancing glycolysis attenuates Parkinson's disease progression in models and clinical databases', *J Clin Invest*, 129: 4539-49.

Calzi, F., R. Bellasio, G. Guiso, S. Caccia, and M. T. Tacconi. 1997. 'Effect of piribedil and its metabolite, S584, on brain lipid peroxidation in vitro and in vivo', *Eur J Pharmacol*, 338: 185-90.

Cardarelli, F., L. Digiacomo, C. Marchini, A. Amici, F. Salomone, G. Fiume, A. Rossetta, E. Gratton, D. Pozzi, and G. Caracciolo. 2016. 'The intracellular trafficking mechanism of Lipofectamine-based transfection reagents and its implication for gene delivery', *Sci Rep*, 6: 25879.

Cashman, N. R., H. D. Durham, J. K. Blusztajn, K. Oda, T. Tabira, I. T. Shaw, S. Dahrouge, and J. P. Antel. 1992. 'Neuroblastoma x spinal cord (NSC) hybrid cell lines resemble developing motor neurons', *Dev Dyn*, 194: 209-21.

Chai, B., Y. Li, Y. Guo, Z. Zhang, K. Jia, X. Chai, and Y. Suo. 2024. 'ETV7 promotes colorectal cancer progression through upregulation of IFIT3', *Funct Integr Genomics*, 24: 8.

Chaytow, Helena, Emily Carroll, David Gordon, Yu-Ting Huang, Dinja van der Hoorn, Hannah Louise Smith, Thomas Becker, Catherina Gwynne Becker, Kiterie Maud Edwige Faller, Kevin Talbot, and Thomas Henry Gillingwater. 2022. 'Targeting phosphoglycerate kinase 1 with terazosin improves motor neuron phenotypes in multiple models of amyotrophic lateral sclerosis', *eBioMedicine*: 104202.

Cheetham, S. W., G. J. Faulkner, and M. E. Dinger. 2020. 'Overcoming challenges and dogmas to understand the functions of pseudogenes', *Nat Rev Genet*, 21: 191-201.

Chen, H., Y. Li, J. Gao, Q. Cheng, L. Liu, and R. Cai. 2023. 'Activation of Pgk1 Results in Reduced Protein Aggregation in Diverse Neurodegenerative Conditions', *Mol Neurobiol*, 60: 5090-101.

Chen, J., H. Luo, X. Wu, M. Dong, D. Wang, Y. Ou, Y. Wang, S. Sun, Z. Liu, Z. Yang, Q. Guan, and Q. Zhang. 2025. 'Inhibition of Phosphoglycerate Kinase 1 Enhances Radiosensitivity of Esophageal Squamous Cell Carcinoma to X-rays and Carbon Ion Irradiation', *Front Biosci (Landmark Ed)*, 30: 36430.

Chen, S., H. Wang, J. Chen, J. Cheng, J. Gao, S. Chen, X. Yao, J. Sun, J. Ren, S. Li, F. Che, and Q. Wan. 2024. 'Upregulation of mitochondrial PGK1 by ROS-TBC1D15 pathway promotes neuronal death after oxygen-glucose deprivation/reoxygenation injury', *Brain Res*, 1825: 148724.

Chen, X., C. Zhao, X. Li, T. Wang, Y. Li, C. Cao, Y. Ding, M. Dong, L. Finci, J. H. Wang, X. Li, and L. Liu. 2015. 'Terazosin activates Pgk1 and Hsp90 to promote stress resistance', *Nat Chem Biol*, 11: 19-25.

Chen, Y. S., Z. X. Hong, Y. T. Lin, E. C. Tsao, P. Y. Chen, C. A. Liu, H. J. Harn, T. W. Chiou, and S. Z. Lin. 2024. 'Efficiency of PGK1 proteins delivered to the brain via a liposomal system through intranasal route administration for the treatment of spinocerebellar ataxia type 3', *Drug Deliv Transl Res*, 14: 1940-53.

Chia, R., A. Chio, and B. J. Traynor. 2018. 'Novel genes associated with amyotrophic lateral sclerosis: diagnostic and clinical implications', *Lancet Neurol*, 17: 94-102.

Chio, A., G. Logroscino, O. Hardiman, R. Swingler, D. Mitchell, E. Beghi, B. G. Traynor, and Consortium Eurals. 2009. 'Prognostic factors in ALS: A critical review', *Amyotroph Lateral Scler*, 10: 310-23.

Chitwood, P. J., S. Juszkiewicz, A. Guna, S. Shao, and R. S. Hegde. 2018. 'EMC Is Required to Initiate Accurate Membrane Protein Topogenesis', *Cell*, 175: 1507-19 e16.

Chu, S. L., J. R. Huang, Y. T. Chang, S. Y. Yao, J. S. Yang, V. W. Hsu, and J. W. Hsu. 2024. 'Phosphoglycerate kinase 1 acts as a cargo adaptor to promote EGFR transport to the lysosome', *Nat Commun*, 15: 1021.

Chung, S., D. K. Arrell, R. S. Faustino, A. Terzic, and P. P. Dzeja. 2010. 'Glycolytic network restructuring integral to the energetics of embryonic stem cell cardiac differentiation', *J Mol Cell Cardiol*, 48: 725-34.

Ciura, S., S. Lattante, I. Le Ber, M. Latouche, H. Tostivint, A. Brice, and E. Kabashi. 2013. 'Loss of function of C9orf72 causes motor deficits in a zebrafish model of amyotrophic lateral sclerosis', *Ann Neurol*, 74: 180-7.

Conte, M., M. Martucci, G. Mosconi, A. Chiariello, M. Cappuccilli, V. Totti, A. Santoro, C. Franceschi, and S. Salvioli. 2020. 'GDF15 Plasma Level Is Inversely Associated With Level of Physical Activity and Correlates With Markers of Inflammation and Muscle Weakness', *Front Immunol*, 11: 915.

Dalby, B., S. Cates, A. Harris, E. C. Ohki, M. L. Tilkins, P. J. Price, and V. C. Ciccarone. 2004. 'Advanced transfection with Lipofectamine 2000 reagent: primary neurons, siRNA, and high-throughput applications', *Methods*, 33: 95-103.

Danshina, P. V., C. B. Geyer, Q. Dai, E. H. Goulding, W. D. Willis, G. B. Kitto, J. R. McCarrey, E. M. Eddy, and D. A. O'Brien. 2010. 'Phosphoglycerate kinase 2 (PGK2) is essential for sperm function and male fertility in mice', *Biol Reprod*, 82: 136-45.

Devlin, A. C., K. Burr, S. Borooah, J. D. Foster, E. M. Cleary, I. Geti, L. Vallier, C. E. Shaw, S. Chandran, and G. B. Miles. 2015. 'Human iPSC-derived motoneurons harbouring TARDBP or C9ORF72 ALS mutations are dysfunctional despite maintaining viability', *Nat Commun*, 6: 5999.

Dewey, C. M., B. Cenik, C. F. Sephton, D. R. Dries, P. Mayer, 3rd, S. K. Good, B. A. Johnson, J. Herz, and G. Yu. 2011. 'TDP-43 is directed to stress granules by sorbitol, a novel physiological osmotic and oxidative stressor', *Mol Cell Biol*, 31: 1098-108.

Dewey, C. M., B. Cenik, C. F. Sephton, B. A. Johnson, J. Herz, and G. Yu. 2012. 'TDP-43 aggregation in neurodegeneration: are stress granules the key?', *Brain Res*, 1462: 16-25.

Ding, H., Y. J. Cheng, H. Yan, R. Zhang, J. B. Zhao, C. F. Qian, W. B. Zhang, H. Xiao, and H. Y. Liu. 2014. 'Phosphoglycerate kinase 1

promotes radioresistance in U251 human glioma cells', *Oncol Rep*, 31: 894-900.

Ding, Q., J. Chaplin, M. J. Morris, M. A. Hilliard, E. Wolvetang, D. C. H. Ng, and P. G. Noakes. 2021. 'TDP-43 Mutation Affects Stress Granule Dynamics in Differentiated NSC-34 Motoneuron-Like Cells', *Front Cell Dev Biol*, 9: 611601.

Doble, A. 1996. 'The pharmacology and mechanism of action of riluzole', *Neurology*, 47: S233-41.

Du, H., Z. Huo, Y. Chen, Z. Zhao, F. Meng, X. Wang, S. Liu, H. Zhang, F. Zhou, J. Liu, L. Zhang, S. Zhou, Y. Guan, and X. Wang. 2023. 'Induced Pluripotent Stem Cells and Their Applications in Amyotrophic Lateral Sclerosis', *Cells*, 12.

Eyster, C., S. Matsuzaki, A. Pranay, J. R. Giorgione, A. Faakye, M. Ahmed, and K. M. Humphries. 2025. 'Mechanistic studies of PFKFB2 reveal a novel inhibitor of its kinase activity', *PLoS One*, 20: e0317167.

Faller, K. M. E., H. Chaytow, and T. H. Gillingwater. 2025. 'Targeting common disease pathomechanisms to treat amyotrophic lateral sclerosis', *Nat Rev Neurol*, 21: 86-102.

Fang, T., A. Al Khleifat, J. H. Meurgey, A. Jones, P. N. Leigh, G. Bensimon, and A. Al-Chalabi. 2018. 'Stage at which riluzole treatment prolongs survival in patients with amyotrophic lateral sclerosis: a retrospective analysis of data from a dose-ranging study', *Lancet Neurol*, 17: 416-22.

Feldman, E. L., S. A. Goutman, S. Petri, L. Mazzini, M. G. Savelieff, P. J. Shaw, and G. Sobue. 2022. 'Amyotrophic lateral sclerosis', *Lancet*, 400: 1363-80.

Feneberg, E., D. Gordon, A. G. Thompson, M. J. Finelli, R. Dafinca, A. Candalija, P. D. Charles, I. Mager, M. J. Wood, R. Fischer, B. M. Kessler, E. Gray, M. R. Turner, and K. Talbot. 2020. 'An ALS-linked mutation in TDP-43 disrupts normal protein interactions in the motor neuron response to oxidative stress', *Neurobiol Dis*, 144: 105050.

Ferraiuolo, L., and N. J. Maragakis. 2021. 'Mini-Review: Induced pluripotent stem cells and the search for new cell-specific ALS therapeutic targets', *Neurosci Lett*, 755: 135911.

Ferrari, R., D. Kapogiannis, E. D. Huey, and P. Momeni. 2011. 'FTD and ALS: a tale of two diseases', *Curr Alzheimer Res*, 8: 273-94.

Fiorillo, A., M. Petrosino, A. Ilari, A. Pasquo, A. Cipollone, M. Maggi, R. Chiaraluce, and V. Consalvi. 2018. 'The phosphoglycerate kinase 1 variants found in carcinoma cells display different catalytic activity and conformational stability compared to the native enzyme', *PLoS One*, 13: e0199191.

Firth, J. D., B. L. Ebert, C. W. Pugh, and P. J. Ratcliffe. 1994. 'Oxygen-regulated control elements in the phosphoglycerate kinase 1 and lactate dehydrogenase A genes: similarities with the erythropoietin 3' enhancer', *Proc Natl Acad Sci U S A*, 91: 6496-500.

Flanagan-Steet, H., M. A. Fox, D. Meyer, and J. R. Sanes. 2005. 'Neuromuscular synapses can form in vivo by incorporation of initially aneural postsynaptic specializations', *Development*, 132: 4471-81.

Floare, M. L., and S. P. Allen. 2020. 'Why TDP-43? Why Not? Mechanisms of Metabolic Dysfunction in Amyotrophic Lateral Sclerosis', *Neurosci Insights*, 15: 2633105520957302.

Franco, R., and A. Cedazo-Minguez. 2014. 'Successful therapies for Alzheimer's disease: why so many in animal models and none in humans?', *Front Pharmacol*, 5: 146.

Fu, C. Y., H. Y. Chen, C. Y. Lin, S. J. Chen, J. C. Sheu, and H. J. Tsai. 2023. 'Extracellular Pgk1 interacts neural membrane protein enolase-2 to improve the neurite outgrowth of motor neurons', *Commun Biol*, 6: 849.

Fu, T., H. Tian, H. Rong, P. Ai, and X. Li. 2023. 'LncRNA PVT1 induces apoptosis and inflammatory response of bronchial epithelial cells by regulating miR-30b-5p/BCL2L11 axis in COPD', *Genes Environ*, 45: 24.

Fujimori, K., M. Ishikawa, A. Otomo, N. Atsuta, R. Nakamura, T. Akiyama, S. Hadano, M. Aoki, H. Saya, G. Sobue, and H. Okano. 2018. 'Modeling sporadic ALS in iPSC-derived motor neurons identifies a potential therapeutic agent', *Nat Med*, 24: 1579-89.

Gao, C., Q. Shi, X. Pan, J. Chen, Y. Zhang, J. Lang, S. Wen, X. Liu, T. L. Cheng, and K. Lei. 2024. 'Neuromuscular organoids model spinal neuromuscular pathologies in C9orf72 amyotrophic lateral sclerosis', *Cell Rep*, 43: 113892.

Gao, M., L. Zhu, J. Chang, T. Cao, L. Song, C. Wen, Y. Chen, Y. Zhuo, and F. Chen. 2023. 'Safety and Efficacy of Edaravone in Patients with Amyotrophic Lateral Sclerosis: A Systematic Review and Meta-analysis', *Clin Drug Investig*, 43: 1-11.

Gautam, M., A. Gunay, N. S. Chandel, and P. H. Ozdinler. 2022. 'Mitochondrial dysregulation occurs early in ALS motor cortex with TDP-43 pathology and suggests maintaining NAD(+) balance as a therapeutic strategy', *Sci Rep*, 12: 4287.

Gero, D., P. Szoleczky, K. Modis, J. P. Pribis, Y. Al-Abed, H. Yang, S. Chevan, T. R. Billiar, K. J. Tracey, and C. Szabo. 2013. 'Identification of pharmacological modulators of HMGB1-induced inflammatory response by cell-based screening', *PLoS One*, 8: e65994.

Gerou, M., B. Hall, R. Woof, J. Allsop, S. J. Kolb, K. Meyer, P. J. Shaw, and S. P. Allen. 2021. 'Amyotrophic lateral sclerosis alters the metabolic aging profile in patient derived fibroblasts', *Neurobiol Aging*, 105: 64-77.

Geser, F., M. Martinez-Lage, L. K. Kwong, V. M. Lee, and J. Q. Trojanowski. 2009. 'Amyotrophic lateral sclerosis, frontotemporal dementia and beyond: the TDP-43 diseases', *J Neurol*, 256: 1205-14.

Gitcho, M. A., R. H. Baloh, S. Chakraverty, K. Mayo, J. B. Norton, D. Levitch, K. J. Hatanpaa, C. L. White, 3rd, E. H. Bigio, R. Caselli, M. Baker, M. T. Al-Lozi, J. C. Morris, A. Pestronk, R. Rademakers, A. M. Goate, and N. J. Cairns. 2008. 'TDP-43 A315T mutation in familial motor neuron disease', *Ann Neurol*, 63: 535-8.

Goutman, S. A., O. Hardiman, A. Al-Chalabi, A. Chio, M. G. Savelieff, M. C. Kiernan, and E. L. Feldman. 2022. 'Emerging insights into the complex genetics and pathophysiology of amyotrophic lateral sclerosis', *Lancet Neurol*, 21: 465-79.

Graham, F. L., J. Smiley, W. C. Russell, and R. Nairn. 1977. 'Characteristics of a human cell line transformed by DNA from human adenovirus type 5', *J Gen Virol*, 36: 59-74.

Griffin, P., J. M. Dimitry, P. W. Sheehan, B. V. Lananna, C. Guo, M. L. Robinette, M. E. Hayes, M. R. Cedeno, C. J. Nadarajah, L. A. Ezerskiy, M. Colonna, J. Zhang, A. Q. Bauer, T. P. Burris, and E. S. Musiek. 2019. 'Circadian clock protein Rev-erbalpha regulates neuroinflammation', *Proc Natl Acad Sci U S A*, 116: 5102-07.

Grlickova-Duzevik, E., T. M. Reimonn, M. Michael, T. Tian, J. Owyoung, A. McGrath-Conwell, P. Neufeld, M. Mueth, D. C. Molliver, P. J. Ward, and B. J. Harrison. 2023. 'Members of the CUGBP Elav-like family of RNA-binding proteins are expressed in distinct populations of primary sensory neurons', *J Comp Neurol*, 531: 1425-42.

Gros, P., X. Wang, J. Guan, A. E. Lang, P. C. Austin, B. Welk, N. P. Visanji, and C. Marras. 2021. 'Exposure to Phosphoglycerate Kinase 1

Activators and Incidence of Parkinson's Disease', *Mov Disord*, 36: 2419-25.

Guo, Z., Y. Zhang, H. Wang, L. Liao, L. Ma, Y. Zhao, R. Yang, X. Li, J. Niu, Q. Chu, Y. Fu, B. Li, and C. Yang. 2024. 'Hypoxia-induced downregulation of PGK1 crotonylation promotes tumorigenesis by coordinating glycolysis and the TCA cycle', *Nat Commun*, 15: 6915.

Hahn, K. R., H. J. Kwon, Y. S. Yoon, D. W. Kim, and I. K. Hwang. 2022. 'Phosphoglycerate kinase 1 protects against ischemic damage in the gerbil hippocampus', *Aging (Albany NY)*, 14: 8886-99.

Hart, A., G. Aldridge, Q. Zhang, N. S. Narayanan, and J. E. Simmering. 2024. 'Association of Terazosin, Doxazosin, or Alfuzosin Use and Risk of Dementia With Lewy Bodies in Men', *Neurology*, 103: e209570.

Harwood, F. C., R. I. Klein Geltink, B. P. O'Hara, M. Cardone, L. Janke, D. Finkelstein, I. Entin, L. Paul, P. J. Houghton, and G. C. Grosveld. 2018. 'ETV7 is an essential component of a rapamycin-insensitive mTOR complex in cancer', *Sci Adv*, 4: eaar3938.

He, Q., Y. Ma, J. Liu, D. Zhang, J. Ren, R. Zhao, J. Chang, Z. N. Guo, and Y. Yang. 2021. 'Biological Functions and Regulatory Mechanisms of Hypoxia-Inducible Factor-1alpha in Ischemic Stroke', *Front Immunol*, 12: 801985.

He, Y., Y. Luo, L. Huang, D. Zhang, H. Hou, Y. Liang, S. Deng, P. Zhang, and S. Liang. 2024. 'Novel inhibitors targeting the PGK1 metabolic enzyme in glycolysis exhibit effective antitumor activity against kidney renal clear cell carcinoma in vitro and in vivo', *Eur J Med Chem*, 267: 116209.

He, Y., Y. Luo, D. Zhang, X. Wang, P. Zhang, H. Li, S. Ejaz, and S. Liang. 2019. 'PGK1-mediated cancer progression and drug resistance', *Am J Cancer Res*, 9: 2280-302.

Hergesheimer, R. C., A. A. Chami, D. R. de Assis, P. Vourc'h, C. R. Andres, P. Corcia, D. Lanznaster, and H. Blasco. 2019. 'The debated toxic role of aggregated TDP-43 in amyotrophic lateral sclerosis: a resolution in sight?', *Brain*, 142: 1176-94.

Howe, K., M. D. Clark, C. F. Torroja, J. Torrance, C. Berthelot, M. Muffato, J. E. Collins, S. Humphray, K. McLaren, L. Matthews, S. McLaren, I. Sealy, M. Caccamo, C. Churcher, C. Scott, J. C. Barrett, R. Koch, G. J. Rauch, S. White, W. Chow, B. Kilian, L. T. Quintais, J. A. Guerra-Assuncao, Y. Zhou, Y. Gu, J. Yen, J. H. Vogel, T. Eyre, S. Redmond, R. Banerjee, J. Chi, B. Fu, E. Langley, S. F. Maguire, G. K. Laird, D. Lloyd, E. Kenyon, S. Donaldson, H. Sehra, J. Almeida-King, J.

Loveland, S. Trevanion, M. Jones, M. Quail, D. Willey, A. Hunt, J. Burton, S. Sims, K. McLay, B. Plumb, J. Davis, C. Clee, K. Oliver, R. Clark, C. Riddle, D. Elliot, G. Threadgold, G. Harden, D. Ware, S. Begum, B. Mortimore, G. Kerry, P. Heath, B. Phillimore, A. Tracey, N. Corby, M. Dunn, C. Johnson, J. Wood, S. Clark, S. Pelan, G. Griffiths, M. Smith, R. Glithero, P. Howden, N. Barker, C. Lloyd, C. Stevens, J. Harley, K. Holt, G. Panagiotidis, J. Lovell, H. Beasley, C. Henderson, D. Gordon, K. Auger, D. Wright, J. Collins, C. Raisen, L. Dyer, K. Leung, L. Robertson, K. Ambridge, D. Leongamornlert, S. McGuire, R. Gilderthorp, C. Griffiths, D. Manthravadi, S. Nichol, G. Barker, S. Whitehead, M. Kay, J. Brown, C. Murnane, E. Gray, M. Humphries, N. Sycamore, D. Barker, D. Saunders, J. Wallis, A. Babbage, S. Hammond, M. Mashreghi-Mohammadi, L. Barr, S. Martin, P. Wray, A. Ellington, N. Matthews, M. Ellwood, R. Woodmansey, G. Clark, J. Cooper, A. Tromans, D. Grafham, C. Skuce, R. Pandian, R. Andrews, E. Harrison, A. Kimberley, J. Garnett, N. Fosker, R. Hall, P. Garner, D. Kelly, C. Bird, S. Palmer, I. Gehring, A. Berger, C. M. Dooley, Z. Ersan-Urun, C. Eser, H. Geiger, M. Geisler, L. Karotki, A. Kirn, J. Konantz, M. Konantz, M. Oberlander, S. Rudolph-Geiger, M. Teucke, C. Lanz, G. Raddatz, K. Osoegawa, B. Zhu, A. Rapp, S. Widaa, C. Langford, F. Yang, S. C. Schuster, N. P. Carter, J. Harrow, Z. Ning, J. Herrero, S. M. Searle, A. Enright, R. Geisler, R. H. Plasterk, C. Lee, M. Westerfield, P. J. de Jong, L. I. Zon, J. H. Postlethwait, C. Nusslein-Volhard, T. J. Hubbard, H. Roest Crollius, J. Rogers, and D. L. Stemple. 2013. 'The zebrafish reference genome sequence and its relationship to the human genome', *Nature*, 496: 498-503.

Hu, H., W. Zhu, J. Qin, M. Chen, L. Gong, L. Li, X. Liu, Y. Tao, H. Yin, H. Zhou, L. Zhou, D. Ye, Q. Ye, and D. Gao. 2017. 'Acetylation of PGK1 promotes liver cancer cell proliferation and tumorigenesis', *Hepatology*, 65: 515-28.

Hu, J., J. Han, H. Li, X. Zhang, L. L. Liu, F. Chen, and B. Zeng. 2018. 'Human Embryonic Kidney 293 Cells: A Vehicle for Biopharmaceutical Manufacturing, Structural Biology, and Electrophysiology', *Cells Tissues Organs*, 205: 1-8.

Huang, Y. T., D. van der Hoorn, L. M. Ledahawsky, A. A. L. Motyl, C. Y. Jordan, T. H. Gillingwater, and E. J. N. Groen. 2019. 'Robust Comparison of Protein Levels Across Tissues and Throughout Development Using Standardized Quantitative Western Blotting', *J Vis Exp*.

Hubers, A., W. Just, A. Rosenbohm, K. Muller, N. Marroquin, I. Goebel, J. Hogel, H. Thiele, J. Altmuller, P. Nurnberg, J. H. Weishaupt, C. Kubisch, A. C. Ludolph, and A. E. Volk. 2015. 'De novo FUS mutations

are the most frequent genetic cause in early-onset German ALS patients', *Neurobiol Aging*, 36: 3117 e1-17 e6.

Invitrogen, Life Technologies. 2013. "Lipofectamine 2000 DNA Transfection Reagent Protocol." In.: Invitrogen, Life Technologies.

Jeffery, C. J. 2017. 'Moonlighting proteins - nature's Swiss army knives', *Sci Prog*, 100: 363-73.

Jiang, Y., R. He, Y. Jiang, D. Liu, L. Tao, M. Yang, C. Lin, Y. Shen, X. Fu, J. Yang, J. Li, Y. Huo, R. Hua, W. Liu, J. Zhang, B. Shen, Z. Zhang, and Y. Sun. 2019. 'Transcription factor NFAT5 contributes to the glycolytic phenotype rewiring and pancreatic cancer progression via transcription of PGK1', *Cell Death Dis*, 10: 948.

Jin, C., X. Zhu, H. Wu, Y. Wang, and X. Hu. 2020. 'Perturbation of phosphoglycerate kinase 1 (PGK1) only marginally affects glycolysis in cancer cells', *J Biol Chem*, 295: 6425-46.

Johann, S., M. Dahm, M. Kipp, U. Zahn, and C. Beyer. 2011. 'Regulation of choline acetyltransferase expression by 17 beta-oestradiol in NSC-34 cells and in the spinal cord', *J Neuroendocrinol*, 23: 839-48.

Josephs, K. A., M. E. Murray, J. L. Whitwell, N. Tosakulwong, S. D. Weigand, L. Petrucelli, A. M. Liesinger, R. C. Petersen, J. E. Parisi, and D. W. Dickson. 2016. 'Updated TDP-43 in Alzheimer's disease staging scheme', *Acta Neuropathol*, 131: 571-85.

Kabashi, E., L. Lin, M. L. Tradewell, P. A. Dion, V. Bercier, P. Bourgouin, D. Rochefort, S. Bel Hadj, H. D. Durham, C. Vande Velde, G. A. Rouleau, and P. Drapeau. 2010. 'Gain and loss of function of ALS-related mutations of TARDBP (TDP-43) cause motor deficits in vivo', *Hum Mol Genet*, 19: 671-83.

Kaluz, S., M. Kaluzova, and E. J. Stanbridge. 2008. 'Regulation of gene expression by hypoxia: integration of the HIF-transduced hypoxic signal at the hypoxia-responsive element', *Clin Chim Acta*, 395: 6-13.

Kawakami, I., T. Arai, and M. Hasegawa. 2019. 'The basis of clinicopathological heterogeneity in TDP-43 proteinopathy', *Acta Neuropathol*, 138: 751-70.

Khalfallah, Y., R. Kuta, C. Grasmuck, A. Prat, H. D. Durham, and C. Vande Velde. 2018. 'TDP-43 regulation of stress granule dynamics in neurodegenerative disease-relevant cell types', *Sci Rep*, 8: 7551.

Kimmel, C. B., W. W. Ballard, S. R. Kimmel, B. Ullmann, and T. F. Schilling. 1995. 'Stages of embryonic development of the zebrafish', *Dev Dyn*, 203: 253-310.

Klusa, V. Z., S. Isajevs, D. Svirina, J. Pupure, U. Beitnere, J. Rumaks, S. Svirskis, B. Jansone, Z. Dzirkale, R. Muceniece, I. Kalvinsh, and H. V. Vinters. 2010. 'Neuroprotective properties of mildronate, a small molecule, in a rat model of Parkinson's disease', *Int J Mol Sci*, 11: 4465-87.

Kokotos, A. C., A. M. Antoniazzi, S. R. Unda, M. S. Ko, D. Park, D. Eliezer, M. G. Kaplitt, P. De Camilli, and T. A. Ryan. 2024. 'Phosphoglycerate kinase is a central leverage point in Parkinson's disease-driven neuronal metabolic deficits', *Sci Adv*, 10: eadn6016.

Kotsikorou, E., G. Sahota, and E. Oldfield. 2006. 'Bisphosphonate inhibition of phosphoglycerate kinase: quantitative structure-activity relationship and pharmacophore modeling investigation', *J Med Chem*, 49: 6692-703.

Kumar, S., B. Ma, C. J. Tsai, H. Wolfson, and R. Nussinov. 1999. 'Folding funnels and conformational transitions via hinge-bending motions', *Cell Biochem Biophys*, 31: 141-64.

Kyncl, J. J. 1986. 'Pharmacology of terazosin', *Am J Med*, 80: 12-9.

Ladd, A. N., N. Charlet, and T. A. Cooper. 2001. 'The CELF family of RNA binding proteins is implicated in cell-specific and developmentally regulated alternative splicing', *Mol Cell Biol*, 21: 1285-96.

Lam, W., C. H. Leung, S. Bussom, and Y. C. Cheng. 2007. 'The impact of hypoxic treatment on the expression of phosphoglycerate kinase and the cytotoxicity of troxacitabine and gemcitabine', *Mol Pharmacol*, 72: 536-44.

Lay, A. J., X. M. Jiang, O. Kisker, E. Flynn, A. Underwood, R. Condron, and P. J. Hogg. 2000. 'Phosphoglycerate kinase acts in tumour angiogenesis as a disulphide reductase', *Nature*, 408: 869-73.

Le Masson, G., S. Przedborski, and L. F. Abbott. 2014. 'A computational model of motor neuron degeneration', *Neuron*, 83: 975-88.

Li, H., H. P. Ko, and J. P. Whitlock. 1996. 'Induction of phosphoglycerate kinase 1 gene expression by hypoxia. Roles of Arnt and HIF1alpha', *J Biol Chem*, 271: 21262-7.

Li, M., A. Zhang, X. Qi, R. Yu, and J. Li. 2023. 'A novel inhibitor of PGK1 suppresses the aerobic glycolysis and proliferation of hepatocellular carcinoma', *Biomed Pharmacother*, 158: 114115.

Li, X., Y. Jiang, J. Meisenhelder, W. Yang, D. H. Hawke, Y. Zheng, Y. Xia, K. Aldape, J. He, T. Hunter, L. Wang, and Z. Lu. 2016. 'Mitochondria-Translocated PGK1 Functions as a Protein Kinase to Coordinate Glycolysis and the TCA Cycle in Tumorigenesis', *Mol Cell*, 61: 705-19.

Li, X., X. Qian, H. Jiang, Y. Xia, Y. Zheng, J. Li, B. J. Huang, J. Fang, C. N. Qian, T. Jiang, Y. X. Zeng, and Z. Lu. 2018. 'Nuclear PGK1 Alleviates ADP-Dependent Inhibition of CDC7 to Promote DNA Replication', *Mol Cell*, 72: 650-60 e8.

Li, X., Q. Yang, H. Yu, L. Wu, Y. Zhao, C. Zhang, X. Yue, Z. Liu, H. Wu, B. G. Haffty, Z. Feng, and W. Hu. 2014. 'LIF promotes tumorigenesis and metastasis of breast cancer through the AKT-mTOR pathway', *Oncotarget*, 5: 788-801.

Liang, J., C. Liu, D. Xu, K. Xie, and A. Li. 2022. 'LncRNA NEAT1 facilitates glioma progression via stabilizing PGK1', *J Transl Med*, 20: 80.

Liao, L., W. Dang, T. Lin, J. Yu, T. Liu, W. Li, S. Xiao, L. Feng, J. Huang, R. Fu, J. Li, L. Liu, M. Wang, H. Tao, H. Jiang, K. Chen, X. Diao, B. Zhou, X. Shen, and C. Luo. 2022. 'A potent PGK1 antagonist reveals PGK1 regulates the production of IL-1beta and IL-6', *Acta Pharm Sin B*, 12: 4180-92.

Liberti, M. V., and J. W. Locasale. 2016. 'The Warburg Effect: How Does it Benefit Cancer Cells?', *Trends Biochem Sci*, 41: 211-18.

Lin, Y. H., C. T. Yeh, C. Y. Chen, and K. H. Lin. 2025. 'Pseudogene: Relevant or Irrelevant?', *Biomed J*, 48: 100790.

Ling, J. P., O. Pletnikova, J. C. Troncoso, and P. C. Wong. 2015. 'TDP-43 repression of nonconserved cryptic exons is compromised in ALS-FTD', *Science*, 349: 650-5.

Little, A. C., I. Kovalenko, L. E. Goo, H. S. Hong, S. A. Kerk, J. A. Yates, V. Purohit, D. B. Lombard, S. D. Merajver, and C. A. Lyssiotis. 2020. 'High-content fluorescence imaging with the metabolic flux assay reveals insights into mitochondrial properties and functions', *Commun Biol*, 3: 271.

Liu, F., H. He, W. Yang, D. Wang, X. Sui, Y. Sun, S. Wang, Y. Yang, Z. Xiao, J. Yang, Y. Wang, and Y. Luo. 2024. 'Novel energy optimizer, meldonium, rapidly restores acute hypobaric hypoxia-induced brain

injury by targeting phosphoglycerate kinase 1', *Cell Commun Signal*, 22: 383.

Liu, H., L. Shen, Z. Sun, W. Wu, and M. Xu. 2023. 'Downregulated Phosphoglycerate Kinase 1 Attenuates Cerebral Ischemia-Reperfusion Injury by Reversing Neuroinflammation and Oxidative Stress through the Nuclear Factor Erythroid 2 Related Factor 2/ARE Pathway', *Neuroscience*, 524: 94-107.

Loewa, A., J. J. Feng, and S. Hedtrich. 2023. 'Human disease models in drug development', *Nat Rev Bioeng*: 1-15.

Lu, G., Z. Wen, L. Yu, C. Wang, and Y. Gao. 2024. 'HIF1A overexpression caused by etomidate activates PGK1-induced oxidative stress in postoperative cognitive dysfunction', *Brain Res*, 1841: 149069.

Luan, H. H., A. Wang, B. K. Hilliard, F. Carvalho, C. E. Rosen, A. M. Ahasic, E. L. Herzog, I. Kang, M. A. Pisani, S. Yu, C. Zhang, A. M. Ring, L. H. Young, and R. Medzhitov. 2019. 'GDF15 Is an Inflammation-Induced Central Mediator of Tissue Tolerance', *Cell*, 178: 1231-44 e11.

Luo, J. W., W. H. Duan, L. Song, Y. Q. Yu, and D. Z. Shi. 2021. 'A Meta-Analysis of Growth Differentiation Factor-15 and Prognosis in Chronic Heart Failure', *Front Cardiovasc Med*, 8: 630818.

Luo, Y., J. Yang, L. Zhang, Z. Tai, H. Huang, Z. Xu, and H. Zhang. 2023. 'Phosphoglycerate kinase (PGK) 1 succinylation modulates epileptic seizures and the blood-brain barrier', *Exp Anim*, 72: 475-89.

Mackenzie, I. R., E. H. Bigio, P. G. Ince, F. Geser, M. Neumann, N. J. Cairns, L. K. Kwong, M. S. Forman, J. Ravits, H. Stewart, A. Eisen, L. McClusky, H. A. Kretzschmar, C. M. Monoranu, J. R. Highley, J. Kirby, T. Siddique, P. J. Shaw, V. M. Lee, and J. Q. Trojanowski. 2007. 'Pathological TDP-43 distinguishes sporadic amyotrophic lateral sclerosis from amyotrophic lateral sclerosis with SOD1 mutations', *Ann Neurol*, 61: 427-34.

Madji Hounoum, B., P. Vourc'h, R. Felix, P. Corcia, F. Patin, M. Gueguinou, M. Potier-Cartereau, C. Vandier, C. Raoul, C. R. Andres, S. Mavel, and H. Blasco. 2016. 'NSC-34 Motor Neuron-Like Cells Are Unsuitable as Experimental Model for Glutamate-Mediated Excitotoxicity', *Front Cell Neurosci*, 10: 118.

Maier, O., J. Bohm, M. Dahm, S. Bruck, C. Beyer, and S. Johann. 2013. 'Differentiated NSC-34 motoneuron-like cells as experimental model for cholinergic neurodegeneration', *Neurochem Int*, 62: 1029-38.

Majounie, E., A. E. Renton, K. Mok, E. G. Dopper, A. Waite, S. Rollinson, A. Chio, G. Restagno, N. Nicolaou, J. Simon-Sanchez, J. C. van Swieten, Y. Abramzon, J. O. Johnson, M. Sendtner, R. Pamphlett, R. W. Orrell, S. Mead, K. C. Sidle, H. Houlden, J. D. Rohrer, K. E. Morrison, H. Pall, K. Talbot, O. Ansorge, A. L. S. F. T. D. Consortium Chromosome, Ftld Ftld Als French research network on, Italsgen Consortium, D. G. Hernandez, S. Arepalli, M. Sabatelli, G. Mora, M. Corbo, F. Giannini, A. Calvo, E. Englund, G. Borghero, G. L. Floris, A. M. Remes, H. Laaksovirta, L. McCluskey, J. Q. Trojanowski, V. M. Van Deerlin, G. D. Schellenberg, M. A. Nalls, V. E. Drory, C. S. Lu, T. H. Yeh, H. Ishiura, Y. Takahashi, S. Tsuji, I. Le Ber, A. Brice, C. Drepper, N. Williams, J. Kirby, P. Shaw, J. Hardy, P. J. Tienari, P. Heutink, H. R. Morris, S. Pickering-Brown, and B. J. Traynor. 2012. 'Frequency of the C9orf72 hexanucleotide repeat expansion in patients with amyotrophic lateral sclerosis and frontotemporal dementia: a cross-sectional study', *Lancet Neurol*, 11: 323-30.

Malo, N., J. A. Hanley, S. Cerquozzi, J. Pelletier, and R. Nadon. 2006. 'Statistical practice in high-throughput screening data analysis', *Nat Biotechnol*, 24: 167-75.

Manzo, E., I. Lorenzini, D. Barrameda, A. G. O'Conner, J. M. Barrows, A. Starr, T. Kovalik, B. E. Rabichow, E. M. Lehmkuhl, D. D. Shreiner, A. Joardar, J. C. Lievens, R. Bowser, R. Sattler, and D. C. Zarnescu. 2019. 'Glycolysis upregulation is neuroprotective as a compensatory mechanism in ALS', *Elife*, 8.

Marin, B., F. Boumediene, G. Logroscino, P. Couratier, M. C. Babron, A. L. Leutenegger, M. Copetti, P. M. Preux, and E. Beghi. 2017. 'Variation in worldwide incidence of amyotrophic lateral sclerosis: a meta-analysis', *Int J Epidemiol*, 46: 57-74.

Marquez, J., F. Aslam, and M. K. Khokha. 2023. 'Expanding EMC foldopathies: Topogenesis deficits alter the neural crest', *Genesis*, 61: e23520.

McComb, R. B., L. W. Bond, R. W. Burnett, R. C. Keech, and G. N. Bowers, Jr. 1976. 'Determination of the molar absorptivity of NADH', *Clin Chem*, 22: 141-50.

McHale-Owen, H., K. M. E. Faller, H. Chaytow, and T. H. Gillingwater. 2025. 'Phosphoglycerate kinase 1 as a therapeutic target in neurological disease', *Trends Mol Med*.

Meskyte, E. M., L. Pezze, L. Bartolomei, M. Forcato, I. A. Bocci, G. Bertalot, M. Barbareschi, L. Oliveira-Ferrer, A. Bisio, S. Bicciato, D. Baltriukiene, and Y. Ciribilli. 2023. 'ETV7 reduces inflammatory

responses in breast cancer cells by repressing the TNFR1/NF-kappaB axis', *Cell Death Dis*, 14: 263.

Miller, T. M., M. E. Cudkowicz, A. Genge, P. J. Shaw, G. Sobue, R. C. Bucelli, A. Chio, P. Van Damme, A. C. Ludolph, J. D. Glass, J. A. Andrews, S. Babu, M. Benatar, C. J. McDermott, T. Cochrane, S. Chary, S. Chew, H. Zhu, F. Wu, I. Nestorov, D. Graham, P. Sun, M. McNeill, L. Fanning, T. A. Ferguson, S. Fradette, Valor, and O. L. E. Working Group. 2022. 'Trial of Antisense Oligonucleotide Tofersen for SOD1 ALS', *N Engl J Med*, 387: 1099-110.

Mills, M., N. Yang, R. Weinberger, D. L. Vander Woude, A. H. Beggs, S. Easteal, and K. North. 2001. 'Differential expression of the actin-binding proteins, alpha-actinin-2 and -3, in different species: implications for the evolution of functional redundancy', *Hum Mol Genet*, 10: 1335-46.

Mitsumoto, H., and R. K. Olney. 1996. 'Drug combination treatment in patients with ALS: current status and future directions', *Neurology*, 47: S103-7.

Morales-Briceno, H., A. D. Ha, K. London, D. Farlow, F. C. F. Chang, and V. S. C. Fung. 2019. 'Parkinsonism in PGK1 deficiency implicates the glycolytic pathway in nigrostriatal dysfunction', *Parkinsonism Relat Disord*, 64: 319-23.

Morris, H. R., M. G. Spillantini, C. M. Sue, and C. H. Williams-Gray. 2024. 'The pathogenesis of Parkinson's disease', *Lancet*, 403: 293-304.

Muddapu, V. R., S. A. P. Dharshini, V. S. Chakravarthy, and M. M. Gromiha. 2020. 'Neurodegenerative Diseases - Is Metabolic Deficiency the Root Cause?', *Front Neurosci*, 14: 213.

Nango, H., Y. Kosuge, M. Sato, Y. Shibukawa, Y. Aono, T. Saigusa, Y. Ito, and K. Ishige. 2020. 'Highly Efficient Conversion of Motor Neuron-Like NSC-34 Cells into Functional Motor Neurons by Prostaglandin E(2)', *Cells*, 9.

Neumann, M., L. K. Kwong, E. B. Lee, E. Kremmer, A. Flatley, Y. Xu, M. S. Forman, D. Troost, H. A. Kretzschmar, J. Q. Trojanowski, and V. M. Lee. 2009. 'Phosphorylation of S409/410 of TDP-43 is a consistent feature in all sporadic and familial forms of TDP-43 proteinopathies', *Acta Neuropathol*, 117: 137-49.

Neumann, M., D. M. Sampathu, L. K. Kwong, A. C. Truax, M. C. Micsenyi, T. T. Chou, J. Bruce, T. Schuck, M. Grossman, C. M. Clark, L. F. McCluskey, B. L. Miller, E. Masliah, I. R. Mackenzie, H. Feldman, W. Feiden, H. A. Kretzschmar, J. Q. Trojanowski, and V. M. Lee. 2006.

'Ubiquitinated TDP-43 in frontotemporal lobar degeneration and amyotrophic lateral sclerosis', *Science*, 314: 130-3.

Nie, H., H. Ju, J. Fan, X. Shi, Y. Cheng, X. Cang, Z. Zheng, X. Duan, and W. Yi. 2020. 'O-GlcNAcylation of PGK1 coordinates glycolysis and TCA cycle to promote tumor growth', *Nat Commun*, 11: 36.

Noureddine, M., H. Mikolajek, N. V. Morgan, C. Denning, S. Loughna, K. Gehmlich, and F. Mohammed. 2025. 'Structural and functional insights into alpha-actinin isoforms and their implications in cardiovascular disease', *J Gen Physiol*, 157.

Opheim, K. M., E. Y. Uc, M. A. Cantrell, and B. C. Lund. 2024. 'Reprint of: The impact of alpha-1-adrenergic receptor antagonists on the progression of Parkinson disease', *J Am Pharm Assoc (2003)*: 102173.

Oprisoreanu, A. M., H. L. Smith, S. Krix, H. Chaytow, N. O. Carragher, T. H. Gillingwater, C. G. Becker, and T. Becker. 2021. 'Automated in vivo drug screen in zebrafish identifies synapse-stabilising drugs with relevance to spinal muscular atrophy', *Dis Model Mech*, 14.

Pacelli, C., N. Giguere, M. J. Bourque, M. Levesque, R. S. Slack, and L. E. Trudeau. 2015. 'Elevated Mitochondrial Bioenergetics and Axonal Arborization Size Are Key Contributors to the Vulnerability of Dopamine Neurons', *Curr Biol*, 25: 2349-60.

Palmai, Z., L. Chaloin, C. Lionne, J. Fidy, D. Perahia, and E. Balog. 2009. 'Substrate binding modifies the hinge bending characteristics of human 3-phosphoglycerate kinase: a molecular dynamics study', *Proteins*, 77: 319-29.

Park, H. B., B. C. Choi, and K. H. Baek. 2023. 'PGK1 modulates balance between pro- and anti-inflammatory cytokines by interacting with ITI-H4', *Biomed Pharmacother*, 161: 114437.

Park, M. K., L. Zhang, K. W. Min, J. H. Cho, C. C. Yeh, H. Moon, D. Hormaechea-Agulla, H. Mun, S. Ko, J. W. Lee, S. Jathar, A. S. Smith, Y. Yao, N. T. Giang, H. H. Vu, V. C. Yan, M. C. Bridges, A. Kourtidis, F. Muller, J. H. Chang, S. J. Song, S. Nakagawa, T. Hirose, J. H. Yoon, and M. S. Song. 2021. 'NEAT1 is essential for metabolic changes that promote breast cancer growth and metastasis', *Cell Metab*, 33: 2380-97 e9.

Patton, E. E., L. I. Zon, and D. M. Langenau. 2021. 'Zebrafish disease models in drug discovery: from preclinical modelling to clinical trials', *Nat Rev Drug Discov*, 20: 611-28.

Pfeiffer, T., S. Schuster, and S. Bonhoeffer. 2001. 'Cooperation and competition in the evolution of ATP-producing pathways', *Science*, 292: 504-7.

Pink, R. C., K. Wicks, D. P. Caley, E. K. Punch, L. Jacobs, and D. R. Carter. 2011. 'Pseudogenes: pseudo-functional or key regulators in health and disease?', *RNA*, 17: 792-8.

Poewe, W., K. Seppi, C. M. Tanner, G. M. Halliday, P. Brundin, J. Volkmann, A. E. Schrag, and A. E. Lang. 2017. 'Parkinson disease', *Nat Rev Dis Primers*, 3: 17013.

Protter, D. S. W., and R. Parker. 2016. 'Principles and Properties of Stress Granules', *Trends Cell Biol*, 26: 668-79.

Pupure, J., S. Isajevs, E. Skapare, J. Rumaks, S. Svirskis, D. Svirina, I. Kalvinsh, and V. Klusa. 2010. 'Neuroprotective properties of mildronate, a mitochondria-targeted small molecule', *Neurosci Lett*, 470: 100-5.

Qian, X., X. Li, Q. Cai, C. Zhang, Q. Yu, Y. Jiang, J. H. Lee, D. Hawke, Y. Wang, Y. Xia, Y. Zheng, B. H. Jiang, D. X. Liu, T. Jiang, and Z. Lu. 2017. 'Phosphoglycerate Kinase 1 Phosphorylates Beclin1 to Induce Autophagy', *Mol Cell*, 65: 917-31 e6.

Qiang, S. J., Y. Q. Shi, T. Y. Wu, J. Q. Wang, X. L. Chen, J. Su, X. P. Chen, J. Z. Li, and Z. S. Chen. 2022. 'The Discovery of Novel PGK1 Activators as Apoptotic Inhibiting and Neuroprotective Agents', *Front Pharmacol*, 13: 877706.

Qiu, A., X. Wen, Q. Zou, L. Yin, S. Zhu, Y. Sheng, Y. He, Q. Liu, D. Luo, and Z. Guo. 2024. 'Phosphoglycerate Kinase 1: An Effective Therapeutic Target in Cancer', *Front Biosci (Landmark Ed)*, 29: 92.

Raman, R., S. P. Allen, E. F. Goodall, S. Kramer, L. L. Ponger, P. R. Heath, M. Milo, H. C. Hollinger, T. Walsh, J. R. Highley, S. Olpin, C. J. McDermott, P. J. Shaw, and J. Kirby. 2015. 'Gene expression signatures in motor neurone disease fibroblasts reveal dysregulation of metabolism, hypoxia-response and RNA processing functions', *Neuropathol Appl Neurobiol*, 41: 201-26.

Reineke, L. C., and J. R. Neilson. 2019. 'Differences between acute and chronic stress granules, and how these differences may impact function in human disease', *Biochem Pharmacol*, 162: 123-31.

Ribeiro, Gbes, F. R. Rodrigues, E. Pasqualotto, J. M. Dantas, and D. G. Di Luca. 2024. 'Exposure to Glycolysis-Enhancing Drugs and Risk of Parkinson's Disease: A Meta-Analysis', *J Parkinsons Dis*.

Riley, M. J., C. C. Mitchell, S. E. Ernst, E. B. Taylor, and M. J. Welsh. 2024. 'A model for stimulation of enzyme activity by a competitive inhibitor based on the interaction of terazosin and phosphoglycerate kinase 1', *Proc Natl Acad Sci U S A*, 121: e2318956121.

Rojas-Pirela, M., D. Andrade-Alviarez, V. Rojas, U. Kemmerling, A. J. Caceres, P. A. Michels, J. L. Concepcion, and W. Quinones. 2020. 'Phosphoglycerate kinase: structural aspects and functions, with special emphasis on the enzyme from Kinetoplastea', *Open Biol*, 10: 200302.

Rosa, J. G. S., C. Lima, and M. Lopes-Ferreira. 2022. 'Zebrafish Larvae Behavior Models as a Tool for Drug Screenings and Pre-Clinical Trials: A Review', *Int J Mol Sci*, 23.

Rosen, D. R., T. Siddique, D. Patterson, D. A. Figlewicz, P. Sapp, A. Hentati, D. Donaldson, J. Goto, J. P. O'Regan, H. X. Deng, and et al. 1993. 'Mutations in Cu/Zn superoxide dismutase gene are associated with familial amyotrophic lateral sclerosis', *Nature*, 362: 59-62.

Sadick, J. S., M. R. O'Dea, P. Hasel, T. Dykstra, A. Faustin, and S. A. Liddelow. 2022. 'Astrocytes and oligodendrocytes undergo subtype-specific transcriptional changes in Alzheimer's disease', *Neuron*, 110: 1788-805 e10.

Sakaue, S., T. Kasai, I. Mizuta, M. Suematsu, S. Osone, Y. Azuma, T. Imamura, T. Tokuda, H. Kanno, O. M. A. El-Agnaf, M. Morimoto, M. Nakagawa, H. Hosoi, and T. Mizuno. 2017. 'Early-onset parkinsonism in a pedigree with phosphoglycerate kinase deficiency and a heterozygous carrier: do PGK-1 mutations contribute to vulnerability to parkinsonism?', *NPJ Parkinsons Dis*, 3: 13.

Salameti, V., P. G. Bhosale, A. Ames-Draycott, K. Sipila, and F. M. Watt. 2019. 'NOTCH1 signaling in oral squamous cell carcinoma via a TEL2/SERPINE1 axis', *Oncotarget*, 10: 6791-804.

Saleem, S., and R. R. Kannan. 2018. 'Zebrafish: an emerging real-time model system to study Alzheimer's disease and neurospecific drug discovery', *Cell Death Discov*, 4: 45.

Sasane, R., A. Bartels, M. Field, M. I. Sierra, S. Duvvuri, D. L. Gray, S. S. Pin, J. J. Renger, and D. J. Stone. 2021. 'Parkinson disease among patients treated for benign prostatic hyperplasia with alpha1 adrenergic receptor antagonists', *J Clin Invest*, 131.

Schmid, B., A. Hruscha, S. Hogl, J. Banzhaf-Strathmann, K. Strecker, J. van der Zee, M. Teucke, S. Eimer, J. Hegermann, M. Kittelmann, E. Kremmer, M. Cruts, B. Solchenberger, L. Hasenkamp, F. van Bebber,

C. Van Broeckhoven, D. Edbauer, S. F. Lichtenthaler, and C. Haass. 2013. 'Loss of ALS-associated TDP-43 in zebrafish causes muscle degeneration, vascular dysfunction, and reduced motor neuron axon outgrowth', *Proc Natl Acad Sci U S A*, 110: 4986-91.

Schroeder, A., O. Mueller, S. Stocker, R. Salowsky, M. Leiber, M. Gassmann, S. Lightfoot, W. Menzel, M. Granzow, and T. Ragg. 2006. 'The RIN: an RNA integrity number for assigning integrity values to RNA measurements', *BMC Mol Biol*, 7: 3.

Schultz, J. L., A. N. Brinker, J. Xu, S. E. Ernst, F. Tayyari, A. J. Rauckhorst, L. Liu, E. Y. Uc, E. B. Taylor, J. E. Simmering, V. A. Magnotta, M. J. Welsh, and N. S. Narayanan. 2022. 'A pilot to assess target engagement of terazosin in Parkinson's disease', *Parkinsonism Relat Disord*, 94: 79-83.

Shaker, B., S. Ahmad, J. Lee, C. Jung, and D. Na. 2021. 'In silico methods and tools for drug discovery', *Comput Biol Med*, 137: 104851.

Shimizu, J., T. Kasai, H. Yoshida, A. M. Huynh, Y. Nakao-Azuma, M. Shinomoto, T. Tokuda, T. Mizuno, and M. Yamaguchi. 2020. 'Novel Drosophila model for parkinsonism by targeting phosphoglycerate kinase', *Neurochem Int*, 139: 104816.

Simmering, J. E., M. J. Welsh, L. Liu, N. S. Narayanan, and A. Pottegard. 2021. 'Association of Glycolysis-Enhancing alpha-1 Blockers With Risk of Developing Parkinson Disease', *JAMA Neurol*, 78: 407-13.

Simmering, J. E., M. J. Welsh, J. Schultz, and N. S. Narayanan. 2022. 'Use of Glycolysis-Enhancing Drugs and Risk of Parkinson's Disease', *Mov Disord*, 37: 2210-16.

Sjoblom, B., A. Salmazo, and K. Djinovic-Carugo. 2008. 'Alpha-actinin structure and regulation', *Cell Mol Life Sci*, 65: 2688-701.

Sourbron, J., M. Partoens, C. Scheldeman, Y. Zhang, L. Lagae, and P. de Witte. 2019. 'Drug repurposing for Dravet syndrome in scn1Lab(-/-) mutant zebrafish', *Epilepsia*, 60: e8-e13.

Streisinger, G., C. Walker, N. Dower, D. Knauber, and F. Singer. 1981. 'Production of clones of homozygous diploid zebra fish (Brachydanio rerio)', *Nature*, 291: 293-6.

Suk, T. R., and M. W. C. Rousseaux. 2020. 'The role of TDP-43 mislocalization in amyotrophic lateral sclerosis', *Mol Neurodegener*, 15: 45.

Swerdlow, R. H., J. K. Parks, S. W. Miller, J. B. Tuttle, P. A. Trimmer, J. P. Sheehan, J. P. Bennett, Jr., R. E. Davis, and W. D. Parker, Jr. 1996. 'Origin and functional consequences of the complex I defect in Parkinson's disease', *Ann Neurol*, 40: 663-71.

Szebenyi, K., L. M. D. Wenger, Y. Sun, A. W. E. Dunn, C. A. Limegrover, G. M. Gibbons, E. Conci, O. Paulsen, S. B. Mierau, G. Balmus, and A. Lakatos. 2021. 'Human ALS/FTD brain organoid slice cultures display distinct early astrocyte and targetable neuronal pathology', *Nat Neurosci*, 24: 1542-54.

Takahashi, K., K. Tanabe, M. Ohnuki, M. Narita, T. Ichisaka, K. Tomoda, and S. Yamanaka. 2007. 'Induction of pluripotent stem cells from adult human fibroblasts by defined factors', *Cell*, 131: 861-72.

Talbot K, Al-Chalabi A, Ajram L, Bendotti C, Bonetto V, Bose S, Bruijn LI, Cole N, Coney L, Dickie BG, Greensmith L, Latimer J, Malaspina A, McGrath S, Mead RJ, Nyberg S, Phelan A, Richardson JC, Turner MR, Van Den Bosch L, Waters J, Wright PD, and Lee JL. 2023. 'Guiding Principles for Drug Discovery and Development in Amyotophic Lateral Sclerosis', *myname5doddie*.

Talbot, K. 2009. 'Motor neuron disease: the bare essentials', *Pract Neurol*, 9: 303-9.

Tamaoka, A., M. Arai, M. Itokawa, T. Arai, M. Hasegawa, K. Tsuchiya, H. Takuma, H. Tsuji, A. Ishii, M. Watanabe, Y. Takahashi, J. Goto, S. Tsuji, and H. Akiyama. 2010. 'TDP-43 M337V mutation in familial amyotrophic lateral sclerosis in Japan', *Intern Med*, 49: 331-4.

Tang, B. L. 2020. 'Glucose, glycolysis, and neurodegenerative diseases', *J Cell Physiol*, 235: 7653-62.

Tang, S. W., W. H. Chang, Y. C. Su, Y. C. Chen, Y. H. Lai, P. T. Wu, C. I. Hsu, W. C. Lin, M. K. Lai, and J. Y. Lin. 2009. 'MYC pathway is activated in clear cell renal cell carcinoma and essential for proliferation of clear cell renal cell carcinoma cells', *Cancer Lett*, 273: 35-43.

Technologies, Agilent. 2017a. 'Characterizing Your Cells', Accessed 16/06/25. https://www.agilent.com/cs/library/technicaloverviews/public/5991-7994EN.pdf.

———. 2017b. 'Seeding Adherent Cells in Agilent Seahorse XF24 Cell Culture Microplates ', Accessed 16/06/25. https://www.agilent.com/cs/library/usermanuals/public/XFe24_DAY_BEFORE_CELL_SEEDING.pdf.

———. 2019. 'Agilent Seahorse XF Glycolysis Stress Test Kit', Accessed 16/06/2025. https://www.agilent.com/cs/library/usermanuals/public/XF_Glycolysis_Stress_Test_Kit_User_Guide.pdf.

———. 2022. 'FCCP Optimization Using the Agilent Seahorse XF Cell Mito Stress Test with the Agilent Seahorse XF Pro Analyzer', Accessed 16/06/25. https://www.agilent.com/cs/library/instructionsheet/public/is-fccp-optimization-5994-4807en-agilent.pdf.

———. 2024. 'Agilent Seahorse XF Cell Mito Stress Test Kit', Accessed 18/06/2025. https://www.agilent.com/cs/library/usermanuals/public/XF_Cell_Mito_Stress_Test_Kit_User_Guide.pdf.

Thomas, P., and T. G. Smart. 2005. 'HEK293 cell line: a vehicle for the expression of recombinant proteins', *J Pharmacol Toxicol Methods*, 51: 187-200.

Thomson, S. R., J. E. Nahon, C. A. Mutsaers, D. Thomson, G. Hamilton, S. H. Parson, and T. H. Gillingwater. 2012. 'Morphological characteristics of motor neurons do not determine their relative susceptibility to degeneration in a mouse model of severe spinal muscular atrophy', *PLoS One*, 7: e52605.

Tong, J., J. Yang, H. Lv, S. Lv, C. Zhang, and Z. J. Chen. 2018. 'Dysfunction of pseudogene PGK1P2 is involved in preeclampsia by acting as a competing endogenous RNA of PGK1', *Pregnancy Hypertens*, 13: 37-45.

Tran, T., J. Yang, J. Gardner, and Y. Xiong. 2018. 'GDF15 deficiency promotes high fat diet-induced obesity in mice', *PLoS One*, 13: e0201584.

Turrens, J. F. 2003. 'Mitochondrial formation of reactive oxygen species', *J Physiol*, 552: 335-44.

Uechi, H., S. Sridharan, J. Nijssen, J. Bilstein, J. M. Iglesias-Artola, S. Kishigami, V. Casablancas-Antras, I. Poser, E. J. Martinez, E. Boczek, M. Wagner, N. Tomschke, A. M. de Jesus Domingues, A. Pal, T. Doeleman, S. Kour, E. N. Anderson, F. Stein, H. O. Lee, X. Zhang, A. W. Fritsch, M. Jahnel, J. Fursch, A. C. Murthy, S. Alberti, M. Bickle, N. L. Fawzi, A. Nadler, D. C. David, U. B. Pandey, A. Hermann, F. Stengel, B. G. Davis, A. J. Baldwin, M. M. Savitski, A. A. Hyman, and R. J. Wheeler. 2025. 'Small-molecule dissolution of stress granules by redox modulation benefits ALS models', *Nat Chem Biol*.

Valbuena, G. N., M. Rizzardini, S. Cimini, A. P. Siskos, C. Bendotti, L. Cantoni, and H. C. Keun. 2016. 'Metabolomic Analysis Reveals Increased Aerobic Glycolysis and Amino Acid Deficit in a Cellular Model of Amyotrophic Lateral Sclerosis', *Mol Neurobiol*, 53: 2222-40.

Vander Heiden, M. G., L. C. Cantley, and C. B. Thompson. 2009. 'Understanding the Warburg effect: the metabolic requirements of cell proliferation', *Science*, 324: 1029-33.

Vandoorne, T., K. De Bock, and L. Van Den Bosch. 2018. 'Energy metabolism in ALS: an underappreciated opportunity?', *Acta Neuropathol*, 135: 489-509.

Vaz, R. L., S. Sousa, D. Chapela, H. C. van der Linde, R. Willemsen, A. D. Correia, T. F. Outeiro, and N. D. Afonso. 2020. 'Identification of antiparkinsonian drugs in the 6-hydroxydopamine zebrafish model', *Pharmacol Biochem Behav*, 189: 172828.

Wallach, I., M. Dzamba, and A. Heifets. 2016. 'AtomNet: A deep, convolutional neural network for bioactivity prediction in structure-based drug discovery', *Abstracts of Papers of the American Chemical Society*, 251.

Wang, C., C. Yuan, L. Zhang, C. Wu, and N. Li. 2007. 'Differential gene expression of phosphoglyceric kinase (PGK) and hypoxic adaptation in chicken', *Sci China C Life Sci*, 50: 335-42.

Wang, D., F. Liu, W. Yang, Y. Sun, X. Wang, X. Sui, J. Yang, Q. Wang, W. Song, M. Zhang, Z. Xiao, T. Wang, Y. Wang, and Y. Luo. 2022. 'Meldonium Ameliorates Hypoxia-Induced Lung Injury and Oxidative Stress by Regulating Platelet-Type Phosphofructokinase-Mediated Glycolysis', *Front Pharmacol*, 13: 863451.

Wang, J., Q. S. Gao, Y. Wang, R. Lafyatis, S. Stamm, and A. Andreadis. 2004. 'Tau exon 10, whose missplicing causes frontotemporal dementia, is regulated by an intricate interplay of cis elements and trans factors', *J Neurochem*, 88: 1078-90.

Wang, S., B. Jiang, T. Zhang, L. Liu, Y. Wang, Y. Wang, X. Chen, H. Lin, L. Zhou, Y. Xia, L. Chen, C. Yang, Y. Xiong, D. Ye, and K. L. Guan. 2015. 'Insulin and mTOR Pathway Regulate HDAC3-Mediated Deacetylation and Activation of PGK1', *PLoS Biol*, 13: e1002243.

Wang, Y., L. Sun, G. Yu, X. Qi, A. Zhang, Z. Lu, D. Li, and J. Li. 2021. 'Identification of a novel non-ATP-competitive protein kinase inhibitor of PGK1 from marine nature products', *Biochem Pharmacol*, 183: 114343.

Wang, Yang, Shihu Qian, Fang Zhao, Yujie Wang, and Jiaming Li. 2022. 'Terazosin Analogs Targeting Pgk1 as Neuroprotective Agents: Design, Synthesis, and Evaluation', *Frontiers in Chemistry*, 10.

Wang, Z., J. Tian, L. Wang, H. Yan, S. Feng, and Y. Zhang. 2024. 'PGK1 Is Involved in the HIF-1 Signaling Pathway as a Hub Gene for Ferroptosis After Traumatic Brain Injury', *Mol Neurobiol*.

Watson, H. C., and J. A. Littlechild. 1990. 'Isoenzymes of phosphoglycerate kinase: evolutionary conservation of the structure of this glycolytic enzyme', *Biochem Soc Trans*, 18: 187-90.

Watson, H. C., N. P. Walker, P. J. Shaw, T. N. Bryant, P. L. Wendell, L. A. Fothergill, R. E. Perkins, S. C. Conroy, M. J. Dobson, M. F. Tuite, and et al. 1982. 'Sequence and structure of yeast phosphoglycerate kinase', *EMBO J*, 1: 1635-40.

Weber, M. A., S. Schnyder-Candrian, B. Schnyder, V. Quesniaux, V. Poli, C. L. Stewart, and B. Ryffel. 2005. 'Endogenous leukemia inhibitory factor attenuates endotoxin response', *Lab Invest*, 85: 276-84.

Weber, M. A., K. Sivakumar, E. E. Tabakovic, M. Oya, G. M. Aldridge, Q. Zhang, J. E. Simmering, and N. S. Narayanan. 2023. 'Glycolysis-enhancing alpha(1)-adrenergic antagonists modify cognitive symptoms related to Parkinson's disease', *NPJ Parkinsons Dis*, 9: 32.

Wei, Y., Q. Miao, Q. Zhang, S. Mao, M. Li, X. Xu, X. Xia, K. Wei, Y. Fan, X. Zheng, Y. Fang, M. Mei, Q. Zhang, J. Ding, Y. Fan, M. Lu, and G. Hu. 2023. 'Aerobic glycolysis is the predominant means of glucose metabolism in neuronal somata, which protects against oxidative damage', *Nat Neurosci*, 26: 2081-89.

Weiskirchen, S., S. K. Schroder, E. M. Buhl, and R. Weiskirchen. 2023. 'A Beginner's Guide to Cell Culture: Practical Advice for Preventing Needless Problems', *Cells*, 12.

Winton, M. J., L. M. Igaz, M. M. Wong, L. K. Kwong, J. Q. Trojanowski, and V. M. Lee. 2008. 'Disturbance of nuclear and cytoplasmic TAR DNA-binding protein (TDP-43) induces disease-like redistribution, sequestration, and aggregate formation', *J Biol Chem*, 283: 13302-9.

Witzel, S., A. Maier, R. Steinbach, J. Grosskreutz, J. C. Koch, A. Sarikidi, S. Petri, R. Gunther, J. Wolf, A. Hermann, J. Prudlo, I. Cordts, P. Lingor, W. N. Loscher, Z. Kohl, T. Hagenacker, C. Ruckes, B. Koch, S. Spittel, K. Gunther, S. Michels, J. Dorst, T. Meyer, A. C. Ludolph, and Network German Motor Neuron Disease. 2022. 'Safety and Effectiveness of Long-term Intravenous Administration of Edaravone

for Treatment of Patients With Amyotrophic Lateral Sclerosis', *JAMA Neurol*, 79: 121-30.

Wolf, J., A. Safer, J. C. Wohrle, F. Palm, W. A. Nix, M. Maschke, and A. J. Grau. 2014. 'Variability and prognostic relevance of different phenotypes in amyotrophic lateral sclerosis - data from a population-based registry', *J Neurol Sci*, 345: 164-7.

Wu, L. S., W. C. Cheng, and C. K. Shen. 2012. 'Targeted depletion of TDP-43 expression in the spinal cord motor neurons leads to the development of amyotrophic lateral sclerosis-like phenotypes in mice', *J Biol Chem*, 287: 27335-44.

Wu, Y., L. Ma, X. Li, J. Yang, X. Rao, Y. Hu, J. Xi, L. Tao, J. Wang, L. Du, G. Chen, and S. Liu. 2024. 'The role of artificial intelligence in drug screening, drug design, and clinical trials', *Front Pharmacol*, 15: 1459954.

Xu, L., T. Liu, L. Liu, X. Yao, L. Chen, D. Fan, S. Zhan, and S. Wang. 2020. 'Global variation in prevalence and incidence of amyotrophic lateral sclerosis: a systematic review and meta-analysis', *J Neurol*, 267: 944-53.

Xu, Y. F., T. F. Gendron, Y. J. Zhang, W. L. Lin, S. D'Alton, H. Sheng, M. C. Casey, J. Tong, J. Knight, X. Yu, R. Rademakers, K. Boylan, M. Hutton, E. McGowan, D. W. Dickson, J. Lewis, and L. Petrucelli. 2010. 'Wild-type human TDP-43 expression causes TDP-43 phosphorylation, mitochondrial aggregation, motor deficits, and early mortality in transgenic mice', *J Neurosci*, 30: 10851-9.

Xu, Y. F., Y. J. Zhang, W. L. Lin, X. Cao, C. Stetler, D. W. Dickson, J. Lewis, and L. Petrucelli. 2011. 'Expression of mutant TDP-43 induces neuronal dysfunction in transgenic mice', *Mol Neurodegener*, 6: 73.

Yang, P., C. Mathieu, R. M. Kolaitis, P. Zhang, J. Messing, U. Yurtsever, Z. Yang, J. Wu, Y. Li, Q. Pan, J. Yu, E. W. Martin, T. Mittag, H. J. Kim, and J. P. Taylor. 2020. 'G3BP1 Is a Tunable Switch that Triggers Phase Separation to Assemble Stress Granules', *Cell*, 181: 325-45 e28.

Yang, W., X. Lei, F. Liu, X. Sui, Y. Yang, Z. Xiao, Z. Cui, Y. Sun, J. Yang, X. Yang, X. Lin, Z. Bao, W. Li, Y. Ma, Y. Wang, and Y. Luo. 2024. 'Meldonium, as a potential neuroprotective agent, promotes neuronal survival by protecting mitochondria in cerebral ischemia-reperfusion injury', *J Transl Med*, 22: 771.

Yatsuga, S., Y. Fujita, A. Ishii, Y. Fukumoto, H. Arahata, T. Kakuma, T. Kojima, M. Ito, M. Tanaka, R. Saiki, and Y. Koga. 2015. 'Growth

differentiation factor 15 as a useful biomarker for mitochondrial disorders', *Ann Neurol*, 78: 814-23.

Yin, L., N. Wu, and M. A. Lazar. 2010. 'Nuclear receptor Rev-erbalpha: a heme receptor that coordinates circadian rhythm and metabolism', *Nucl Recept Signal*, 8: e001.

Yip, P. K., M. Bremang, I. Pike, V. Ponnusamy, A. T. Michael-Titus, and D. K. Shah. 2023. 'Newborns with Favourable Outcomes after Perinatal Asphyxia Have Upregulated Glucose Metabolism-Related Proteins in Plasma', *Biomolecules*, 13.

Yu, Z., J. Gao, Z. Zhou, L. Li, and S. Hu. 2025. 'Circulating growth differentiation factor-15 concentration and hypertension risk: a dose-response meta-analysis', *Front Cardiovasc Med*, 12: 1500882.

Zhang, K., L. Sun, and Y. Kang. 2023. 'Regulation of phosphoglycerate kinase 1 and its critical role in cancer', *Cell Commun Signal*, 21: 240.

Zhang, P., S. Gong, S. Li, and Z. Yuan. 2023. 'PVT1 alleviates hypoxia-induced endothelial apoptosis by enhancing autophagy via the miR-15b-5p/ATG14 and miR-424-5p/ATG14 axis', *Biochem Biophys Res Commun*, 671: 1-9.

Zhang, T., Y. Wang, H. Yu, T. Zhang, L. Guo, J. Xu, X. Wei, N. Wang, Y. Wu, X. Wang, and L. Huang. 2022. 'PGK1 represses autophagy-mediated cell death to promote the proliferation of liver cancer cells by phosphorylating PRAS40', *Cell Death Dis*, 13: 68.

Zhang, Y., G. Yu, H. Chu, X. Wang, L. Xiong, G. Cai, R. Liu, H. Gao, B. Tao, W. Li, G. Li, J. Liang, and W. Yang. 2018. 'Macrophage-Associated PGK1 Phosphorylation Promotes Aerobic Glycolysis and Tumorigenesis', *Mol Cell*, 71: 201-15 e7.

Zhao, Z., X. Chen, A. M. Dowbaj, A. Sljukic, K. Bratlie, L. Lin, E. L. S. Fong, G. M. Balachander, Z. Chen, A. Soragni, M. Huch, Y. A. Zeng, Q. Wang, and H. Yu. 2022. 'Organoids', *Nat Rev Methods Primers*, 2.

Zheng, J., J. L. Zhu, Y. Zhang, H. Zhang, Y. Yang, D. R. Tang, and J. Sun. 2020. 'PGK1 inhibitor CBR-470-1 protects neuronal cells from MPP+', *Aging (Albany NY)*, 12: 13388-99.